Lecture Notes in Physics 844

Tilman Plehn

Lectures on LHC Physics

Springer

Lecture Notes in Physics

Volume 844

For further volumes:
http://www.springer.com/series/5304

The Lecture Notes in Physics

The series Lecture Notes in Physics (LNP), founded in 1969, reports new developments in physics research and teaching—quickly and informally, but with a high quality and the explicit aim to summarize and communicate current knowledge in an accessible way. Books published in this series are conceived as bridging material between advanced graduate textbooks and the forefront of research and to serve three purposes:

- to be a compact and modern up-to-date source of reference on a well-defined topic
- to serve as an accessible introduction to the field to postgraduate students and nonspecialist researchers from related areas
- to be a source of advanced teaching material for specialized seminars, courses and schools

Both monographs and multi-author volumes will be considered for publication. Edited volumes should, however, consist of a very limited number of contributions only. Proceedings will not be considered for LNP.

Volumes published in LNP are disseminated both in print and in electronic formats, the electronic archive being available at springerlink.com. The series content is indexed, abstracted and referenced by many abstracting and information services, bibliographic networks, subscription agencies, library networks, and consortia.

Proposals should be sent to a member of the Editorial Board, or directly to the managing editor at Springer:

Christian Caron
Springer Heidelberg
Physics Editorial Department I
Tiergartenstrasse 17
69121 Heidelberg/Germany
christian.caron@springer.com

Tilman Plehn

Lectures on LHC Physics

Springer

Tilman Plehn
Institut für Theoretische Physik
Universität Heidelberg
Philosophenweg 16
69120 Heidelberg
Germany
e-mail: plehn@uni-heidelberg.de

ISSN 0075-8450
ISBN 978-3-642-24039-3
DOI 10.1007/978-3-642-24040-9
Springer Heidelberg Dordrecht London New York

e-ISSN 1616-6361
e-ISBN 978-3-642-24040-9

Library of Congress Control Number: 2011938666

Cover design: eStudio Calamar, Berlin/Figueres

Printed on acid-free paper

Springer is part of Springer Science+Business Media (www.springer.com)

for Thomas Binoth

Preface

These notes are based on lecture courses at Heidelberg University in the Summer 2009 and in the Winter 2010/2011 and on many topical lectures for graduate students, written up in coffee shops around the world. Its target audience are students who know at least some field theory and are starting their diploma or master thesis; carefully studying these notes should put you into a position to start actual research in LHC physics.

One thing to keep in mind when reading is that the Heidelberg lecture course includes four hours a week without exercises. This means I calculate everything in detail on the blackboard. This is why the notes look the way they look. When reading these notes, take a break here and there, get a coffee and think about the physics behind the calculation you just followed.

The text is divided into three distinct parts:

- In the first part I focus on Higgs physics and collider searches. To understand what we are looking for I start with the most minimalistic and not renormalizable models describing massive gauge bosons. I then slowly advance to the usual fundamental Higgs scalar we are really searching for. At the end of this part what everybody should understand is the usual set of ATLAS or CMS graphs shown in Fig. 1.6, where many colored lines represent different search channels and their discovery potential. Many QCD issues affecting Higgs searches I will skip in the Higgs part and postpone to the…
- …QCD part. Here, I am taking at least one step back and study the theory which describes Higgs production and everything else at the LHC. Two core discussions shape this part: first, I derive the DGLAP equation by constructing the splitting kernels. This leads us to the parton shower and to the physical interpretation of resumming different logarithms in the QCD perturbation series. Second, there are two modern approaches combining parton shower and matrix element descriptions of jet radiation, which I introduce at least on the level of simplified models. Throughout the QCD discussion I avoid the more historically

interesting deep inelastic scattering process and instead rely on the Drell–Yan process or its inverted R ratio process for motivation and illustration.
- Finally, there are many aspects of LHC physics we need to take into account simulating LHC events. Some of them, like old fashioned and fat jets, helicity amplitudes, or missing transverse energy I cover in the third part. This part should expand in an earlier online version (arXiv:0910.4182), where I will keep these lecture notes up to date with actual discussions of LHC data.

What is almost entirely missing in this review is an introduction to searches for new physics completing the Standard Model of particle physics beyond the weak scale. Covering this topic appropriately would at least double the length of these notes. For the structure of such models and their signatures I instead refer to our review article Ref. [1] and in particular to its second chapter.

Last, but not least, the literature listed at the end of each part is not meant to cite original or relevant research papers. Instead, I collected a set of review papers or advanced lecture notes supplementing these lecture notes in different directions. Going through some of these mostly introductory papers will be instructive and fun once the basics have been covered by these lecture notes.

Heidelberg, June 2011 Tilman Plehn

Reference

1. Morrissey, D.E., Plehn, T., Tait, T.M.P.: New physics at the LHC. arXiv:0912.3259 [hep-ph]

Acknowledgments

The list of people I would like to thank is long and historically grown: starting with Peter Zerwas, Wim Beenakker, Roland Höpker, Michael Spira and Michael Krämer I would like to thank all the people who taught me theoretical physics and phenomenology over many years. This later on included Tao Han, Dieter Zeppenfeld and Uli Baur. Sorry, guys, but what you are holding in your hands is really the best I could do. Dirk Zerwas I would like to thank for continuous insight into experimental physics from our first semester at Heidelberg to the last day of writing these notes. Manfred Lindner I am grateful for his many comments on my black board notes when his class started right after mine. As a long-term collaborator I am missing Dave Rainwater who should have stayed in LHC physics.

The QCD part of this lecture is based on my 2008 TASI lectures, and I would like to thank Tom DeGrand and Ben Allanach for their comments on the TASI notes and Sally Dawson for her encouragement to put these notes on the web. For this longer version I am indebted to Steffen Schumann and Thomas Binoth for helping me out on many QCD questions over the past years, to Jan Pawlowski for uncountable cups of coffee on field theory and QCD, to Fabio Maltoni and Johan Alwall for teaching me jet merging, and to Michelangelo Mangano for many detailed comments. Alert readers like David Lopez-Val, Sebastian Bock, Florian Görtz or Michael Spannowsky followed my appeal to give me lists of typos, and Manuela Wirschke carefully read the notes removing language mistakes—thank you very much to everyone who helped make this writeup more correct and more readable.

Most importantly, I would like to thank all the people who have convinced me that theoretical physics even including QCD is fun—at least most of the time. Not surprisingly this includes many US colleagues from our TASI year 1997.

Contents

Chapter 1
Higgs Physics

Understanding the nature of electroweak symmetry breaking—or slightly more specifically deciphering the Higgs mechanism—is the main goal of the ATLAS and CMS experiments at the LHC. Observing some kind of Higgs boson and studying its properties involves many experimental and theoretical issues focused around understanding hadron collider data and QCD predictions to unprecedented precision. The latter will be the main topic of the second half of this lecture.

On the other hand, before we discuss the details of Higgs signatures, backgrounds, and related QCD aspects we should start with a discussion of electroweak symmetry breaking. Higgs physics at the LHC might well mean much more than just finding a light fundamental Higgs boson as predicted by the Standard Model of particle physics. Therefore, we prefer to follow an effective theory approach. This means we do not start by writing down the Higgs potential and deriving the measured gauge boson and fermion masses. Instead, we step by step include gauge boson and fermion masses in our gauge theories, see what this means for the field content, and show how we can embed this mechanism in a renormalizable fundamental gauge theory. Only this last step will lead us to the Standard Model and the Higgs potential.

1.1 Electroweak Symmetry Breaking

As a starting point, let us sketch the Standard Model Lagrangian and what we need to do to accommodate mass terms for gauge bosons and fermions. As a matter of fact, in a first step in Sect. 1.1.1 we will try to make our gauge bosons massive without introducing a physical Higgs field. Even for the $SU(2)$ gauge theory of the electroweak Standard Model we might get away without a fundamental Higgs boson, as we will show in Sect. 1.1.2. Only when we worry about quantum fluctuations of the relevant degrees of freedom we are led to the usual picture of the Higgs potential, the Higgs boson, and the symmetries related to its implementation.

T. Plehn, *Lectures on LHC Physics*, Lecture Notes in Physics 844,
DOI: 10.1007/978-3-642-24040-9_1, © Springer-Verlag Berlin Heidelberg 2012

1.1.1 Massive Photon

Even though this is not the physical problem we are interested in, we start by breaking electrodynamics, i.e. giving a mass to the (massless) photon of our usual locally $U(1)_Q$-symmetric Lagrangian. To its kinetic $F \cdot F$ term we would like to add a photon mass $m^2 A^2/2$, which we know is forbidden by the gauge symmetry. The way around is also adding an innocent looking real (uncharged) scalar field without a mass and without a coupling to the photon, but with a *scalar-photon mixing* term and a non-trivial gauge transformation. The result is called the Boulware–Gilbert model

$$\begin{aligned}\mathscr{L} &= -\frac{1}{4}F_{\mu\nu}F^{\mu\nu} + \frac{1}{2}e^2 f^2 A_\mu^2 + \frac{1}{2}(\partial\mu\phi)^2 - ef A_\mu \partial^\mu \phi \\ &= -\frac{1}{4}F_{\mu\nu}F^{\mu\nu} + \frac{1}{2}e^2 f^2 \left(A_\mu - \frac{1}{ef}\partial_\mu \phi\right)^2 ,\end{aligned} \tag{1.1}$$

where f is a common mass scale for the photon mass and the mixing. It ensures that all terms in the Lagrangian have mass dimension four—remembering that bosonic fields like A_μ and ϕ have mass dimension one. The additional factor e will become the usual electric charge, but at this stage it is a dimensionless number without any specific relevance in this interaction-less Lagrangian. Because all terms in Eq. 1.1 have mass dimension four our theory should be renormalizable.

We can define a simultaneous gauge transformation of both fields in the Lagrangian

$$A_\mu \longrightarrow A_\mu + \frac{1}{ef}\partial_\mu \chi \quad \phi \longrightarrow \phi + \chi , \tag{1.2}$$

under which the Lagrangian is indeed invariant: the kinetic term for the photon we leave untouched, so it will be gauge invariant just as it was before. The simultaneous gauge invariance is then defined to keep the second term in Eq. 1.1 invariant. If we now re-define the photon field as $B_\mu = A_\mu - \partial_\mu \phi/(ef)$ we need to compare the new and the old kinetic terms

$$\begin{aligned}F_{\mu\nu}\Big|_B &= \partial_\mu B_\nu - \partial_\nu B_\mu = \partial_\mu \left(A_\nu - \frac{1}{ef}\partial_\nu \phi\right) - \partial_\nu \left(A_\mu - \frac{1}{ef}\partial_\mu \phi\right) \\ &= \partial_\mu A_\nu - \partial_\nu A_\mu = F_{\mu\nu}\Big|_A ,\end{aligned} \tag{1.3}$$

and then rewrite the Lagrangian of Eq. 1.1 as

$$\boxed{\mathscr{L} = -\frac{1}{4}F_{\mu\nu}F^{\mu\nu} + \frac{1}{2}e^2 f^2 B_\mu^2 = -\frac{1}{4}F_{\mu\nu}F^{\mu\nu} + \frac{1}{2}m_B^2 B_\mu^2} . \tag{1.4}$$

This Lagrangian effectively describes a *massive photon field* B_μ, which has absorbed the real scalar ϕ as its additional longitudinal component. This is because a massless gauge boson A_μ has only two on-shell degrees of freedom, namely a left handed

and a right handed polarization, while the massive B_μ has an additional longitudinal polarization degree of freedom. Without any fundamental Higgs boson appearing, the massive photon has 'eaten' the real scalar field ϕ. Of course, the new field B_μ is not simply a photon with a mass term, because this is still forbidden by gauge invariance. Our way out is to split the massive photon field into the transverse degrees of freedom A_μ and the longitudinal mode ϕ with their different gauge transformations given by Eq. 1.2.

What kind of properties does this field ϕ need to have, so that we can use it to provide a photon mass? From the combined gauge transformation in Eq. 1.2 we immediately see that any additional purely scalar term in the Lagrangian, like a scalar potential $V(\phi)$, needs to be symmetric under the linear shift $\phi \to \phi + \chi$, not to spoil gauge invariance. This means that we cannot write down polynomial terms ϕ^n, like a mass or a self coupling of ϕ. An interaction term ϕAA would not be possible, either. Only *derivative interactions* proportional to $\partial\phi$ coupling to conserved currents are allowed. In that case we can absorb the shift by χ into a total derivative in the Lagrangian.

This example illustrates a few vital properties of *Nambu–Goldstone bosons* (NGB). Such massless physical states appear in many areas of physics and are described by *Goldstone's theorem*:

If a global symmetry group is spontaneously broken into a group of lower rank, its broken generators correspond to physical Goldstone modes. These fields transform non-linearly under the larger and linearly under the smaller group. They are massless and cannot form a potential, because the non-linear transformation only allows derivative terms in the Lagrangian. If the smaller symmetry is also broken, the NGBs become pseudo-NGBs and acquire a mass of the size of this hard-breaking term.

In the special case that the spontaneously broken symmetry is a gauge symmetry and its breaking induces gauge boson masses, these massive degrees of freedom are made out of 'eaten' Goldstone modes. The gauge boson mass is given by the vacuum expectation value (VEV) breaking the larger symmetry.

1.1.2 Standard Model Doublets

One of the complications of the Standard Model is its $SU(2)$ doublet structure. In the last section we have chosen not to introduce a charged $SU(2)$ doublet, which is why there are no degrees of freedom left after the photon gets its mass. This means that our toy model is not going to be well suited to provide the three degrees of freedom needed to make $SU(2)$ gauge bosons massive. What it illustrates is only how by introducing a neutral scalar particle without an interaction but with a mixing term we make gauge bosons heavy, in spite of gauge invariance.

Fermion fields have mass dimension 3/2, so we know how mass and interaction terms in the renormalizable dimension-4 Lagrangian have to look. For example, the interaction of fermions with gauge bosons is most easily written in terms of *covariant derivatives*. The terms

$$\mathscr{L}_{D4} = \overline{Q}_L i\not{D} Q_L + \overline{Q}_R i\not{D} Q_R + \overline{L}_L i\not{D} L_L + \overline{L}_R i\not{D} L_R - \frac{1}{4} F_{\mu\nu} F^{\mu\nu} \cdots \tag{1.5}$$

describe electromagnetic interactions introducing a covariant derivative $D_\mu = \partial_\mu + ieqA_\mu$ with the photon field also appearing in the field strength tensor $F_{\mu\nu} = \partial_\mu A_\nu - \partial_\nu A_\mu$. The same form works for the weak $SU(2)$ interactions, except that the weak interaction knows about the chirality of the fermion fields, so we have to distinguish $\not{D}_L$ and $\not{D}_R$. The covariant derivatives we write in terms of the $SU(2)$ basis matrices $\tau_{1,2,3}$ or $\tau_{+,-,3}$, with $\tau_\pm = (\tau_1 \pm i\tau_2)/2$.

$$\begin{aligned}
D_{L\mu} &= \partial_\mu + ig' \left(q - \frac{\tau_3}{2}\right) B_\mu + igW_\mu^a \frac{\tau_a}{2} \\
&= \partial_\mu + ieqA_\mu + ig_Z \left(-qs_w^2 + \frac{\tau_3}{2}\right) Z_\mu + i\frac{g}{\sqrt{2}} \left(\tau_+ W_\mu^+ + \tau_- W_\mu^-\right) \\
D_{R\mu} &= D_{L\mu}\Big|_{\tau=0} \\
\tau_+ &= \begin{pmatrix} 0 & 1 \\ 0 & 0 \end{pmatrix} \qquad \tau_- = \begin{pmatrix} 0 & 0 \\ 1 & 0 \end{pmatrix} \\
\tau_1 &= \begin{pmatrix} 0 & 1 \\ 1 & 0 \end{pmatrix} \qquad \tau_2 = \begin{pmatrix} 0 & -i \\ i & 0 \end{pmatrix} \qquad \tau_3 = \begin{pmatrix} 1 & 0 \\ 0 & -1 \end{pmatrix},
\end{aligned} \tag{1.6}$$

The fields B_μ and W_μ^a are the new gauge bosons. In the second line we re-write the covariant derivative in the mass eigenstates, i.e. the photon A_μ and the Z boson. At this level the two weak couplings g and g_Z do not necessarily coincide, but we will get back to this issue in Sect. 1.1.5.

Before we generalize the Boulware–Gilbert model to the weak gauge symmetry of the Standard Model it is instructive to review the form of the mass term for massive gauge bosons following from Eq. 1.6. In particular, there will appear a relative factor two between the two bases of the Pauli matrices, i.e. in terms of $W^{1,2}$ and $W^\pm$, which often causes confusion.

Products of the *Pauli matrices* $\tau_{1,2,3}$ satisfy the relation $\tau_i \tau_j = \delta_{ij} + i\varepsilon_{ijk}\tau_k$ or the commutator relation $[\tau_i, \tau_j] = 2i\varepsilon_{ijk}\tau_k$. Summing over indices we see that

$$\begin{aligned}
\sum_{i,j} \tau_i \tau_j &= \sum_{i,j} \left(\delta^{ij} + i\varepsilon^{ijk}\tau_k\right) = \sum \delta^{ij} + i \sum_{i \neq j} \varepsilon^{ijk}\tau_k \\
&= \sum \delta^{ij} + i \sum_{i<j} \left(\varepsilon^{ijk} + \varepsilon^{jik}\right) \tau_k \\
&= \sum \delta^{ij}.
\end{aligned} \tag{1.7}$$

The basis of three Pauli matrices we can write in terms of $\tau_{1,2,3}$ as well as in terms of $\tau_{+,-,3}$. The latter form of the generators corresponds to the two charged and one neutral vector bosons. While the usual basis is written in terms of complex numbers, the second set of generators reflects the fact that for $SU(2)$ as for any $SU(N)$ group

we can find a set of real generators of the adjoint representation. When we switch between the two bases we only have to make sure we get the factors $\sqrt{2}$ right

$$\begin{aligned}\sqrt{2}\left(\tau_+ W_\mu^+ + \tau_- W_\mu^-\right) &= \sqrt{2}\begin{pmatrix} 0 & W_\mu^+ \\ 0 & 0 \end{pmatrix} + \sqrt{2}\begin{pmatrix} 0 & 0 \\ W_\mu^- & 0 \end{pmatrix} \\ &\stackrel{!}{=} \tau_1 W_\mu^1 + \tau_2 W_\mu^2 = \begin{pmatrix} 0 & W_\mu^1 \\ W_\mu^1 & 0 \end{pmatrix} + \begin{pmatrix} 0 & -i W_\mu^2 \\ i W_\mu^2 & 0 \end{pmatrix} \\ \Leftrightarrow \qquad W_\mu^\pm &= \frac{1}{\sqrt{2}}\left(W_\mu^1 \mp i W_\mu^2\right). \end{aligned} \tag{1.8}$$

To track these numbers of two in the definitions of the weak gauge field we have a close look at is the dimension-2 mass term for charged and neutral gauge bosons

$$\mathscr{L}_{D2} = \frac{m_W^2}{2}\left(W^{1,\mu} W_\mu^1 + W^{2,\mu} W_\mu^2\right) + \frac{m_Z^2}{2} Z^\mu Z_\mu = m_W^2 W^{+,\mu} W_\mu^- + \frac{m_Z^2}{2} Z^\mu Z_\mu. \tag{1.9}$$

The relative factor two in front of the W mass corresponds to the factors $1/\sqrt{2}$ in the $SU(2)$ generators $\tau_\pm$.

Of course, in the complete Standard Model Lagrangian there are many additional terms, e.g. kinetic terms of all kinds, but they do not affect our discussion of $U(1)_Y$ and $SU(2)_L$ gauge invariance.

Guessing the form of the fermion masses the one thing we have to ensure is that we combine the left handed and right handed doublets (Q_L, L_L) and singlets (Q_R, L_R) properly:

$$\mathscr{L}_{D3} = -\overline{Q}_L m_Q Q_R - \overline{L}_L m_L L_R + \cdots \tag{1.10}$$

Following our labeling scheme by mass dimension fermion masses will be included as $\mathscr{L}_{D3}$. *Dirac mass* terms simply link $SU(2)$ doublet fields for leptons and quarks with right handed singlets and give mass to all fermions in the Standard Model. This helicity structure of mass terms we can easily derive by introducing left handed and right handed projectors

$$\psi_L = \frac{\mathbb{1} - \gamma_5}{2}\psi \equiv \mathbb{P}_L \psi \qquad \psi_R = \frac{\mathbb{1} + \gamma_5}{2}\psi \equiv \mathbb{P}_R \psi, \tag{1.11}$$

where ψ is a generic Dirac spinor and $\mathbb{P}_{L,R}$ are projectors in this 4×4 Dirac space. At this stage we do not need the explicit form of the gamma matrices which we will introduce in Eq. (2.106). The mass term for a Dirac fermion reads

$$\begin{aligned}\overline{\psi}\mathbb{1}\psi &= \overline{\psi}\left(\mathbb{P}_L + \mathbb{P}_R\right)\psi \\ &= \overline{\psi}\left(\mathbb{P}_L^2 + \mathbb{P}_R^2\right)\psi \\ &= \psi^\dagger \gamma_0 \left(\mathbb{P}_L^2 + \mathbb{P}_R^2\right)\psi \qquad \text{with} \quad \overline{\psi} = \psi^\dagger \gamma^0 \\ &= \psi^\dagger \left(\mathbb{P}_R \gamma^0 \mathbb{P}_L + \mathbb{P}_L \gamma^0 \mathbb{P}_R\right)\psi \qquad \text{with} \quad \{\gamma_5, \gamma_\mu\} = 0 \end{aligned}$$

$$
\begin{aligned}
&= (\mathbb{P}_R\psi)^\dagger\gamma^0(\mathbb{P}_L\psi) + (\mathbb{P}_L\psi)^\dagger\gamma^0(\mathbb{P}_R\psi) \qquad \text{with} \quad \gamma_5^\dagger = \gamma_5, \mathbb{P}_{L,R}^\dagger = \mathbb{P}_{L,R} \\
&= (\overline{\mathbb{P}_R\psi})\mathbb{1}(\mathbb{P}_L\psi) + (\overline{\mathbb{P}_L\psi})\mathbb{1}(\mathbb{P}_R\psi) \\
&= \overline{\psi}_R\mathbb{1}\psi_L + \overline{\psi}_L\mathbb{1}\psi_R,
\end{aligned}
\tag{1.12}
$$

while the kinetic term stays diagonal

$$
\begin{aligned}
\overline{\psi}\partial\!\!\!/\psi &= \overline{\psi}i\partial\!\!\!/\left(\mathbb{P}_L^2 + \mathbb{P}_R^2\right)\psi \\
&= \overline{\psi}\left(\mathbb{P}_R\partial\!\!\!/\mathbb{P}_L + \mathbb{P}_L\partial\!\!\!/\mathbb{P}_R\right)\psi \\
&= (\overline{\mathbb{P}_L\psi})\partial\!\!\!/(\mathbb{P}_L\psi) + (\overline{\mathbb{P}_R\psi})\partial\!\!\!/(\mathbb{P}_R\psi) \\
&= \overline{\psi}_L\partial\!\!\!/\psi_L + \overline{\psi}_R\partial\!\!\!/\psi_R.
\end{aligned}
\tag{1.13}
$$

In general, these mass terms can be matrices in generation space, which implies that we might have to rotate the fermion fields from an interaction basis into the mass basis where these mass matrices are diagonal. Flavor physics dealing with such 3×3 mass matrices is its own field of physics with its own reviews and lecture notes, so we will omit this complication here. For our discussion of electroweak symmetry breaking it is sufficient to study one fermion generation at a time.

The well-known problem with the mass terms in Eq. 1.10 is that they are not gauge invariant. To understand this issue of *fermion masses* we check the local weak $SU(2)_L$ transformation

$$
U(x) = \exp\left(-i\alpha^a(x)\frac{\tau_a}{2}\right) \equiv e^{-i(\alpha\cdot\tau)/2}, \tag{1.14}
$$

which only transforms the left-handed fermion fields and leaves the right-handed fields untouched

$$
\begin{aligned}
L_L &\xrightarrow{U} U L_L \qquad & Q_L &\xrightarrow{U} U Q_L \\
L_R &\xrightarrow{U} L_R \qquad & Q_R &\xrightarrow{U} Q_R.
\end{aligned}
\tag{1.15}
$$

It is obvious that there is no way we can make left-right mixing fermion mass terms as shown in Eq. 1.10 invariant under this left handed $SU(2)$ gauge transformation, where one of the fermion field picks up a factor U and the other is unchanged,

$$
\overline{Q}_L m_Q Q_R \xrightarrow{U} \overline{Q}_L U^{-1} m_Q Q_R \neq \overline{Q}_L m_Q Q_R. \tag{1.16}
$$

In analogy to the massive photon case, to write a gauge-invariant Lagrangian for massive fermions we have to add something else to our minimal Standard Model Lagrangian. Note that this addition does not have to be a fundamental scalar Higgs field, dependent on how picky we are with the properties of our new Lagrangian beyond the issue of gauge invariance.

To see what we need to add let us also look at the local $U(1)$ transformations involved. We start with a slightly complicated-looking way of writing the abelian *hypercharge* $U(1)_Y$ and *electric charge* $U(1)_Q$ transformations, making it more obvious how they mix with the neutral component of $SU(2)$ to give the electric charge.

Let us start with the neutral component of the $SU(2)$ transformation, i.e. $V = \exp(i\beta\tau_3/2)$. Acting on a field with an $SU(2)$ charge this it not a usual $U(1)$ transformation. What we can do is combine it with another, appropriately chosen transformation. This hypercharge transformation is proportional to the unit matrix and hence commutes with all other matrices

$$\begin{aligned}\exp(i\beta q)\, V^\dagger &= \exp(i\beta q)\, \exp\left(-\frac{i}{2}\beta\tau_3\right) \\ &= \exp\left(i\beta\frac{y\mathbb{1}+\tau_3}{2}\right)\, \exp\left(-\frac{i}{2}\beta\tau_3\right) \qquad \text{with} \quad \boxed{q \equiv \frac{y\mathbb{1}+\tau_3}{2}} \\ &= \exp\left(i\frac{\beta}{2}y\mathbb{1}\right),\end{aligned} \tag{1.17}$$

The hypercharge values are $y_Q = 1/3$ and $y_L = -1$. This relation between the charges is called the Gell–Mann–Nishijima formula. Acting on a left handed field the factor τ_3 above is replaced by its eigenvalue ± 1 for up-type and down-type fermions. The $U(1)_Y$ charges or quantum numbers y are the quark and lepton hypercharges of the Standard Model. As required by the above argument, properly combined with the isospin they give the correct electric charges $q_{Q,L}$. Since τ_3 and the unit matrix commute with each other the combined exponentials have no additional factor a la Baker–Campbell–Hausdorff $e^A e^B = e^{A+B} e^{[A,B]/2}$. In analogy to Eq. 1.15 left handed and right handed quark and lepton fields transform under this $U(1)_Y$ symmetry as

$$\begin{aligned} L_L &\to \exp(i\beta q_L)\, V^\dagger L_L = \exp\left(i\frac{\beta}{2}y_L\mathbb{1}\right) L_L \\ Q_L &\to \exp\left(i\beta q_Q\right) V^\dagger Q_L = \exp\left(i\frac{\beta}{2}y_Q\mathbb{1}\right) Q_L \\ L_R &\to \exp(i\beta q_L)\, L_R \\ Q_R &\to \exp\left(i\beta q_Q\right) Q_R. \end{aligned} \tag{1.18}$$

Under a combined $SU(2)_L$ and $U(1)_Y$ transformation the left handed fermions see the hypercharge, while the right handed fermions only see the electric charge. Just as for the $SU(2)$ transformation U we do not even have to compute anything to see that such different transformations of the left handed and right handed fermion fields do not allow for a Dirac mass term.

1.1.3 Sigma Model

One way of solving this problem which at this point really looks like a cheap trick is to introduce an additional field $\Sigma(x)$. This field will in some way play the role of the real scalar field we used for the photon mass generation. Its physical properties will become clear piece by piece from the way it appears in the Lagrangian and from the required gauge invariance. The equation of motion for the Σ field will also have to follow from the way we introduce it in the Lagrangian.

Following the last section, we first introduce Σ into the *fermion mass* term to see what it takes to make this mass term gauge invariant under the weak $SU(2)$ transformation

$$\begin{aligned} &\overline{Q}_L \Sigma m_Q Q_R \xrightarrow{U} \overline{Q}_L U^{-1} \Sigma^{(U)} m_Q Q_R \stackrel{!}{=} \overline{Q}_L \Sigma m_Q Q_R \\ &\quad \Leftrightarrow \qquad \Sigma \to \Sigma^{(U)} = U \Sigma. \end{aligned} \tag{1.19}$$

If the result should be a dimension-4 Lagrangian the mass dimension of Σ has to be $m^0 = 1$. The same we can do for the $U(1)_Y$ transformation V

$$\begin{aligned} \overline{Q}_L \Sigma m_Q Q_R \xrightarrow{V} &\overline{Q}_L \exp\left(-i\frac{\beta}{2} y \mathbb{1}\right) \Sigma^{(V)} m_Q \exp\left(i\beta q\right) Q_R \\ &= \overline{Q}_L \Sigma^{(V)} \exp\left(-i\frac{\beta}{2} y \mathbb{1}\right) \exp\left(i\beta q\right) m_Q Q_R \\ &= \overline{Q}_L \Sigma^{(V)} V m_Q Q_R \\ &\stackrel{!}{=} \overline{Q}_L \Sigma m_Q Q_R \qquad \Leftrightarrow \qquad \Sigma \to \Sigma^{(V)} = \Sigma V^\dagger. \end{aligned} \tag{1.20}$$

where in the second line we use the fact that $\exp\left(i\beta y \mathbb{1}/2\right)$ always commutes. Together with Eq. 1.19 this gives us the *transformation property* we need

$$\boxed{\Sigma \to U \Sigma V^\dagger}. \tag{1.21}$$

For any Σ with this property the $\mathscr{L}_{D3}$ part of the Lagrangian has the required $U(1)_Y \times SU(2)_L$ symmetry, independent of what this field really means. From the way it transforms we see that Σ is a 2×2 matrix with mass dimension zero. In other words, including a Σ field in the fermion mass terms gives a $U(1)_Y$ and $SU(2)_L$-invariant Lagrangian, without saying anything about possible representations of Σ in terms of physical fields

$$\boxed{\mathscr{L}_{D3} = -\overline{Q}_L \Sigma m_Q Q_R - \overline{L}_L \Sigma m_L L_R + \text{h.c.} + \cdots} \tag{1.22}$$

In the second step, we worry about the *gauge boson masses*, starting with the left handed covariant derivative

$$D_{L\mu} = \partial_\mu + ig'\left(q - \frac{\tau_3}{2}\right) B_\mu + igW_\mu^a \frac{\tau_a}{2} = \partial_\mu + ig'\frac{y}{2} B_\mu + igW_\mu^a \frac{\tau_a}{2}. \tag{1.23}$$

Instead of deriving the gauge transformation of Σ let us start with a well-chosen ansatz and work backwards step by step, as to check that we indeed arrive at the correct masses.

First, we consistently require that the covariant derivative acting on the Σ field in the gauge-symmetric Lagrangian reads

$$D_\mu \Sigma = \partial_\mu \Sigma - i g' \Sigma B_\mu \frac{\tau_3}{2} + i g W_\mu^a \frac{\tau_a}{2} \Sigma. \tag{1.24}$$

If we introduce the abbreviations $V_\mu \equiv \Sigma (D_\mu \Sigma)^\dagger$ and $T \equiv \Sigma \tau_3 \Sigma^\dagger$ we claim we can write the gauge boson mass terms as

$$\boxed{\mathscr{L}_{D2} = -\frac{v^2}{4} \text{Tr}[V_\mu V^\mu] + \Delta\rho \frac{v^2}{8} \text{Tr}[T V_\mu] \, \text{Tr}[T V^\mu]}. \tag{1.25}$$

The trace acts on the 2×2 $SU(2)$ matrices. The parameter $\Delta\rho$ is conventional and will be the focus of Sect. 1.1.5. What we need to show is that this form is gauge invariant and gives the correct gauge boson masses.

Another question is what additional terms of mass dimension four we can write down using the dimensionless field Σ and which are gauge invariant. Our first attempt of a building block

$$\Sigma^\dagger \Sigma \overset{U,V}{\to} (U \Sigma V^\dagger)^\dagger (U \Sigma V^\dagger) = V \Sigma^\dagger U^\dagger U \Sigma V^\dagger = V \Sigma^\dagger \Sigma V^\dagger \neq \Sigma^\dagger \Sigma \tag{1.26}$$

is forbidden by gauge invariance according to the $SU(2)$ transformation of the sigma field, Eq. 1.20. On the other hand, a circularly symmetric trace $\text{Tr}(\Sigma^\dagger \Sigma) \to \text{Tr}(V \Sigma^\dagger \Sigma V^\dagger) = \text{Tr}(\Sigma^\dagger \Sigma)$ changes this into a gauge invariant combination, which allows for the additional *potential terms*, meaning terms with no derivatives

$$\boxed{\mathscr{L}_\Sigma = -\frac{\mu^2 v^2}{4} \text{Tr}(\Sigma^\dagger \Sigma) - \frac{\lambda v^4}{16} \left(\text{Tr}(\Sigma^\dagger \Sigma)\right)^2 + \cdots}, \tag{1.27}$$

with properly chosen prefactors μ, v, λ. This fourth term finalizes our construction of the relevant weak Lagrangian

$$\mathscr{L} = \mathscr{L}_{D2} + \mathscr{L}_{D3} + \mathscr{L}_{D4} + \mathscr{L}_\Sigma, \tag{1.28}$$

organized by mass dimension.

As rule of thumb we will later notice that once we express this potential in terms of the usual Higgs doublet $|\phi|^2$, the prefactors will just be μ and λ. The parameter μ and the factor v appearing with every power of Σ have mass dimension one, while λ has mass dimension zero. Higher dimensional terms in a dimension-4 Lagrangian are possible as long as we limit ourselves to powers of $\text{Tr}(\Sigma^\dagger \Sigma)$. However, they lead to higher powers in v which we will see makes them higher-dimensional operators in our complete quantum theory.

To check for the correct masses in the Standard Model we start with $\mathrm{Tr}(\Sigma^\dagger \Sigma)$ and assume it acquires a finite (expectation) value after we properly deal with Σ. The definitely simplest way to achieve this is to assume

$$\boxed{\Sigma(x) = \mathbb{1}}\,. \tag{1.29}$$

This choice is called *unitary gauge*. It looks like a dirty trick to first introduce $\Sigma(x) = \mathbb{1}$ and then use this field for a gauge invariant implementation of gauge boson masses. Clearly, a constant does not exhibit the correct transformation property under the U and V symmetries, but we can always work in a specific gauge and only later check the physical predictions for gauge invariance. Even the way the sigma field breaks our gauge symmetry we can schematically see from

$$\Sigma \to U \Sigma V^\dagger = U \mathbb{1} V^\dagger = U V^\dagger \stackrel{!}{=} \mathbb{1}, \tag{1.30}$$

which requires $U = V$ to be the remaining $U(1)$ gauge symmetry after including the Σ field. Certainly, $\Sigma = \mathbb{1}$ gives the correct fermion masses in $\mathscr{L}_{D3}$ and makes the potential $\mathscr{L}_\Sigma$ an irrelevant constant. What we need to check is $\mathscr{L}_{D2}$ which is supposed to reproduce the correct gauge boson masses. Using the covariant derivative from Eq. 1.24 acting on a constant field we can compute the auxiliary field V_μ in unitary gauge

$$\begin{aligned} V_\mu = \Sigma (D_\mu \Sigma)^\dagger &= -ig W_\mu^a \frac{\tau_a}{2} + ig' B_\mu \frac{\tau_3}{2} \\ &= -ig W_\mu^+ \frac{\tau_+}{\sqrt{2}} - ig W_\mu^- \frac{\tau_-}{\sqrt{2}} - ig W_\mu^3 \frac{\tau_3}{2} + ig' B_\mu \frac{\tau_3}{2} \\ &= -i \frac{g}{\sqrt{2}} \left(W_\mu^+ \tau_+ + W_\mu^- \tau_- \right) - i g_Z Z_\mu \frac{\tau_3}{2} \end{aligned} \tag{1.31}$$

with $Z_\mu = c_w W_\mu^3 - s_w B_\mu$ and the two coupling constants $g_Z = g/c_w$ and $g' = g s_w / c_w$. What is not obvious from this argument is that we can actually write the ratio g'/g in terms of a rotation angle, which implicitly assumes that we can rotate the B and W^3 fields into the physical mass-eigenstate photon and Z fields

$$\begin{pmatrix} A_\mu \\ Z_\mu \end{pmatrix} = \begin{pmatrix} c_w & s_w \\ -s_w & c_w \end{pmatrix} \begin{pmatrix} B_\mu \\ W_\mu^3 \end{pmatrix}. \tag{1.32}$$

The result in Eq. 1.31 gives us the first of the two terms in the gauge boson mass Lagrangian $\mathscr{L}_{D2}$

$$\begin{aligned} \mathrm{Tr}[V_\mu V^\mu] &= -2 \frac{g^2}{2} W_\mu^+ W^{-\mu} \mathrm{Tr}(\tau_+ \tau_-) - \frac{g_Z^2}{4} Z_\mu Z^\mu \mathrm{Tr}(\tau_3^2) \\ &= -g^2 W_\mu^+ W^{-\mu} - \frac{g_Z^2}{2} Z_\mu Z^\mu, \end{aligned} \tag{1.33}$$

using $\tau_\pm^2 = 0$, $\mathrm{Tr}(\tau_3\tau_\pm) = 0$, $\mathrm{Tr}\tau_\pm\tau_\mp = 1$, and $\mathrm{Tr}(\tau_3^2) = \mathrm{Tr}\mathbb{1} = 2$. The second mass term in $\mathscr{L}_{D2}$ proportional to $\Delta\rho$ is equally simple in unitary gauge

$$\begin{aligned} T &= \Sigma\tau_3\Sigma^\dagger = \tau_3 \\ \Rightarrow \quad \mathrm{Tr}(TV_\mu) &= \mathrm{Tr}\left(-ig_Z Z_\mu \frac{\tau_3^2}{2}\right) = -ig_Z Z_\mu \\ \Rightarrow \ \mathrm{Tr}(TV_\mu)\,\mathrm{Tr}(TV^\mu) &= -g_Z^2 Z_\mu Z^\mu . \end{aligned} \tag{1.34}$$

Inserting both terms into Eq. 1.25 yields the complete gauge boson mass term

$$\begin{aligned} \mathscr{L}_{D2} &= -\frac{v^2}{4}\left(-g^2 W_\mu^+ W^{-\mu} - \frac{g_Z^2}{2} Z_\mu Z^\mu\right) + \Delta\rho\frac{v^2}{8}\left(-g_Z^2 Z_\mu Z^\mu\right) \\ &= \frac{v^2 g^2}{4} W_\mu^+ W^{-\mu} + \frac{v^2 g_Z^2}{8} Z_\mu Z^\mu - \Delta\rho\frac{v^2 g_Z^2}{8} Z_\mu Z^\mu \\ &= \frac{v^2 g^2}{4} W_\mu^+ W^{-\mu} + \frac{v^2 g_Z^2}{8}(1-\Delta\rho)\, Z_\mu Z^\mu . \end{aligned} \tag{1.35}$$

Identifying the masses with the form given in Eq. 1.9 and assuming universality of *neutral and charged current* interactions ($\Delta\rho = 0$) we find

$$\boxed{m_W = \frac{gv}{2}} \qquad \boxed{m_Z = \sqrt{1-\Delta\rho}\,\frac{g_Z v}{2} \overset{\Delta\rho=0}{=} \frac{g_Z v}{2} = \frac{gv}{2c_w}} \tag{1.36}$$

The role of a possible additional and unwanted Z-mass contribution $\Delta\rho$ we will discuss in Sect. 1.1.5 on custodial symmetry. Given that we know the heavy gauge boson masses ($m_W \sim 80\,\mathrm{GeV}$) and the weak coupling ($g \sim 0.7$) from experiment, these relations experimentally tell us $v \sim 246\,\mathrm{GeV}$.

Let us just recapitulate what we did until now—using this Σ field and its finite constant value $\Sigma = \mathbb{1}$ in unitary gauge we have made the fermions and electroweak gauge boson massive. Choosing this constant finite field value for Σ is not the only and not the minimal assumption needed to make the gauge bosons heavy, but it leads to the most compact Lagrangian. From the photon mass example, however, we know that there must be more to this mechanism. We should for example be able to see the additional degrees of freedom of the longitudinal gauge boson modes if we step away from unitary gauge.

If a finite expectation value of the terms in the potential $\mathscr{L}_\Sigma$ should be linked to electroweak symmetry breaking and the gauge boson masses we can guess that the *minimal assumption* leading to finite gauge boson masses is $\langle \mathrm{Tr}(\Sigma^\dagger(x)\Sigma(x))\rangle \neq 0$ in the vacuum. Every parameterization of Σ with this property will lead to the same massive gauge bosons, so they are all physically equivalent—as they should be given that they are only different gauge choices. In the canonical normalization we write

$$\boxed{\frac{1}{2}\,\langle \mathrm{Tr}(\Sigma^\dagger(x)\Sigma(x))\rangle = 1} \qquad \forall x, \tag{1.37}$$

which instead of our previous $\Sigma(x) = \mathbb{1}$ we can also fulfill through

$$\Sigma^\dagger(x)\Sigma(x) = \mathbb{1} \qquad \forall x. \tag{1.38}$$

This means that $\Sigma(x)$ is a unitary matrix which like any 2×2 unitary matrix can be expressed in terms of the Pauli matrices. Even though this solution still forbids fluctuations which in the original condition on the expectation value only vanish on average, in contrast to $\Sigma(x) = \mathbb{1}$ it allows a non-trivial x dependence. The unitary matrix can be parameterized as

$$\boxed{\Sigma(x) = \exp\left(-\frac{i}{v}\vec{w}(x)\right)} \qquad \text{with} \quad \vec{w}(x) = w_a(x)\tau_a, \tag{1.39}$$

where $\vec{w}(x)$ has mass dimension one which is absorbed by the mass scale v. These fields are a set of scalar *Nambu–Goldstone modes*. From the photon mass example for Goldstone's theorem we know that they will become the missing degrees of freedom for the three now massive gauge bosons $W^\pm$ and Z. The normalization scale v fixes the relevant energy scale of our Lagrangian. Because the relation between Σ and $\vec{w}$ is not linear, this is referred to as a *non-linear representation* of the Σ field. Using the commutation properties of the Pauli matrices we can expand Σ as

$$\begin{aligned}
\Sigma &= \mathbb{1} - \frac{i}{v}\vec{w} + \frac{1}{2}\frac{(-1)}{v^2} w_a\tau_a w_b\tau_b + \frac{1}{6}\frac{i}{v^3} w_a\tau_a w_b\tau_b w_c\tau_c + \mathcal{O}(w^4) \\
&= \mathbb{1} - \frac{i}{v}\vec{w} - \frac{1}{2v^2} w_a w_a \mathbb{1} + \frac{i}{6v^3} w_a w_a \vec{w} + \mathcal{O}(w^4) \qquad \text{using Eq. 1.7} \\
&= \left(1 - \frac{1}{2v^2} w_a w_a + \mathcal{O}(w^4)\right)\mathbb{1} - \frac{i}{v}\left(1 - \frac{1}{6v^2} w_a w_a + \mathcal{O}(w^4)\right)\vec{w}.
\end{aligned} \tag{1.40}$$

From this expression we can for example read off Feynman rules for the longitudinal gauge fields $\vec{w}$, which we will use later.

Yet another way of parameterizing the unitary field Σ in terms of the Pauli matrices is the properly normalized expression

$$\Sigma(x) = \frac{1}{\sqrt{1 + \frac{w_a w_a}{v^2}}}\left(1 - \frac{i}{v}\vec{w}(x)\right). \tag{1.41}$$

The different ways of writing the Σ field in terms of the Pauli matrices cannot have any impact on the physics.

Before we move on and introduce a physical Higgs boson we briefly discuss different gauge choices and the appearance of Goldstone modes. If we break $SU(2)_L \times U(1)_Y \to U(1)_Q$ we expect three Goldstone bosons which become part of the weak gauge bosons and promote those from massless gauge bosons (with

two degrees of freedom each) to massive gauge bosons (with three degrees of freedom each). This is the point of view of the unitary gauge, in which we never see Goldstone modes.

In the general $(R-\xi)$ gauge we can actually see these Goldstone modes appear in the *gauge boson propagators*

$$\begin{aligned}\Delta^{\mu\nu}_{VV}(q) &= \frac{-i}{q^2-m_V^2+i\varepsilon}\left[g^{\mu\nu}+(\xi-1)\frac{q^\mu q^\nu}{q^2-\xi m_V^2}\right]\\ &= \begin{cases}\dfrac{-i}{q^2-m_V^2+i\varepsilon}\left[g^{\mu\nu}-\dfrac{q^\mu q^\nu}{m_V^2}\right] & \text{unitary gauge } \xi\to\infty\\ \dfrac{-i}{q^2-m_V^2+i\varepsilon}\,g^{\mu\nu} & \text{Feynman gauge } \xi=1\\ \dfrac{-i}{q^2-m_V^2+i\varepsilon}\left[g^{\mu\nu}-\dfrac{q^\mu q^\nu}{q^2}\right] & \text{Landau gauge } \xi=0\end{cases}\end{aligned} \tag{1.42}$$

Obviously, these gauge choices are physically equivalent. However, something has to compensate, for example, for the fact that in Feynman gauge the whole Goldstone term vanishes and the polarization sum looks like a massless gauge bosons, while in unitary gauge we can see the effect of these modes directly. The key is the Goldstone propagator, i.e. additional propagating scalar degrees of freedom

$$\Delta_{VV}(q^2)=\frac{-i}{q^2-\xi m_V^2+i\varepsilon}, \tag{1.43}$$

for both heavy gauge bosons ($V=Z,W^+$). The Goldstone mass $\sqrt{\xi}m_V$ depends on the gauge: in unitary gauge the infinitely heavy Goldstones do not propagate ($\Delta_{VV}(q^2)\to 0$), while in Feynman gauge and in Landau gauge we have to include them as particles. From the form of the Goldstone propagators we can guess that they will indeed cancel the second term of the gauge boson propagators.

These different gauges have different Feynman rules and Green's functions, even a different particle content, so for a given problem one or the other might be the most efficient to use in computations or proofs. For example, the proof of renormalizability was first formulated in unitary gauge. Loop calculations might be more efficient in Feynman gauge, because of the simplified propagator structure, while many QCD processes benefit from an explicit projection on the physical external gluons. Tree-level helicity amplitudes are usually computed in unitary gauge, etc.

1.1.4 Higgs Boson

At this stage we have defined a perfectly fine electroweak theory with massive gauge bosons. All we need is a finite vacuum expectation value for Σ, which means this field *spontaneously breaks* the electroweak symmetry not by explicit terms in the

Lagrangian but via the vacuum and relying on an unknown origin of this finite VEV. If we are interested in physics at or above the electroweak energy scale $E \sim v$ some kind of ultraviolet completion of this Σ model should tell us what the Σ field's properties as a quantum object are.

If we consider our Σ model itself the fundamental theory and promote the Σ field to a quantum field like all other Standard Model fields, we need to allow for *quantum fluctuations* of $\mathrm{Tr}(\Sigma^\dagger \Sigma)$ around the vacuum value $\mathrm{Tr}\Sigma^\dagger \Sigma = 2$. We can parameterize these new degrees of freedom as a real scalar field

$$\boxed{\Sigma \to \left(1 + \frac{H}{v}\right) \Sigma}\,, \tag{1.44}$$

as long as this physical field H has a vanishing vacuum expectation value and therefore

$$\frac{1}{2} \langle \mathrm{Tr}(\Sigma^\dagger \Sigma) \rangle = \left\langle \left(1 + \frac{H}{v}\right)^2 \right\rangle = 1 \tag{1.45}$$

The factor in front of the fluctuation term H/v is not fixed until we properly define the physical Higgs field and make sure that its kinetic term does not come with an unexpected prefactor different from unity. On the other hand, if we assume that the neutral Goldstone mode w_3 has the correct normalization, the Higgs field should be added to Σ such that it matches this Goldstone, as we will see later in this section and then in more detail in Sect. 1.2.

The non-dynamical limit of this Higgs ansatz is indeed our sigma model in unitary gauge $\Sigma^\dagger \Sigma = \mathbb{1}$, equivalent to $H = 0$. Interpreting the fluctuations around the non-trivial vacuum as a *physical Higgs field* is the usual Higgs mechanism, named after one of The University of Edinburgh's most famous sons.

For this new Higgs field $\mathscr{L}_\Sigma$ defines a potential following the original form Eq. 1.27

$$\mathscr{L}_\Sigma = -\frac{\mu^2 v^2}{2} \left(1 + \frac{H}{v}\right)^2 - \frac{\lambda v^4}{4} \left(1 + \frac{H}{v}\right)^4 + \cdots \tag{1.46}$$

The dots stand for higher-dimensional terms which might or might not be there. We will have a look at them in Sect. 1.2.1. Some of them are not forbidden by any symmetry, but they are not realized at tree level in the Standard Model either. The minimum of this potential occurs at $H = 0$. But as mentioned already, we will have the entire Sect. 1.2.1 on the Higgs potential.

Let us recall one last time how we got to the Higgs mechanism from a static gauge invariant theory, the Σ model. From an effective field theory point of view we can introduce the Goldstone modes and with them gauge boson masses without introducing a fundamental Higgs scalar. All we need is the finite vacuum expectation value for Σ to spontaneously break electroweak symmetry. For this symmetry

breaking we do not care about quantum fluctuations of the Σ field, i.e. we do not distinguish between the invariant $\mathrm{Tr}\,\Sigma^\dagger\Sigma$ and its expectation value. Any properties of the Σ field as a quantum field are left to the ultraviolet completion, which has to decide for example if Σ is a fundamental or composite field. This way, the Higgs field could just be one step in a ladder built out of effective theories. Such a non-fundamental Higgs field is the basis for so-called strongly interacting light Higgs models where the Higgs field is a light composite field with a different canonical normalization as compared to a fundamental scalar.

Counting degrees of freedom we should be able to write Σ as a complex doublet with four degrees of freedom, three of which are eaten Goldstones and one is the fundamental Higgs scalar. For example, we can write

$$\Sigma \to \left(1+\frac{H}{v}\right)\mathbb{1} - \frac{i}{v}\vec{w} = \frac{1}{v}\begin{pmatrix} v+H-iw_3 & -w_2-iw_1 \\ w_2-iw_1 & v+H+iw_3 \end{pmatrix} = \frac{\sqrt{2}}{v}(\widetilde{\phi}\,\phi). \quad (1.47)$$

The last step is just another way to write the 2×2 matrix as a bi-doublet in terms of the two $SU(2)$ doublets containing the physical Higgs field and the Goldstone modes for the massive vector bosons W and Z

$$\widetilde{\phi} = \frac{1}{\sqrt{2}}\begin{pmatrix} v+H-iw_3 \\ w_2-iw_1 \end{pmatrix} \qquad \phi = \frac{1}{\sqrt{2}}\begin{pmatrix} -w_2-iw_1 \\ v+H+iw_3 \end{pmatrix}. \quad (1.48)$$

The vacuum expectation value v appearing in the ϕ and $\widetilde{\phi}$ doublets corresponds to $\langle\Sigma\rangle = \mathbb{1}$. In this form the normalization of the two real scalars w_3 and H is indeed the same, so their kinetic terms will be of the same form. The over-all factors $1/\sqrt{2}$ in the definition of the doublets are purely conventional and sometimes lead to confusion when for some people $v = 246\,\mathrm{GeV}$ while for others $v = 174\,\mathrm{GeV}$. The latter choice is a little less common but has the numerological advantage of $v \sim m_t$. In the Standard Model the two Higgs doublets ϕ and $\widetilde{\phi}$ give mass to up-type and down-type fermions.

Apart from problems arising when we ask for higher precision and quantum corrections, the effective sigma model clearly breaks down at large enough energies which can excite the fluctuations of the sigma field and for example produce a Higgs boson. This is the *job of the LHC*, which is designed and built to take us into an energy range where we can observe the structure of electroweak symmetry breaking beyond the effective theory and the Goldstone modes.

A last side remark—instead of deriving both relevant doublets for up and down-type fermion masses from one physical Higgs field ϕ and $\widetilde{\phi}$ we can include *two sigma fields* in the fermion-mass terms

$$\mathscr{L}_{D3} = -\overline{Q}_L m_{Qu}\Sigma_u \frac{\mathbb{1}+\tau_3}{2} Q_R - \overline{Q}_L m_{Qd}\Sigma_d \frac{\mathbb{1}-\tau_3}{2} Q_R + \cdots \quad (1.49)$$

with the isospin projectors $(\mathbb{1}\pm\tau_3)/2$. In the gauge boson mass terms they appear as

$$\mathscr{L}_{D2} = \frac{v_u^2}{2}\,\mathrm{Tr}\left[V_\mu^{(u)}V^{(u)\mu}\right] + \frac{v_d^2}{2}\,\mathrm{Tr}\left[V_\mu^{(d)}V^{(d)\mu}\right]. \quad (1.50)$$

Each of the two Σ fields we can express in the usual representation

$$\Sigma^{(u,d)} = \mathbb{1} + \frac{H^{(u,d)}}{v_{u,d}} - \frac{i\vec{w}^{(u,d)}}{v_{u,d}} \qquad \vec{w}^{(u,d)} = w_a^{(u,d)}\tau_a. \tag{1.51}$$

From the gauge-boson masses we know that

$$v_u^2 + v_d^2 = v^2 \qquad \Leftrightarrow \qquad v_u = v\sin\beta \quad \text{and} \quad v_d = v\cos\beta, \tag{1.52}$$

which means that the longitudinal vector bosons are

$$\vec{w} = \cos\beta\ \vec{w}^{(u)} + \sin\beta\ \vec{w}^{(d)}. \tag{1.53}$$

This two-Higgs doublet model is for example the minimal choice in supersymmetric extensions of the Standard Model. The ratio of its two vacuum expectation values $\tan\beta = v_u/v_d$ is one of the most important new physics parameters for example in B physics. But type-II two-Higgs doublet models where one Higgs doublet gives mass to up-type and another one to down-type fermions are much more general than that.

1.1.5 Custodial Symmetry

Analyzing the appearance of $\Delta\rho$ in Eqs. 1.25 and 1.36 we will see that not only higher energies, but also higher precision leads to a breakdown of the effective sigma model. At some point we start seeing how the relative size of the W and Z masses are affected by quantum fluctuations of the sigma field, i.e. the Higgs boson.

From the construction in Sect. 1.1.3 we know that electroweak symmetry breaking by a sigma field or Higgs doublet links the couplings of neutral and charged currents firmly to the masses of the W and Z bosons. On the other hand, the general renormalizable Lagrangian for the gauge boson masses in Eq. 1.25 involves two terms, both symmetric under $SU(2)_L \times U(1)_Y$ and hence allowed in the electroweak Standard Model. The mass values coming from $\text{Tr}[V_\mu V^\mu]$ give m_W and m_Z proportional to $g \equiv g_W$ and g_Z. Their relative size can be expressed in terms of the weak mixing angle θ_w, together with the assumption that G_F or g universally govern charged current ($W^\pm$) and neutral-current (W^3) interactions. At tree level this experimentally very well tested relation is

$$\frac{m_W^2}{m_Z^2} = \frac{g^2}{g_Z^2} = \cos^2\theta_w \equiv c_w^2. \tag{1.54}$$

In general, we can introduce a free parameter ρ which breaks this relation

$$\boxed{g_Z^2 \to g_Z^2\,\rho} \qquad m_Z \to m_Z\sqrt{\rho}, \tag{1.55}$$

which from measurements is very strongly constrained to be unity. In $\mathcal{L}_{D2}$ the Z-mass term proportional to $\Delta\rho$ precisely predicts such a deviation $\rho \neq 1$.

To bring our Lagrangian into agreement with measurements we better find a reason to constrain $\Delta\rho$ to zero, and the $SU(2) \times U(1)$ gauge symmetry unfortunately does not do the job.

Looking ahead, we will find that in the Standard Model $\rho = 1$ is actually violated at the one-loop level. This means we are looking for an *approximate symmetry* of the Standard Model. What we can hope for is that this symmetry is at least a good symmetry in the $SU(2)_L$ gauge sector and slightly broken elsewhere. One possibility along those lines is to replace the $SU(2)_L \times U(1)_Y$ symmetry with a larger $SU(2)_{L\times SU}(2)_R$ symmetry. At this stage this extended symmetry does not have to be a local gauge symmetry, a global version of $SU(2)_L$ combined with a global $SU(2)_R$ is sufficient. This global symmetry would have to act like

$$\begin{aligned} &\Sigma \to U\Sigma V^\dagger \qquad U \in SU(2)_L \qquad V \in SU(2)_R \\ &\mathrm{Tr}(\Sigma^\dagger\Sigma) \to \mathrm{Tr}\left(V\Sigma^\dagger U^\dagger U\Sigma V^\dagger\right) = \mathrm{Tr}(\Sigma^\dagger\Sigma). \end{aligned} \tag{1.56}$$

In this setup, the three components of W^μ form a triplet under $SU(2)_L$ and a singlet under $SU(2)_R$. If we cannot extract τ_3 as a special generator of $SU(2)_L$ and combine it with the $U(1)$ hypercharge the W and Z masses have to be identical, corresponding to $c_w = 1$ at tree level.

In the gauge boson and fermion mass terms computed in unitary gauge the Σ field becomes identical to its vacuum expectation value $\mathbb{1}$. On the symmetry breaking VEV the combined global $SU(2)$ transformations act as

$$\langle\Sigma\rangle \to \langle U\Sigma V^\dagger\rangle = \langle U\mathbb{1}V^\dagger\rangle = UV^\dagger \stackrel{!}{=} \mathbb{1}. \tag{1.57}$$

The last step, i.e. the symmetry requirement for the Lagrangian can only be satisfied if we require $U = V$. In other words, the vacuum expectation value for Σ breaks $SU(2)_L \times SU(2)_R$ to the *diagonal subgroup* $SU(2)_{L+R}$. The technical term is precisely defined this way—the two $SU(2)$ symmetries reduce to one remaining symmetry which can be written as $U = V$. Depending on if we look at the global symmetry structure in the unbroken or broken phase the *custodial symmetry* group is either $SU(2)_R$ or $SU(2)_{L+R}$. Its effect should nevertheless be the same.

Beyond tree level the global $SU(2)_L \times SU(2)_R$ symmetry structure can protect the relation between the gauge boson masses shown in Eq. 1.54. In other words, the custodial symmetry structure protects the tree-level value of $\rho = 1$.

From Eq. 1.56 we immediately see that it allows all terms in the Higgs potential $\mathscr{L}_\Sigma$, but it changes the picture not only for gauge boson but also for fermion masses. If fermions reside in $SU(2)_L$ as well as $SU(2)_R$ doublets we cannot implement any difference between up-type and down-type fermions in the Lagrangian. The custodial symmetry is only intact in the limit for example of identical third generation fermion masses $m_b = m_t$.

The measured masses $m_t \gg m_b$ affect the protected tree-level value $\rho = 1$: self energy loops in the W propagator involve a mixture of the bottom and top quark, while the Z propagator includes pure bottom and top loops. Skipping the loop calculation we quote their different contributions to the gauge boson masses as

$$
\begin{aligned}
\Delta\rho &\supset \frac{3G_F}{8\sqrt{2}\pi^2}\left(m_t^2+m_b^2-2\frac{m_t^2m_b^2}{m_t^2-m_b^2}\log\frac{m_t^2}{m_b^2}\right)\\
&= \frac{3G_F}{8\sqrt{2}\pi^2}\left(2m_b^2+m_b^2\delta-2m_b^2\frac{1+\delta}{\delta}\log(1+\delta)\right) \qquad m_t^2=m_b^2(1+\delta)\\
&= \frac{3G_F}{8\sqrt{2}\pi^2}\left(2m_b^2+m_b^2\delta-2m_b^2\left(\frac{1}{\delta}+1\right)\left(\delta-\frac{\delta^2}{2}+\frac{\delta^3}{3}+\mathcal{O}(\delta^4)\right)\right)\\
&= \frac{3G_F}{8\sqrt{2}\pi^2}m_b^2\left(2+\delta-2-2\delta+\delta+\delta^2-\frac{2}{3}\delta^2+\mathcal{O}(\delta^3)\right)\\
&= \frac{3G_F}{8\sqrt{2}\pi^2}m_b^2\left(\frac{1}{3}\delta^2+\mathcal{O}(\delta^3)\right)\\
&= \frac{G_Fm_W^2}{8\sqrt{2}\pi^2}\left(\frac{\left(m_t^2-m_b^2\right)^2}{m_W^2m_b^2}+\cdots\right)
\end{aligned}
\tag{1.58}
$$

In the Taylor series above the assumption of δ being small is of course not realistic, but the result is nevertheless instructive: the shift vanishes very rapidly towards the chirally symmetric limit $m_t \sim m_b$. The sign of the contribution of a chiral fermion doublet to $\Delta\rho$ is always positive. In terms of realistic Standard Model mass ratios it scales like m_t^2/m_W^2.

We have already argued that hypercharge or electric charge break custodial symmetry. From the form of the covariant derivative $D_\mu\Sigma$ including a single τ_3 we can guess that the $SU(2)_R$ symmetry will not allow B field interactions which are proportional to $s_w \sim \sqrt{1/4}$. A second contribution to the ρ parameter therefore arises from Higgs loops in the presence of $g' \neq 0$

$$
\Delta\rho \supset -\frac{11G_Fm_Z^2s_w^2}{24\sqrt{2}\pi^2}\log\frac{m_H^2}{m_Z^2}. \tag{1.59}
$$

The sign of this contribution implies that larger Higgs masses give negative contributions to the ρ parameter.

There is another parameterization of the same effect, namely the T parameter. It is part of an effective theory parameterization of deviations from the tree-level relations between gauge boson masses, mixing angles, and neutral and charged current couplings. In general, for example the mass ratio m_W/m_Z depends on all three parameters *S,T,U*. Typical experimental constraints form an ellipse in the S vs T plane along the diagonal. However, for example the leading contribution from the different bottom and top masses can be translated into a contribution $\alpha\Delta T \sim \Delta\rho$, centered around $T=0$.

There are two reasons to discuss these loop contributions breaking the custodial symmetry in the Standard Model. First, $\Delta\rho$ is experimentally very strongly

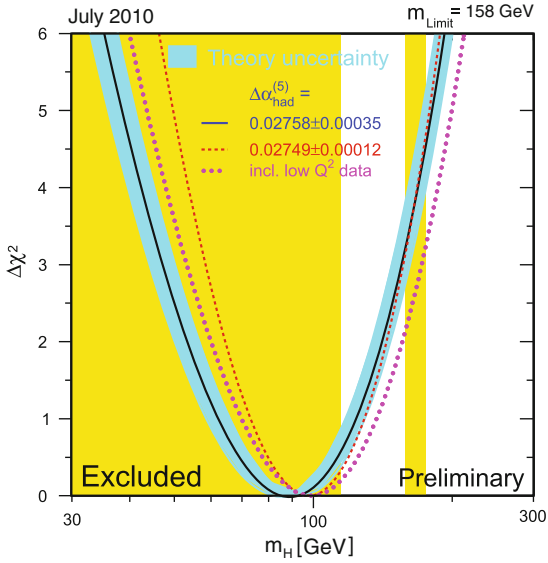

Fig. 1.1 Allowed range of Higgs masses in the Standard Model after taking into account electroweak precision data, most notably the ρ parameter contribution from the Higgs itself, Eq. 1.59. Figure from the LEP electroweak working group, with updates available under http://lepewwg.web.cern.ch/LEPEWWG

constrained by *electroweak precision measurements*, which means that alternative models for electroweak symmetry breaking usually include the same kind of approximate custodial symmetry by construction. As a matter of fact, this constraint is responsible for the almost death of (technicolor) models which describe the Higgs boson as a bound state under a new QCD-like interaction.

Even more importantly, in the Standard Model we can measure the symmetry violations from the heavy quarks and from the Higgs sector shown in Eqs. 1.58 and 1.59 in electroweak precision measurements. Even though the Higgs contributions depend on the Higgs mass only logarithmically, we can then derive an *upper bound* on the Higgs mass of the order of $\mathcal{O}(200\,\text{GeV})$, as shown in Fig. 1.1. This strongly suggests that if we are faced (mostly) with the Standard Model at the weak scale the Tevatron and at the LHC will be looking for a fairly light Higgs boson—or something that very much looks like a light fundamental Higgs boson.

However, we should firmly keep in mind that the ρ parameter only points to a light fundamental Higgs boson if we assume the Standard Model Higgs mechanism. For any other model it might point to something similar to a light Higgs field, but does not have to be fundamental. Including additional fields in a model can even turn around this prediction and prefer a heavy Higgs state.

One last question is: how do physical modes which we introduce as $\Sigma(x) = \exp(-i\vec{w}/v)$ transform under the different global $SU(2)$ symmetries which make up the custodial symmetry and can we construct a model of electroweak symmetry breaking around the custodial symmetry? This brings us back to the example of the photon mass, where we first saw Goldstone's theorem at work.

Under the usual $SU(2)_L$ symmetry we know the transformation reads $\Sigma \to U\Sigma$ with $U = \exp(-i\alpha\cdot\tau/2)$. The transformation properties of the Goldstone modes $\vec{w}$ follow from the infinitesimal transformations

$$\begin{aligned}
\mathbb{1} - i\frac{w\cdot\tau}{v} &\to \left(\mathbb{1} - i\frac{\alpha\cdot\tau}{2}\right)\left(\mathbb{1} - i\frac{w\cdot\tau}{v}\right) \\
&= \mathbb{1} - \frac{i}{v}\left(w\cdot\tau + \frac{v}{2}\alpha\right) + \cdots \\
&\stackrel{!}{=} \mathbb{1} - i\frac{w'\cdot\tau}{v} \qquad \text{implying} \quad \boxed{w \to w' = w + \frac{v}{2}\alpha}\,,
\end{aligned} \tag{1.60}$$

so U is a *non-linear transformation*, since w'_a is not proportional to w_a. The same structure we find for the $SU(2)_R$ transformation. This model of electroweak symmetry breaking we call a non-linear sigma model. When we construct a Lagrangian this non-linear symmetry transformation forbids mass terms, gauge interactions, Yukawa couplings, and quadratic potential terms for these modes in Σ. As discussed in Sect. 1.1.1 only derivative terms like the kinetic term and derivative couplings are allowed under the $SU(2)_L$ and $SU(2)_R$ symmetries.

Similarly, we can evaluate the transformation of these physical modes under the diagonal symmetry group $SU(2)_{L+R}$ with $\Sigma \to U\Sigma U^\dagger$ and instead find

$$\begin{aligned}
\mathbb{1} - i\frac{w\cdot\tau}{v} &\to \left(\mathbb{1} - i\frac{\alpha\cdot\tau}{2}\right)\left(\mathbb{1} - i\frac{w\cdot\tau}{v}\right)\left(\mathbb{1} + i\frac{\alpha\cdot\tau}{2}\right) \\
&= \left(\mathbb{1} - i\frac{\alpha\cdot\tau}{2}\right)\left(\left[\left(\mathbb{1} - i\frac{w\cdot\tau}{v}\right), \left(\mathbb{1} + i\frac{\alpha\cdot\tau}{2}\right)\right]\right. \\
&\qquad \left. + \left(\mathbb{1} + i\frac{\alpha\cdot\tau}{2}\right)\left(\mathbb{1} - i\frac{w\cdot\tau}{v}\right)\right) \\
&= \left(\mathbb{1} - i\frac{\alpha\cdot\tau}{2}\right)\left[-i\frac{w\cdot\tau}{v}, i\frac{\alpha\cdot\tau}{2}\right] + \left(\mathbb{1} - i\frac{w\cdot\tau}{v}\right) + \cdots \\
&= \left(\mathbb{1} - i\frac{\alpha\cdot\tau}{2}\right)\frac{1}{2v}\,2i\tau(\alpha\times w) + \left(\mathbb{1} - i\frac{w\cdot\tau}{v}\right) + \cdots \\
&= \mathbb{1} - i\frac{w\cdot\tau}{v} + i\frac{\tau(\alpha\times w)}{v} + \cdots \\
&\quad \text{implying} \quad \boxed{w_i \to w'_i = w_i - \varepsilon_{ijk}\alpha_j w_k}\,,
\end{aligned} \tag{1.61}$$

which is a *linear transformation*. In the fourth line we have used the commutator

$$\begin{aligned}
[\tau_i, \tau_j] = 2i\varepsilon_{ijk}\tau_k \quad &\Rightarrow \quad (\alpha\cdot\tau)(w\cdot\tau) = \alpha\cdot w + i\tau(\alpha\times w) \qquad \text{using Eq. 1.7} \\
&\Rightarrow \quad [(\alpha\cdot\tau), (w\cdot\tau)] = 2i\tau(\alpha\times w).
\end{aligned} \tag{1.62}$$

In other words, when we transform the physical modes corresponding to the broken generators in Σ by the larger symmetry $SU(2)_L \times SU(2)_R$ we find a non-linear transformation, while the approximate symmetry $SU(2)_{L+R}$ leads to a linear transformation. This is precisely what Goldstone's theorem predicts for the spontaneous breaking of a global electroweak symmetry.

1.2 The Standard Model

Before we discuss all the ways we can look for a Higgs Boson at the LHC we briefly review the Higgs mechanism in the Standard Model. In the last sections we have seen that there does not really need to be such a fundamental scalar, but electroweak precision data tells us whatever it is the Higgs should look very similar to a light fundamental scalar, unless we see some seriously new states and effects around the weak scale.

To make it a little more interesting and since we are already in the mood of not taking the Standard Model Higgs sector too literally, in Sect. 1.2.1 we include higher dimensional operators on top of the usual *renormalizable* (dimension-4) operators in the Higgs potential. Such operators generally occur in effective theories based on ultraviolet completions of our Standard Model, but their effects are often small or assumed to be small.

Once we want to analyze the behavior of the Higgs sector over a wide range of energy scales, like we will do in Sects. 1.2.2 and 1.2.3, we need to take the Standard Model seriously and in turn find constraints on the structure and the validity of our Standard Model with a fundamental Higgs boson.

1.2.1 Higgs Potential to Dimension Six

In the *renormalizable Standard Model* all terms in the Lagrangian are defined to be of mass dimension four, like $m_f \bar{\psi}\psi$ or $\bar{\psi}\partial_\mu\psi$ or $F_{\mu\nu}F^{\mu\nu}$. This mass dimension is easy to read off if we remember that for example scalar fields or vector-boson fields contribute mass dimension one while fermion spinors carry mass dimension 3/2. The same renormalizability assumption we usually make for the Higgs potential, even though from the previous discussion it is clear that higher dimensional terms—stemming from higher powers of $\mathrm{Tr}(\Sigma^\dagger\Sigma)$—can and should exist.

Starting from the Higgs doublets introduced in Eq. 1.48 and for now ignoring the Goldstone modes the simplified doublet

$$\phi = \frac{1}{\sqrt{2}} \begin{pmatrix} -w_2 - i w_1 \\ v + H + i w_3 \end{pmatrix} \sim \frac{1}{\sqrt{2}} \begin{pmatrix} 0 \\ v + H \end{pmatrix} \tag{1.63}$$

leaves us with only two renormalizable potential terms in Eq. 1.46, now written in terms of the Higgs doublet and with μ^2 and λ as prefactors

$$-\mathcal{L}_\Sigma = V_{\mathrm{SM}} = \mu^2|\phi|^2 + \lambda|\phi|^4 + \mathrm{const.} \tag{1.64}$$

To emphasize that renormalizability is a strong and not necessarily very justified theoretical assumption in LHC Higgs physics, we allow for more operators in the Higgs potential. If we expand the possible mass dimensions and the operator basis, there are exactly *two gauge-invariant operators* of dimension six we can write down in terms of the Higgs doublet $|\phi|^2$, i.e. before electroweak symmetry breaking

$$\mathcal{O}_1 = \frac{1}{2}\partial\mu(\phi^\dagger\phi)\ \partial^\mu(\phi^\dagger\phi) \qquad \mathcal{O}_2 = -\frac{1}{3}(\phi^\dagger\phi)^3. \tag{1.65}$$

The prefactors in the Lagrangian are conventional, because to construct a Lagrangian we have to multiply these operators with general coefficients of mass dimension minus two, parameterized in terms of an unknown mass scale Λ

$$\mathcal{L}_{D6} = \sum_{i=1}^{2} \frac{f_i}{\Lambda^2}\mathcal{O}_i. \tag{1.66}$$

As long as the typical energy scale E in the numerator in our matrix element is small ($E \ll \Lambda$), the corrections from the additional operators are small as well.

There is in principle one more possible operator $(\partial_\mu\phi)^\dagger(\phi^\dagger\phi)(\partial^\mu\phi)$, but it violates the custodial symmetry and leads to a very large contribution to the electroweak precision parameter $\Delta S = -f_3 v^2/(2\Lambda^2)$. Such large contributions to S are firmly ruled out by electroweak precision data, so we ignore this operator in our analysis.

Before we compute the Higgs potential including $\mathcal{O}_2$ we look at the effects of the dimension-6 operator $\mathcal{O}_1$. It contributes to the kinetic term the Higgs field in the Lagrangian, before or after symmetry breaking

$$\begin{aligned}\mathcal{O}_1 &= \frac{1}{2}\partial\mu(\phi^\dagger\phi)\ \partial^\mu(\phi^\dagger\phi) \\ &= \frac{1}{2}\partial\mu\left(\frac{(\widetilde{H}+v)^2}{2}\right)\partial^\mu\left(\frac{(\widetilde{H}+v)^2}{2}\right) \\ &= \frac{1}{2}\,(\widetilde{H}+v)^2\ \partial_\mu\widetilde{H}\ \partial^\mu\widetilde{H}.\end{aligned} \tag{1.67}$$

We use the symbol $\widetilde{H}$ for the Higgs field as part of ϕ, because from the formula above it is likely that there will be a difference between $\widetilde{H}$ and the physical Higgs field H at the end of the day. The contribution from $\mathcal{O}_1$ leaves us with a combined kinetic term

$$\begin{aligned}\mathcal{L}_{\text{kin}} &= \frac{1}{2}\partial_\mu\widetilde{H}\partial^\mu\widetilde{H}\left(1+\frac{f_1 v^2}{\Lambda^2}\right) \stackrel{!}{=} \frac{1}{2}\partial_\mu H\ \partial^\mu H \\ \Leftrightarrow \qquad & \boxed{H = \sqrt{1+\frac{f_1 v^2}{\Lambda^2}}\,\widetilde{H} \equiv N\ \widetilde{H}}\,.\end{aligned} \tag{1.68}$$

This is a simple rescaling to define the *canonical kinetic term* in the Lagrangian, but it also means we have to make sure we replace $\widetilde{H}$ with H in the entire Higgs sector.

Taking into account the additional dimension-6 operator $\mathcal{O}_2$ we can write the Higgs potential as

$$\boxed{V = \mu^2|\phi|^2 + \lambda|\phi|^4 + \frac{f_2}{3\Lambda^2}|\phi|^6}\,. \tag{1.69}$$

The positive sign in the last term of the potential V ensures that for $f_2 > 0$ the potential is bounded from below for large field values ϕ. The non-trivial minimum at $\phi \neq 0$ is given by

$$\frac{\partial V}{\partial |\phi|^2} = \mu^2 + 2\lambda|\phi|^2 + \frac{3f_2}{3\Lambda^2}|\phi|^4 \stackrel{!}{=} 0 \quad \Leftrightarrow \quad |\phi|^4 + \frac{2\lambda\Lambda^2}{f_2}|\phi|^2 + \frac{\mu^2\Lambda^2}{f_2} \stackrel{!}{=} 0, \tag{1.70}$$

defining the minimum position $|\phi|^2 = v^2/2$. The two solutions of the quadratic equation for $v^2/2$ are

$$\begin{aligned}
\frac{v^2}{2} &= -\frac{\lambda\Lambda^2}{f_2} \pm \left[\left(\frac{\lambda\Lambda^2}{f_2}\right)^2 - \frac{\mu^2\Lambda^2}{f_2}\right]^{\frac{1}{2}} = \frac{\lambda\Lambda^2}{f_2}\left[-1 \pm \sqrt{1 - \frac{\mu^2 f_2}{\Lambda^2\lambda^2}}\right] \\
&= \frac{\lambda\Lambda^2}{f_2}\left[-1 \pm \left(1 - \frac{f_2\mu^2}{2\lambda^2\Lambda^2} - \frac{f_2^2\mu^4}{8\lambda^4\Lambda^4} + \mathcal{O}(\Lambda^{-6})\right)\right] \\
&= \begin{cases} -\dfrac{\mu^2}{2\lambda} - \dfrac{f_2\mu^4}{8\lambda^3\Lambda^2} + \mathcal{O}(\Lambda^{-4}) = \dfrac{v_0^2}{2}\left(1 + \dfrac{f_2 v_0^2}{4\lambda\Lambda^2} + \mathcal{O}(\Lambda^{-4})\right) \\ -\dfrac{2\lambda\Lambda^2}{f_2^2} + \mathcal{O}(\Lambda^0) \end{cases}
\end{aligned} \tag{1.71}$$

The first solution we have expanded around the Standard Model minimum, $v_0^2 = -\mu^2/\lambda$. The second, high-scale solution is not the vacuum relevant for our Standard Model. Note that from the W, Z masses we know that $v = 246\,\text{GeV}$ so v is really our first observable in the Higgs sector, sensitive to the higher-dimensional operators.

To compute the mass of the Higgs state we could study the second derivative of the potential in the different directions, but we can also simply collect all quadratic terms contributing to the Lagrangian by hand. The regular dimension-4 contributions in terms of the shifted Higgs field $\widetilde{H}$ are

$$V_{\text{SM}} = \mu^2\frac{(\widetilde{H}+v)^2}{2} + \lambda\frac{(\widetilde{H}+v)^4}{4} = \frac{\mu^2}{2}\left(\widetilde{H}^2\cdots\right) + \frac{\lambda}{4}\left(\cdots 6\widetilde{H}^2v^2\cdots\right). \tag{1.72}$$

Only the terms in the parentheses contribute to the Higgs mass in terms of μ, v and λ. Including the additional potential operator in terms of $\widetilde{H}$ gives

$$\begin{aligned}
\mathcal{O}_2 &= -\frac{1}{3}(\phi^\dagger\phi)^3 \\
&= -\frac{1}{3}\frac{(\widetilde{H}+v)^6}{8} \\
&= -\frac{1}{24}\left(\widetilde{H}^6 + 6\widetilde{H}^5 v + 15\widetilde{H}^4v^2 + 20\widetilde{H}^3v^3 + 15\widetilde{H}^2v^4 + 6\widetilde{H}v^5 + v^6\right).
\end{aligned} \tag{1.73}$$

Combining both gives us the complete mass term to dimension six

$$
\begin{aligned}
\mathscr{L}_{\text{mass}} &= -\frac{\mu^2}{2}\tilde{H}^2 - \frac{3}{2}\lambda v^2 \tilde{H}^2 - \frac{f_2}{\Lambda^2}\frac{15}{24}v^4\tilde{H}^2 \\
&= -\frac{1}{2}\left(\mu^2 + 3\lambda v^2 + \frac{5}{4}\frac{f_2 v^4}{\Lambda^2}\right)\tilde{H}^2 \\
&= -\frac{1}{2}\left(-\lambda v^2\left(1+\frac{f_2 v^2}{4\lambda\Lambda^2}\right) + 3\lambda v^2 + \frac{5}{4}\frac{f_2 v^4}{\Lambda^2}\right)\tilde{H}^2 \qquad \text{Eq. 1.71 twice} \\
&= -\frac{1}{2}\left(2\lambda v^2 - \frac{f_2 v^4}{4\Lambda^2} + \frac{5}{4}\frac{f_2 v^4}{\Lambda^2}\right)\left(1+\frac{f_1 v^2}{\Lambda^2}\right)^{-1} H^2 \qquad \text{using Eq. 1.68} \\
&= -\frac{1}{2}\left(2\lambda v^2 + \frac{f_2 v^4}{\Lambda^2}\right)\left(1 - \frac{f_1 v^2}{\Lambda^2} + \mathscr{O}(\Lambda^{-4})\right) H^2 \\
&= -\lambda v^2\left(1+\frac{f_2 v^2}{2\lambda\Lambda^2}\right)\left(1 - \frac{f_1 v^2}{\Lambda^2} + \mathscr{O}(\Lambda^{-4})\right) H^2 \\
&= -\lambda v^2\left(1 - \frac{f_1 v^2}{\Lambda^2} + \frac{f_2 v^2}{2\Lambda^2\lambda} + \mathscr{O}(\Lambda^{-4})\right) H^2 \overset{!}{=} -\frac{m_H^2}{2}H^2 \\
m_H^2 &= -2\lambda v^2\left(1 - \frac{f_1 v^2}{\Lambda^2} + \frac{f_2 v^2}{2\Lambda^2\lambda}\right).
\end{aligned}
\tag{1.74}
$$

Including dimension-6 operators the relation between the vacuum expectation value, the Higgs mass and the factor in front of the $|\phi|^4$ term in the potential changes. Once we measure the Higgs mass at the LHC, we can compute the trilinear and quadrilinear *Higgs self couplings* by collecting the right powers of H in the Higgs potential, in complete analogy to the Higgs mass above. We find

$$
\begin{aligned}
\mathscr{L}_{\text{self}} = &-\frac{m_H^2}{2v}\left[\left(1 - \frac{f_1 v^2}{2\Lambda^2} + \frac{2 f_2 v^4}{3\Lambda^2 m_H^2}\right)H^3 - \frac{2 f_1 v^2}{\Lambda^2 m_H^2} H\partial_\mu H \partial^\mu H\right] \\
&-\frac{m_H^2}{8v^2}\left[\left(1 - \frac{f_1 v^2}{\Lambda^2} + \frac{4 f_2 v^4}{\Lambda^2 m_H^2}\right)H^4 - \frac{4 f_1 v^2}{\Lambda^2 m_H^2} H^2 \partial_\mu H \partial^\mu H\right].
\end{aligned}
\tag{1.75}
$$

This gives the Feynman rules

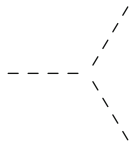

$$
-i\frac{3m_H^2}{v}\left(1 - \frac{f_1 v^2}{2\Lambda^2} + \frac{2 f_2 v^4}{3\Lambda^2 m_H^2} + \frac{2 f_1 v^2}{3\Lambda^2 m_H^2}\sum_{j<k}^{3}(p_j p_k)\right) \tag{1.76}
$$

and

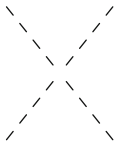

$$
-i\frac{3m_H^2}{v^2}\left(1 - \frac{f_1 v^2}{\Lambda^2} + \frac{4 f_2 v^4}{\Lambda^2 m_H^2} + \frac{2 f_1 v^2}{3\Lambda^2 m_H^2}\sum_{j<k}^{4}(p_j p_k)\right) \tag{1.77}
$$

From this discussion we see that in the Higgs sector the Higgs self couplings as well as the Higgs mass can be computed from the Higgs potential and depend on the operators we take into account. As mentioned before, in the Standard Model we use only the dimension-4 operators which appear in the renormalizable Lagrangian and which give us for the Higgs mass and self couplings

$$\boxed{m_H^2 = 2\lambda v^2 = -2\mu^2} \quad \text{and} \quad \mathscr{L}_{\text{self}} = -\frac{m_H^2}{2v} H^3 - \frac{m_H^2}{8v^2} H^4, \tag{1.78}$$

with $v = v_0 = 246\,\text{GeV}$. When the Higgs sector becomes more complicated, not the existence but the form of such relations between masses and couplings will change.

With this information we could now start computing Higgs observables at the LHC, but let us first see what else we can say about the Higgs potential from a theoretical point of view.

1.2.2 Unitarity

If we want to compute transition amplitudes at very high energies the Goldstone modes become very useful. In the V rest frame we can write the three polarization vectors of a massive gauge boson as

$$\varepsilon_{T,1}^\mu = \begin{pmatrix} 0 \\ 1 \\ 0 \\ 0 \end{pmatrix} \quad \varepsilon_{T,2}^\mu = \begin{pmatrix} 0 \\ 0 \\ 1 \\ 0 \end{pmatrix} \quad \varepsilon_L^\mu = \begin{pmatrix} 0 \\ 0 \\ 0 \\ 1 \end{pmatrix}. \tag{1.79}$$

If we boost V into the z direction, giving it a four-momentum $p^\mu = (E, 0, 0, |\vec{p}|)$, the polarization vectors become

$$\varepsilon_{T,1}^\mu = \begin{pmatrix} 0 \\ 1 \\ 0 \\ 0 \end{pmatrix} \quad \varepsilon_{T,2}^\mu = \begin{pmatrix} 0 \\ 0 \\ 1 \\ 0 \end{pmatrix} \quad \varepsilon_L^\mu = \frac{1}{m_V} \begin{pmatrix} |\vec{p}| \\ 0 \\ 0 \\ E \end{pmatrix} \overset{E \gg m_V}{\longrightarrow} \frac{1}{m_V} \begin{pmatrix} |\vec{p}| \\ 0 \\ 0 \\ |\vec{p}| \end{pmatrix} \equiv \frac{1}{m_V} p^\mu. \tag{1.80}$$

Very relativistic gauge bosons are dominated by their longitudinal polarization $|\varepsilon_L^\mu| \sim E/m_V \gg 1$. This longitudinal degree of freedom is precisely the Goldstone boson. This means that at high energies we can approximate the complicated vector bosons Z, $W^\pm$ as scalar Goldstone bosons w_0, $w_\pm$. This comes in handy for example when we next talk about unitarity as a constraint on the Higgs sector. This relation between Goldstones and gauge bosons at very high energies is called the *equivalence theorem*.

Based on the equivalence theorem we can compute the amplitude for $W^+W^- \to W^+W^-$ scattering at very high energies ($E \gg m_W$) in terms of scalar Goldstones

bosons. Three diagrams contribute to this processes: a four-point vertex, the s-channel Higgs exchange and the t-channel Higgs exchange:

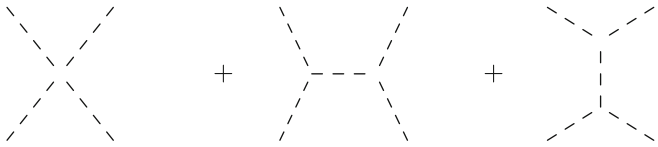

For that we need some basic Feynman rules, for example the Goldstone couplings to the Higgs boson and the four-Goldstone couplings. We start with the Higgs doublet, now including the Goldstone modes

$$\begin{aligned}
\phi &= \frac{1}{\sqrt{2}}\begin{pmatrix} -w_2 - iw_1 \\ v + H + iw_3 \end{pmatrix} \\
\phi^\dagger\phi &= \frac{1}{2}\left(w_1^2 + w_2^2 + w_3^2 + (v+H)^2\right) \\
\left(\phi^\dagger\phi\right)^2 &= \frac{1}{4}\left(\sum_i w_i^2\right)^2 + \frac{1}{2}(v+H)^2\sum_i w_i^2 + \frac{1}{4}(v+H)^4 \\
&= \frac{1}{4}\left(\sum_i w_i^2\right)^2 + \left(vH + \frac{v^2}{2} + \frac{H^2}{2}\right)\sum_i w_i^2 + \mathcal{O}(w^0),
\end{aligned} \tag{1.81}$$

where in the last step we neglect all terms without the Goldstone fields. For the potential we then get, only keeping the relevant terms contributing to the four-Goldstone and Higgs–Goldstone–Goldstone couplings at dimension four

$$\begin{aligned}
V &= \mu^2|\phi|^2 + \lambda|\phi|^4 \supset \lambda|\phi|^4 = \frac{m_H^2}{2v^2}\,|\phi|^4 \\
&= \frac{m_H^2}{2v^2}\left[\frac{1}{4}\left(\sum_i w_i^2\right)^2 + vH\sum_i w_i^2 + \mathcal{O}(w^0)\right] \\
&= \frac{m_H^2}{8v^2}\left(\sum_i w_i^2\right)^2 + \frac{m_H^2}{2v}H\sum_i w_i^2 + \mathcal{O}(w^0)
\end{aligned} \tag{1.82}$$

Focussing on the scattering of charged Goldstones $w_\pm w_\pm \to w_\pm w_\pm$ we use the corresponding fields $w_\pm = (w_1 \pm iw_2)/\sqrt{2}$. They appear in the above expression as $w_1^2 + w_2^2 = 2w_+w_-$, so we find the terms

$$\begin{aligned}
V &= \frac{m_H^2}{8v^2}4(w_+w_-)^2 + \frac{m_H^2}{2v}H2w_+w_- + \cdots \\
&= \frac{m_H^2}{2v^2}w_+w_-w_+w_- + \frac{m_H^2}{v}Hw_+w_- + \cdots,
\end{aligned} \tag{1.83}$$

which fix the two Feynman rules we need. Linking the Lagrangian to a Feynman rule involves one complication: for each positively charged Goldstone in the vertex there are two ways we can identify them with the Lagrangian fields. In addition, there are also two choices to identify the two negatively charged Goldstones, which implies an additional combinatorial factor four in the Feynman rule. Including a common factor $(-i)$ the two Feynman rules then become $-2im_H^2/v^2$ and $-im_H^2/v$.

The amplitude is given in terms of the Mandelstam variables s and t which describe the momentum flow p^2 through the two Higgs propagators and which we will properly introduce in Sect. 2.1.1

$$\begin{aligned} A &= \frac{-2im_H^2}{v^2} + \left(\frac{-im_H^2}{v}\right)^2 \frac{i}{s-m_H^2} + \left(\frac{-im_H^2}{v}\right)^2 \frac{i}{t-m_H^2} \\ &= -\frac{im_H^2}{v^2}\left[2 + \frac{m_H^2}{s-m_H^2} + \frac{m_H^2}{t-m_H^2}\right]. \end{aligned} \tag{1.84}$$

For this process we want to test the unitarity of the S matrix, which we write in terms of a transition amplitude $S = \mathbb{1} + iA$. The S matrix should be unitary to conserve probability

$$\begin{aligned} \mathbb{1} &\overset{!}{=} S^\dagger S = (\mathbb{1} - iA^\dagger)(\mathbb{1} + iA) = \mathbb{1} + i(A - A^\dagger) + A^\dagger A \\ &\Leftrightarrow \quad A^\dagger A = -i(A - A^\dagger). \end{aligned} \tag{1.85}$$

If we sandwich $(A - A^\dagger)$ between identical asymptotically free fields, which means that we are looking at forward scattering with a scattering angle $\theta \to 0$, we find in the high-energy limit or for massless external particles

$$\begin{aligned} -i\langle j|A - A^{*T}|j\rangle &= -i\langle j|A - A^*|j\rangle = 2\mathrm{Im}A(\theta = 0) \\ \Rightarrow \qquad & \boxed{\sigma \equiv \frac{1}{2s}\langle j|A^\dagger A|j\rangle = \frac{1}{s}\,\mathrm{Im}A(\theta = 0)}. \end{aligned} \tag{1.86}$$

Assuming that our Lagrangian is hermitian this imaginary part corresponds only to absorptive terms in the scattering amplitude. This is the usual formulation of the *optical theorem* reflecting unitarity in terms of the transition amplitude A.

To include the dependence on the scattering angle θ we decompose the transition amplitude into partial waves

$$A = 16\pi \sum_{l=0}^{\infty} (2l+1) P_l(\cos\theta) a_l \qquad \text{with} \qquad \int_{-1}^{1} dx\, P_l(x) P_{l'}(x) = \frac{2}{2l+1}\delta_{ll'}, \tag{1.87}$$

ordered by the orbital angular momentum l. P_l are the Legendre polynomials of the scattering angle θ, which obey an orthogonality condition. The scattering cross section including all prefactors and the phase space integration is then given by

$$\begin{aligned}\sigma &= \int d\Omega \frac{|A|^2}{64\pi^2 s} \\ &= \frac{(16\pi)^2}{64\pi^2 s} 2\pi \int_{-1}^{1} d\cos\theta \sum_l \sum_{l'} (2l+1)(2l'+1)\; a_l a_{l'}^*\; P_l(\cos\theta) P_{l'}(\cos\theta) \\ &= \frac{8\pi}{s} \sum_l 2(2l+1)\; |a_l|^2 = \frac{16\pi}{s} \sum_l (2l+1)\; |a_l|^2 .\end{aligned} \tag{1.88}$$

The relation between the integral over the scattering angle θ and the Mandelstam variable t we will discuss in more detail in Sect. 2.1.1. Applied to this perturbative series in partial waves the optical theorem requires

$$\frac{16\pi}{s}(2l+1)\; |a_l|^2 \stackrel{!}{=} \frac{1}{s}\; 16\pi (2l+1)\; \text{Im}\, a_l \qquad \Leftrightarrow \qquad |a_l|^2 \stackrel{!}{=} \text{Im}\, a_l . \tag{1.89}$$

using $P_l(\cos\theta = 1) = 1$. This condition we can rewrite as

$$(\text{Re}\; a_l)^2 + \left(\text{Im}\; a_l - \frac{1}{2}\right)^2 = \frac{1}{4} \qquad \Rightarrow \qquad \boxed{|\text{Re}\; a_l| < \frac{1}{2}} \tag{1.90}$$

once we recognize that the condition on $\text{Im}\, a_l$ and on $\text{Re}\; a_l$ is a unit cycle around $a_l = (0, 1/2)$ with radius 1/2.

It is important to remember that in the above argument we have formulated the constraint for each term in the sum over the Legendre polynomials. Mathematically, this is well justified, but of course there might be physics effects which lead to a systematic cancellation between different terms. This is why the constraint we compute is referred to as *perturbative unitary*. For Goldstone scattering we compute the supposedly leading first term in the partial wave expansion from the amplitude

$$\begin{aligned} a_0 = \frac{1}{16\pi s} \int_{-s}^{0} dt |A| &= \frac{1}{16\pi s} \int_{-s}^{0} dt \frac{m_H^2}{v^2} \left[2 + \frac{m_H^2}{s - m_H^2} + \frac{m_H^2}{t - m_H^2} \right] \\ &= \frac{m_H^2}{16\pi v^2} \left[2 + \frac{m_H^2}{s - m_H^2} - \frac{m_H^2}{s} \log\left(1 + \frac{s}{m_H^2}\right) \right] \\ &= \frac{m_H^2}{16\pi v^2} \left[2 + \mathcal{O}\left(\frac{m_H^2}{s}\right) \right]. \end{aligned} \tag{1.91}$$

In the high-energy limit $s \gg m_H^2$ this translates into an upper limit on the Higgs mass which in Eq. 1.84 enters as the Goldstone coupling in the numerator

$$\frac{m_H^2}{8\pi v^2} < \frac{1}{2} \qquad \Leftrightarrow \qquad \boxed{m_H^2 < 4\pi v^2 = (870\ \text{GeV})^2} . \tag{1.92}$$

This is the maximum value of m_H maintaining perturbative unitarity for $WW \to WW$ scattering. Replacing the Higgs mass by the self coupling we can formulate the same constraint as $\lambda < 2\pi$. In this form we see that perturbative unitarity goes right to the limitations of perturbation theory, which means that we should include higher order effects as well as higher dimensional operators to get a reliable numerical prediction in the range of $m_H \lesssim 1$ TeV. In the following section we will have another less perturbatively limited look at the behavior of large λ.

Of course, if we limit s to a finite value this bound changes, and we can compute a maximum scale s_{max} which leaves $WW \to WW$ perturbatively unitary for fixed m_H: for $m_H \lesssim v$ this typically becomes $\sqrt{s_{\text{max}}} \sim 1.2\,\text{TeV}$. This number is one of the motivations to build the LHC as a high energy collider with a partonic center-of-mass energy in the few-TeV range. If something should go wrong with the Standard Model Higgs sector we can expect to see something else curing unitarity around the TeV scale.

One last but very important comment we need to make: this unitarity argument only works if the *WWH* coupling is exactly what it should be. While perturbative unitarity only gives us a fairly rough upper limit on m_H, it also uniquely fixes g_{WWH} to its Standard Model value. Any sizeable deviation from this value again means new physics appearing at the latest around the mass scales of Eq. 1.92.

Looking at processes like $WW \to f\bar{f}$ or $WW \to WWH$ or $WW \to HHH$ we can exactly the same way fix *all Higgs couplings* in the Standard Model, including g_{Hff}, g_{HHH}, g_{HHHH}. The most important result of the unitarity test is probably not the upper bound on the Higgs mass, but the underlying assumption that the unitarity test only works in the presence of one Higgs boson if all Higgs couplings look exactly as predicted by the Standard Model.

1.2.3 Renormalization Group Analysis

Two additional theoretical constraints we can derive from the renormalization group equation of the Higgs potential, specifically from the *renormalization scale* dependence of the self coupling $\lambda(Q^2)$. Such a scale dependence arises automatically when we encounter ultraviolet divergences and absorb the $1/\varepsilon$ poles into a minimal counter term. We will discuss this running of couplings in more detail in Sect. 2.2.1 for the running QCD coupling α_s. In the case of a running quartic Higgs coupling λ the relevant *s, t* and *u*-channel diagrams only depending on λ itself are

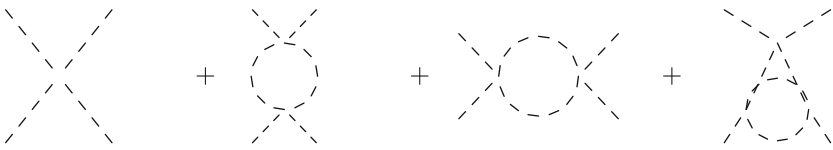

Skipping the calculation we quote the complete renormalization group equation including diagrams with the Higgs boson, the top quark and the weak gauge bosons inside the loops

$$\boxed{\frac{d\lambda}{d\log Q^2} = \frac{12\lambda^2 + 6\lambda\lambda_t^2 - 3\lambda_t^4 - \frac{3}{2}\lambda\left(3g_2^2 + g_1^2\right) + \frac{3}{16}\left(2g_2^4 + (g_2^2 + g_1^2)^2\right)}{16\pi^2}}, \tag{1.93}$$

with $\lambda_t = \sqrt{2}m_t/v$. This formula will be the basis of the discussion in this section.

The first regime we study is where the Higgs self coupling λ becomes strong. Fixed order perturbation theory as we use it in the unitarity argument runs into problems in this regime and the renormalization group equation is the appropriate tool to describe this region. The leading term in Eq. 1.93 reads

$$\frac{d\lambda}{d\log Q^2} = \frac{1}{2Q}\frac{d\lambda}{dQ} = \frac{1}{16\pi^2}12\lambda^2 + \mathcal{O}(\lambda) = \frac{3}{4\pi^2}\lambda^2 + \mathcal{O}(\lambda). \tag{1.94}$$

Because of the positive sign on the right-hand side the quartic coupling will become stronger and stronger and eventually diverge for larger scales Q^2. Obviously, this divergence should not happen in a physical model and will give us a constraint on the maximum value of λ allowed. The approximate renormalization group equation we can solve by replacing $\lambda = g^{-1}$

$$\begin{aligned}
&\frac{d\lambda}{d\log Q^2} = \frac{d}{d\log Q^2}\frac{1}{g} = -\frac{1}{g^2}\frac{dg}{d\log Q^2} \stackrel{!}{=} \frac{3}{4\pi^2}\frac{1}{g^2} \\
\Leftrightarrow \quad &\frac{dg}{d\log Q^2} = -\frac{3}{4\pi^2} \quad \Leftrightarrow \quad g(Q^2) = -\frac{3}{4\pi^2}\log Q^2 + C.
\end{aligned} \tag{1.95}$$

A boundary condition $\lambda(Q^2 = v^2) = \lambda_0$ fixes the integration constant C

$$\begin{aligned}
&g_0 = \frac{1}{\lambda_0} = -\frac{3}{4\pi^2}\log v^2 + C \quad \Leftrightarrow \quad C = g_0 + \frac{3}{4\pi^2}\log v^2 \\
\Rightarrow \quad &g(Q^2) = -\frac{3}{4\pi^2}\log Q^2 + g_0 + \frac{3}{4\pi^2}\log v^2 = -\frac{3}{4\pi^2}\log\frac{Q^2}{v^2} + g_0 \\
\Leftrightarrow \quad &\boxed{\lambda(Q^2) = \left[-\frac{3}{4\pi^2}\log\frac{Q^2}{v^2} + \frac{1}{\lambda_0}\right]^{-1} = \lambda_0\left[1 - \frac{3}{4\pi^2}\lambda_0\log\frac{Q^2}{v^2}\right]^{-1}}.
\end{aligned} \tag{1.96}$$

Starting from scales $Q \sim v$ where the expression in brackets is close to one and moving towards larger scales the denominator becomes smaller until λ actually hits a pole at the critical value Q_{pole}

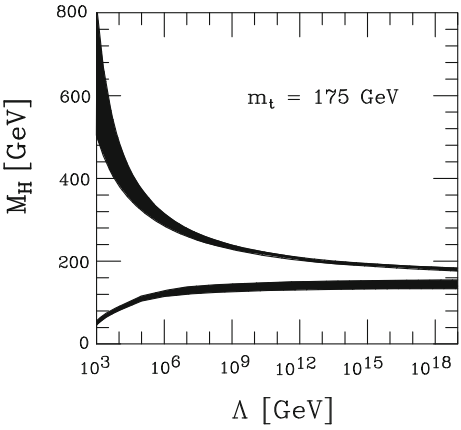

Fig. 1.2 Triviality or Landau pole (*upper*) and stability bounds (*lower*) for the Standard Model Higgs boson in the $m_H - Q$ plane. Similar figures first appeared in Ref. [1], involving this kind of physics argument from Ref. [2]

$$
\begin{aligned}
1 - \frac{3}{4\pi^2}\lambda_0 \log \frac{Q^2_{\text{pole}}}{v^2} \stackrel{!}{=} 0 \quad &\Leftrightarrow \quad \frac{3}{4\pi^2}\lambda_0 \log \frac{Q^2_{\text{pole}}}{v^2} = 1 \\
&\Leftrightarrow \quad \log \frac{Q^2_{\text{pole}}}{v^2} = \frac{4\pi^2}{3\lambda_0} \\
&\Leftrightarrow \quad Q_{\text{pole}} = v \, \exp \frac{2\pi^2}{3\lambda_0} = v \, \exp \frac{4\pi^2 v^2}{3m_H^2}
\end{aligned}
\tag{1.97}
$$

Such a pole is called a *Landau pole* and gives us a maximum scale beyond which we cannot rely on our perturbative theory to work. In the upper line of Fig. 1.2 we show Q_{pole} versus the Higgs mass, approximately computed in Eq. 1.97. As a function of the Higgs mass Q_{pole} gives the maximum scale were our theory is valid, which means we have to reside below the upper line in Fig. 1.2. Turning the argument around, for given Q_{pole} we can read off the maximum allowed Higgs mass which in the limit of large cutoff values around the Planck scale 10^{19} GeV becomes $m_H \lesssim 180\,\text{GeV}$.

This limit is often referred to as the *triviality bound*, which at first glance is precisely not what this theory is—trivial or non-interacting. The name originates from the fact that if we want our Higgs potential to be perturbative at all scales, the coupling λ can only be zero everywhere. Any finite coupling will hit a Landau pole at some scale. Such a theory with zero interaction is called trivial.

After looking at the ultraviolet regime we can go back to the full renormalization group equation Eq. 1.93 and ask a completely different question: how long will $\lambda > 0$ ensure that our Higgs potential is bounded from below?

This bound is called the *stability bound*. On the right hand side of Eq. 1.93 there are two terms with a negative sign which in principle drive λ through zero. One

of them vanishes for small $\lambda \sim 0$, so we can neglect it. In the small-λ regime we therefore encounter two finite competing terms

$$\begin{aligned} \frac{d\lambda}{d\log Q^2} &\sim \frac{1}{16\pi^2}\left[-3\frac{4m_t^4}{v^4} + \frac{3}{16}\left(2g_2^4 + \left(g_2^2+g_1^2\right)^2\right)\right] \\ \Leftrightarrow \quad \lambda(Q^2) &\sim \lambda(v^2) + \frac{1}{16\pi^2}\left[-\frac{12m_t^4}{v^4} + \frac{3}{16}\left(2g_2^4 + \left(g_2^2+g_1^2\right)^2\right)\right]\log\frac{Q^2}{v^2}. \end{aligned} \tag{1.98}$$

The usual boundary condition at $\lambda(v^2) = m_H^2/(2v^2)$ is the starting point from which the top Yukawa coupling drives λ to zero at another critical scale $\lambda(Q^2_{\text{stable}}) = 0$ which depends on the Higgs mass m_H. The second (smaller) contribution from the weak gauge coupling ameliorates this behavior

$$\begin{aligned} \lambda(v^2) = \frac{m_H^2}{2v^2} &\stackrel{!}{=} -\frac{1}{16\pi^2}\left[-\frac{12m_t^4}{v^4} + \frac{3}{16}\left(2g_2^4 + \left(g_2^2+g_1^2\right)^2\right)\right]\log\frac{Q^2_{\text{stable}}}{v^2} \\ \Leftrightarrow \quad \frac{m_H^2}{v^2} &= \frac{1}{8\pi^2}\left[\frac{12m_t^4}{v^4} - \frac{3}{16}\left(2g_2^4 + \left(g_2^2+g_1^2\right)^2\right)\right]\log\frac{Q^2_{\text{stable}}}{v^2} \\ \Leftrightarrow \quad m_H &= \begin{cases} 70\,\text{GeV} & \text{for} \quad Q_{\text{stable}} = 10^3\,\text{GeV} \\ 130\,\text{GeV} & \text{for} \quad Q_{\text{stable}} = 10^{16}\,\text{GeV} \end{cases}. \end{aligned} \tag{1.99}$$

From Eq. 1.98 we see that only for energy scales below $Q_{\text{stable}}(m_H)$ the Higgs potential is bounded from below and our vacuum stable. For a given maximum validity scale Q_{stable} this stability bound translates into a minimum Higgs mass balancing the negative slope in Eq. 1.98 for which our theory is then well defined. In Fig. 1.2 we show Q_{stable} as the lower curve, above which our consistent theory has to reside.

Summarizing what we know about the Higgs mass in the Standard Model we already have indirect experimental as well as theory constraints on this otherwise undetermined parameter.

Strictly in the Standard Model, electroweak precision data points to the mass range $m_H \lesssim 200\,\text{GeV}$. This means at the LHC we are either looking for a light Higgs boson or we should expect some drastic modifications to our Standard Model which could alter this picture significantly and would be hard to miss and even more exciting to observe.

From the renormalization group we have two pieces of information on the Higgs mass, again in the renormalizable Standard model: the Landau pole or triviality bound gives an upper limit on m_H as a function of the cutoff scale. Vacuum stability gives a lower bound on m_H as a function of the cutoff scale. Running both cutoff scales towards the Planck mass $Q_{\text{pole}}, Q_{\text{stable}} \to 10^{19}\,\text{GeV}$, we see in Fig. 1.2 that only Higgs mass values around $m_H = 130 \cdots 180\,\text{GeV}$ are allowed for a fundamental Standard Model.

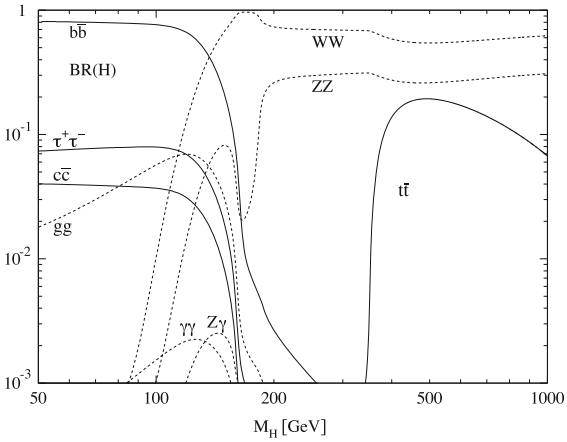

Fig. 1.3 Branching ratios of the Standard-Model Higgs boson as a function of its mass, computed with HDECAY. Off-shell effects in the decays to *WW* and *ZZ* are taken into account. Figure found for example in Refs. [3, 4]

1.3 Higgs Decays

Signatures for new particles at colliders consist of a production process and a decay pattern. Both, the production and the decay can contribute to unique kinematic features which we can use to extract signal from background events. The actual new particle is then described by a Breit–Wigner propagator for unstable particles which we will discuss in detail in Sect. 2.1.2. Since the Higgs boson is a scalar there are no correlations between production and decay process, which simplifies the calculation and simulation of Higgs signatures.

Unlike the production processes the Higgs decay pattern is as simple as it can be. At tree level all decay rates are determined by the Higgs coupling to Standard Model particles, which are *fixed by unitarity*. The rule for different Higgs decays is simple; because by definition the Higgs field couples to all particles (including itself) proportional to their masses it will preferably decay to the heaviest states allowed by phase space. This goes back to the condition $\langle \Sigma \rangle = \mathbb{1}$ translated into the exclusive appearance of the combination $(v + H)$ in the Higgs field ϕ and in the Lagrangian.

This behavior we see in Fig. 1.3. Starting at low masses this first applies to decays to $\tau\tau$ and $b\bar{b}$. The relative size of their branching ratios around $10:90\%$ is given by their Yukawa couplings in the appropriate renormalization scheme ($y_b/y_\tau \sim 1.4$) times an additional color factor $N_c = 3$ for the bottom quarks. Once the (off-shell) decays to *WW* open, they very soon dominate. The dominant decays to bottom pairs and *W* pairs become equal for Higgs masses around 130 GeV.

Because of the small mass difference between the *W* and *Z* bosons the decay to *ZZ* is not as dominant, compared to the *WW* decay which has two degrees of freedom (W^+W^- and W^-W^+) in the final state. In particular in the region where the *W* decays first becomes on-shell we see a drop of in the still off-shell *Z* decays. For large Higgs masses the ratio of $H \to WW$ and $H \to ZZ$ decays is fixed by the relative factor of two, corresponding to the number of degrees of freedom forming

the final state. Above the top threshold the $t\bar{t}$ decay becomes sizeable, but never really dominant.

Because the bottom Yukawa coupling is so small, $m_b/m_W \lesssim 1/30$, one-loop induced couplings can almost compete with it. In particular the loop-induced decay to two photons plays an important role in LHC phenomenology. It proceeds via a top and a W triangle which enter with opposite signs in the amplitude, i.e. interfering destructively. The larger W contribution fixes the sign of the loop-induced coupling.

The structure of the $\gamma\gamma H$ coupling is similar to the production via the loop-induced ggH coupling which we will discuss in Sect. 1.4. The reason for considering this decay channel are the LHC detectors. To extract a Higgs signal from the backgrounds we usually try to measure the four-momenta of the Higgs decay products and reconstruct their invariant mass. The signal should then peak around m_H while the backgrounds we expect to be more or less flat. The LHC detectors, in particular CMS, are designed to measure the photon momentum and energy particularly well. The resolution on $m_{\gamma\gamma}$ will at least be a factor of 10 better than for any other decay channel, except for muons. Moreover, photons do not decay, so we can use all photon events in the Higgs search, while for example hadronically decaying $W/Z \to 2$ jets are not particularly useful at the LHC. These enhancement factors make the Higgs decay to two photons a promising signature, in spite of its small branching ratio around $2 \cdot 10^{-3}$.

Because an observed Higgs sector can deviate from the minimal Standard Model assumptions in many ways the LHC or other future colliders will study the different Higgs decays and, as a function of m_H, answer the questions

- Are gauge-boson couplings proportional to $m_{W,Z}$?
- Are these couplings dimension-3 operators?
- Are fermion Yukawa couplings proportional to m_f?
- Is there a Higgs self coupling, i.e. a remnant of the Higgs potential?
- Do λ_{HHH} and λ_{HHHH} show signs of higher-dimensional operators?
- Are there any other unexpected effects, like a Higgs decay to invisible particles?

But before we decay the Higgs we need to produce it ...

1.4 Higgs Production in Gluon Fusion

Looking for the Higgs boson at hadron colliders starts with bad news: at tree level the Higgs hardly couples to light-flavor quarks and has no coupling to gluons. This is because the Higgs boson couples to all Standard Model particles proportional to their mass—this is the same operator they get their mass from. Because the $SU(3)_C$ symmetry of QCD is not broken there is no coupling to gluons at all.

On the other hand, the protons at the LHC contain a lot of gluons, again something we will talk about in more detail in Chap. 2, so the question is if we can find and use a loop-induced coupling of two gluons to the Higgs. In spite of the expected suppression

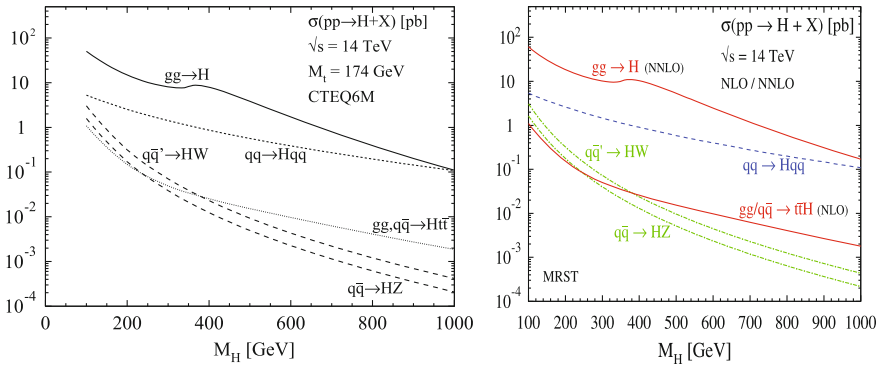

Fig. 1.4 *Left* production cross section for a Standard-Model Higgs boson at the LHC, as a function of the Higgs mass. Figure from Ref. [3]. *Right* updated version including higher order corrections

of the corresponding cross section by a one-loop factor $(g^2/(16\pi^2))^2$ we would hope to arrive at an observable production cross-section $pp \to H$. Numerically, it will turn out that the production of Higgs bosons in gluon fusion is actually the dominant process at the LHC, as shown in Fig. 1.4.

1.4.1 Effective Gluon–Higgs Coupling

If an effective ggH coupling should be mediated by a closed Standard Model *particle loop* the top is the perfect candidate: on the one hand it has a strong coupling to gluons, and on the other hand it has the largest of all Standard Model couplings to the Higgs boson, $m_t/v \sim 0.7$. The corresponding Feynman diagram is

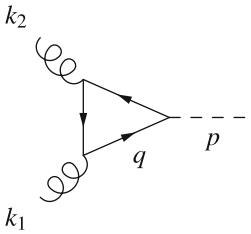

We construct this effective coupling in three steps, starting with the Dirac trace occurring the top loop. All momenta are defined as incoming with $k_1^2 = k_2^2 = 0$ and $p^2 = m_H^2$. The Dirac indices of the two gluons are μ, ν and the loop momentum is q, so in the first step we need to compute

$$T^{\mu\nu} = \mathrm{Tr}\left[(\not{q} + m_t)\gamma^\mu(\not{q} + \not{k}_1 + m_t)\gamma^\nu(\not{q} + \not{k}_1 + \not{k}_2 + m_t)\right]. \qquad (1.100)$$

The calculational problem is the tensor structure of this trace. Because of gauge invariance we can neglect terms proportional to k_1^μ and k_2^ν; they would not survive the multiplication with the transverse gluon polarization ($k \cdot \varepsilon = 0$). In a so-called axial gauge we could also get rid of the remaining terms proportional to k_1^ν and k_2^μ.

However, there is a better way to compute this trace. We know that there is no tree-level Higgs coupling of the Higgs to two gluons, which would correspond to the fields $HG_\mu G^\mu$ with mass dimension three in the Lagrangian. So we need to find another operator mediating such a coupling, keeping in mind that it is loop induced and can therefore include a mass suppression by powers of the top mass. The Higgs can also couple to the *field strength* in the invariant form $HG_{\mu\nu}G^{\mu\nu}$ with $G_{\mu\nu} \equiv \partial_\mu A_\nu - \partial_\nu A_\mu + \mathcal{O}(A^2)$. This operator has mass dimension five and arises from the dimension-6 gauge-invariant object $\phi^\dagger \phi G_{\mu\nu} G^{\mu\nu}$ after breaking $SU(2)_L$.

The factor in front of this term is the effective coupling we are going to compute in this section. Before that it pays to briefly look at the operator itself. Switching from position space and its momentum operator into momentum space $\partial \to ik$

$$\begin{aligned} G^{\mu\nu}G_{\mu\nu} &= -\left(k_{1\mu}A_{1\nu} - k_{1\nu}A_{1\mu}\right)\left(k_{2\mu}A_{2\nu} - k_{2\nu}A_{2\mu}\right) + \mathcal{O}(A^3) \\ &= -2\left[(k_1k_2)(A_1A_2) - (k_1A_2)(k_2A_1)\right] + \mathcal{O}(A^3) \\ &= -2(k_1k_2)A_{1\mu}A_{2\nu}\left[g^{\mu\nu} - \frac{k_1^\nu k_2^\mu}{k_1k_2}\right] + \mathcal{O}(A^3) \\ &= -m_H^2 A_{1\mu}A_{2\nu}\left[g^{\mu\nu} - \frac{k_1^\nu k_2^\mu}{k_1k_2}\right] + \mathcal{O}(A^3) \end{aligned} \tag{1.101}$$

shows that the gauge invariant operator linking exactly two gluon fields to a Higgs field has to be proportional to the transverse tensor

$$\begin{aligned} &P_T^{\mu\nu} = \frac{1}{\sqrt{2}}\left(g^{\mu\nu} - \frac{k_1^\nu k_2^\mu}{(k_1k_2)}\right) \\ &\text{with} \quad P_T^{\mu\nu}P_{T\mu\nu} = 1 \quad \text{and} \quad P_T^{\mu\nu}k_{1\mu} = 0 = P_T^{\mu\nu}k_{2\nu}. \end{aligned} \tag{1.102}$$

Using this known tensor structure of $T^{\mu\nu}$ as defined in Eq. 1.100 we can extract the scalar *form factor F* from the Dirac trace using

$$T^{\mu\nu} = F\ P_T^{\mu\nu} \qquad \Leftrightarrow \qquad P_{T\mu\nu}T^{\mu\nu} = P_{T\mu\nu}P_T^{\mu\nu}\ F = F. \tag{1.103}$$

This way we project out the relevant gluon tensor structure or the relevant degrees of freedom of the two gluons contributing to this effective coupling. Terms involving a larger number of gluon fields are related to this ggH coupling by non-abelian $SU(3)$ gauge invariance.

One thing to admit at this stage is that nobody in the world really computes Dirac traces by hand anymore. There are powerful programs, like FORM, which do this job for us. Using it we find

$$P_{T\,\mu\nu}T^{\mu\nu} = \frac{4m_t}{\sqrt{2}}\left(-m_H^2 + 3m_t^2 - \frac{8}{m_H^2}(k_1q)(k_2q) - 2(k_1q) + q^2\right). \quad (1.104)$$

Inside this trace there appears the loop momentum q, which we in our second step we have to consider as part of the loop integration. The effective ggH vertex includes the loop integral

$$\int \frac{d^4q}{i\pi^2}\frac{T^{\mu\nu}}{[q^2-m_t^2][(q+k_1)^2-m_t^2][(q+k_1+k_2)^2-m_t^2]}. \quad (1.105)$$

The non-trivial q^μ dependence of the numerator observed in Eq. 1.104 we can take care of using a few tricks. For example, we use the relation $q^2/(q^2-m_t^2) = 1+m_t^2/(q^2-m_t^2)$ and then shift q, knowing that the final result for this integral will be finite. This is non-trivial piece of information, because most loop calculations lead to ultraviolet divergences, which need to be removed by first regularizing the integral and then renormalizing the parameters. The reason why we do not see any divergences in this process is that for a renormalization we would need something to renormalize, i.e. a leading order process which receives quantum corrections. However, we only compute this one-loop amplitude because there is no tree-level vertex, i.e. nothing to renormalize, which means no ultraviolet divergences.

While these tricks help a little, we still do not know how to remove the $(k_1q)(k_2q)$ term in Eq. 1.104. The method of choice is a *Passarino-Veltman reduction* which turns tensor integrals into scalar integrals, where a scalar integral does not have powers of the loop momentum in the numerator. For example, the scalar three-point function is given by

$$C(k_1^2,k_2^2,m_H^2;m_t,m_t,m_t) \equiv \int \frac{d^4q}{i\pi^2}\frac{1}{[q^2-m_t^2][(q+k_1)^2-m_t^2][(q+k_1+k_2)^2-m_t^2]}. \quad (1.106)$$

Combining our Dirac trace in Eq. 1.104 with the tensor integral in Eq. 1.105 and the applying a reduction algorithm gives us

$$\int \frac{d^4q}{i\pi^2}\frac{P_{T\,\mu\nu}T^{\mu\nu}}{[...][...][...]} = \frac{4m_t}{\sqrt{2}}\left[2+\left(4m_t^2-m_H^2\right)C(0,0,m_H^2;m_t,m_t,m_t)\right]. \quad (1.107)$$

The first term not proportional to any scalar integral has a curious origin. It comes from a combination of $\mathcal{O}(\varepsilon)$ terms from the Dirac trace in $n = 4-2\varepsilon$ dimensions and a two-point function which for the integration measure $1/i\pi^2$ always includes the ultraviolet divergence $1/\varepsilon$.

Scalar integrals we can for example calculate using the Feynman parameterization

$$\frac{1}{A_1A_2\cdots A_n} = \int_0^1 dx_1\cdots dx_n\,\delta\left(\sum x_i - 1\right)\frac{(n-1)!}{(x_1A_1+x_2A_2+\cdots+x_nA_n)^n}, \quad (1.108)$$

but we usually obtain shorter analytical expressions using the *Cuskosky cutting rule* which links the imaginary part of a diagram or a scalar integral to the sum of all cut Feynman graphs.

The cut rule is directly related to the unitarity of the S matrix and the optical theorem discussed in Sect. 1.2.2. Limiting ourselves to scalar amplitudes/integrals, the cut rule tells us that the sum of all cut one-loop or squared scalar diagrams has to vanish, including the two external cuts which correspond to the untouched amplitude A and its complex conjugate A^*. This gives us a very useful expression for the imaginary part of the amplitude

$$-i\left(A - A^*\right) = 2\mathrm{Im}A \stackrel{!}{=} 16\pi^2 \sum_{\text{cut graphs}} A. \tag{1.109}$$

The factor $16\pi^2$ corresponds to the integral measure in the scalar integrals which can be arranged such that $d^4q/(i\pi^2)$ gives a typical prefactor of one. Cutting diagrams means replacing all internal propagators by $1/(q^2 - m^2) \to 2\pi\theta(q_0)\delta(q^2 - m^2)$. From this imaginary part we compute the complete amplitude or scalar integral. If we know the pole or cut structure of the amplitude, we can make use of the *Cauchy integral* for a complex analytic function $A(z)$

$$A(z) = \frac{1}{2\pi i} \oint_{\text{counter-clockwise}} dz' \frac{A(z')}{z' - z}, \tag{1.110}$$

and compute the unknown real part of $A(q^2)$ integrating such that the kinematic cut for real values to the right of $q^2 = m_1^2 + m_2^2$ is outside the integration path

$$\begin{aligned}
\mathrm{Re}A(q^2) &= \frac{1}{2\pi i} \oint dq'^2 \, \frac{i\,\mathrm{Im}A(q'^2)}{q'^2 - q^2} \\
&= \frac{1}{2\pi} \int_{(m_1^2+m_2^2)}^{\infty} dq'^2 \, \frac{\mathrm{Im}A(q'^2 + i\varepsilon) - \mathrm{Im}A(q'^2 - i\varepsilon)}{q'^2 - q^2} \\
&\equiv \frac{1}{\pi} \int_{(m_1^2+m_2^2)}^{\infty} dq'^2 \, \frac{\mathrm{Im}_+ A(q'^2)}{q'^2 - q^2}.
\end{aligned} \tag{1.111}$$

This step assumes a sufficiently fast convergence on the integration contour for large momenta. This method of computing for example scalar integrals is known to produce the most compact results.

The finite scalar three point function which appears in our effective coupling Eq. 1.107 has the form

$$
\begin{aligned}
C(0,0,m_H^2;m_t,m_t,m_t) &= \frac{1}{m_H^2}\int_0^1 \frac{dx}{x}\log\left(\frac{m_H^2 x(1-x)-m_t^2}{(-m_t^2)}\right)\\
&= \frac{1}{m_H^2}\int_0^1 \frac{dx}{x}\log\left(1-x(1-x)\frac{m_H^2}{m_t^2}\right)\\
&= \frac{1}{2m_H^2}\log^2\left[-\frac{1+\sqrt{1-4m_t^2/m_H^2}}{1-\sqrt{1-4m_t^2/m_H^2}}\right] \quad \frac{4m_t^2}{m_H^2}\equiv\tau<1.
\end{aligned}
\tag{1.112}
$$

For general top and Higgs masses it reads

$$
\begin{aligned}
C(0,0,m_H^2;m_t,m_t,m_t) &= -\frac{2f(\tau)}{m_H^2}\\
\text{with}\qquad f(\tau) &= \begin{cases} \left[\sin^{-1}\sqrt{\frac{1}{\tau}}\right]^2 & \tau>1 \\ -\frac{1}{4}\left[\log\left(\frac{1+\sqrt{1-\tau}}{1-\sqrt{1-\tau}}\right)-i\pi\right]^2 & \tau<1 \end{cases},
\end{aligned}
\tag{1.113}
$$

including imaginary or absorptive terms for $\tau < 1$. The dimensionless variable τ is the appropriate parameter to describe the behavior of this scalar integral. For example the low-energy limit of the scalar integral, i.e. the limit in which the top loop becomes heavy and cannot be resolved by the external energy of the order of the Higgs mass, will be given by $\tau \gtrsim 1$ which means $m_H < 2m_t$. In contrast to what many people who use such effective vertices assume, the expression in Eq. 1.113 is valid for *arbitrary Higgs and top masses* not just in the heavy top limit.

Expressing our Dirac trace and loop integral in terms of this function $f(\tau)$ we find for our effective coupling in Eq. 1.107

$$
\begin{aligned}
\int \frac{d^4q}{i\pi^2}\frac{P_{T\mu\nu}T^{\mu\nu}}{[...][...][...]} &= \frac{4m_t}{\sqrt{2}}\left(2-\left(4m_t^2-m_H^2\right)\frac{2f(\tau)}{m_H^2}\right)\\
&= \frac{4m_t}{\sqrt{2}}\left(2-2\left(\tau-1\right)f(\tau)\right)\\
&= \frac{8m_t}{\sqrt{2}}\left(1+(1-\tau)f(\tau)\right).
\end{aligned}
\tag{1.114}
$$

Using this result we can as the third and last step of our calculation collect all factors from our Feynman diagram and compute the *effective ggH coupling*

$$
\begin{aligned}
F &= -\,i^3\,(-ig_s)^2\,\frac{im_t}{v}\,\mathrm{Tr}(T^aT^b)\,\frac{i\pi^2}{16\pi^4}\,\frac{8m_t}{\sqrt{2}}\,(1+(1-\tau)f(\tau)) \\
&= \frac{g_s^2 m_t}{v}\,\frac{\delta^{ab}}{2}\,\frac{i}{16\pi^2}\,\frac{8m_t}{\sqrt{2}}\,(1+(1-\tau)f(\tau)) \\
&= \frac{g_s^2}{v}\,\frac{\delta^{ab}}{2}\,\frac{i}{16\pi^2}\,\frac{8}{\sqrt{2}}\,\frac{m_H^2\tau}{4}\,(1+(1-\tau)f(\tau)) \\
&= ig_s^2\,\delta^{ab}\,\frac{1}{16\sqrt{2}\pi^2}\,\frac{m_H^2}{v}\,\tau\;(1+(1-\tau)f(\tau)) \\
&= i\alpha_s\,\delta^{ab}\,\frac{1}{4\sqrt{2}\pi}\,\frac{m_H^2}{v}\,\tau\;(1+(1-\tau)f(\tau)),
\end{aligned}
\tag{1.115}
$$

where the numerical factors originate from the closed fermion loop, the three top propagators, the two top-gluon couplings, the top Yukawa coupling, the color trace, the unmatched loop integration measure, and finally the result computed in Eq. 1.114.

Based on Eq. 1.101 which including prefactors reads

$$
F P_T^{\mu\nu} A_{1\mu} A_{2\nu} = F\,\frac{-G^{\mu\nu}G_{\mu\nu}}{\sqrt{2}m_H^2},
\tag{1.116}
$$

we can include the complete form factor in the effective Lagrangian. This finally defines the Feynman rule we are interested in

$$
\boxed{\mathscr{L}_{ggH} \supset \frac{g_{ggH}}{v}\,HG^{\mu\nu}G_{\mu\nu}} \quad \text{with} \quad g_{ggH} = -i\,\frac{\alpha_s}{8\pi}\,\tau\,[1+(1-\tau)f(\tau)],
\tag{1.117}
$$

dropping the δ^{ab}. It is important to notice that the necessary factor in front of the dimension-5 operator is $1/v$ and not $1/m_t$. This is a particular feature of this coupling, which does not decouple for heavy top quarks because we have included the top Yukawa coupling in the numerator. Without this Yukawa coupling, the heavy top limit $\tau \to \infty$ of the expression would be zero, as we will see in a minute.

Of course, just like we have three-gluon and four-gluon couplings in QCD we can compute the $gggH$ and the $ggggH$ couplings from the ggH coupling simply using gauge invariance. This set of n-gluon couplings to the Higgs boson is again not an approximate result in the top mass. Gauge invariance completely fixes the n-gluon coupling to the Higgs via one exact dimension-5 operator in the Lagrangian. These additional gluon field arise from the commutator of two gluon field in the field strength tensor, so they only exist in non-abelian QCD and cannot be generalized to the photon-photon-Higgs coupling.

1.4.2 Low-Energy Theorem

The general expression for g_{ggH} is not particularly handy, but for light Higgs bosons we can write it in a more compact form. We start with a Taylor series for $f(\tau)$ in the

heavy-top limit $\tau \gg 1$

$$f(\tau) = \left[\sin^{-1}\frac{1}{\tau^{1/2}}\right]^2 = \left[\frac{1}{\tau^{1/2}} + \frac{1}{6\tau^{3/2}} + \mathcal{O}(\tau^{-5/2})\right]^2$$
$$= \frac{1}{\tau} + \frac{1}{3\tau^2} + \mathcal{O}(\tau^{-3}) \overset{\tau\to\infty}{\longrightarrow} 0, \tag{1.118}$$

and combine it with all other τ-dependent terms from Eq. 1.117

$$\begin{aligned}\tau\,[1 + (1-\tau) f(\tau)] &= \tau\left[1 + (1-\tau)\left(\frac{1}{\tau} + \frac{1}{3\tau^2} + \mathcal{O}(\tau^{-3})\right)\right] \\ &= \tau\left[1 + \frac{1}{\tau} - 1 - \frac{1}{3\tau} + \mathcal{O}(\tau^{-2})\right] \\ &= \tau\left[\frac{2}{3\tau} + \mathcal{O}(\tau^{-2})\right] \\ &= \frac{2}{3} + \mathcal{O}(\tau^{-1}), \quad \text{implying} \quad \boxed{g_{ggH} = -i\,\frac{\alpha_s}{12\pi}}\,. \end{aligned} \tag{1.119}$$

In this low-energy or heavy-top limit where we have *decoupled the top quark* from the set of propagating Standard Model particles. The *ggH* coupling does not depend on m_t anymore and gives a finite result. Computing this finite result in Eq. 1.115 we included the top Yukawa coupling in the numerator. We emphasize again that while this low-energy approximation is very compact to analytically write down the effective *ggH* coupling, it is not necessary to numerically compute processes involving the effective *ggH* coupling.

In this low-energy limit we can easily add more Higgs bosons to the loop. Attaching an external Higgs leg to the gluon self energy diagram simply means replacing one of the two top propagators with two top propagators and adding a Yukawa coupling

$$\frac{1}{\not{q} - m_t} \;\mapsto\; \frac{1}{\not{q} - m_t}\,\frac{\sqrt{2}m_t}{v}\,\frac{1}{\not{q} - m_t}. \tag{1.120}$$

This we can compare to a differentiation with respect to m_t

$$\frac{\sqrt{2}m_t}{v}\,\frac{\partial}{\partial m_t}\,\frac{1}{\not{q} - m_t} \sim -\frac{\sqrt{2}m_t}{v}\,\frac{-1}{(\not{q} - m_t)(\not{q} - m_t)} \sim \frac{1}{\not{q} - m_t}\,\frac{\sqrt{2}m_t}{v}\,\frac{1}{\not{q} - m_t}. \tag{1.121}$$

This treatment including a gamma matrix in $\not{q} = \gamma_\mu q^\mu$ is, strictly speaking, nonsense. However, it gives us an idea how we can in the limit of a heavy top derive the ggH^n couplings from the gluon self energy or the *ggH* coupling

$$g_{ggH^{n+1}} = m_t^2\,\frac{\partial}{\partial m_t}\left(\frac{1}{m_t} g_{ggH^n}\right). \tag{1.122}$$

The first two effective couplings with one or two external Higgs legs are the triangular form factor $g_{ggH} = -i\alpha_s/(12\pi)$ and the box form factor $g_{ggHH} = +i\alpha_s/(12\pi)$. To obtain the correct mass dimension each external Higgs field appears as H/v. Using $\log(1+x) = -\sum_{n=1}(-x)^n/n$ we can eventually re-sum this series of effective couplings in the form

$$\boxed{\mathscr{L}_{ggH} = G^{\mu\nu}G_{\mu\nu}\,\frac{\alpha_s}{\pi}\left(\frac{H}{12v} - \frac{H^2}{24v^2} + \cdots\right) = \frac{\alpha_s}{12\pi}\,G^{\mu\nu}G_{\mu\nu}\log\left(1+\frac{H}{v}\right)}\,. \tag{1.123}$$

In Sect. 1.2.2 we note that there should be a relative factor between the Lagrangian and the Feynman rule accounting for more than one way to identify the external legs of the Feynman rule with the fields in the Lagrangian. For n neutral Higgs fields the effective coupling has to include a factor of $1/n$ which is precisely the denominator of the logarithm's Taylor series.

Such a closed form of the Lagrangian is very convenient for simple calculations and gives surprisingly exact results for the $gg \to H$ production rate at the LHC, as long as the Higgs mass does not exceed roughly twice the top mass. However, for example for $gg \to H+$ jets production its results only hold in the limit that *all* jet momenta are much smaller than m_t. It also becomes problematic for example in the $gg \to HH$ process close to threshold, where the momenta of slow-moving Higgs bosons lead to an additional scale in the process. We will come back to this process later.

1.4.3 Signatures

To discuss the Higgs production for example in gluon fusion we would normally need to know how to deal with gluons inside the incoming protons, how to parameterize the phase space of the Higgs decay products, and how to kinematically distinguish interesting events from others. All of this we will piece by piece introduce in Sect. 2.1. In contrast, throughout the following sections on Higgs production at the LHC we will limit ourselves to some very basic phenomenological features and postpone any discussion on how to compute these features.

Without knowing any theoretical particle physics we can discuss the main feature or problem of hadron collider physics: there is no such thing as a signal without a background. More precisely, there is no kinematic configuration which is unique to a signal event and cannot appear as an unlucky combination of uninteresting Standard Model or QCD processes and detector effects. This implies that any LHC measurement will always be a *statistics exercise* in some kind of event counting combined with a probability estimate on the signal nature of a given event.

The first quantity we can compute and analyze at colliders is the total number of events expected from a certain production process in a given time interval. This

number of events is the product of the proton–proton LHC luminosity measured in inverse femtobarns, the total production cross section measured in femtobarns, and the detection efficiency measured in per-cent. In other words, a predicted event event rate it is split into a collider-specific number describing the initial state, a process-specific number describing the physical process, and a detector-specific efficiency for each particle in the final state.

The latter is the easiest number to deal with: over the sensitive region of the detector, the fiducial volume, the detection efficiency is a set of numbers depending on the nature of the detected particle and its energy. This number is very good for muons, somewhere between 90 and 100%, and less than 1/3 for tau leptons. Other particles typically range somewhere in between.

For theorists luminosity is simply a conversion number between cross sections which we compute for a living and event numbers. People who build colliders use units involving seconds and square meters, but for us inverse femtobarns work better. Typical numbers are: a typical year of LHC running at design luminosity could deliver up to 10 inverse femtobarns per year in the first few years and three to ten times that later. At the end of 2011 one inverse femtobarn is a realistic estimate. The key numbers and their orders of magnitude for typical signals are

$$N_{\text{events}} = \sigma_{\text{tot}} \cdot \mathscr{L} \qquad \mathscr{L} = 10 \cdots 300\,\text{fb}^{-1} \qquad \sigma_{\text{tot}} = 1 \cdots 10^4\,\text{fb}. \tag{1.124}$$

Different cross sections for Tevatron and LHC processes are shown in Fig. 1.5.

Finally, talking about cross sections and how to compute them we need to remember that at the LHC there exist two kinds of processes. The first involves all particles which we know and love, like old-fashioned electrons or slightly more modern W and Z bosons or most recently top quarks. All of these processes we call *backgrounds*. They are described by QCD, which means QCD is the theory of the evil. Top quarks have an interesting history, because when I was a graduate student they still belonged to the second class of processes, the *signals*. These either involve particles we have not seen before or particles we want to know something about. Such new particles are usually produced via QCD effects as well, so QCD as we will discuss it in Chap. 2 is not entirely evil. If we actually see new particles someone gets the Nobel prize, while for the rest of the community the corresponding processes instantly turn into backgrounds.

Because signals are things we had not seen before they are rare compared to much more rare that backgrounds. Digging out signal events from a large number of background events is what the remaining Higgs section will be about. Figure 1.5 shows that at the LHC the production cross section for a pair of bottom quarks is larger than 10^5 nb or 10^{11} fb, the typical production rate for W or Z bosons ranges around 200 nb or 2×10^8 fb, the rate for a pair of 500 GeV supersymmetric gluinos is 4×10^4 fb, and the Higgs rate can be as big as 2×10^5 fb. To extract such signals from huge backgrounds we need to describe the backgrounds with an incredible precision, at least those background events which populate the signal region in phase space. The high-energy community has agreed that we call a five sigma excess over the known backgrounds a signal discovery

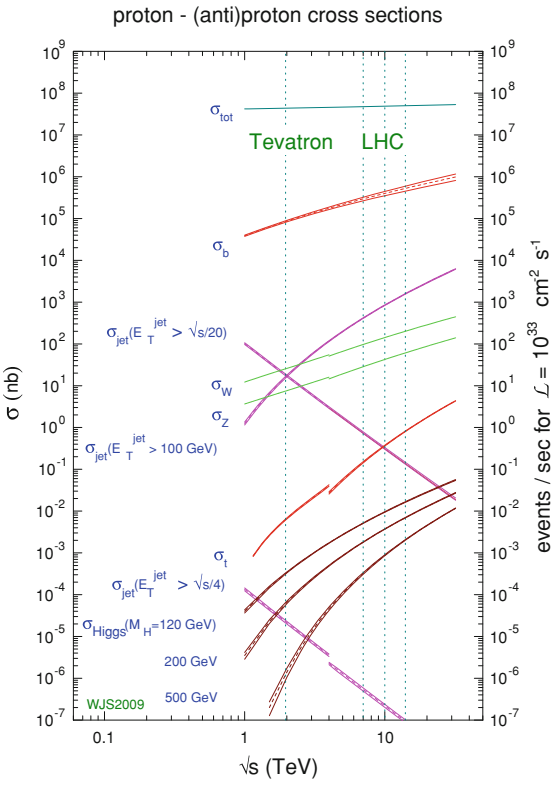

Fig. 1.5 Production rates for signal and background processes at hadron colliders. The discontinuity is due to the Tevatron being a proton–antiproton collider while the LHC is a proton–proton collider. The two colliders correspond to the x–axis values of 2 TeV and something between 7 and 14 TeV. Figure from Ref. [5]

$$\begin{aligned} \frac{S}{\sqrt{B}} &= N_\sigma > 5 && \text{(Gaussian limit)} \\ P_{\text{fluct}} &< 5.8 \times 10^{-7} && \text{(fluctuation probability).} \end{aligned} \tag{1.125}$$

Never trust anybody who wants to sell you a three sigma evidence as a discovery, because everyone who has been around for a few years has seen a great number of those go away. People usually have some kind of reason to advertize such effects, but all they are really saying is that their errors do not allow them to make a conclusive statement. On the other hand, in the Gaussian limit the statistical significance improves with $\sqrt{\mathcal{L}}$. So all we need to do is wait for the significance to hit five sigma.

One last aspect we have to at least mention is the *trigger*. Because of the sheer mass of data at the LHC, we will not be able to write every LHC event on tape. As a matter of fact, we could not even write every top pair event on tape. Instead, we have to decide very fast if an event has the potential of being interesting in the light of the physics questions we are asking at the LHC. Only these events we keep. Before there is a mis-understanding: while experimentalists are reluctant to change triggers these are not carved in stone, so as a functioning high energy physics community we will not miss great new physics just because we forgot to include it in the trigger menu.

For now we can safely assume that above an energy threshold we will keep all events with leptons or photons, plus as much as we can events with missing energy (i.e. neutrinos in the Standard Model and dark matter particles in new-physics models) and jets with high energy coming from resonance decays. This trigger menu reflects the general attitude that the LHC is not built to study QCD, and that very soft final states for example from bottom decays are best studied in the LHCb experiment instead of ATLAS and CMS.

With this minimal background of collider phenomenology we can look at Higgs production in gluon fusion, combined with different Higgs decays. The total Higgs production cross section through the loop induced ggH coupling we show in Fig. 1.4. For a reasonably light Higgs boson the cross section ranges around at least 30 pb, which for relevant luminosities starting around 30 fb^{-1} means 10^6 events. The question is: after multiplying with the relevant branching ratio and detection efficiencies, which of the decays can be distinguished from the Standard Model background statistically? Since gluon fusion really only produces the Higgs boson the details of the production process do not help much with the background suppression. The results of experimental simulations, for example by the ATLAS collaboration, are shown in Fig. 1.6. The complete list of possible Higgs decays, ordered by decreasing branching ratio according to Fig. 1.3, is:

- $gg \to H \to b\bar{b}$ is hopeless, because of sheer size of the QCD continuum background $gg \to b\bar{b}$, which according to Fig. 1.5 exceeds the signal by roughly eight orders of magnitude. There is little to cut on except for the invariant mass of the $b\bar{b}$ pair with an $\mathcal{O}(10\%)$ mass resolution. What makes things worse, this channel will as it stands not be triggered on.
- $gg \to H \to \tau^+\tau^-$ is problematic, because of the low velocity of the Higgs which makes the reconstruction of $m_{\tau\tau} \sim m_H$ hard. We will discuss this decay and its reconstruction in detail in Sect. 1.5.3. It is widely assumed that Higgs production in gluon fusion is too close to threshold to see the decay to tau leptons, but this might still change.
- $gg \to H \to \gamma\gamma$ is, in spite of the small rate, very promising. Because $m_{\gamma\gamma}$ can be reconstructed to $\mathcal{O}(1\%)$ this observable has incredibly precise side bins to the left and the to right of the Higgs peak. This is what for example the electromagnetic calorimeter of CMS has been designed for. The main problem is backgrounds for example from pions mistaken for photons, while theory input will play no role in this analysis. Moreover, the peak in the invariant mass of the photons is great to measure the *Higgs mass*: once we see a Gaussian peak we can determine its central value with a precision of $\Gamma_{\text{detector}}/\sqrt{S}$ (in a signal dominated sample with S signal events), i.e. at the per-mille level.
- $gg \to H \to W^+W^-$ has a large rate, but once one of the W bosons decays leptonically the Higgs mass is hard to reconstruct. All we can do is reconstruct a transverse mass variable, which we discuss in Sect. 3.3. On the other hand, the backgrounds are electroweak and therefore small. The most promising analysis relies on angular correlations—if the two gauge bosons come from a spin-zero resonance they have to have opposite polarization; because the W coupling to

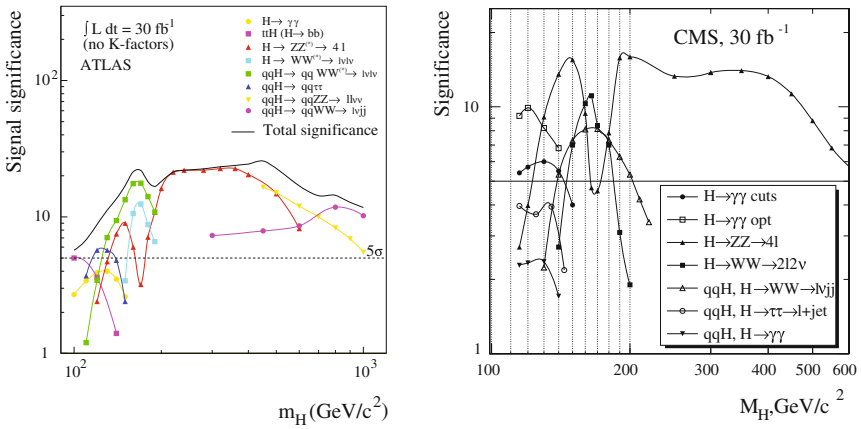

Fig. 1.6 Simulated statistical significance for different Higgs production and decay channels for an integrated luminosity of 30 fb^{-1} (*left* ATLAS [6]; *right* CMS [7]). Five standard deviations over the backgrounds are required for discovery

fermions is purely left handed this implies that the two leptons prefer to move into the same direction as opposed to back-to-back. Because there is not much more to cut on the expected significance drops sharply with the decreasing branching ratio once we require off-shell W decays.

- $gg \to H \to ZZ$ works great for ZZ to four leptons, in particular muons, because of the fully reconstructed $m_{4L_l l} \sim m_{ZZ} \sim m_H$. Of all Higgs channels it requires the least understanding of the LHC detectors. Therefore it is referred to as *golden channel*. Its limitation are the leptonic Z branching ratio and the sharp drop in the off-shell Higgs branching ratio towards smaller Higgs masses. The semi-leptonic decay of the Z pair might work once we ask for a boosted hadronically decaying Z, as we will discuss in Sect. 3.1.2.
- $gg \to H \to Z\gamma$ is a little like $\gamma\gamma$, but with a smaller rate and a further reduced branching ratio of $Z \to \mu^+\mu^-$ or $Z \to e^+e^-$. Instead of combining the advantages of $H \to ZZ$ and $H \to \gamma\gamma$ this channel combines more of the disadvantages, so it is not likely to be helpful. Of course, as for any channel seeing it will give us more information on the Higgs boson, so we should not give up.
- $gg \to H \to$ invisible is not predicted in Standard Model; it is obviously hopeless if only the Higgs is produced, because we would be trying to extract a signal of missing energy and nothing else. 'Absolutely nothing' in addition to some QCD remnant is not a good signature for the trigger.

1.5 Higgs Production in Weak Boson Fusion

Going back to Fig. 1.4 we see that while gluon fusion gives the largest Higgs production rate at the LHC, there are other promising channels to study. In the Standard Model the Higgs has sizeable couplings only to the W and Z bosons and to the top quark, so instead of via the top Yukawa coupling we can produce Higgs bosons via their gauge boson couplings. This induces two channels, the larger of which is weak boson fusion $qq \to qqH$: two incoming quarks each radiate a W or Z boson which merge and form a Higgs. Because the LHC is a pp collider and because the proton mostly contains the valence quarks (uud) and low-x gluons it is important that this process can proceed as $ud \to duH$, where the u radiates a W^+ and the d radiates a W^-. The Feynman diagram for this process is

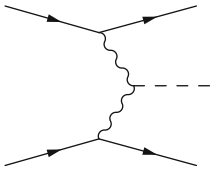

If the Higgs were a Z boson, it could also bremsstrahlung off the incoming or outgoing quarks, but for Higgs production at colliders we safely assume that the first two generation fermions are massless. That is at least unless we discuss a muon collider as a specific way to produce Higgs bosons.

In a way, weak boson fusion looks like double deep inelastic scattering, one from each of the protons. This is one of the key observations which in Sect. 1.5.2 we will use for background suppression via the central jet veto. The double deep inelastic scattering approximation is also a good way to compute corrections to the weak boson fusion production rate, at least provided we neglect kinematic distributions

1.5.1 Production Kinematics

In the Feynman diagrams for weak-boson fusion Higgs production we encounter intermediate massive gauge boson propagators. They induce a particular shape of the kinematic distributions of the final state jet. First, we need to quote the exact calculation showing that in the matrix element squared we will usually find one power of p_T in the numerator. With this information we can look for the maximum in the $p_{T,j} = p_{T,W}$ spectrum as a function of the momentum in the beam direction, p_3, and the absolute value of the two-dimensional transverse momentum p_T

$$
\begin{aligned}
0 &\stackrel{!}{=} \frac{\partial}{\partial p_T} \frac{p_T}{E^2 - p_T^2 - p_3^2 - m_W^2} \\
&= \frac{1}{E^2 - p_T^2 - p_3^2 - m_W^2} + p_T \frac{(-1)}{(E^2 - p_T^2 - p_3^2 - m_W^2)^2} (-2p_T) \\
&= \frac{E^2 + p_T^2 - p_3^2 - m_W^2}{(E^2 - p_T^2 - p_3^2 - m_W^2)^2} \\
&\sim \frac{C m_W^2 + p_T^2 - m_W^2}{(E^2 - p_T^2 - p_3^2 - m_W^2)^2} \quad \text{with } E^2 \sim p_3^2 \gg m_W^2 \text{ but } E^2 - p_3^2 = C\, m_W^2 \\
&= \frac{p_T^2 - (1-C) m_W^2}{(E^2 - p_T^2 - p_3^2 - m_W^2)^2} \\
\Leftrightarrow \quad & \boxed{p_T^2 = (1-C) m_W^2}
\end{aligned}
\tag{1.126}
$$

for some number $C < 1$. This admittedly hand-waving argument shows that in weak-boson-fusion Higgs production the transverse momenta of the outgoing jets peak at values below the W mass. In reality, the peak occurs around $p_T \sim 30\,\text{GeV}$. This transverse momentum scale we need to compare to the longitudinal momentum given by the energy scale of valence quarks at the LHC, i.e. several hundreds of GeV.

These two forward jets are referred to as *tagging jets*. They offer a very efficient cut against QCD backgrounds: because of their back-to-back geometry and their very large longitudinal momentum, their invariant mass m_{jj} will easily exceed a TeV. For any kind of QCD background this will not be the case. Compared to Higgs production in gluon fusion the tagging jets are an example how features of the production process which have little or nothing to do with the actual Higgs kinematics can help reduce backgrounds—the largest production rate does not automatically yield the best discovery prospects.

Moving on to the Higgs kinematics, in contrast to the jets the Higgs and its decay products are expected to hit the detector centrally. So we are looking for two forward jets and for example two τ leptons or two W bosons in the central detector. Last but not least, the Higgs is produced with finite transverse momentum which is largely determined by the kinematic and the acceptance cuts on the forward jets and their typical transverse momentum scale $p_{T\,H} \sim m_W$.

Compared to the Higgs production in gluon fusion we buy this distinctive signature and its efficient extraction from the background at the expense of the rate. Let us start with the partonic cross sections: the one-loop amplitude for $gg \to H$ is suppressed by $\alpha_s y_t/(4\pi) \sim (1/10)(2/3)(1/12) = 1/180$. For the production cross section this means a factor of $(1/180)^2 \sim 1/40000$. The cross section for weak boson fusion is proportional to g^6, but with two additional jets in the final state. Including the additional phase-space for two jets this roughly translates into $(2/3)^6 1/(16\pi)^2 = (64/729)(1/2500) \sim 1/25000$. These two numbers governing the main LHC production cross sections roughly balance each other.

The difference in rate which we see in Fig. 1.4 instead arises from the quark and gluon luminosities. In weak boson fusion the two forward jets always combine to a large partonic center-of-mass energy $x_1 x_2 s > (p_{j,1} + p_{j,2})^2 = 2(p_{j,1} p_{j,2})$, with the two parton momentum fractions $x_{1,2}$ and the hadronic center of mass energy $\sqrt{s} = 14\,\text{TeV}$. Producing a single Higgs in gluon fusion probes the large gluon parton density at typical parton momentum fractions $x \sim m_H/\sqrt{s} \sim 10^{-3}$. This means that each of the two production processes with their specific incoming partons probes its most favorable parton momentum fraction: low-x for gluon fusion and high-x for valence quark scattering. Looking at typical LHC energies, the gluon parton density grows very steeply for $x \lesssim 10^{-2}$. This means that gluon fusion wins: for a 150 GeV Higgs the gluon fusion rate of $\sim 30\,\text{pb}$ clearly exceeds the weak boson fusion rate of $\sim 4\,\text{pb}$. On the other hand, these numbers mean little when we battle an 800 pb $t\bar{t}$ background relying on kinematic cuts either on forward jets or on Higgs decay products.

In Fig. 1.6 we see that for large Higgs mass the weak boson fusion rate approaches the gluon fusion rate. The two reasons for this behavior we mentioned already in this section: first of all, for larger x values the rate for $gg \to H$ decreases steeply with the gluon density, while in weak boson fusion the already huge partonic center of mass energy due to the tagging jets ensures that an increase in m_H makes no difference anymore. Even more importantly, there appear *large logarithms* because the low-p_T enhancement of the quark-W splitting. If we neglect m_W in the weak boson fusion process the $p_{T,j}$ distributions will diverge for small $p_{T,j}$ like $1/p_{T,j}$, as we will see in Sect. 2.3.3. After integrating over $p_{T,j}$ this yields a $\log p_{T,j}^{\max}/p_{T,j}^{\min}$ dependence of the total rate. With the W mass cutoff and a typical hard scale given by m_H this logarithm becomes

$$\sigma_{\text{WBF}} \propto \left(\log \frac{p_{T,j}^{\max}}{p_{T,j}^{\min}}\right)^2 \sim \left(\log \frac{m_H}{m_W}\right)^2 . \tag{1.127}$$

For $m_H = \mathcal{O}(\text{TeV})$ this logarithm gives us an enhancement by factors of up to 10, which makes weak boson fusion the dominant Higgs production process.

Motivated by such logarithms, we will talk about partons inside the proton and their probability distributions for given momenta in Sect. 2.3.3. In the *effective W approximation* we can resum the logarithms appearing in Eq. 1.127 or compute such a probability for W bosons inside the proton. This number is a function of the partonic momentum fraction x and can be evaluated as a function of the transverse momentum p_T. Because the incoming quark inside the proton has negligible transverse momentum, the transverse momenta of the W boson and the forward jet are identical. These transverse momentum distributions in $p_{T,W} = p_{T,j}$ look different for transverse and longitudinal gauge bosons

$$
\begin{aligned}
P_T(x, p_T) &\sim \frac{g_V^2 + g_A^2}{4\pi^2} \frac{1 + (1-x)^2}{2x} \frac{p_T^2}{(p_T^2 + (1-x)m_W^2)^2} \\
&\to \frac{g_V^2 + g_A^2}{4\pi^2} \frac{1 + (1-x)^2}{2x} \frac{1}{p_T^2} \\
P_L(x, p_T) &\sim \frac{g_V^2 + g_A^2}{4\pi^2} \frac{(1-x)^2}{x} \frac{m_W^2}{(p_T^2 + (1-x)m_W^2)^2} \\
&\to \frac{g_V^2 + g_A^2}{4\pi^2} \frac{(1-x)^2}{x} \frac{m_W^2}{p_T^4}.
\end{aligned} \tag{1.128}
$$

The couplings $g_{A,V}$ describe the gauge coupling of the W bosons to the incoming quarks. Looking at large transverse momenta $p_T \gg m_W$ the radiation of longitudinal W bosons falls off sharper than the radiation of transverse W bosons. This different behavior of transverse and longitudinal W bosons is interesting, because it allows us to gain information on the centrally produced particle and which modes it couples to just from the transverse momentum spectrum of the forward jets and without looking at the actual central particle.

The problem with the effective W approximation is that it is a poor description of Higgs production at the LHC. The simple reason is that the Higgs mass is of the order of the W mass, as are the transverse momenta of the W and the final state jets, and none of them are very small. Neglecting for example the transverse momentum of the W bosons or the final-state jets will not give us useful predictions for the kinematic distributions, neither for the tagging jets nor for the Higgs. For the SSC, the competing design to the LHC in Texas which unfortunately was never built, this might have been a different story, but at the LHC we should not describe W bosons (or for that matter top quarks) as essentially massless partons inside the proton.

1.5.2 Jet Ratios and Central Jet Veto

From the Feynman diagram for weak boson fusion we see that the diagram describing a gluon exchange between the two quark lines multiplied with the Born diagram is proportional to the color factor $\mathrm{Tr}T^a \mathrm{Tr}T^b \delta^{ab} = 0$. The only way to avoid this suppression is the interference of two identical final-state quarks, for example in ZZ fusion. First, this does not involve only valence quarks and second, this assumes a phase space configuration where one of the two supposedly forward jets turns around and goes backwards, so the interfering diagrams contribute in the same phase spare region. This means that virtual gluon exchange in weak boson fusion is practically absent.

In Chap. 2 we will see that virtual gluon exchange and real gluon emission are very closely related. Radiating a gluon off any of the quarks in the weak boson fusion process will lead to a double infrared divergence, one because the gluon can be radiated at small angles and one because the gluon can be radiated with vanishing energy. The divergence at small angles is removed by redefining the quark parton

densities in the proton. The soft divergence has to cancel between real gluon emission and virtual gluon exchange. However, if virtual gluon exchange does not appear, non-collinear gluon radiation cannot appear either. This means that additional QCD jet activity as part of the weak boson fusion process is limited to collinear radiation, i.e. radiation along the beam line or at least in the same direction as the far forward tagging jets. Gluon radiation into the central detector is suppressed by the color structure of the weak boson fusion process.

While it is not immediately clear how to quantify such a statement it is a very useful feature, for example looking at the top pair backgrounds. The $WWb\bar{b}$ final state as a background to $qqH, H \to WW$ searches includes two bottom jets which can mimic the signal's tagging jets. At the end, it turns out that it is much more likely that we will produce another jet $pp \to t\bar{t}$+jet so only one of the two bottom jets from the top decays needs to be forward. In any case, the way to isolate the Higgs signal is to look at additional central jets.

As described above, for the signal additional jet activity is limited to small-angle radiation off the initial-state and final-state quarks. For background like top pairs this is not the case, which means we can reduce all kinds of background by vetoing jets in the central region above $p_{T,j} \gtrsim 30$ GeV. This strategy is referred to as central jet veto or *mini-jet veto*. Note that it has nothing to do with rapidity gaps at HERA or pomeron exchange, it is a QCD feature completely accounted for by standard perturbative QCD.

From QCD we then need to compute the probability of not observing additional central jets for different signal and background processes. Postponing the discussion of QCD parton splitting to Sect. 2.3.2 we already know that for small transverse momenta the $p_{T,j}$ spectra for massless states will diverge, as shown in Eq. 1.127. Looking at some kind of n-particle final state and an additional jet radiation we can implicitly define a reference point p_T^{crit} at which the diverging rate for one jet radiation σ_{n+1} starts to exceed the original rate σ_n, whatever the relevant process might be

$$\sigma_{n+1}(p_T^{\text{crit}}) = \int_{p_T^{\text{crit}}}^{\infty} dp_{T,j} \, \frac{d\sigma_{n+1}}{dp_{T,j}} \stackrel{!}{=} \sigma_n . \tag{1.129}$$

This condition defines a point in p_T below which our perturbation theory in α_s, i.e. in counting the number of external partons, breaks down. For weak boson fusion Higgs production we find $p_T^{\text{crit}} \sim 10\,\text{GeV}$, while for QCD processes like $t\bar{t}$ production it becomes $p_T^{\text{crit}} = 40\,\text{GeV}$. In other words, jets down to $p_T = 10$ GeV are perturbatively well defined for Higgs signatures, while for the QCD backgrounds jets below 40 GeV are much more frequent than they should be looking at the perturbative series in α_s. This fixes the p_T range where a central jet veto will be helpful to reject backgrounds

$$p_{T,j} > 30\,\text{GeV} \qquad \text{and} \qquad \eta_j^{(\text{tag } 1)} < \eta_j < \eta_j^{(\text{tag } 2)} . \tag{1.130}$$

The second condition reminds us of the fact that only central jets will be rare in weak boson fusion. The smaller the p_T threshold the more efficient the central jet veto

becomes, but at some point experimental problems as well as non-perturbative QCD effects will force us to stay above 20 or 30 or even 40 GeV.

If we assign a probability pattern to the radiation of jets from the core process we can compute the *survival probability* of such a jet veto. If we assume that we can describe successive jet radiation using Poisson statistics the probability of observing exactly n jets given an expected n_0 jets is

$$f(n;n_0) = \frac{n_0^n e^{-n_0}}{n!} \quad \Rightarrow \quad \boxed{f(0;n_0) = e^{-n_0}}. \tag{1.131}$$

This defines the so-called exponentiation model. We consistently fix the expectation value in terms of the inclusive cross sections producing at least zero or at least one jet,

$$n_0 = \frac{\sigma_1(p_T^{\min})}{\sigma_0}. \tag{1.132}$$

This ensures that the inclusive jet ratio σ_1/σ_0 is reproduced by the ratio of the corresponding Poisson distributions. In Sect. 2.3.4 we will see why such inclusive cross sections for the production of a certain final state together with an unspecified number of jets is an appropriate observable. Only in Sect. 2.5.3 we will actually be able to formulate observables for final states with a fixed number of jets. Including this expectation value n_0 into Eq. 1.131 returns a veto survival probability of $\exp(-\sigma_1/\sigma_0)$. This comes out roughly as 88% for the weak boson fusion signal and as 24% for the $t\bar{t}$ background. For the signal-to-background ratio this is an increase by a factor three.

An alternative model starts from a constant probability of radiating a jet, which in terms of the inclusive cross sections σ_j, i.e. the production rate for the radiation of at least j jets, reads

$$\frac{\sigma_{j+1}(p_T^{\min})}{\sigma_j(p_T^{\min})} = P_{\text{rad}}(p_T^{\min}). \tag{1.133}$$

The expected number of jets is then given by

$$\begin{aligned} n_0 &= \frac{1}{\sigma_0} \sum_{j=1} j(\sigma_j - \sigma_{j+1}) = \frac{1}{\sigma_0} \left(\sum_{j=1} j\sigma_j - \sum_{j=2} (j-1)\sigma_j \right) = \frac{1}{\sigma_0} \sum_{j=1} \sigma_j \\ &= \frac{\sigma_1}{\sigma_0} \sum_{j=1} P_{\text{rad}}^j = \frac{P_{\text{rad}}}{1 - P_{\text{rad}}}, \end{aligned} \tag{1.134}$$

which, assuming the series converges, turns into a requirement on $p_T^{\min}$. Radiating jets with a constant probability has been observed at many experiments, including most recently the LHC, and is in the context of W+jets referred to as staircase scaling. Some advanced simulational results we will discuss in Sect. 2.5.3. Even without

saying anything on how to calculate exclusive processes with a fixed number of jets we can derive a particular property of the constant probability of staircase scaling: the ratios of the $(n+1)$-jet rate to the n-jet rate for inclusive and exclusive jet rates are identical. We can see this by computing the inclusive P_{rad} in terms of exclusive jet rates

$$\begin{aligned} P_{\text{rad}} = \frac{\sigma_{n+1}}{\sigma_n} &= \frac{\sum_{j=n+1}^{\infty} \sigma_j^{(\text{excl})}}{\sigma_n^{(\text{excl})} + \sum_{j=n+1}^{\infty} \sigma_j^{(\text{excl})}} \\ &= \frac{\sigma_{n+1}^{(\text{excl})} \sum_{j=0}^{\infty} P_{\text{excl}}^j}{\sigma_n^{(\text{excl})} + \sigma_{n+1}^{(\text{excl})} \sum_{j=0}^{\infty} P_{\text{excl}}^j} \qquad \text{with} \quad P_{\text{excl}} = \frac{\sigma_{n+1}^{(\text{excl})}}{\sigma_n^{(\text{excl})}} \\ &= \frac{\frac{P_{\text{excl}} \sigma_n^{(\text{excl})}}{1-P_{\text{excl}}}}{\sigma_n^{(\text{excl})} + \frac{P_{\text{excl}} \sigma_n^{(\text{excl})}}{1-P_{\text{excl}}}} = \frac{P_{\text{excl}}}{1 - P_{\text{excl}} + P_{\text{excl}}} \\ &= P_{\text{excl}}. \end{aligned} \tag{1.135}$$

Using this result we can check the validity of the Poisson ansatz from Eq. 1.131 for staircase scaling

$$\frac{\sigma_{n+1}^{(\text{excl})}}{\sigma_n^{(\text{excl})}} \overset{\text{Poisson}}{=} \frac{n_0^n (n+1)!}{n! n_0^{n+1}} = \frac{n+1}{n_0} = (n+1)\frac{1-P_{\text{rad}}}{P_{\text{rad}}} \neq P_{\text{rad}}, \tag{1.136}$$

so the exponentiation model does not correspond to a constant probability of radiating jets, i.e. to staircase scaling.

To show that the exponentiation model and staircase scaling are not the only assumptions we can make to compute jet rates we show yet another, but similar ansatz which tries to account for an increasing number of legs to radiate jets off. Based on

$$\frac{\sigma_{j+1}(p_T^{\min})}{\sigma_j(p_T^{\min})} = \frac{j+1}{j} P_{\text{rad}}(p_T^{\min}), \tag{1.137}$$

the expectation for the number of jets radiated gives, again following Eq. 1.134

$$\begin{aligned} n_0 &= \frac{1}{\sigma_0} \sum_{j=1} \sigma_j = \frac{1}{\sigma_0} \sigma_0 \sum_{j=1} j P_{\text{rad}}^j \\ &= P_{\text{rad}} \sum_{j=1} j P_{\text{rad}}^{j-1} = \frac{P_{\text{rad}}}{(1-P_{\text{rad}})^2}. \end{aligned} \tag{1.138}$$

All of these models are more or less well motivated statistical approximations. The do not incorporate experimental effects or the non-perturbative underlying event, i.e. additional energy dependent but process independent jet activity in the detectors from many not entirely understood sources. For many reasons none of them is guaranteed to give us the correct numbers. By the time we get to Sect. 2.5.3 we will be able to more accurately describe the central jet veto in QCD.

1.5.3 Decay Kinematics and Signatures

The sizeable transverse momentum of the decaying Higgs boson in the weak boson fusion process allows us to reconstruct the invariant mass of a $\tau\tau$ system in the *collinear approximation*: if we assume that a τ with momentum $\vec{p}$ decays into a lepton with the momentum $x\,\vec{p}$ and a neutrino, both moving into the same direction as the tau, we can write the two-dimensional transverse momentum of the two taus from the Higgs decay in two ways

$$\vec{p}_1 + \vec{p}_2 \equiv \frac{\vec{k}_1}{x_1} + \frac{\vec{k}_2}{x_2} \stackrel{!}{=} \vec{k}_1 + \vec{k}_2 + \not{\vec{k}}. \tag{1.139}$$

The missing transverse momentum $\not{\vec{k}}$ is the measured vector sum of the two neutrino momenta. This equation is useful because we can measure the missing energy vector at the LHC in the transverse plane, i.e. as two components, which means Eq. 1.139 is really two equations for the two unknowns x_1 and x_2. Skipping the calculation of solving these two equations for $x_1 x_2$ we quote the result for the invariant $\tau\tau$ mass

$$\boxed{m_{\tau\tau} = 2(p_1 p_2) = 2\frac{(k_1 k_2)}{x_1 x_2}}\,, \tag{1.140}$$

which for the signal has to correspond to the Higgs mass. From the formula above it is obvious that this approximation does not only require a sizeable $p_i \gg m_\tau$, but also that back-to-back taus will not work—the two vectors contributing to $\not{\vec{k}}$ then largely cancel and the computation fails. This is what happens for the production channel $gg \to H \to \tau\tau$, where the Higgs boson is essentially produced at rest.

Again, we can make a list of *signatures* which work more or less well in connection to weak boson fusion production. These channels are also included in the summary plot by ATLAS, shown in Fig. 1.6.

- $qqH, H \to b\bar{b}$ is problematic because of large QCD backgrounds and because of the trigger in ATLAS. The most worrisome background is overlapping events, one producing the two tagging jets and the other one two bottom jets. This overlapping scattering gives a non-trivial structure to the background events, so a brute force side-bin analysis will not work.
- $qqH, H \to \tau\tau$ can be a discovery channel for a light Higgs boson with $m_H \lesssim 130\,\text{GeV}$. The approximate mass reconstruction might be as good as $\sim$5 GeV. This channel is particularly useful in scenarios beyond the Standard Model, like its minimal supersymmetric extension. It guarantees the discovery of one Higgs boson over the entire supersymmetric parameter space without a dedicated SUSY search.
- $qqH, H \to \gamma\gamma$ should be compatible with $gg \to H \to \gamma\gamma$ with its smaller rate but improved background suppression. It is included in inclusive $H \to \gamma\gamma$ analyses, and for neural net analyses zooming in on large Higgs transverse momenta it will dominate the inclusive analysis.

- $qqH, H \to Z\gamma$ is difficult due to a too small event rate and no apparent experimental advantages.
- $qqH, H \to WW$ is a *discovery channel* for $m_H \gtrsim 135\,\text{GeV}$. In contrast to $gg \to H \to WW$ it also works for off-shell W decays, i.e. for Higgs masses below 150 GeV. This is where a multitude of background rejection cuts and a better signal-to-background ratio win over the large rate in gluon fusion.
- $qqH, H \to ZZ$ is likely to work in spite of the smaller rate compared to gluon fusion. It might even be possible with one hadronic Z decay, but there are not many detailed studies available.
- $qqH, H \to$ invisible is the only discovery channel for an invisible Higgs which really works at the LHC. It relies on the pure tagging-jet signature, which means it is seriously hard and requires a very good understanding of the detector and of QCD effects.

Just a side remark for younger LHC physicists: weak boson fusion was essentially unknown as a production mode for light Higgses until around 1998 and started off as a very successful PhD project. This meant that for example the Higgs chapter in the ATLAS TDR had to be re-written. While it sometime might appear that way, there is no such thing as a completely understood field of LHC physics. Every aspect of LHC physics continuously moves around and your impact only depends on how good your ideas and their technical realizations are.

1.6 Associated Higgs Production

In Fig. 1.4 there appears a third class of processes at smaller rates: associated Higgs production with heavy Standard Model particles, like W or Z bosons or $t\bar{t}$ pairs. Until the summer of 2008 the Higgs community at the LHC was convinced that (a) we would not be able to make use of WH and ZH production at the LHC and (b) we would not be able to see most of the light Higgs bosons produced at the LHC, because $H \to b\bar{b}$ is no promising signature in gluon fusion or weak boson fusion production.

One key to argument (a) are the two different initial states for signal and background: at the Tevatron the processes $q\bar{q} \to ZH$ and $q'\bar{q} \to WH$ arise from valence quarks. At the LHC with its proton-proton beam this is not possible, so the signal rate will suffer when we go from Tevatron to LHC. The QCD background at leading order is $q\bar{q} \to Zg^* \to Zb\bar{b}$ production, with an off-shell gluon splitting into a low mass bottom quark pair. At next-to-leading order, we also have to consider the t-channel process $q\bar{q} \to Z\bar{b}bg$ and its flipped counter part $qg \to Z\bar{b}bq$. This background becomes more dangerous for larger initial state gluon densities. Moving from Tevatron to LHC the Higgs signal will decrease while the background increases—not a very promising starting point.

With Ref. [8] the whole picture changed. We will discuss this search strategy in detail in Sect. 3.1.2 in the context of jets and jet algorithms at the LHC. It turns out

that searches for *boosted Higgs bosons* are not only promising in the $VH, H \to b\bar{b}$ channel, but might also resurrect the $t\bar{t}H, H \to b\bar{b}$ channel. These new channels are not yet included in the ATLAS list of processes shown in Fig. 1.6 because the simulations are still at an early stage. But we can expect them to play a role in LHC searches for a light Higgs boson.

This is another example of what is possible and what not in LHC phenomenology: it all really depends only on how creative you are; that even applies to a field like Standard Model Higgs searches, which is supposedly studied to death.

1.7 Beyond Higgs Discovery

The prime goal of the LHC is to discover a new light scalar particle which we would suspect to be the Higgs boson. However, the Standard Model makes many predictions concerning the properties of a Higgs boson; as a matter of fact, all its properties except for its mass are fixed in the minimal one-doublet Higgs sector of the Standard Model. The question is, can we test at least some of these predictions?

In this section we will briefly touch on two interesting questions relevant to LHC Higgs physics and to determining if what we might see at the LHC is really a Higgs boson. This is where we have seen the most progress in LHC Higgs physics over recent years: not only will we be able to see a light Higgs boson simultaneously in different production and decay channels, as discussed in Sects. 1.4 and 1.5, we can also study many of its properties. In a way this section ties in with the effective theory picture we use to introduce the Higgs mechanism: the obvious requirements to include massive gauge bosons in an effective electroweak gauge theory leads us towards the Standard Model Higgs boson only step by step, and at any of these steps we could have stopped and postulated some alternative ultraviolet completion of our theory.

1.7.1 CP Properties

One question for the LHC is: once we see a Higgs boson at the LHC, how do we test its quantum numbers? One such quantum number is its spin. A spin-one Higgs boson would not couple to two photons, so we only need to look at angular distributions for example in weak boson fusion to distinguish spin zero from spin two.

Once we know that we are talking about a scalar field we still need to measure its CP properties. The fundamental CP-even Standard-Model Higgs bosons couples to the W and Z bosons proportional to $g^{\mu\nu}$. For general *CP-even* and *CP-odd* Higgs bosons there are two more gauge invariant ways to couple to W bosons, which altogether give us the three coupling tensor structures

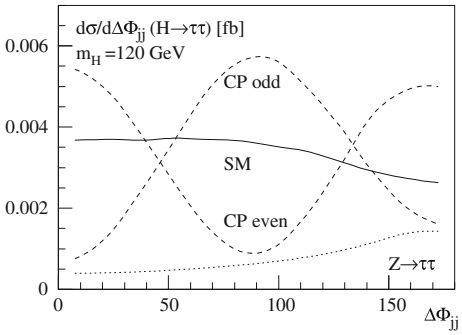

Fig. 1.7 Distribution for the azimuthal angle between the two forward jets in WBF production with a subsequent decay $H \to \tau\tau$. The signal and the leading Z background are simulated at parton level. All signal rates are normalized to the Standard-Model value. Figure from Ref. [11]

$$g^{\mu\nu} \qquad g^{\mu\nu} - \frac{p_1^\mu p_2^\nu}{p_1 p_2} \qquad \varepsilon_{\mu\nu\rho\sigma}\, p_1^\rho p_2^\sigma . \tag{1.141}$$

These are the only gauge invariant dimension-5 couplings of two gauge bosons to a (pseudo-) scalar field. The second one appears in the effective one-loop gluon-gluon-Higgs coupling in Eqs. 1.117 and 1.123. This second tensor is not orthogonal to $g^{\mu\nu}$, but we can replace it with any linear combination with $g^{\mu\nu}$. On the other hand, these two coupling structures nicely correspond to the gauge-invariant forms $W^{\mu\nu}W_{\mu\nu}$ and $W^{\mu\nu}\widetilde{W}_{\mu\nu}$ in the electroweak Lagrangian, so we leave them like this.

Going back to the transverse momentum spectra for the tagging jets shown in Eq. 1.128 we already know one way of telling apart these couplings: by construction, the dimension-3 *WWH* coupling proportional to $g^{\mu\nu}$ comes out of the Higgs potential as a side product of the W mass term, i.e. it couples the longitudinal Goldstone modes in the W boson to the Higgs. In contrast, the CP-even dimension-6 operator is proportional to the transverse tensor, which means it couples the transverse W polarizations to the Higgs and therefore produces a harder p_T spectrum of the tagging jets.

A very useful observable is the *azimuthal angle* between the two tagging jets in weak boson fusion, i.e. the angle separating the two jets in the transverse plane. For the three gauge-invariant coupling structures shown in Eq. 1.141 we find three distinctly different normalized distributions of the azimuthal angle $\Delta\phi$, shown in Fig. 1.7.

The tree-level coupling should in principle show no dependence of $\Delta\phi$ at all. The decrease towards larger angular separation is an effect of kinematic cuts against the Z background which prefers large angular separation. Therefore, the signal is depleted in the background-rich region. The CP-odd and therefore antisymmetric $\varepsilon^{\mu\nu\rho\sigma}$ coupling vanishes once two momenta contracted by the Levi–Civita tensor are equal. This explains the zeros at $\phi = 0, \pi$, where the two transverse jet momenta are no more linearly independent. To explain the opposite shape of the CP-even Higgs we use the low transverse momentum limit of the tagging jets. In that case the Higgs

production matrix element becomes proportional to the scalar product $(p_T^{\text{tag}\,1}\, p_T^{\text{tag}\,2})$ which vanishes for a relative angle $\Delta\phi = \pi/2$.

A related method of telling apart the $g^{\mu\nu}$ structure and the CP-odd coupling is looking at the *decay kinematics*. Each of the decaying Z bosons defines a plane opened by the two lepton momenta. If the angle between these two planes in the Higgs rest frame is ϕ, its distribution can be written as

$$\frac{d\sigma}{d\phi} \propto 1 + a\cos(\phi) + b\cos(2\phi). \tag{1.142}$$

For the CP-odd Higgs coupling to $W^{\mu\nu}\widetilde{W}_{\mu\nu}$ we find $a = 0$ and $b = 1/4$, while for the CP-even Higgs coupling $g^{\mu\nu}$ we find $a > 1/4$ depending on m_H. This method only works if we observe the decay $H \to ZZ \to 4\,\ell$ with a good signal-to-background ratio S/B. Both methods of determining the Higgs coupling structure are equivalent, as we can see from their Feynman diagrams: starting from the Feynman diagram for $H \to ZZ \to 4\,\ell$ we can switch two fermion legs from the final state into the initial state

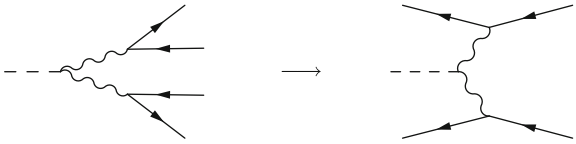

and read the diagram right-to-left. The same information which we can find in the angular correlation of the tagging jets is encoded in the decay plane correlation. The advantage of the first is that a production-side correlation in weak boson fusion is independent of the Higgs decay and can be used for all Higgs masses and decay signatures.

1.7.2 Higgs Self Coupling

If we should ever observe a scalar particle at the LHC, the crucial question will be if this is indeed our Higgs boson arising from electroweak symmetry breaking. In other words, Does this observed scalar field have a *potential* with a minimum at a non-vanishing vacuum expectation value?

Of course we could argue that a dimension-3 Higgs coupling to massive W bosons really is a Higgs–Goldstone self coupling, so we see it by finding a Higgs in weak boson fusion. On the other hand, it would be far more convincing to actually measure the self coupling of the actual Higgs field. This trilinear coupling we can probe at the LHC studying Higgs pair production, for example in gluon fusion via the usual top quark loop

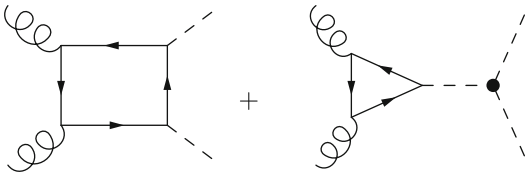

Following exactly the same argument as presented in Sect. 1.4.1 we can derive the two tensor structures contributing to Higgs pair production for transverse gluons

$$\begin{aligned}
\sqrt{2}P_T^{\mu\nu} &= g^{\mu\nu} - \frac{k_1^\nu k_2^\mu}{(k_1 k_2)} \\
\sqrt{2}P_2^{\mu\nu} &= g^{\mu\nu} + \frac{k_3^2 k_1^\nu k_2^\mu}{k_T^2 (k_1 k_2)} - \frac{2(k_2 k_3) k_1^\nu k_3^\mu}{k_T^2 (k_1 k_2)} - \frac{2(k_1 k_3) k_2^\mu k_3^\nu}{k_T^2 (k_1 k_2)} + \frac{k_3^\nu k_3^\mu}{k_T^2} \\
&\text{with} \quad k_T^2 = 2\frac{(k_1 k_3)(k_2 k_3)}{(k_1 k_2)} - k_3^2 .
\end{aligned} \tag{1.143}$$

The third momentum is one of the two Higgs momenta, so $k_3^2 = m_H^2$. In this representation the two tensors are orthonormal, which means $P_T^2 = \mathbb{1}$, $P_2^2 = \mathbb{1}$ and $P_T \cdot P_2 = 0$. The second tensor structure is missing in single Higgs production, so it only appears in the continuum (box) diagram and turns out to be numerically sub-leading over most of the relevant phase space.

From Sect. 1.4.2 on the effective Higgs-gluon coupling we know that in the low-energy limit we can compute the leading form factors associated with the triangle and box diagrams, both multiplying the transverse tensor $g^{\mu\nu} - k_1^\mu k_2^\nu/(k_1 k_2)$ for the incoming gluons

$$g_{ggH} = -g_{ggHH} = -i\frac{\alpha_s}{12\pi} + \mathcal{O}\left(\frac{m_H^2}{4m_t^2}\right). \tag{1.144}$$

Close to the production threshold $s \sim (2m_H)^2$ the leading contribution to the loop-induced production cross section for $gg \to HH$ involving the two Feynman diagrams above and the Higgs self coupling derived in Sect. 1.2.1 is then proportional to

$$\begin{aligned}
\left[3m_H^2 \frac{g_{ggH}}{s - m_H^2} + g_{ggHH}\right]^2 &= g_{ggH} \left[3m_H^2 \frac{1}{s - m_H^2} - 1\right]^2 \\
&\sim g_{ggH} \left[3m_H^2 \frac{1}{3m_H^2} - 1\right]^2 \to 0,
\end{aligned} \tag{1.145}$$

so the triangle diagram and the box diagram cancel.

In this argument we assume that the Higgs self coupling in the Standard Model is proportional to m_H. To see deviations from this self coupling in the first term

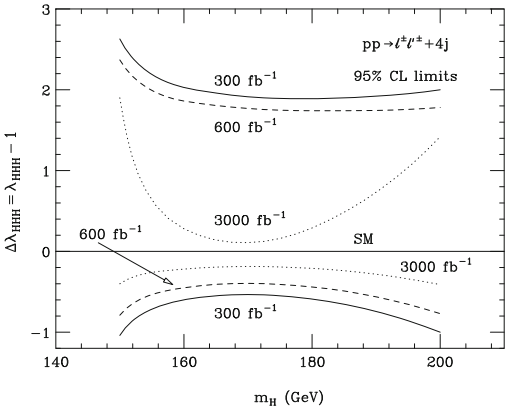

Fig. 1.8 The (parton-level) sensitivity limits for Higgs pair production and a measurement of the Higgs self coupling. The analysis is based on the decay $HH \to WW$. Figure from Ref. [13]

of Eq. 1.145 we can look at something like the m_{HH} distribution and measure the threshold behavior. In the *absence of any self coupling* this threshold cancellation of the self coupling contribution with the continuum should be absent as well. The threshold contribution to Higgs pair production would be huge. This way a shape analysis of the threshold behavior will allow us to experimentally exclude the case of $\lambda_{HHH} = 0$ which predicts an unobserved large enhancement of the production cross section at threshold. At this point it is still under study if such a measurement will work at the LHC and what kind of LHC luminosities would be required.

Of course, the Higgs self coupling sticks out of the Higgs parameters, but all Higgs couplings would be interesting to measure. If the Higgs is light and if all the of gluon fusion and weak boson fusion channels are indeed observed with sufficient luminosity, a numerical fit of all couplings to all Higgs observables will be possible, for example using the SFitter reconstruction tool [10]. As you can see in the original paper, for integrated luminosities around $30\,\text{fb}^{-1}$ the accuracy on the extracted couplings ranges from 30 to 70% error bands. Contrasting more specific hypotheses, like a strongly interacting light Higgs, with the Standard Model reduces these errors bars, possibly to $\mathcal{O}(10\%)$.

1.8 Further Reading

At this point we are done with our brief review of the Higgs sector in the Standard Model and of contemporary Higgs phenomenology. From the discussions it should be clear that we have to move on to QCD, to understand the strengths and weaknesses of these searches and what distinguishes a good from a bad search channel (Fig. 1.8).

Before moving on we mention a few papers where you can learn more about Higgs phenomenology at the LHC. Luckily, for Higgs searches there are several very complete and useful reviews available:

- You can look at the original articles by Higgs [12, 13] or Brout and Englert [14], but they are rather short and not really on top of the phenomenological aspects of the topic. Other papers for example by Guralnik, Hagen, Kibble [17] tend to be harder to read for phenomenologically interested students.
- Wolfgang Kilian's book [16] on the effective field theory approach to the Higgs mechanism is what the corresponding sections in these lecture notes are largely based on it. The underlying symmetry structure, including the custodial symmetry is nicely described in Scott Willenbrock's TASI lectures [17].
- Abdelhak Djouadi's compilation on 'absolutely everything we know about Higgs phenomenology' is indeed exhaustive. It has two volumes, one on the Standard Model [4] and another one on its minimal supersymmetric extension [18].
- For more experimental details you might want to have a look at Karl Jakobs' and Volker Büscher's review of LHC Higgs physics [19].
- As a theory view on LHC Higgs physics, mostly focused on gluon fusion production and its QCD aspects, there is Michael Spira's classic [3]. This is where you can find more information on the low-energy theorem. Michael and his collaborators also published a set of lecture notes on Higgs physics [20]. Watch out for how Michael summarizes the state of the art concerning weak boson fusion production of light Higgs bosons.
- As always, there is a TASI lecture on the topic. TASI lecture notes are generally what you should look for when you are interested in an area of high energy physics. Dave Rainwater did not only write his thesis on Higgs searches in weak boson fusion [21], he also left us all he knows about Higgs phenomenology at the LHC in his TASI notes [22].
- Tao Han wrote a very comprehensible set of TASI lecture notes on basic LHC phenomenology, in case you need to catch up on this [23].
- For some information on electroweak precision data and the ρ parameter, there are James Wells' TASI lectures [24].
- If you are interested in Higgs production in association with a W or Z boson and the way to observe boosted $H \to b\bar{b}$ decays you need to read the original paper [9]. The same is true for the $t\bar{t}H$ analysis.
- For cut rules and scalar integrals the best writeup I know is Wim Beenakker's PhD thesis. Unfortunately, I am not sure where to get it from except from the author by request.

References

1. Cabibbo, N., Maiani, L., Parisi, G., Petronzio, R.: Bounds on the Fermions and Higgs boson masses in grand unified theories. Nucl. Phys. B **158**, 295 (1979)
2. Lindner, M.: Implications of triviality for the standard model. Z. Phys. C **31**, 295 (1986)
3. Spira, M.: QCD effects in Higgs physics. Fortsch. Phys. **46**, 203 (1998)
4. Djouadi, A.: The anatomy of electro-weak symmetry breaking. I: the Higgs boson in the standard model. Phys. Rept. **457**, 1 (2008)

5. Campbell, J.M., Huston, J.W., Stirling, W.J.: Hard interactions of quarks and gluons: a primer for LHC physics. Rept. Prog. Phys. **70**, 89 (2007)
6. Asai, S. et al.: Prospects for the search for a standard model Higgs boson in ATLAS using vector boson fusion. Eur. Phys. J. C **32**(2), 19 (2004)
7. Bayatian, G.L. et al.: CMS collaboration, CMS technical design report, volume II: physics performance. J. Phys. G **34**, 995 (2007)
8. Butterworth, J.M., Davison, A.R., Rubin, M., Salam, G.P.: Jet substructure as a new Higgs search channel at the LHC. Phys. Rev. Lett. **100**, 242001 (2008)
9. Plehn, T., Rainwater, D., Zeppenfeld, D.: Determining the structure of Higgs couplings at the LHC. Phys. Rev. Lett. **88**, 051801 (2002)
10. Lafaye, R., Plehn, T., Rauch, M., Zerwas, D., Dührssen, M.: Measuring the Higgs sector. JHEP **0908**, 009 (2009)
11. Baur, U., Plehn, T., Rainwater, D.L.: Determining the Higgs boson selfcoupling at hadron colliders. Phys. Rev. D **67**, 033003 (2003)
12. Higgs, P.W.: Broken symmetries, massless particles and gauge fields. Phys. Lett. **12**, 132 (1964)
13. Higgs, P.W.: Broken symmetries and the masses of gauge bosons. Phys. Rev. Lett. **13**, 508 (1964)
14. Englert, F., Brout, R.: Broken symmetry and the mass of gauge vector mesons. Phys. Rev. Lett. **13**, 321 (1964)
15. Guralnik, G.S., Hagen, C.R., Kibble, T.W.B.: Global conservation laws and massless particles. Phys. Rev. Lett. **13**, 585 (1964)
16. Kilian, W.: Electroweak symmetry breaking: the bottom-up approach. Springer Tracts Mod. Phys. **198**, 1 (2003)
17. Willenbrock, S.: Symmetries of the standard model. arXiv:hep-ph/0410370
18. Djouadi, A.: The Anatomy of electro-weak symmetry breaking. II. The Higgs bosons in the minimal supersymmetric model. Phys. Rept. **459**, 1 (2008)
19. Büscher, V., Jakobs, K.: Higgs boson searches at hadron colliders. Int. J. Mod. Phys. A **20**, 2523 (2005)
20. Gomez-Bock, M., Mondragon, M., Mühlleitner, M., Spira, M., Zerwas, P.M.: Concepts of electroweak symmetry breaking and Higgs physics. arXiv:0712.2419 [hep-ph]
21. Rainwater, D.L.: Intermediate-mass Higgs searches in weak boson fusion. arXiv:hep-ph/9908378
22. Rainwater, D.: Searching for the Higgs boson. arXiv:hep-ph/0702124
23. Han, T.: Collider phenomenology: basic knowledge and techniques. arXiv:hep-ph/0508097
24. Wells, J.D.: TASI lecture notes: introduction to precision electroweak analysis. arXiv:hep-ph/0512342

Chapter 2
QCD

Just as Chap. 1 is not meant to be a complete introduction to electroweak symmetry breaking but is aimed at introducing the aspects of Higgs physics most relevant to the LHC this section cannot cover the entire field of QCD. Instead, we will focus on QCD as it impacts LHC physics and searches for new physics at the LHC, like for example the Higgs searches discussed in the first part of the lecture.

In Sect. 2.1 we will introduce the most important process at the LHC, the Drell–Yan process or lepton pair production. This process will lead us through all of the introduction into QCD. Ultraviolet divergences and renormalization we will only mention in passing, to get an idea how much of the treatment of ultraviolet and infrared divergences works the same way. After discussing in detail infrared divergences in Sects. 2.3–2.5 we will spend some time on modern approaches on combining QCD matrix element calculations at leading order and next-to-leading order in perturbative QCD with parton showers. This last part is fairly close to current research with the technical details changing rapidly. Therefore, we will rely on toy models to illustrate the different approaches.

2.1 Drell–Yan Process

Most text books on QCD start from a very simple class of QCD processes, namely deep inelastic scattering. These are processes with the HERA initial state $e^{\pm}p$. The problem with this approach is that for the LHC era such processes are not very useful. What we would like to understand instead are processes of the kind $pp \to W+\text{jets}$, $pp \to H+\text{jets}$, $pp \to t\bar{t}+\text{jets}$, or the production of new particles with or without jets. These kind of signal and background processes and their relevance in an LHC analysis we already mentioned in Sect. 1.4.3.

From a QCD perspective such processes are very complex, so we need to step back a little and start with a simple question: we know how to compute the production rate and distributions for photon and Z production for example at LEP, $e^+e^- \to \gamma, Z \to$

T. Plehn, *Lectures on LHC Physics*, Lecture Notes in Physics 844,
DOI: 10.1007/978-3-642-24040-9_2, © Springer-Verlag Berlin Heidelberg 2012

$\ell^+\ell^-$. What is the production rate for this final state at the LHC, how do we account for quarks inside the protons, and what are the best-suited kinematic variables to use at a hadron collider?

2.1.1 Gauge Boson Production

The simplest question we can ask at the LHC is: How do we compute the production of a weak gauge boson? This process is referred to as *Drell–Yan production*. In our first attempts we will explicitly not care about additional jets, so if we assume the proton to consist of quarks and gluons and simply compute the process $q\bar{q} \to \gamma, Z$ under the assumption that the quarks are partons inside protons. Gluons do not couple to electroweak gauge bosons, so we only have to consider valence quark versus sea anti-quark scattering in the initial state. Modulo the $SU(2)$ and $U(1)$ charges which describe the $Zf\bar{f}$ and $\gamma\bar{f}f$ couplings in the Feynman rules

$$\boxed{-i\gamma^\mu\left(\ell\mathbb{P}_L + r\mathbb{P}_R\right)} \quad \text{with } \ell = \frac{e}{s_w c_w}\left(T_3 - 2Qs_w^2\right) \quad r = \ell\Big|_{T_3=0} \quad (Zf\bar{f}) \qquad \ell = r = Qe \quad (\gamma f\bar{f}), \tag{2.1}$$

with $T_3 = \pm 1/2$, the matrix element and the squared matrix element for the partonic process

$$q\bar{q} \to \gamma, Z \tag{2.2}$$

will be the same as the corresponding matrix element squared for $e^+e^- \to \gamma, Z$, with an additional color factor. The general amplitude for *massless fermions* is

$$\mathscr{M} = -i\bar{v}(k_2)\gamma^\mu\left(\ell\mathbb{P}_L + r\mathbb{P}_R\right)u(k_1)\varepsilon_\mu. \tag{2.3}$$

Massless fermions are a good approximation at the LHC for all particles except for the top quark. For the bottom quark we need to be careful with some aspects of this approximation, but the first two generation quarks and all leptons are usually assumed to be massless in LHC simulations. Once we will arrive at infrared divergences in LHC cross sections we will specifically discuss ways of regulating them without introducing masses.

Squaring the matrix element in Eq. 2.3 means adding the same structure once again, just walking through it in the opposite direction. Luckily, we do not have to care about factors of $(-i)$ since we are only interested in the absolute value squared. Because the chiral projectors $\mathbb{P}_L r = (\mathbb{1} \mp \gamma_5)/2$ are real and $\gamma_5^T = \gamma_5$ is symmetric the left and right-handed gauge boson vertices described by the Feynman rules in Eq. 2.1 do not change under transposition, so for the production of a massive Z boson we obtain

$$
\begin{aligned}
|\mathscr{M}|^2 = & \sum_{\text{spin,pol,color}} \bar{u}(k_1)\gamma^\nu \left(\ell \mathbb{P}_L + r\mathbb{P}_R\right) v(k_2)\bar{v}(k_2)\gamma^\mu \\
& \times \left(\ell \mathbb{P}_L + r\mathbb{P}_R\right) u(k_1)\varepsilon_\mu \varepsilon_\nu^* \\
= & N_c \mathrm{Tr}\big[\not{k}_1\gamma^\nu \left(\ell \mathbb{P}_L + r\mathbb{P}_R\right)\not{k}_2\gamma^\mu \\
& \times \left(\ell \mathbb{P}_L + r\mathbb{P}_R\right)\big]\left(-g_{\mu\nu} + \frac{q_\mu q_\nu}{m_Z^2}\right) && \text{in unitary gauge} \\
= & N_c \mathrm{Tr}\Big[\not{k}_1\gamma^\nu \left(\ell \mathbb{P}_L + r\mathbb{P}_R\right) \\
& \times \left(\ell \mathbb{P}_L + r\mathbb{P}_R\right)\not{k}_2\gamma^\mu\Big]\left(-g_{\mu\nu} + \frac{q_\mu q_\nu}{m_Z^2}\right) && \text{with } \{\gamma_\mu, \gamma_5\} = 0 \\
= & N_c \mathrm{Tr}\left[\not{k}_1\gamma^\nu \left(\ell^2 \frac{\mathbb{1}}{2} + r^2 \frac{\mathbb{1}}{2}\right)\not{k}_2\gamma^\mu\right] \\
& \times \left(-g_{\mu\nu} + \frac{q_\mu q_\nu}{m_Z^2}\right) && \text{symmetric polarization sum} \\
= & \frac{N_c}{2}\left(\ell^2 + r^2\right)\mathrm{Tr}\left[\not{k}_1\gamma^\nu\not{k}_2\gamma^\mu\right]\left(-g_{\mu\nu} + \frac{q_\mu q_\nu}{m_Z^2}\right) \\
= & 2N_c\left(\ell^2 + r^2\right)\left[k_1^\mu k_2^\nu + k_1^\nu k_2^\mu - (k_1k_2)g^{\mu\nu}\right] \\
& \times \left(-g_{\mu\nu} + \frac{q_\mu q_\nu}{m_Z^2}\right) \\
= & 2N_c\left(\ell^2 + r^2\right)\Bigg[-2(k_1k_2) + 4(k_1k_2) \\
& + 2\frac{(-k_1k_2)^2}{m_Z^2} - \frac{(k_1k_2)q^2}{m_Z^2}\Bigg] && \text{with } (qk_1) = -(k_1k_2) \\
= & 2N_c\left(\ell^2 + r^2\right)\left[2(k_1k_2) + \frac{q^4}{2m_Z^2} - \frac{q^4}{2m_Z^2}\right] && \text{with } q^2 = (k_1 + k_2)^2 \\
= & 2N_c\left(\ell^2 + r^2\right)q^2 \\
= & 2N_c\left(\ell^2 + r^2\right)m_Z^2
\end{aligned}
\tag{2.4}
$$

The momenta are k_1 and k_2 for the massless incoming (anti-) fermions and $q = -k_1 - k_2$ for the outgoing gauge boson. The color factor N_c accounts for the number of $SU(3)$ states which can be combined to form a color singlet like the Z.

An interesting aspect coming out of our calculation is that the $1/m_Z$-dependent terms in the polarization sum do not contribute—as far as the matrix element squared is concerned the Z boson could as well be transverse. This reflects the fact that the Goldstone modes do not couple to massless fermions, just like the Higgs boson.

It also means that the corresponding matrix element squared for the photon production simply means not replacing $q^2 \to m_Z^2$ in the last step.

What is still missing is an averaging factor for initial-state spins and colors, only the sum is included in Eq. 2.4. For incoming electrons as well as incoming quarks this factor K_{ij} includes $1/4$ for the spins. Since we do not observe color in the initial state, and the color structure of the incoming $q\bar{q}$ pair has no impact on the Z–production matrix element, we also average over the color. This means another factor $1/N_c^2$ in the averaged matrix element, which altogether becomes (in four space–time dimensions)

$$K_{ij} = \frac{1}{4N_c^2} \tag{2.5}$$

In spite of our specific case in Eq. 2.4 looking that way, matrix elements we compute from our Feynman rules are not automatically numbers with mass unit zero.

If for the invariant mass of the two quarks we introduce the *Mandelstam variable* $s = (k_2 + k_2)^2 = 2(k_1 k_2)$ momentum conservation implies $s = q^2 = m_Z^2$. In four space–time dimensions (this detail will become important later) we can compute a *total cross section* from the matrix element squared, for example as given in Eq. 2.4, as

$$\boxed{s \left.\frac{d\sigma}{dy}\right|_{2\to 1} = \frac{\pi}{(4\pi)^2} K_{ij} \, (1-\tau) \, |\mathcal{M}|^2} \qquad \tau = \frac{m_Z^2}{s}. \tag{2.6}$$

The mass of the final state appears in τ, with $\tau = 0$ for a massless photon. It would be replaced to include m_W or the Higgs mass or the mass of a Kaluza–Klein graviton if needed.

From LEP we know that such a heavy gauge boson we do not actually observe at colliders. What we should really calculate is the production for example of a pair of fermions through an s-channel Z and γ, where the Z might or might not be on its mass shell. The matrix element for this process we can derive from the same Feynman rules in Eq. 2.1, now for an incoming fermion k_1, incoming anti-fermion k_2, outgoing fermion p_1 and outgoing anti-fermion p_2. To make it easy to switch particles between initial and final states, we can define all momenta as incoming, so momentum conservation means $k_1 + k_2 + p_1 + p_2 = 0$. The additional *Mandelstam variables* we need to describe this $(2 \to 2)$ process are $t = (k_1 + p_1)^2 < 0$ and $u = (k_1 + p_2)^2 < 0$, as usually with $s + t + u = 0$ for massless final state particles. The $(2 \to 2)$ matrix element for the two sets of incoming and outgoing fermions becomes

$$\begin{aligned} \mathcal{M} = (-i)^2 \bar{u}(p_1) \gamma^\nu \left(\ell' \mathbb{P}_L + r' \mathbb{P}_R\right) v(p_2) \\ \times \bar{v}(k_2) \gamma^\mu \left(\ell \mathbb{P}_L + r \mathbb{P}_R\right) u(k_1) \frac{i}{q^2 - m_Z^2} \left(-g_{\mu\nu} + \frac{q_\mu q_\nu}{m_Z^2}\right). \end{aligned} \tag{2.7}$$

The coupling to the gauge bosons are ℓ and r for the incoming quarks and ℓ' and r' for the outgoing leptons. When we combine the four different spinors and their momenta correctly the matrix element squared factorizes into twice the trace we have computed before. The corresponding picture is two fermion currents interacting with each other through a gauge boson. All we have to do is combine the traces properly. If the incoming trace includes the indices μ and ν and the outgoing trace the indices ρ and σ, the Z bosons link μ and ρ as well as ν and σ.

To make the results a little more compact we continue computing this process for a *massless photon* instead of the Z boson, i.e. for the physical scenario where the initial-state fermions do not have enough energy to excite the intermediate Z boson. The specific features of an intermediate massive Z boson we postpone to Sect. 2.1.2. The assumption of a massless photon simplifies the couplings to $(\ell^2 + r^2) = 2Q^2 e^2$ and the polarization sums to $-g_{\mu\nu}$:

$$
\begin{aligned}
|\mathcal{M}|^2 &= 4N_c(2Q^2e^2)(2Q'^2e^2)\frac{1}{q^4}\left[k_1^\mu k_2^\nu + k_1^\nu k_2^\mu - (k_1k_2)g^{\mu\nu}\right](-g_{\mu\rho}) \\
&\qquad \times \left[p_1^\rho p_2^\sigma + p_1^\sigma p_2^\rho - (p_1p_2)g^{\rho\sigma}\right](-g_{\nu\sigma}) \\
&= \frac{16N_cQ^2Q'^2e^4}{q^4}\left[k_{1\rho}k_2^\nu + k_1^\nu k_{2\rho} - (k_1k_2)g_\rho^\nu\right]\left[p_1^\rho p_{2\nu} + p_{1\nu}p_2^\rho - (p_1p_2)g_\nu^\rho\right] \\
&= \frac{16N_cQ^2Q'^2e^4}{q^4}\Big[2(k_1p_1)(k_2p_2) + 2(k_1p_2)(k_2p_1) \\
&\qquad - 2(k_1k_2)(p_1p_2) - 2(k_1k_2)(p_1p_2) + 4(k_1k_2)(p_1p_2)\Big] \\
&= \frac{32N_cQ^2Q'^2e^4}{q^4}\left[(k_1p_1)(k_2p_2) + (k_1p_2)(k_2p_1)\right] \\
&= \frac{32N_cQ^2Q'^2e^4}{s^2}\left[\frac{t^2}{4} + \frac{u^2}{4}\right] \\
&= \frac{8N_cQ^2Q'^2e^4}{s^2}\left[s^2 + 2st + 2t^2\right] \\
&= 8N_cQ^2Q'^2e^4\left[1 + 2\frac{t}{s} + 2\frac{t^2}{s^2}\right] \qquad (2.8)
\end{aligned}
$$

We can briefly check if this number is indeed positive, using the definition of the Mandelstam variable t for massless external particles in terms of the polar angle $t = s(-1 + \cos\theta)/2 = -s \cdots 0$: the upper phase space boundary $t = 0$ inserted into the brackets in Eq. 2.8 gives $[\cdots] = 1$, just as the lower boundary $t = -s$ with $[\cdots] = 1 - 2 + 2 = 1$. For the central value $t = -s/2$ the minimum value of the brackets is $[\cdots] = 1 - 1 + 0.5 = 0.5$.

The azimuthal angle ϕ plays no role at colliders, unless you want to compute gravitational effects on Higgs production at ATLAS and CMS. Any LHC Monte Carlo will either random-generate a reference angle ϕ for the partonic process or pick one and keep it fixed.

The two-particle phase space integration for massless particles then gives us

$$\boxed{s^2 \frac{d\sigma}{dt}\bigg|_{2\to 2} = \frac{\pi}{(4\pi)^2} K_{ij} |\mathcal{M}|^2} \qquad t = \frac{s}{2}(-1+\cos\theta). \tag{2.9}$$

For our Drell–Yan process we then find the differential cross section in four space–time dimensions, using $\alpha = e^2/(4\pi)$

$$\begin{aligned} \frac{d\sigma}{dt} &= \frac{1}{s^2}\frac{\pi}{(4\pi)^2}\frac{1}{4N_c} 8Q^2 Q'^2 (4\pi\alpha)^2 \left(1 + 2\frac{t}{s} + 2\frac{t^2}{s^2}\right) \\ &= \frac{1}{s^2}\frac{2\pi\alpha^2}{N_c} Q^2 Q'^2 \left(1 + 2\frac{t}{s} + 2\frac{t^2}{s^2}\right), \end{aligned} \tag{2.10}$$

which we can integrate over the polar angle or the Mandelstam variable t to compute the total cross section

$$\begin{aligned} \sigma &= \frac{1}{s^2}\frac{2\pi\alpha^2}{N_c} Q^2 Q'^2 \int_{-s}^{0} dt \left(1 + 2\frac{t}{s} + 2\frac{t^2}{s^2}\right) \\ &= \frac{1}{s^2}\frac{2\pi\alpha^2}{N_c} Q^2 Q'^2 \left[t + \frac{t^2}{s} + \frac{2t^3}{3s^2}\right]_{-s}^{0} \\ &= \frac{1}{s^2}\frac{2\pi\alpha^2}{N_c} Q^2 Q'^2 \left(s - \frac{s^2}{s} + \frac{2t^s}{3s^2}\right) \\ &= \frac{1}{s}\frac{2\pi\alpha^2}{N_c} Q^2 Q'^2 \frac{2}{3} \quad \Rightarrow \quad \boxed{\sigma(q\bar{q}\to \ell^+\ell^-)\Big|_{\text{QED}} = \frac{4\pi\alpha^2}{3N_c s} Q_\ell^2 Q_q^2} \end{aligned} \tag{2.11}$$

As a side remark—in the history of QCD, the same process but read *right-to-left* played a crucial role, namely the production rate of quarks in e^+e^- scattering. For small enough energies we can neglect the Z exchange contribution. At leading order we can then compute the corresponding production cross sections for muon pairs and for quark pairs in e^+e^- collisions. Moving the quarks into the final state means that we do not average of the color in the initial state, but sum over all possible color combinations, which in Eq. 2.9 gives us an averaging factor $K_{ij} = 1/4$. Everything else stays the same as for the Drell–Yan process

$$\boxed{R \equiv \frac{\sigma(e^+e^-\to \text{hadrons})}{\sigma(e^+e^-\to \ell^+\ell^-)}} = \frac{\sum_{\text{quarks}} \frac{4\pi\alpha^2 N_c}{3s} Q_e^2 Q_q^2}{\frac{4\pi\alpha^2}{3s} Q_e^2 Q_\ell^2} = N_c \left(3\frac{1}{9} + 2\frac{4}{9}\right) = \frac{11 N_c}{9}, \tag{2.12}$$

for example for five quark flavors where the top quark is too heavy to be produced at the given e^+e^- collider energy. For those interested in the details we did take one short cut: hadrons are also produced in the hadronic decays of $e^+e^-\to\tau^+\tau^-$ which we strictly speaking need to subtract. This way, R as a function of the collider energy is a beautiful measurement of the weak and color charges of the quarks in QCD.

2.1.2 Massive Intermediate States

Before we move on to describing incoming quarks inside protons we should briefly consider the second Feynman diagram contributing to the Drell–Yan production rate in Eq. 2.11, the on-shell or off-shell Z boson

$$|\mathscr{M}|^2 = |\mathscr{M}_\gamma + \mathscr{M}_Z|^2 = |\mathscr{M}_\gamma|^2 + |\mathscr{M}_Z|^2 + 2\text{Re}\mathscr{M}_Z\mathscr{M}_\gamma . \tag{2.13}$$

Interference occurs in phase space regions where for both intermediate states the invariant masses of the muon pair are the same. For the photon the on-shell pole is not a problem. It has zero mass, which means that we hit the pole $1/q^2$ in the matrix element squared only in the limit of zero incoming energy. Strictly speaking we never hit it, because the energy of the incoming particles has to be large enough to produce the final state particles with their tiny but finite masses and with some kind of momentum driving them through the detector.

A problem arises when we consider the intermediate Z boson. In that case, the propagator contributes as $|\mathscr{M}|^2 \propto 1/(s-m_Z^2)^2$ which diverges for on-shell Z bosons. Before we can ask what such a pole means for LHC simulations we have to recall how we deal with it in field theory. There, we encounter the same issue when we solve for example the *Klein–Gordon equation*. The Green function for a field obeying this equation is the inverse of the Klein–Gordon operator

$$\left(\Box + m^2\right) G(x-x') = \delta^4(x-x'). \tag{2.14}$$

Fourier transforming $G(x-x')$ into momentum space we find

$$\begin{aligned}
G(x-x') &= \int \frac{d^4q}{(2\pi)^4} e^{-iq\cdot(x-x')} \tilde{G}(q) \\
\left(\Box + m^2\right) G(x-x') &= \int \frac{d^4q}{(2\pi)^4} \left(\Box + m^2\right) e^{-iq\cdot(x-x')} \tilde{G}(q) \\
&= \int \frac{d^4q}{(2\pi)^4} \left((iq)^2 + m^2\right) e^{-iq\cdot(x-x')} \tilde{G}(q) \\
&= \int \frac{d^4q}{(2\pi)^4} e^{-iq\cdot(x-x')} \left(-q^2 + m^2\right) \tilde{G}(q) \\
&\overset{!}{=} \delta^4(x-x') = \int \frac{d^4q}{(2\pi)^4} e^{-iq\cdot(x-x')} \\
\Leftrightarrow \quad (-q^2+m^2)\tilde{G}(q) = 1 \quad &\Leftrightarrow \quad \tilde{G}(q) \sim -\frac{1}{q^2-m^2}.
\end{aligned} \tag{2.15}$$

The problem with the Green function in momentum space is that as an inverse it is not defined for $q^2 = m^2$. We usually avoid this problem by slightly shifting this pole following the *Feynman* $i\,\varepsilon$ prescription to $m^2 \to m^2 - i\varepsilon$, or equivalently deforming our integration contours appropriately. The sign of this infinitesimal shift we need to understand because it will become relevant for phenomenology when we introduce an actual finite decay width of intermediate states.

In the Feynman $i\varepsilon$ prescription the sign is crucial to correctly complete the q_0 integration of the Fourier transform in the complex plane

$$\begin{aligned}
&\int_{-\infty}^{\infty} dq_0 \frac{e^{-iq_0x_0}}{q^2 - m^2 + i\varepsilon} \\
&= (\theta(x_0) + \theta(-x_0)) \int_{-\infty}^{\infty} dq_0 \frac{e^{-iq_0x_0}}{q_0^2 - (\omega^2 - i\varepsilon)} \quad \text{with} \quad \omega^2 = \vec{q}^{\,2} + m^2 \\
&= (\theta(x_0) + \theta(-x_0)) \int_{-\infty}^{\infty} dq_0 \frac{e^{-iq_0x_0}}{(q_0 - \sqrt{\omega^2 - i\varepsilon})(q_0 + \sqrt{\omega^2 - i\varepsilon})} \\
&= \left(\theta(x_0) \oint_{C_2} + \theta(-x_0) \oint_{C_1}\right) dq_0 \frac{e^{-iq_0x_0}}{(q_0 - \omega(1 - i\varepsilon'))(q_0 + \omega(1 - i\varepsilon'))}, \qquad (2.16)
\end{aligned}$$

defining $\varepsilon' = \varepsilon/(2\omega^2)$. In the last step we close the integration contour along the real q_0 axis in the complex q_0 plane. Because the integrand has to vanish for large q_0, we have to make sure the exponent $-ix_0 i\mathrm{Im}q_0 = x_0\mathrm{Im}q_0$ is negative. For $x_0 > 0$ this means $\mathrm{Im}q_0 < 0$ and vice versa. This argument forces C_1 to close for positive and C_2 for negative imaginary parts in the complex q_0 plane.

The contour integrals we can solve using Cauchy's formula, keeping in mind that the integrand has two poles at $q_0 = \pm\omega(1 - i\varepsilon')$. They lie in the upper (lower) half plane for negative (positive) real parts of q_0. The contour C_1 through the upper half plane includes the pole at $q_0 \sim -\omega$ while the contour C_2 includes the pole at $q_0 \sim \omega$, all assuming $\omega > 0$:

$$\begin{aligned}
\int_{-\infty}^{\infty} dq_0 \frac{e^{-iq_0x_0}}{q^2 - m^2 + i\varepsilon} &= 2\pi i \left[\theta(x_0) \frac{(-1)e^{-i\omega x_0}}{\omega + \omega(1 - i\varepsilon')} + \theta(-x_0) \frac{e^{i\omega x_0}}{-\omega - \omega(1 - i\varepsilon')}\right] \\
&\overset{\varepsilon' \to 0}{=} -i\frac{\pi}{\omega}\left[\theta(x_0)e^{-i\omega x_0} + \theta(-x_0)e^{i\omega x_0}\right]. \qquad (2.17)
\end{aligned}$$

The factor (-1) in the C_2 integration arises because Cauchy's integration formula requires us to integrate counter-clockwise, while going from negative to positive $\mathrm{Re}q_0$ the contour C_2 is defined clockwise. Using this result we can complete the four–dimensional Fourier transform from Eq. 2.15

$$
\begin{aligned}
G(x) &= \int d^4q e^{-i(q\cdot x)} \tilde{G}(q) \\
&= \int d^4q \frac{e^{-i(q\cdot x)}}{q^2 - m^2 + i\varepsilon} \\
&= -i\pi \int d^3\vec{q} e^{i\vec{q}\vec{x}} \frac{1}{\omega} \left[\theta(x_0) e^{-i\omega x_0} + \theta(-x_0) e^{i\omega x_0}\right] \\
&= -i\pi \int d^4q e^{i\vec{q}\vec{x}} \frac{1}{\omega} \left[\theta(x_0) e^{-iq_0 x_0} \delta(q_0 - \omega) + \theta(-x_0) e^{-iq_0 x_0} \delta(q_o + \omega)\right] \\
&= -i\pi \int d^4q e^{-i(q\cdot x)} \frac{1}{\omega} \left[\theta(x_0)\delta(\omega - q_0) + \theta(-x_0)\delta(\omega + q_0)\right] \\
&= -i\pi \int d^4q e^{-i(q\cdot x)} \frac{1}{\omega} 2\omega \left[\theta(x_0)\delta(\omega^2 - q_0^2) + \theta(-x_0)\delta(\omega^2 - q_0^2)\right] \\
&= -2\pi i \int d^4q e^{-i(q\cdot x)} \left[\theta(x_0) + \theta(-x_0)\right] \delta(q_0^2 - \omega^2) \\
&= -2\pi i \int d^4q e^{-i(q\cdot x)} \left[\theta(x_0) + \theta(-x_0)\right] \delta(q^2 - m^2),
\end{aligned}
\tag{2.18}
$$

with $q_0^2 - \omega^2 = q^2 - m^2$. This is exactly the usual decomposition of the propagator function $\Delta_F(x) = \theta(x_0)\Delta^+(x) + \theta(-x_0)\Delta^-(x)$ into positive and negative energy contributions.

Let us briefly recapitulate what would have happened if we instead had chosen the Feynman parameter $\varepsilon < 0$. All steps leading to the propagator function in Eq. 2.18 we summarize in Table 2.1. For the wrong sign of $i\varepsilon$ the two poles in the complex q_0 plane would be mirrored by the real axis. The solution with Re $q_0 > 0$ would sit in the quadrant with Im $q_0 > 0$ and the second pole at a negative real and imaginary part. To be able to close the integration path in the upper half plane in the mathematically positive direction the real pole would have to be matched up with $\theta(-x_0)$. The residue in the Cauchy integral would now include a factor $+1/(2\omega)$. At the end, the two poles would give the same result as for the correct sign of $i\varepsilon$, except with a wrong over-all sign.

When we are interested in the kinematic distributions of on-shell massive states the situation is a little different. Measurements of differential distributions for example at LEP include information on the *physical width* of the decaying particle, which means we cannot simply apply the Feynman $i\varepsilon$ prescription as if we were dealing with an asymptotic stable state. From the same couplings governing the Z decay, the Z propagator receives corrections, for example including fermion loops:

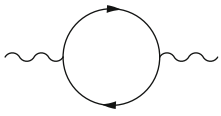

Such one-particle irreducible diagrams can occur in the same propagator repeatedly. Schematically written as a scalar they are of the form

Table 2.1 Contributions to the propagator function Eq. 2.18 for both signs of $i\varepsilon$

	$\frac{1}{q^2-m^2+i\varepsilon}$		$\frac{1}{q^2-m^2-i\varepsilon}$	
Pole	$q_0=\omega(1-i\varepsilon)$	$q_0=-\omega(1-i\varepsilon)$	$q_0=\omega(1+i\varepsilon)$	$q_0=-\omega(1+i\varepsilon)$
Complex quadrant	$(+,-)$	$(-,+)$	$(+,+)$	$(-,-)$
Convergence: x_0 Im $q_0<0$	$x_0>0$	$x_0<0$	$x_0<0$	$x_0>0$
Part of real axis	$\theta(x_0)$	$\theta(-x_0)$	$\theta(-x_0)$	$\theta(x_0)$
Closed contour	Im $q_0<0$	Im $q_0>0$	Im $q_0>0$	Im $q_0<0$
Direction of contour	-1	$+1$	$+1$	-1
Residue	$+\frac{1}{2\omega}$	$-\frac{1}{2\omega}$	$+\frac{1}{2\omega}$	$-\frac{1}{2\omega}$
Fourier exponent	$e^{-i\omega x_0}$	$e^{+i\omega x_0}$	$e^{+i\omega x_0}$	$e^{-i\omega x_0}$
All combined	$-\frac{e^{-i\omega x_0}}{2\omega}\theta(x_0)$	$-\frac{e^{+i\omega x_0}}{2\omega}\theta(-x_0)$	$+\frac{e^{+i\omega x_0}}{2\omega}\theta(-x_0)$	$+\frac{e^{-i\omega x_0}}{2\omega}\theta(x_0)$

$$
\begin{aligned}
&\frac{i}{q^2-m_0^2+i\varepsilon}+\frac{i}{q^2-m_0^2+i\varepsilon}(-iM^2)\frac{i}{q^2-m_0^2+i\varepsilon}\\
&\quad+\frac{i}{q^2-m_0^2+i\varepsilon}(-iM^2)\frac{i}{q^2-m_0^2+i\varepsilon}(-iM^2)\frac{i}{q^2-m_0^2+i\varepsilon}+\cdots\\
&\quad=\frac{i}{q^2-m_0^2+i\varepsilon}\sum_{n=0}\left(\frac{M^2}{q^2-m_0^2+i\varepsilon}\right)^n\\
&\quad=\frac{i}{q^2-m_0^2+i\varepsilon}\frac{1}{1-\dfrac{M^2}{q^2-m_0^2+i\varepsilon}}\quad\text{summing the geometric series}\\
&\quad=\frac{i}{q^2-m_0^2+i\varepsilon-M^2},
\end{aligned}
\tag{2.19}
$$

where we denote the loop as M^2 for reasons which will become obvious later. Requiring that the residue of the propagator be unity at the pole we *renormalize* the wave function and the mass in the corresponding process. For example for a massive scalar or gauge boson with a real correction $M^2(q^2)$ this reads

$$
\boxed{\frac{i}{q^2-m_0^2-M^2(q^2)}=\frac{iZ}{q^2-m^2}\quad\text{for}\,q^2\sim m^2}\,, \tag{2.20}
$$

including a renormalized mass m and a wave function renormalization constant Z.

The important step in our argument is that in analogy to the effective ggH coupling discussed in Sect. 1.4.1 the one-loop correction M^2 depends on the momentum flowing through the propagator. Above a certain threshold it can develop an imaginary part because the momentum flowing through the diagram is large enough to produce on-shell states in the loop. Just as for the ggH coupling such *absorptive parts* appear

when a real decay like $Z \to \ell^+\ell^-$ becomes kinematically allowed. After splitting $M^2(q^2)$ into its real and imaginary parts we know what to do with the real part: the solution to $q^2 - m_0^2 - \text{Re}M^2(q^2) \stackrel{!}{=} 0$ defines the renormalized particle mass $q^2 = m^2$ and the wave function renormalization Z. The imaginary part looks like the Feynman $i\varepsilon$ term discussed before

$$\begin{aligned} \frac{i}{q^2 - m_0^2 + i\varepsilon - \text{Re}M^2(q^2) - i\text{Im}M^2} &= \frac{iZ}{q^2 - m^2 + i\varepsilon - iZ\text{Im}M^2} \\ &\equiv \frac{iZ}{q^2 - m^2 + im\Gamma} \\ \Leftrightarrow \quad \Gamma &= -\frac{Z}{m}\text{Im}M^2(q^2 = m^2), \end{aligned} \tag{2.21}$$

for $\varepsilon \to 0$ and finite $\Gamma \neq 0$. The link between the self energy matrix element squared M^2 and the partial width we can illustrate remembering one way to compute scalar integrals or one-loop amplitudes by gluing them together using tree-level amplitudes. The Cuskosky cutting rule discussed in Sect. 1.4.1 tells us schematically written $\text{Im}\, M^2 \sim M^2|_{\text{cut}} \equiv \Gamma$ because cutting the one-loop bubble diagram at the one possible place is nothing but squaring the two tree-level matrix element for the decay $Z \to \ell^+\ell^-$. One thing that we need to keep track of, apart from the additional factor m due to dimensional analysis, is the sign of the $im\Gamma$ term which just like the $i\varepsilon$ prescription is fixed by causality.

Going back to the Drell–Yan process $q\bar{q} \to \ell^+\ell^-$ we now know that for massive unstable particles the Feynman epsilon which we need to define the Green function for internal states acquires a finite value, proportional to the total width of the unstable particle. This definition of a propagator of an unstable particle in the s channel is what we need for the second Feynman diagram contributing to the Drell–Yan process: $q\bar{q} \to Z^* \to \ell^+\ell^-$. The resulting shape of the propagator squared is a *Breit–Wigner propagator*

$$\boxed{\sigma(q\bar{q} \to Z \to \ell^+\ell^-) \propto \left| \frac{1}{s - m_Z^2 + im\Gamma} \right|^2 = \frac{1}{(s-m_Z^2)^2 + m^2\Gamma^2}}\,. \tag{2.22}$$

When taking everything into account, the $(2 \to 2)$ production cross section also includes the squared matrix element for the decay $Z \to \ell^+\ell^-$ in the numerator. In the *narrow width approximation*, the $(2 \to 2)$ matrix element factorizes into the production process times the branching ratio for $Z \to \ell^+\ell^-$, simply by definition of the Breit–Wigner distribution

$$\lim_{\Gamma \to 0} \frac{\Gamma_{\ell\ell}}{(s - m_Z^2)^2 + m^2\Gamma_{\text{tot}}^2} = \Gamma_{\ell\ell}\frac{\pi}{\Gamma_{\text{tot}}}\delta(s - m_Z^2) \equiv \pi \text{BR}(Z \to \ell\ell)\delta(s - m_Z^2). \tag{2.23}$$

The additional factor π will be absorbed in the different one-particle and two-particle phase space definitions. We immediately see that this narrow width approximation

is only exact for scalar particles. It does not keep information about the structure of the matrix element, e.g. when a non-trivial structure of the numerator gives us the spin and angular correlations between the production and decay processes.

Equation 2.23 uses a mathematical relation we might want to remember for life, and that is the definition of the one-dimensional *Dirac delta distribution* in three ways and including all factors of 2 and π

$$\delta(x) = \int \frac{dq}{2\pi} e^{-ixq} = \lim_{\sigma\to 0} \frac{1}{\sigma\sqrt{\pi}} e^{-x^2/\sigma^2} = \lim_{\Gamma\to 0} \frac{1}{\pi} \frac{\Gamma}{x^2+\Gamma^2}. \tag{2.24}$$

The second distribution is a *Gaussian* and the third one we would refer to as a *Breit–Wigner* shape while most other people call it a Cauchy distribution.

Now, we know everything necessary to compute all Feynman diagrams contributing to muon pair production at a hadron collider. Strictly speaking, the two amplitudes interfere, so we end up with three distinct contributions: γ exchange, Z exchange and the $\gamma - Z$ interference terms. They have the properties

- For small energies the γ contribution dominates and can be linked to R.
- On the Z pole the rate is regularized by the Z width and Z contribution dominates over the photon.
- In the tails of the Breit–Wigner distribution we expect $Z - \gamma$ interference.
- For large energies we are again dominated by the photon channel.
- Quantum effects allow unstable particles like the Z to decay off-shell, defining a Breit–Wigner propagator.
- In the limit of vanishing width the Z contribution factorizes into $\sigma \cdot \text{BR}$.

2.1.3 Parton Densities

At the end of Sect. 2.1.1 the discussion of different energy regimes for R experimentally makes sense—at an e^+e^- collider we can tune the energy of the initial state. At hadron colliders the situation is very different. The energy distribution of incoming quarks as parts of the colliding protons has to be taken into account. If we assume that quarks move collinearly with the surrounding proton, i.e. that at the LHC incoming partons have zero p_T, we can define a probability distribution for finding a parton just depending on the respective fraction of the proton's momentum. For this momentum fraction $x = 0 \cdots 1$ the *parton density function* (pdf) is denoted as $f_i(x)$, where i denote the different partons in the proton, for our purposes u,d,c,s,g and depending on the details b. All incoming partons we assume to be massless.

In contrast to so-called structure functions a pdf is not an observable. It is a distribution in the mathematical sense, which means it has to produce reasonable results when integrated over together with a test function. Different parton densities have very different behavior—for the valence quarks (uud) they peak somewhere around $x \lesssim 1/3$, while the gluon pdf is small at $x \sim 1$ and grows very rapidly towards small x. For some typical part of the relevant parameter space ($x = 10^{-3} \ldots 10^{-1}$) it

roughly scales like $f_g(x) \propto x^{-2}$. Towards smaller x values it becomes even steeper. This steep gluon distribution was initially not expected and means that for small enough x LHC processes will dominantly be gluon fusion processes.

While we cannot actually compute parton distribution functions $f_i(x)$ as a function of the momentum fraction x there are a few predictions we can make based on symmetries and properties of the hadrons. Such arguments for example lead to *sum rules*:

The parton distributions inside an anti-proton are linked to those inside a proton through CP symmetry, which is an exact symmetry of QCD. Therefore, for all partons we know

$$f_q^{\bar{p}}(x) = f_{\bar{q}}(x) \qquad f_{\bar{q}}^{\bar{p}}(x) = f_q(x) \qquad f_g^{\bar{p}}(x) = f_g(x) \tag{2.25}$$

for all values of x.

If the proton consists of three valence quarks *uud*, plus quantum fluctuations from the vacuum which can either involve gluons or quark–antiquark pairs, the contribution from the sea quarks has to be symmetric in quarks and antiquarks. The expectation values for the signed numbers of up and down quarks inside a proton have to fulfill

$$\langle N_u \rangle = \int_0^1 dx \, (f_u(x) - f_{\bar{u}}(x)) = 2 \qquad \langle N_d \rangle = \int_0^1 dx \, \left(f_d(x) - f_{\bar{d}}(x)\right) = 1. \tag{2.26}$$

Similarly, the total momentum of the proton has to consist of sum of all parton momenta. We can write this as the expectation value of $\sum x_i$

$$\left\langle \sum x_i \right\rangle = \int_0^1 dx x \left(\sum_q f_q(x) + \sum_{\bar{q}} f_{\bar{q}}(x) + f_g(x) \right) = 1 \tag{2.27}$$

What makes this prediction interesting is that we can compute the same sum only taking into account the measured quark and antiquark parton densities. We find that the momentum sum rule only comes to 1/2. Half of the proton momentum is carried by gluons.

Given the correct definition and normalization of the pdf we can now compute the *hadronic cross section* from its partonic counterpart, like the QED result in Eq. 2.11, as

$$\boxed{\sigma_{\text{tot}} = \int_0^1 dx_1 \int_0^1 dx_2 \sum_{ij} f_i(x_1) f_j(x_2) \hat{\sigma}_{ij}(x_1 x_2 S)}, \tag{2.28}$$

where i,j are the incoming partons with the momentum factions $x_{i,j}$. The partonic energy of the scattering process is $s = x_1 x_2 S$ with the LHC proton energy of eventually $\sqrt{S} = 14\,\text{TeV}$. The partonic cross section $\hat{\sigma}$ corresponds to the cross sections σ computed for example in Eq. 2.11. It has to include all the necessary θ and δ functions for energy–momentum conservation. When we express a general n-particle

cross section $\hat{\sigma}$ including the phase space integration, the x_i integrations and the phase space integrations can of course be interchanged, but Jacobians will make life hard when we attempt to get them right. In Sect. 2.1.5 we will discuss an easier way to compute kinematic distributions instead of the fully integrated total rate in Eq. 2.28.

2.1.4 Hadron Collider Kinematics

Hadron colliders have a particular kinematic feature in that event by event we do not know the longitudinal velocity of the initial state, i.e. the relative longitudinal boost from the laboratory frame to the partonic center of mass. This sensitivity to longitudinal boosts is reflected in the choice of kinematic variables. The first thing we can do is consider the projection of all momenta onto the transverse plane. These transverse components are trivially invariant under longitudinal boosts because the two are orthogonal to each other.

In addition, for the production of a single electroweak gauge boson we remember that the produced particle does not have any momentum transverse to the beam direction. This reflects the fact that the incoming quarks are collinear with the protons, i.e. they have zero transverse momentum. Such a gauge boson not recoiling against anything else cannot develop a finite transverse momentum. Of course, once we decay this gauge boson, for example into a pair of muons, each muon will have transverse momentum, only their vector sum will be zero:

$$\sum_{\text{final state}} \vec{p}_{T,j} = \vec{0}. \tag{2.29}$$

This is a relation between two-dimensional, not three-dimensional vectors. For several particles in the final state we can define an azimuthal angle in the plane transverse to the beam direction. While differences of azimuthal angles, e.g. two such differences between three particles in the final state, are observables the overall angle is a symmetry of the detector as well as of our physics.

In addition to the transverse plane we need to parameterize the longitudinal momenta in a way which makes it easy to implement longitudinal boosts. In Eq. 2.28 we integrate over the two momentum fractions $x_{1,2}$ and can at best determine their product $x_1 x_2 = s/S$ from the final state kinematics. Our task is to replace both, x_1 and x_2 with more physical variables which should be well behaved under longitudinal boosts.

A longitudinal boost for example from the rest frame of a massive particle reads

$$\begin{aligned}\begin{pmatrix} E \\ p_L \end{pmatrix} &= \exp\left[y \begin{pmatrix} 0 & 1 \\ 1 & 0 \end{pmatrix} \right] \begin{pmatrix} m \\ 0 \end{pmatrix} \\ &= \left[\mathbb{1} + y \begin{pmatrix} 0 & 1 \\ 1 & 0 \end{pmatrix} + \frac{y^2}{2} \mathbb{1} + \frac{y^3}{6} \begin{pmatrix} 0 & 1 \\ 1 & 0 \end{pmatrix} \cdots \right] \begin{pmatrix} m \\ 0 \end{pmatrix}\end{aligned}$$

$$= \left[\mathbb{1} \sum_{j\text{even}} \frac{y^j}{j!} + \begin{pmatrix} 0 & 1 \\ 1 & 0 \end{pmatrix} \sum_{j\text{odd}} \frac{y^j}{j!} \right] \begin{pmatrix} m \\ 0 \end{pmatrix}$$
$$= \left[\mathbb{1} \cosh y + \begin{pmatrix} 0 & 1 \\ 1 & 0 \end{pmatrix} \sinh y \right] \begin{pmatrix} m \\ 0 \end{pmatrix} = m \begin{pmatrix} \cosh y \\ \sinh y \end{pmatrix}. \tag{2.30}$$

In the first line we already see that the combination of two such exponentials involving y_1 and y_2 is additive $y = y_1 + y_2$. The *rapidity* y as defined in Eq. 2.30 we can re-write in a way which allows us to compute it from the four-momentum for example in the LHC lab frame

$$\frac{1}{2} \log \frac{E + p_L}{E - p_L} = \frac{1}{2} \log \frac{\cosh y + \sinh y}{\cosh y - \sinh y} = \frac{1}{2} \log \frac{e^y}{e^{-y}} = y. \tag{2.31}$$

We can explicitly check that the rapidity is indeed additive by applying a second longitudinal boost to (E, p_L) in Eq. 2.30

$$\begin{pmatrix} E' \\ p'_L \end{pmatrix} = \exp \left[y' \begin{pmatrix} 0 & 1 \\ 1 & 0 \end{pmatrix} \right] \begin{pmatrix} E \\ p_L \end{pmatrix} = \left[\mathbb{1} \cosh y' + \begin{pmatrix} 0 & 1 \\ 1 & 0 \end{pmatrix} \sinh y' \right] \begin{pmatrix} E \\ p_L \end{pmatrix}$$
$$= \begin{pmatrix} E \cosh y' + p_L \sinh y' \\ p_L \cosh y' + E \sinh y' \end{pmatrix}, \tag{2.32}$$

which gives for the combined rapidity, following its extraction in Eq. 2.21

$$\frac{1}{2} \log \frac{E' + p'_L}{E' - p'_L} = \frac{1}{2} \log \frac{(E + p_L)(\cosh y' + \sinh y')}{(E - p_L)(\cosh y' - \sinh y')} = \frac{1}{2} \log \frac{E + p_L}{E - p_L} + y' = y + y'. \tag{2.33}$$

This combination of several longitudinal boosts is important in the case of massless particles. They do not have a rest frame, which means we can only boost them from one finite-momentum frame to the other. For such massless particles we can simplify the formula for the rapidity Eq. 2.31, instead expressing the rapidity in terms of the polar angle θ. We use the fact that (only) for massless particles $E = |\vec{p}|$

$$y = \frac{1}{2} \log \frac{E + p_L}{E - p_L} = \frac{1}{2} \log \frac{|\vec{p}| + p_L}{|\vec{p}| - p_L} = \frac{1}{2} \log \frac{1 + \cos\theta}{1 - \cos\theta} = \frac{1}{2} \log \frac{1}{\tan^2 \frac{\theta}{2}}$$
$$= -\log \tan \frac{\theta}{2} \equiv \eta \tag{2.34}$$

This *pseudo-rapidity* η is more handy, but coincides with the actual rapidity only for massless particles. To get an idea about the experimental setup at the LHC—in CMS and ATLAS we can observe particles to polar angles of 10 or even 1.3°, corresponding to maximum pseudo-rapidities of 2.5–4.5. Because this is about the same range as the range of the *azimuthal angle* $[0, \pi]$ we define a distance measure inside the detector

$$
\begin{aligned}
(\Delta R)^2 &= (\Delta y)^2 + (\Delta\phi)^2 \\
&= (\Delta\eta)^2 + (\Delta\phi)^2 \qquad\qquad \text{massless particles} \\
&= \left(\log \frac{\tan\frac{\theta+\Delta\theta}{2}}{\frac{\theta}{2}} \right)^2 + (\Delta\phi)^2 \\
&= \frac{(\Delta\theta)^2}{\sin^2\theta} + (\Delta\phi)^2 + \mathcal{O}((\Delta\theta)^3)
\end{aligned}
\tag{2.35}
$$

The angle θ is the polar angle of one of the two particles considered and in our leading approximation can be chosen as each of them without changing Eq. 2.35.

Still studying the production of a single gauge boson at the LHC we can express the final state kinematics in terms of two parameters, the invariant mass of the final-state particle q^2 and its rapidity. The transverse momentum we already know is zero. The two incoming and approximately massless protons have the momenta

$$
p_1 = (E, 0, 0, E) \quad p_2 = (E, 0, 0, -E) \quad S = (2E)^2, \tag{2.36}
$$

which for the momentum of the final-state gauge boson in terms of the parton momentum fractions means, when we include the definition of the rapidity in Eq. 2.30

$$
\begin{aligned}
q = x_1 p_1 + x_2 p_2 = E \begin{pmatrix} x_1 + x_2 \\ 0 \\ 0 \\ x_1 - x_2 \end{pmatrix} &\overset{!}{=} \sqrt{q^2} \begin{pmatrix} \cosh y \\ 0 \\ 0 \\ \sinh y \end{pmatrix} = 2E\sqrt{x_1 x_2} \begin{pmatrix} \cosh y \\ 0 \\ 0 \\ \sinh y \end{pmatrix} \\
\Leftrightarrow \quad \cosh y &= \frac{x_1 + x_2}{2\sqrt{x_1 x_2}} = \frac{1}{2}\left(\sqrt{\frac{x_1}{x_2}} + \sqrt{\frac{x_2}{x_1}} \right) \\
\Leftrightarrow \quad e^y &= \sqrt{\frac{x_1}{x_2}}.
\end{aligned}
\tag{2.37}
$$

This result can be combined with $x_1 x_2 = q^2/S$ to obtain

$$
x_1 = \sqrt{\frac{q^2}{S}} e^y \qquad x_2 = \sqrt{\frac{q^2}{S}} e^{-y}. \tag{2.38}
$$

These relations allow us to for example compute the hadronic *total cross section* for lepton pair production in QED

$$
\boxed{\sigma(pp \to \ell^+\ell^-)\Big|_{\text{QED}} = \frac{4\pi\alpha^2 Q_\ell^2}{3N_c} \int_0^1 dx_1 dx_2 \sum_j Q_j^2 f_j(x_1) f_{\bar{j}}(x_2) \frac{1}{q^2}}, \tag{2.39}
$$

instead in terms of the hadronic phase space variables $x_{1,2}$ in terms of the kinematic final state observables q^2 and y. Remember that the partonic or quark–antiquark

cross section $\hat{\sigma}$ is already integrated over the (symmetric) azimuthal angle ϕ and the polar angle Mandelstam variable t. The transverse momentum of the two leptons is therefore fixed by momentum conservation.

The Jacobian for this change of variables reads

$$\frac{\partial(q^2, y)}{\partial(x_1, x_2)} = \begin{vmatrix} x_2 S & x_1 S \\ 1/(2x_1) & -1/(2x_2) \end{vmatrix} = S = \frac{q^2}{x_1 x_2}, \tag{2.40}$$

which inserted into Eq. 2.39 gives us

$$\begin{aligned} \sigma(pp \to \ell^+\ell^-)\Big|_{\text{QED}} &= \frac{4\pi\alpha^2 Q_\ell^2}{3N_c} \int dq^2 dy \frac{x_1 x_2}{q^2} \frac{1}{q^2} \sum_j Q_j^2 f_j(x_1) f_{\bar{j}}(x_2) \\ &= \frac{4\pi\alpha^2 Q_\ell^2}{3N_c} \int dq^2 dy \frac{1}{q^4} \sum_j Q_j^2 x_1 f_j(x_1) x_2 f_{\bar{j}}(x_2). \end{aligned} \tag{2.41}$$

In contrast to the original form of the integration over the hadronic phase space this form reflects the kinematic observables. For the Drell–Yan process at leading order the q^2 distribution is the same as $m_{\ell\ell}^2$, one of the most interesting distributions to study because of different contributions from the photon, the Z boson, or extra dimensional gravitons. On the other hand, the rapidity integral still suffers from the fact that at hadron colliders we do not know the longitudinal kinematics of the initial state and therefore have to integrate over it.

2.1.5 Phase Space Integration

In the previous example we have computed the simple two-dimensional distribution, by leaving out the double integration in Eq. 2.41

$$\frac{d\sigma(pp \to \ell^+\ell^-)}{dq^2 dy}\Big|_{\text{QED}} = \frac{4\pi\alpha^2 Q_\ell^2}{3N_c q^4} \sum_j Q_j^2 x_1 f_j(x_1) x_2 f_{\bar{j}}(x_2). \tag{2.42}$$

This expression we can numerically evaluate and compare to experiment. However, the rapidity y and the momentum transfer q^2 are by no means the only distribution we would like to look at. Moreover, over the parton densities $f(x)$ we will have to integrate numerically, so we will have to rely on numerical integration tools no matter what we are doing. Looking at a simple $(2 \to 2)$ process we can write the total cross section as

$$\sigma_{\text{tot}} = \int d\phi \int d\cos\theta \int dx_1 \int dx_2 F_{\text{PS}} |\mathscr{M}|^2 = \int_0^1 dy_1 \cdots dy_4 J_{\text{PS}}(\vec{y}) |\mathscr{M}|^2, \tag{2.43}$$

with an appropriate function F_{PS}. In the second step we have re-written the phase space integral as an integral over the four-dimensional unit cube, with the appropriate

Jacobian. Like any integral we can numerically evaluate this phase space integral by binning the variable we integrate over

$$\int_0^1 dy f(y) \quad \longrightarrow \quad \sum_j (\Delta y)_j f(y_j) \sim \Delta y \sum_j f(y_j). \tag{2.44}$$

Without any loss of generality we assume that the integration boundaries are $0 \cdots 1$. The integration variable y we can divide into a discrete set of points y_j, for example equidistant in y and by choosing a chain of random numbers $y_j \varepsilon [0, 1]$. In the latter case we need to keep track of the bin widths $(\Delta y)_j$. When we extend the integral over N dimensions we can in principle divide each axis into bins and compute the functional values for this grid. For not equidistant bins generated by random numbers we again keep track of the associated phase space volume for each random number vector. However, once we know these phase space weights for each phase space point there is no reason to consider the set of random numbers as in any way linked to the N axes. All we need is a chain of random points with an associated phase space weight and their transition matrix element, to integrate over the phase space in complete analogy to Eq. 2.24.

The obvious question arises how such random numbers can be chosen in a smart way; but before we discuss how to best evaluate such an integral numerically, let us first illustrate how this integral is much more useful than just providing the total cross section. If we are interested in the distribution of an observable, like for example the distribution of the transverse momentum of a muon in the Drell–Yan process, we need to compute $d\sigma/dp_T$ as a function of p_T. In terms of Eq. 2.23 any physical y_1 distribution is given by

$$\begin{aligned} \sigma &= \int dy_1 \cdots dy_N f(\vec{y}) = \int dy_1 \frac{d\sigma}{dy_1} \\ \left.\frac{d\sigma}{dy_1}\right|_{y_1^0} &= \int dy_2 \cdots dy_N f(y_1^0) = \int dy_1 \cdots dy_N f(\vec{y}) \delta(y_1 - y_1^0). \end{aligned} \tag{2.45}$$

Numerically we can compute this distribution in two ways: one way corresponds to the first line in Eq. 2.45 and means numerically evaluating the $y_2 \cdots y_N$ integrations and leaving out the y_1 integration. The result will be a function of y_1 which we then evaluate at different points y_1^0.

The second and much more efficient option corresponds to the second line of Eq. 2.45, with the delta distribution defined for discretized y_1. First, we define an array with the size given by the number of bins in the y_1 integration. Then, for each y_1 value of the complete $y_1 \cdots y_N$ integration we decide where the value y_1 goes in this array and add $f(\vec{y})$ to the corresponding column. Finally, we print these columns as a function of y_1 to see the distribution. This set of columns is referred to as a *histogram* and can be produced using publicly available software. This histogram approach does not sound like much, but imagine we want to compute a distribution $d\sigma/dp_T$, where $p_T(\vec{y})$ is a complicated function of the integration variables and kinematic phase space cuts. We then simply evaluate

$$\frac{d\sigma}{dp_T} = \int dy_1 \cdots dy_N \, f(\vec{y}) \delta \left(p_T(\vec{y}) - p_T^0 \right) \tag{2.46}$$

numerically and read off the p_T distribution as a side product of the calculation of the total rate. Histograms mean that computing a total cross section numerically we can trivially extract all distributions in the same process.

The procedure outlined above has an interesting interpretation. Imagine we do the entire phase space integration numerically. Just like computing the interesting observables we can compute the momenta of all external particles. These momenta are not all independent, because of energy–momentum conservation, but this can be taken care of. The tool which translates the vector of integration variables $\vec{y}$ into the external momenta is called a *phase space generator*. Because the phase space is not uniquely defined in terms of the integration variables, the phase space generator also returns the Jacobian J_{PS}, called the phase space weight. If we think of the integration as an integration over the unit cube, this weight needs to be combined with the matrix element squared $|\mathscr{M}|^2$. Once we compute the unique phase space configuration $(k_1, k_2, p_1 \cdots)_j$ corresponding to the vector $\vec{y}_j$, the combined weight $W = J_{\text{PS}} |\mathscr{M}|^2$ is the probability that this configuration will appear at the LHC. This means we do not only integrate over the phase space, we really simulate LHC events. The only complication is that the probability of a certain configuration is not only given by the frequency with which it appears, but also by the explicit weight. So when we run our numerical integration through the phase space generator and histogram all the distributions we are interested in we generate *weighted events*. These events, i.e. the momenta of all external particles and the weight W, we can for example store in a big file.

This simulation is not yet what experimentalists want—they want to represent the probability of a certain configuration appearing only by its frequency. Experimentally measured events do not come with a variable weight, either they are recorded or they are not. This means we have to unweight the events by translating the event weight into frequency.

There are two ways to do that. On the one hand, we can look at the minimum event weight and express all other events in relative probability to this event. Translating this relative event weight into a frequency means replacing an event with the relative weight W_j / W_{min} by W_j / W_{min} events in the same phase space point. The problem with this method is that we are really dealing with a binned phase space, so we would not know how to distribute these events in the given bin. Alternatively, we can start from to the maximum weight W_{max} and compute the ratio $W_j / W_{\text{max}} \in [0, 1]$. Keeping an event with a given probability means we can generate a flat random number $r \in [0, 1]$ and only keep it if $W_j / W_{\text{max}} > r$. The challenge in this translation is that we always lose events. If it was not for the experimentalists we would hardly use such *unweighted events*, but they have good reasons to want such unweighted events which feed best through detector simulations.

The last comment is that if the phase space configuration $(k_1, k_2, p_1 \cdots)_j$ can be measured, its weight W_j better be positive. This is not trivial once we go beyond leading order. There, we need to add several contributions to produce a physical

event, like for example different n-particle final states, and there is no guarantee for each of them to be positive. We have to ensure that after adding up all contributions and after integrating over any kind of unphysical degrees of freedom we might have introduced, the probability of a physics configuration is positive. From this point of view negative values for parton densities $f(x) < 0$ are in principle not problematic, as long as we always keep a positive hadronic rate $d\sigma_{pp\to X} > 0$.

Going back to the numerical phase space integration for many particles, it faces two problems. First, the partonic phase space for n on-shell particles in the final state has $3(n+2)-3$ dimensions. If we divide each of these directions in 100 bins, the number of phase space points we need to evaluate for a $(2 \to 4)$ process is $100^{15} = 10^{30}$, which is not realistic.

To integrate over a large number of dimensions we use *Monte Carlo integration*. In this approach we define a distribution $p_Y(y)$ such that for a one-dimensional integral we can replace the binned discretized phase space integral by a discretized version based on a set of random numbers Y_j over the integration variables y

$$\langle g(Y)\rangle = \int_0^1 dy p_Y(y) g(y) \quad \longrightarrow \quad \frac{1}{N}\sum_j g(Y_j). \tag{2.47}$$

All we have to make sure is that the probability of returning Y_j is given by $p_Y(y)$ for $y < Y_j < y + dy$. As mentioned above, also Eq. 2.47 has the advantage that we can naively generalize it to any number of N dimensions, just by organizing the random numbers Y_j in one large chain instead of an N-dimensional array. Our N-dimensional phase space integral shown in Eq. 2.43 we can re-write in the same manner

$$\int_0^1 d^N y f(y) = \int_0^1 d^N y \frac{f(y)}{p_Y(y)} p_Y(y) = \left\langle \frac{f(Y)}{p_Y(Y)} \right\rangle \to \frac{1}{N}\sum_j \frac{f(Y_j)}{p_Y(Y_j)}. \tag{2.48}$$

To compute the integral we have to average over all phase space values of f/p_Y. In the ideal case where we exactly know the form of the integrand and can map it into our random numbers, the error of the numerical integration will be zero. So what we have to find is a way to encode $f(Y_j)$ into $p_Y(Y_j)$. This task is called *importance sampling* and you can find some documentation for example on the standard implementation VEGAS to look at the details.

Technically, VEGAS will call the function which computes the weight $W = J_{\text{PS}}|\mathscr{M}|^2$ for a number of phase space points and average over these points, but including another weight factor W_{MC} representing the importance sampling. If we want to extract distributions via histograms we have to add the total weight $W = W_{\text{MC}} J_{\text{PS}}|\mathscr{M}|^2$ to the columns.

The second numerical challenge is that the matrix elements for interesting processes are by no means flat. We would therefore like to help our adaptive or importance sampling Monte Carlo by defining the integration variables such that the integrand becomes as flat as possible. For example for the integration over the partonic momentum fraction we know that the integrand usual falls off as $1/x$. In that situation we can substitute

$$\int_\delta dx \frac{C}{x} = \int_{\log\delta} d\log x \left(\frac{d\log x}{dx}\right)^{-1} \frac{C}{x} = \int_{\log\delta} d\log x\, C, \tag{2.49}$$

to obtain a flat integrand. There exists an even more impressive and relevant example: intermediate particles with Breit–Wigner propagators squared are particularly painful to integrate over the momentum $s = p^2$ flowing through it

$$P(s,m) = \frac{1}{(s-m^2)^2 + m^2\Gamma^2}. \tag{2.50}$$

For example, a Standard-Model Higgs boson with a mass of 120 GeV has a width around 0.005 GeV, which means that the integration over the invariant mass of the Higgs decay products $\sqrt{s}$ requires a relative resolution of 10^{-5}. Since this is unlikely to be achievable what we should really do is find a substitution which produces the inverse Breit–Wigner as a Jacobian and leads to a flat integrand—et voilà

$$\begin{aligned}\int ds \frac{C}{(s-m^2)^2 + m^2\Gamma^2} &= \int dz \left(\frac{dz}{ds}\right)^{-1} \frac{C}{(s-m^2)^2 + m^2\Gamma^2} \\ &= \int dz \frac{(s-m^2)^2 + m^2\Gamma^2}{m\Gamma} \frac{C}{(s-m^2)^2 + m^2\Gamma^2} \\ &= \frac{1}{m\Gamma} \int dz C \quad \text{with} \quad \tan z = \frac{s-m^2}{m\Gamma}.\end{aligned} \tag{2.51}$$

This is the most useful *phase space mapping* in LHC physics. Of course, any adaptive Monte Carlo will eventually converge on such an integrand, but a well-chosen set of integration parameters will speed up simulations very significantly.

2.2 Ultraviolet Divergences

From general field theory we know that when we are interested for example in cross section prediction with higher precision we need to compute further terms in its perturbative series in α_s. This computation will lead to ultraviolet divergences which can be absorbed into counter terms for any parameter in the Lagrangian. The crucial feature is that for a renormalizable theory like our Standard Model including a Higgs boson the number of counter terms is finite, which means once we know all parameters including their counter terms our theory becomes predictive.

In Sect. 2.3 we will see that in QCD processes we also encounter another kind of divergences. They arise from the infrared momentum regime. Infrared divergences is what this lecture is really going to be about, but before dealing with them it is very instructive to see what happens to the much better understood ultraviolet divergences. In Sect. 2.2.1 we will review how such ultraviolet divergences arise and how they are removed. In Sect. 2.2.2 we will review how running parameters appear in this procedure, i.e. how scale dependence is linked to the appearance of divergences.

Finally, in Sect. 2.2.3 we will interpret the use of running parameters physically and see that in perturbation theory they re-sum classes of logarithms to all orders in perturbation theory. Later in Sect. 2.3 we will follow exactly the same steps for infrared divergences and develop some crucial features of hadron collider physics.

2.2.1 Counter Terms

Renormalization, i.e. the proper treatment of ultraviolet divergences, is one of the most important things to understand about field theories; more detailed discussions you can find in any book on advanced field theory. The aspect of renormalization which will guide us through this section is the appearance of the renormalization scale.

In perturbation theory, scales automatically arise from the regularization of infrared or ultraviolet divergences. We can see this writing down a simple scalar loop integral, corresponding to two virtual scalars with masses $m_{1,2}$ and with the external momentum p flowing through a diagram similar to those summed in Sect. 2.1.2

$$B(p^2; m_1, m_2) \equiv \int \frac{d^4q}{16\pi^2} \frac{1}{q^2 - m_1^2} \frac{1}{(q+p)^2 - m_2^2}. \tag{2.52}$$

Such two-point functions appear for example in the gluon self energy, with massless scalars for ghosts, with a Dirac trace in the numerator for quarks, and with massive scalars for supersymmetric scalar quarks. In those cases the two masses are identical $m_1 = m_2$. The integration measure $1/(16\pi^2)$ is dictated by the usual Feynman rules for the integration over loop momenta. Counting powers of q in Eq. 2.52 we see that the integrand scales like $1/q$ in the ultraviolet, so it is logarithmically divergent and we have to regularize it. Regularizing means expressing the divergence in a well-defined manner or scheme allowing us to get rid of it by renormalization.

One regularization scheme is to introduce a cutoff into the momentum integral Λ, for example through the so-called Pauli–Villars regularization. Because the ultraviolet behavior of the integrand or integral cannot depend on any parameter living at a small energy scales, the parameterization of the ultraviolet divergence in Eq. 2.52 cannot involve the mass m or the external momentum p^2. The scalar two-point function has mass dimension zero, so its divergence has to be proportional to $\log(\Lambda/\mu_R)$ with a dimensionless prefactor and some scale μ_R^2 which is an artifact of the regularization of such a Feynman diagram.

A more elegant regularization scheme is *dimensional regularization*. It is designed not to break gauge invariance and naively seems to not introduce a mass scale μ_R. When we shift the momentum integration from 4 to $4 - 2\varepsilon$ dimensions and use analytic continuation in the number of space–time dimensions to renormalize the theory a *renormalization scale* μ_R nevertheless appears once we ensure the two-point function and with it observables like cross sections keep their correct mass

dimension

$$\int \frac{d^4q}{16\pi^2}\cdots \longrightarrow \mu_R^{2\varepsilon}\int \frac{d^{4-2\varepsilon}q}{16\pi^2}\cdots = \frac{i\mu_R^{2\varepsilon}}{(4\pi)^2}\left[\frac{C_{-1}}{\varepsilon}+C_0+C_1\varepsilon+\mathcal{O}(\varepsilon^2)\right]. \tag{2.53}$$

At the end, the scale μ_R might become irrelevant and drop out after renormalization and analytic continuation, but to be on the save side we keep it. The constants C_i in the series in $1/\varepsilon$ depend on the loop integral we are considering. To regularize the ultraviolet divergence we assume $\varepsilon > 0$ and find mathematically well-defined poles $1/\varepsilon$. Defining scalar integrals with the integration measure $1/(i\pi^2)$ will make for example C_{-1} come out as of the order $\mathcal{O}(1)$. This is the reason we usually find factors $1/(4\pi)^2 = \pi^2/(2\pi)^4$ in front of the loop integrals.

The poles in $1/\varepsilon$ will cancel with the universal *counter terms* once we renormalize the theory. Counter terms we include by shifting parameters in the Lagrangian and the leading order matrix element. They cancel the poles in the combined leading order and virtual one-loop prediction

$$\begin{aligned} |\mathcal{M}_{\text{LO}}(g)+\mathcal{M}_{\text{virt}}|^2 &= |\mathcal{M}_{\text{LO}}(g)|^2 + 2\text{Re}\,\mathcal{M}_{\text{LO}}(g)\mathcal{M}_{\text{virt}}+\cdots \\ &\to |\mathcal{M}_{\text{LO}}(g+\delta g)|^2 + 2\text{Re}\,\mathcal{M}_{\text{LO}}(g)\mathcal{M}_{\text{virt}}+\cdots \\ \text{with}\quad g \to g^{\text{bare}} &= g+\delta g \quad\text{and}\quad \delta g \propto \alpha_s/\varepsilon. \end{aligned} \tag{2.54}$$

The dots indicate higher orders in α_s, for example absorbing the δg corrections in the leading order and virtual interference. As we can see in Eq. 2.54 the counter terms do not come with a factor $\mu_R^{2\varepsilon}$ in front. Therefore, while the poles $1/\varepsilon$ cancel just fine, the scale factor $\mu_R^{2\varepsilon}$ will not be matched between the actual ultraviolet divergence and the counter term.

We can keep track of the renormalization scale best by expanding the prefactor of the regularized but not yet renormalized integral in Eq. 2.53 in a Taylor series in ε, no question asked about convergence radii

$$\begin{aligned} \mu_R^{2\varepsilon}\left[\frac{C_{-1}}{\varepsilon}+C_0+\mathcal{O}(\varepsilon)\right] &= e^{2\varepsilon\log\mu_R}\left[\frac{C_{-1}}{\varepsilon}+C_0+\mathcal{O}(\varepsilon)\right] \\ &= \left[1+2\varepsilon\log\mu_R+\mathcal{O}(\varepsilon^2)\right]\left[\frac{C_{-1}}{\varepsilon}+C_0+\mathcal{O}(\varepsilon)\right] \\ &= \frac{C_{-1}}{\varepsilon}+C_0+C_{-1}\log\mu_R^2+\mathcal{O}(\varepsilon) \\ &\to \frac{C_{-1}}{\varepsilon}+C_0+C_{-1}\log\frac{\mu_R^2}{M^2}+\mathcal{O}(\varepsilon). \end{aligned} \tag{2.55}$$

In the last step we have by hand corrected for the fact that $\log\mu_R^2$ with a mass dimension inside the logarithm cannot appear in our calculations. From somewhere else in our calculation the scale dependence logarithm will be matched with a $\log M^2$ where M^2 is the typical mass or energy scale in our process. This little argument shows that also in dimensional regularization we introduce a mass scale μ_R which

appears as $\log(\mu_R^2/M^2)$ in the renormalized expression for our observables. There is no way of removing ultraviolet divergences without introducing the renormalization scale if we keep track of the mass dimensions of our regularized result.

In Eq. 2.54 there appear two contributions to a given observable, the expected C_0 and the renormalization induced C_{-1}. Because the factors C_{-1} are linked to the counter terms in the theory we can often guess them without actually computing the loop integral, which is very useful in cases where they numerically dominate.

Counter terms as they schematically appear in Eq. 2.54 are not uniquely defined. They need to include a given divergence, to return finite observables, but we are free to add any finite contribution we want. This opens many ways to define a counter term for example based on physical processes where counter terms do not only cancel the pole but also finite contributions at a given order in perturbation theory. Needless to say, such schemes do not automatically work universally. An example for such a *physical renormalization scheme* is the on-shell scheme for masses, where we define a counter term such that external on-shell particles do not receive any corrections to their masses. For the top mass this means that just like in Eq. 2.54 we replace the leading order mass with the bare mass, for which we then insert the expression in terms of the renormalized mass and the counter term

$$\begin{aligned} m_t^{\text{bare}} &= m_t + \delta m_t \\ &= m_t + m_t \frac{\alpha_s C_F}{4\pi} \left(3 \left(-\frac{1}{\varepsilon} + \gamma_E - \log(4\pi) - \log \frac{\mu_R^2}{M^2} \right) - 4 + 3 \log \frac{m_t^2}{M^2} \right) \\ &\equiv m_t + m_t \frac{\alpha_s C_F}{4\pi} \left(-\frac{3}{\tilde{\varepsilon}} - 4 + 3 \log \frac{m_t^2}{M^2} \right) \\ \Leftrightarrow \quad & \frac{1}{\tilde{\varepsilon}\left(\frac{\mu_R}{M}\right)} \equiv \frac{1}{\varepsilon} - \gamma_E + \log \frac{4\pi\mu_R^2}{M^2}. \end{aligned} \tag{2.56}$$

The convenient scale dependent pole $1/\tilde{\varepsilon}$ includes the universal additional terms like the Euler gamma function and the scaling logarithm. This logarithm is the big problem in this universality argument, since we need to introduce the arbitrary energy scale M to separate the universal logarithm of the renormalization scale and the parameter-dependent logarithm of the physical process.

A theoretical problem with this *on-shell renormalization scheme* is that it is not gauge invariant. On the other hand, it describes for example the kinematic features of top pair production at hadron colliders in a stable perturbation series. This means that once we define a more appropriate scheme for heavy particle masses in collider production mechanisms it better be numerically close to the pole mass. For the computation of total cross sections at hadron colliders or the production thresholds at e^+e^- colliders the pole mass is not well suited at all, but as we will see in Chap. 3 this is not where at the LHC we expect to measure particle masses, so we should do fine with something very similar to the pole mass.

Another example for a process dependent renormalization scheme is the mixing of γ and Z propagators. There we choose the counter term of the weak mixing angle

such that an on-shell Z boson cannot oscillate into a photon, and vice versa. We can generalize this scheme for mixing scalars as they for example appear in supersymmetry, but it is not gauge invariant with respect to the weak gauge symmetries of the Standard Model either. For QCD corrections, on the other hand, it is the most convenient scheme keeping all exchange symmetries of the two scalars.

To finalize this discussion of process dependent mass renormalization we quote the result for a scalar supersymmetric quark, a squark, where in the on-shell scheme we find

$$\begin{aligned} m_{\tilde{q}}^{\text{bare}} &= m_{\tilde{q}} + \delta m_{\tilde{q}} \\ &= m_{\tilde{q}} + m_{\tilde{q}} \frac{\alpha_s C_F}{4\pi} \left(-\frac{2r}{\tilde{\varepsilon}} - 1 - 3r - (1-2r)\log r \right. \\ &\qquad \left. - (1-r)^2 \log\left|\frac{1}{r} - 1\right| - 2r \log\frac{m_{\tilde{q}}^2}{M^2} \right) \end{aligned} \tag{2.57}$$

with $r = m_{\tilde{g}}^2/m_{\tilde{q}}^2$. The interesting aspect of this squark mass counter term is that it also depends on the gluino mass, not just the squark mass itself. The reason why QCD counter terms tend to depend only on the renormalized quantity itself is that the gluon is massless. In the limit of vanishing gluino contribution the squark mass counter term is again only proportional to the squark mass itself

$$m_{\tilde{q}}^{\text{bare}}\Big|_{m_{\tilde{g}}=0} = m_{\tilde{q}} + \delta m_{\tilde{q}} = m_{\tilde{q}} + m_{\tilde{q}} \frac{\alpha_s C_F}{4\pi} \left(-\frac{1}{\tilde{\varepsilon}} - 3 + \log\frac{m_{\tilde{q}}^2}{M^2} \right). \tag{2.58}$$

One common feature of all mass counter terms listed above is $\delta m \propto m$, which means that we actually encounter a multiplicative renormalization

$$m^{\text{bare}} = Z_m m = (1 + \delta Z_m)\, m = \left(1 + \frac{\delta m}{m}\right) m = m + \delta m, \tag{2.59}$$

with $\delta Z_m = \delta m/m$ linking the two ways of writing the mass counter term. This form implies that particles with zero mass will not obtain a finite mass through renormalization. If we remember that chiral symmetry protects a Lagrangian from acquiring fermion masses this means that on-shell renormalization does not break this symmetry. A massless theory cannot become massive by mass renormalization. Regularization and renormalization schemes which do not break symmetries of the Lagrangian are ideal.

When we introduce counter terms in general field theory we usually choose a slightly more model independent scheme—we define a renormalization point. This is the energy scale at which the counter terms cancels all higher order contributions, divergent as well as finite. The best known example is the electric charge which we renormalize in the *Thomson limit* of zero momentum transfer through the photon propagator

$$e \to e^{\text{bare}} = e + \delta e. \tag{2.60}$$

Looking back at δm_t as defined in Eq. 2.56 we also see a way to define a completely general counter term: if dimensional regularization, i.e. the introduction of $4 - 2\varepsilon$ dimensions does not break any of the symmetries of our Lagrangian, like Lorentz symmetry or gauge symmetries, we should simply subtract the ultraviolet pole and nothing else. The only question is: do we subtract $1/\varepsilon$ (MS scheme) or do we subtract $1/\tilde{\varepsilon}$ in the $\overline{MS}$ *scheme*. In the $\overline{\text{MS}}$ scheme the counter term is then scale dependent.

Carefully counting, there are three scales present in such a scheme. First, there is the physical scale in the process. In our case of a top self energy this is for example the top mass m_t appearing in the matrix element for the process $pp \to t\bar{t}$. Next, there is the renormalization scale μ_R, a reference scale which is part of the definition of any counter term. And last but not least, there is the scale M separating the counter term from the process dependent result, which we can choose however we want, but which as we will see implies a running of the counter term. The role of this scale M will become clear when we go through the example of the running strong coupling α_s. Of course, we would prefer to choose all three scales the same, but in a complex physical process this might not always be possible. For example, any massive $(2 \to 3)$ production process naturally involves several external physical scales.

Just a side remark for completeness: a one loop integral which has no intrinsic mass scale is the two-point function with zero mass in the loop and zero momentum flowing through the integral: $B(p^2 = 0; 0, 0)$. It appears for example in the self energy corrections of external quarks and gluons. Based on dimensional arguments this integral has to vanish altogether. On the other hand, we know that like any massive two-point function it has to be ultraviolet divergent $B \sim 1/\varepsilon_{\text{UV}}$ because setting all internal and external mass scales to zero is nothing special from an ultraviolet point of view. This can only work if the scalar integral also has an infrared divergence appearing in dimensional regularization. We can then write the entire massless two-point function as

$$B(p^2 = 0; 0, 0) = \int \frac{d^4q}{16\pi^2} \frac{1}{q^2} \frac{1}{(q+p)^2} = \frac{i\pi^2}{16\pi^2} \left(\frac{1}{\varepsilon_{\text{UV}}} - \frac{1}{\varepsilon_{\text{IR}}} \right), \tag{2.61}$$

keeping track of the divergent contributions from the infrared and the ultraviolet regimes. For this particular integral they precisely cancel, so the result for $B(0; 0, 0)$ is zero, but setting it to zero too early will spoil any ultraviolet and infrared finiteness tests in practical calculations. Treating the two divergences strictly separately and dealing with them one after the other also ensures that for ultraviolet divergences we can choose $\varepsilon > 0$ while for infrared divergences we require $\varepsilon < 0$.

2.2.2 Running Strong Coupling

To get an idea what these different scales which appear in the process of renormalization mean let us compute such a scale dependent parameter, namely the *running strong coupling* $\alpha_s(\mu_R^2)$. The Drell–Yan process is one of the very few relevant process at hadron colliders where the strong coupling does not appear at tree level, so we cannot use it as our toy process this time. Another simple process where we can study this coupling is bottom pair production at the LHC, where at some energy range we will be dominated by valence quarks: $q\bar{q} \to b\bar{b}$. The only Feynman diagram is an s-channel off-shell gluon with a momentum flow $p^2 \equiv s$.

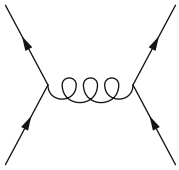

At next-to-leading order this gluon propagator will be corrected by self energy loops, where the gluon splits into two quarks or gluons and re-combines before it produces the two final state bottoms. Let us for now assume that all quarks are massless. The Feynman diagrams for the gluon self energy include a quark look, a gluon loop, and the ghost loop which removes the unphysical degrees of freedom of the gluon inside the loop.

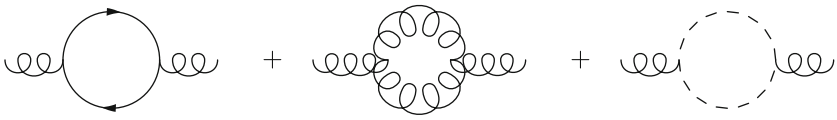

The gluon self energy correction or vacuum polarization, as propagator corrections to gauge bosons are usually labelled, will be a scalar, i.e. all fermion lines close and the Dirac trace is computed inside the loop. In color space the self energy will (hopefully) be diagonal, just like the gluon propagator itself, so we can ignore the color indices for now. In unitary gauge the gluon propagator is proportional to the transverse tensor $T^{\mu\nu} = g^{\mu\nu} - p^\nu p^\mu / p^2$. As mentioned in the context of the effective gluon-Higgs coupling, the same should be true for the gluon self energy, which we therefore write as $\Pi^{\mu\nu} \equiv \Pi T^{\mu\nu}$. A useful simple relation is $T^{\mu\nu} T_\nu^\rho = T^{\mu\rho}$ and $T^{\mu\nu} g_\nu^\rho = T^{\mu\rho}$. Including the gluon, quark, and ghost loops the regularized gluon self energy with a momentum flow p^2 reads

$$-\frac{1}{p^2}\Pi\left(\frac{\mu_R^2}{p^2}\right) = \frac{\alpha_s}{4\pi}\left(-\frac{1}{\tilde{\varepsilon}}+\log\frac{p^2}{M^2}\right)\left(\frac{13}{6}N_c-\frac{2}{3}n_f\right)+\mathcal{O}(\log m_t^2)$$
$$\equiv \alpha_s\left(-\frac{1}{\tilde{\varepsilon}}+\log\frac{p^2}{M^2}\right)b_0+\mathcal{O}(\log m_t^2)$$
$$\text{with}\quad \boxed{b_0=\frac{1}{4\pi}\left(\frac{11}{3}N_c-\frac{2}{3}n_f\right)}. \tag{2.62}$$

The minus sign arises from the factors i in the propagators, as shown in Eq. 2.19. The number of fermions coupling to the gluons is n_f. From the comments on $B(p^2;0,0)$ we could guess that the loop integrals will only give a logarithm $\log p^2$ which is then matched by the logarithm $\log M^2$ implicitly included in the definition of $\tilde{\varepsilon}$. The factor b_0 arises from the one-loop corrections to the gluon self energy, i.e. from diagrams which include one additional factor α_s. Strictly speaking, this form is the first term in a *perturbative series* in the strong coupling $\alpha_s = g_s^2/(4\pi)$. Later on, we will indicate where additional higher order corrections would enter.

In the second step of Eq. 2.62 we have sneaked in additional contributions to the renormalization of the strong coupling from the other one-loop diagrams in the process, replacing the factor 13/6 by a factor 11/3. This is related to the fact that there are actually three types of divergent virtual-gluon diagrams in the physical process $q\bar{q}\to b\bar{b}$: the external quark self energies with renormalization factors $Z_f^{1/2}$, the internal gluon self energy Z_A, and the vertex corrections Z_{Aff}. The only physical parameters we can renormalize in this process are the strong coupling and, if finite, the bottom mass. Wave function renormalization constants are not physical. The entire divergence in our $q\bar{q}\to b\bar{b}$ process which needs to be absorbed in the strong coupling Z_g is given by the combination

$$Z_{Aff} = Z_g Z_A^{1/2} Z_f \quad\Leftrightarrow\quad \frac{Z_{Aff}}{Z_A^{1/2}Z_f}\equiv Z_g. \tag{2.63}$$

We can check this definition of Z_g by comparing all vertices in which the strong coupling g_s appears, namely the gluon coupling to quarks, ghosts as well as the triple and quartic gluon vertex. All of them need to have the same divergence structure

$$\frac{Z_{Aff}}{Z_A^{1/2}Z_f}\stackrel{!}{=}\frac{Z_{A\eta\eta}}{Z_A^{1/2}Z_\eta}\stackrel{!}{=}\frac{Z_{3A}}{Z_A^{3/2}}\stackrel{!}{=}\sqrt{\frac{Z_{4A}}{Z_A^2}}. \tag{2.64}$$

If we had done the same calculation in QED, i.e. looked for a running electric charge, we would have found that the vacuum polarization diagrams for the photon do account for the entire counter term of the electric charge. The other two renormalization constants Z_{Aff} and Z_f cancel because of gauge invariance.

In contrast to QED, the strong coupling diverges in the Thomson limit because QCD is confined towards large distances and weakly coupled at small distances. Lacking a well-enough motivated reference point we are tempted to renormalize α_s

in the $\overline{\text{MS}}$ scheme. From Eq. 2.62 we know that the ultraviolet pole which needs to be cancelled by the counter term is proportional to the function b_0

$$\begin{aligned} g_s^{\text{bare}} &= Z_g g_s = \left(1 + \delta Z_g\right) g_s = \left(1 + \frac{\delta g_s}{g_s}\right) g_s \\ (g_s^2)^{\text{bare}} &= (Z_g g_s)^2 = \left(1 + \frac{\delta g_s}{g_s}\right)^2 g_s^2 = \left(1 + 2\frac{\delta g_s}{g_s}\right) g_s^2 = \left(1 + \frac{\delta g_s^2}{g_s^2}\right) g_s^2 \\ \alpha_s^{\text{bare}} &= \left(1 + \frac{\delta \alpha_s}{\alpha_s}\right) \alpha_s \\ &\stackrel{!}{=} \left(1 - \frac{\Pi}{p^2}\bigg|_{\text{pole}}\right) \alpha_s(M^2) = \left(1 - \frac{\alpha_s}{\tilde{\varepsilon}\left(\frac{\mu_R}{M}\right)} b_0\right) \alpha_s(M^2). \end{aligned} \tag{2.65}$$

Only in the last step we have explicitly included the scale dependence of the counter term. Because the bare coupling does not depend on any scales, this means that α_s depends on the unphysical scale M. Similar to the top mass renormalization scheme we can switch to a more physical scheme for the strong coupling as well: we can absorb also the finite contributions of $\Pi(\mu_R^2/p^2)$ into the strong coupling by simply identifying $M^2 = p^2$. This implies based again on Eq. (6.62)

$$\alpha_s^{\text{bare}} = \alpha_s(p^2) \left(1 - \frac{\alpha_s b_0}{\tilde{\varepsilon}} + \alpha_s b_0 \log \frac{p^2}{M^2}\right) \tag{2.66}$$

This formula defines a running coupling $\alpha_s(p^2)$, because the definition of the coupling now has to account for a possible shift between the original argument p^2 and the scale M^2 coming out of the $\overline{\text{MS}}$ scheme. Since according to Eqs. 2.65 and 2.66 the bare strong coupling can be expressed in terms of $\alpha_s(M^2)$ as well as in terms of $\alpha_s(p^2)$ we can link the two scales through

$$\begin{aligned} & \alpha_s(M^2) = \alpha_s(p^2) + \alpha_s^2 b_0 \log \frac{p^2}{M^2} \\ \Leftrightarrow \quad & \frac{d\alpha_s(p^2)}{d \log p^2} = -\alpha_s^2 b_0 + \mathcal{O}(\alpha_s^3) \end{aligned} \tag{2.67}$$

To the given loop order the argument of the strong coupling squared in this formula can be neglected—its effect is of higher order.

In this first formula for the running coupling constant we see that b_0 is positive in the Standard Model. This means that for $p^2 > M^2$ the ultraviolet limit of the strong coupling is zero. This makes QCD an *asymptotically free* theory. We can compute the function b_0 in general models by simply adding all contributions of strongly interacting particles in this loop

$$b_0 = -\frac{1}{12\pi} \sum_{\text{colored states}} D_j \; T_{R,j}, \tag{2.68}$$

where we need to know some kind of counting factor D_j which is -11 for a vector boson (gluon), +4 for a Dirac fermion (quark), +2 for a Majorana fermion (gluino), +1 for a complex scalar (squark) and +1/2 for a real scalar. The color charges are $T_R = 1/2$ for the fundamental representation of $SU(3)$ and $C_A = N_c$ for the adjoint representation. The masses of the loop particles are not relevant in this approximation because we are only interested in the ultraviolet regime of QCD where all particles can be regarded massless. When we really model the running of α_s we need to take into account threshold effects of heavy particles, because particles can only contribute to the running of α_s at scales above their mass scale. This is why the R ratio computed in Eq. 2.12 is so interesting once we vary the energy of the incoming electron–positron pair.

We can do even better than this fixed order in perturbation theory: while the correction to α_s in Eq. 2.66 is perturbatively suppressed by the usual factor $\alpha_s/(4\pi)$ it includes a logarithm of a ratio of scales which does not need to be small. Instead of simply including these gluon self energy corrections at a given order in perturbation theory we can instead include chains of one-loop diagrams with Π appearing many times in the off-shell gluon propagator. This series of Feynman diagrams is identical to the one we sum for the mass renormalization in Eq. 2.19. It means we replace the off-shell gluon propagator by (schematically written without the factors i)

$$\begin{aligned}\frac{T^{\mu\nu}}{p^2} \to \frac{T^{\mu\nu}}{p^2} &+ \left(\frac{T}{p^2}\cdot(-T\Pi)\cdot\frac{T}{p^2}\right)^{\mu\nu} \\ &+ \left(\frac{T}{p^2}\cdot(-T\Pi)\cdot\frac{T}{p^2}\cdot(-T\Pi)\cdot\frac{T}{p^2}\right)^{\mu\nu} + \cdots \\ = \frac{T^{\mu\nu}}{p^2}\sum_{j=0}^{\infty}\left(-\frac{\Pi}{p^2}\right)^j &= \frac{T^{\mu\nu}}{p^2}\,\frac{1}{1+\Pi/p^2}.\end{aligned} \tag{2.69}$$

To avoid indices we abbreviate $T^{\mu\nu}T^{\rho}_{\nu} = T\cdot T$ which make sense because of $(T\cdot T\cdot T)^{\mu\nu} = T^{\mu\rho}T^{\sigma}_{\rho}T^{\nu}_{\sigma} = T^{\mu\nu}$. This re-summation of the logarithm which appears in the next-to-leading order corrections to α_s moves the finite shift in α_s shown in Eqs. 2.62 and 2.66 into the denominator, while we assume that the pole will be properly taken care off in any of the schemes we discuss

$$\alpha_s^{\text{bare}} = \alpha_s(M^2) - \frac{\alpha_s^2 b_0}{\tilde{\varepsilon}} \equiv \frac{\alpha_s(p^2)}{1-\alpha_s\, b_0\, \log\frac{p^2}{M^2}} - \frac{\alpha_s^2 b_0}{\tilde{\varepsilon}}. \tag{2.70}$$

Just as in the case without re-summation, we can use this complete formula to relate the values of α_s at two reference points, i.e. we consider it a *renormalization group* equation (RGE) which evolves physical parameters from one scale to another in analogy to the fixed order version in Eq. 2.67

$$\frac{1}{\alpha_s(M^2)} = \frac{1}{\alpha_s(p^2)}\left(1-\alpha_s\, b_0\, \log\frac{p^2}{M^2}\right) = \frac{1}{\alpha_s(p^2)} - b_0\, \log\frac{p^2}{M^2} + \mathcal{O}(\alpha_s). \tag{2.71}$$

The factor α_s inside the parentheses we can again evaluate at either of the two scales, the difference is going to be a higher order effect. When we differentiate $\alpha_s(p^2)$ with respect to the momentum transfer p^2 we find, using the relation $d/dx(1/\alpha_s) = -1/\alpha_s^2\ d\alpha_s/dx$

$$\frac{1}{\alpha_s}\ \frac{d\alpha_s}{d\log p^2} = -\alpha_s \frac{d}{d\log p^2}\ \frac{1}{\alpha_s} = -\alpha_s b_0 + \mathcal{O}(\alpha_s^2)$$

$$\boxed{p^2 \frac{d\alpha_s}{dp^2} \equiv \frac{d\alpha_s}{d\log p^2} = \beta = -\alpha_s^2 \sum_{n=0} b_n \alpha_s^n} \tag{2.72}$$

This is the famous running of the strong coupling constant including all higher order terms b_n.

It is customary to replace the renormalization point of α_s in Eq. 2.70 with a reference scale where the denominator of the re-summed running coupling crosses zero and the running coupling itself should diverge. This is the Landau pole of the strong coupling, as discussed for the Higgs self coupling in Sect. 1.2.3. At one loop order this reads

$$1 - \alpha_s\ b_0\ \log\frac{\Lambda_{\rm QCD}^2}{M^2} \stackrel{!}{=} 0 \quad \Leftrightarrow \quad \log\frac{\Lambda_{\rm QCD}^2}{M^2} = \frac{1}{\alpha_s(M^2) b_0}$$

$$\log\frac{p^2}{M^2} = \log\frac{p^2}{\Lambda_{\rm QCD}^2} + \frac{1}{\alpha_s(M^2) b_0}$$

$$\frac{1}{\alpha_s(p^2)} = \frac{1}{\alpha_s(M^2)} + b_0\ \log\frac{p^2}{M^2}$$

$$= \frac{1}{\alpha_s(M^2)}\ + b_0 \log\frac{p^2}{\Lambda_{\rm QCD}^2} - \frac{1}{\alpha_s(M^2)} = b_0 \log\frac{p^2}{\Lambda_{\rm QCD}^2}$$

$$\boxed{\alpha_s(p^2) = \frac{1}{b_0 \log\dfrac{p^2}{\Lambda_{\rm QCD}^2}}} \tag{2.73}$$

This scheme can be generalized to any order in perturbative QCD and is not that different from the Thomson limit renormalization scheme of QED, except that with the introduction of $\Lambda_{\rm QCD}$ we are choosing a reference point which is particularly hard to compute perturbatively. One thing that is interesting in the way we introduce $\Lambda_{\rm QCD}$ is the fact that we introduce a scale into our theory without ever setting it. All we did was renormalize a coupling which becomes strong at large energies and search for the mass scale of this strong interaction. This trick is called *dimensional transmutation*.

In terms of language, there is a little bit of *confusion* between field theorists and phenomenologists: up to now we have introduced the renormalization scale μ_R as the renormalization point, for example of the strong coupling constant. In the $\overline{\rm MS}$

scheme, the subtraction of $1/\tilde{\varepsilon}$ shifts the scale dependence of the strong coupling to M^2 and moves the logarithm $\log M^2/\Lambda^2_{\text{QCD}}$ into the definition of the renormalized parameter. This is what we will from now on call the renormalization scale in the phenomenological sense, i.e. the argument we evaluate α_s at. Throughout this section we will keep the symbol M for this renormalization scale in the $\overline{\text{MS}}$ scheme, but from Sect. 2.3 on we will shift back to μ_R instead of M as the argument of the running coupling.

2.2.3 Re-Summing Scaling Logarithms

In the last Sect. 2.2.2 we have introduced the running strong coupling in a fairly abstract manner. For example, re-summing diagrams and changing the running of α_s from Eqs. 2.67 to 2.72 we did not yet link to any physics. In what way does the re-summation of the one-loop diagrams for the s channel gluon improve our prediction of the bottom pair production rate at the LHC?

To illustrate those effects we best look at a simple observable which depends on just one energy scale, namely p^2. The first observable coming to mind is again the Drell–Yan cross section $\sigma(q\bar{q} \to \mu^+\mu^-)$, but since we are not really sure what to do with the parton densities which are included in the actual hadronic observable, we better use an observable at an e^+e^- collider. Something that will work and includes α_s at least in the one-loop corrections is the R parameter given in Eq. 2.12

$$R = \frac{\sigma(e^+e^- \to \text{hadrons})}{\sigma(e^+e^- \to \mu^+\mu^-)} = N_c \sum_{\text{quarks}} Q_q^2 = \frac{11 N_c}{9}. \tag{2.74}$$

The numerical value at leading order assumes five quarks. Including higher order corrections we can express the result in a power series in the renormalized strong coupling α_s. In the $\overline{\text{MS}}$ scheme we subtract $1/\tilde{\varepsilon}(\mu_R/M)$ and in general include a scale dependence on M in the individual prefactors r_n

$$R\left(\frac{p^2}{M^2}, \alpha_s\right) = \sum_{n=0} r_n\left(\frac{p^2}{M^2}\right) \alpha_s^n(M^2) \qquad r_0 = \frac{11 N_c}{9}. \tag{2.75}$$

The r_n we can assume to be dimensionless—if they are not, we can scale R appropriately using p^2. This implies that the r_n only depend on ratios of two scales, the externally fixed p^2 on the one hand and the artificial M^2 on the other.

At the same time we know that R is an observable, which means that including all orders in perturbation theory it cannot depend on any artificial scale choices M. Writing this dependence as a total derivative and setting it to zero we find an equation which would be called a *Callan–Symanzik equation* if instead of the running coupling we had included a running mass

$$
\begin{aligned}
0 \stackrel{!}{=} M^2 \frac{d}{dM^2} R\left(\frac{p^2}{M^2}, \alpha_s(M^2)\right) &= M^2 \left[\frac{\partial}{\partial M^2} + \frac{\partial \alpha_s}{\partial M^2}\frac{\partial}{\partial \alpha_s}\right] R\left(\frac{p^2}{M^2}, \alpha_s\right) \\
&= \left[M^2 \frac{\partial}{\partial M^2} + \beta \frac{\partial}{\partial \alpha_s}\right] \sum_{n=0} r_n \left(\frac{p^2}{M^2}\right) \alpha_s^n \\
&= \sum_{n=1} M^2 \frac{\partial r_n}{\partial M^2} \alpha_s^n + \sum_{n=1} \beta r_n n \alpha_s^{n-1} \quad \text{with} \quad r_0 = \frac{11 N_c}{9} = \text{const} \\
&= M^2 \sum_{n=1} \frac{\partial r_n}{\partial M^2} \alpha_s^n - \sum_{n=1} \sum_{m=0} n r_n \alpha_s^{n+m+1} b_m \quad \text{with} \quad \beta = -\alpha_s^2 \sum_{m=0} b_m \alpha_s^m \\
&= M^2 \frac{\partial r_1}{\partial M^2} \alpha_s + \left(M^2 \frac{\partial r_2}{\partial M^2} - r_1 b_0\right) \alpha_s^2 \\
&\quad + \left(M^2 \frac{\partial r_3}{\partial M^2} - r_1 b_1 - 2 r_2 b_0\right) \alpha_s^3 + \mathcal{O}(\alpha_s^4).
\end{aligned}
\tag{2.76}
$$

In the second line we have to remember that the M dependence of α_s is already included in the appearance of β, so α_s should be considered a variable by itself. This perturbative series in α_s has to vanish in each order of perturbation theory. The non-trivial structure, namely the mix of r_n derivatives and the perturbative terms in the β function we can read off the α_s^3 term in Eq. 2.76: first, we have the appropriate NNNLO corrections r_3. Next, we have one loop in the gluon propagator b_0 and two loops for example in the vertex r_2. And finally, we need the two-loop diagram for the gluon propagator b_1 and a one-loop vertex correction r_1. The kind-of Callan–Symanzik equation Eq. 2.76 requires

$$
\begin{aligned}
\frac{\partial r_1}{\partial \log M^2} &= 0 \\
\frac{\partial r_2}{\partial \log M^2} &= r_1 b_0 \\
\frac{\partial r_3}{\partial \log M^2} &= r_1 b_1 + 2 r_2(M^2) b_0 \\
&\cdots
\end{aligned}
\tag{2.77}
$$

The dependence on the argument M^2 vanishes for r_0 and r_1. Keeping in mind that there will be integration constants c_n independent of M^2 and that another, in our simple case unique momentum scale p^2 has to cancel the mass units inside $\log M^2$ we find

$$
\begin{aligned}
r_0 &= c_0 = \frac{11 N_c}{9} \\
r_1 &= c_1 \\
r_2 &= c_2 + c_1 b_0 \log \frac{M^2}{p^2}
\end{aligned}
$$

$$
\begin{aligned}
r_3 &= \int d\log\frac{M'^2}{p^2}\left(c_1 b_1 + 2\left(c_2 + c_1 b_0 \log\frac{M'^2}{p^2}\right) b_0\right)\log\frac{M'^2}{p^2} \\
&= c_3 + (c_1 b_1 + 2c_2 b_0)\log\frac{M^2}{p^2} + c_1 b_0^2 \log^2\frac{M^2}{p^2} \\
&\cdots
\end{aligned}
\tag{2.78}
$$

This chain of r_n values looks like we should interpret the apparent fixed-order perturbative series for R in Eq. 2.75 as a series which implicitly includes terms of the order $\log^{n-1} M^2/p^2$ in each r_n. They can become problematic if this logarithm becomes large enough to spoil the fast convergence in terms of $\alpha_s \sim 0.1$, evaluating the observable R at scales far away from the scale choice for the strong coupling constant M.

Instead of the series in r_n we can use the conditions in Eq. 2.78 to express R in terms of the c_n and collect the logarithms appearing with each c_n. The geometric series we then resum to

$$
\begin{aligned}
R &= \sum_n r_n \left(\frac{p^2}{M^2}\right) \alpha_s^n(M^2) \\
&= c_0 + c_1\left(1 + \alpha_s b_0 \log\frac{M^2}{p^2} + \alpha_s^2 b_0^2 \log^2\frac{M^2}{p^2} + \cdots\right)\alpha_s(M^2) \\
&\quad + c_2\left(1 + 2\alpha_s b_0 \log\frac{M^2}{p^2} + \cdots\right)\alpha_s^2(M^2) + \cdots \\
&= c_0 + c_1 \frac{\alpha_s(M^2)}{1 - \alpha_s b_0 \log\frac{M^2}{p^2}} + c_2\left(\frac{\alpha_s(M^2)}{1 - \alpha_s b_0 \log\frac{M^2}{p^2}}\right)^2 + \cdots \\
&\equiv \sum c_n\, \alpha_s^n(p^2).
\end{aligned}
\tag{2.79}
$$

In the last step we use what we know about the running coupling from Eq. 2.71. Note that in contrast to the r_n integration constants the c_n are by definition independent of p^2/M^2 and therefore more suitable as a perturbative series in the presence of potentially large logarithms.

This new organization of the QCD perturbation series for R can be interpreted as *re-summing all logarithms* of the kind $\log M^2/p^2$ in the new organization of the perturbative series and absorbing them into the running strong coupling evaluated at the scale p^2. In this manner, all scale dependence in the perturbative series for the dimensionless observable R is moved into α_s. In Eq. 2.79 we also see that this series in c_n will never lead to a scale-invariant result when we include a finite order in perturbation theory.

Before moving on we collect the logic of the argument given in this section: when we regularize an ultraviolet divergence we automatically introduce a reference scale μ_R. Naively, this could be a ultraviolet cutoff scale, but even the seemingly scale invariant dimensional regularization in the conformal limit of our field theory cannot

avoid the introduction of a scale. There are several ways of dealing with such a scale: first, we can renormalize our parameter at a reference point. Secondly, we can define a running parameter, i.e. absorb the scale logarithm into the $\overline{\text{MS}}$ counter term. In that case introducing Λ_{QCD} leaves us with a compact form of the running coupling $\alpha_s(M^2; \Lambda_{\text{QCD}})$.

Strictly speaking, at each order in perturbation theory the scale dependence should vanish together with the ultraviolet poles, as long as there is only one scale affecting a given observable. However, defining the running strong coupling we sum one-loop vacuum polarization graphs. Even when we compute an observable at a given loop order, we implicitly include higher order contributions. They lead to a dependence of our perturbative result on the artificial scale M^2, which phenomenologists refer to as renormalization scale dependence.

Using the R ratio we see what our definition of the running coupling means in terms of re-summing logarithms: reorganizing our perturbative series to get rid of the ultraviolet divergence $\alpha_s(p^2)$ re-sums the scale logarithms $\log p^2/M^2$ to all orders in perturbation theory. We will need this picture once we introduce infrared divergences in the following section.

2.3 Infrared Divergences

After this brief excursion into ultraviolet divergences and renormalization we can return to the original example, the Drell–Yan process. Last, we wrote down the hadronic cross sections in terms of parton distributions at leading order in Eq. 2.39. At this stage particle distributions (pdfs) are only functions of the collinear momentum fraction of the partons inside the proton about which from a theory point of view we only know a set of sum rules.

The perturbative question we need to ask for $\mu^+\mu^-$ production at the LHC is: what happens if together with the two leptons we produce additional jets which for one reason or another we do not observe in the detector. Such jets could for example come from the radiation of a gluon from the initial state quarks. In Sect. 2.3.1 we will study the kinematics of radiating such jets and specify the infrared divergences this leads to. In Sects. 2.3.2 and 2.3.3 we will show that these divergences have a generic structure and can be absorbed into a re-definition of the parton densities, similar to an ultraviolet renormalization of a Lagrangian parameter. In Sects. 2.3.4 and 2.3.5 we will again follow the example of the ultraviolet divergences and specify what absorbing these divergences means in terms logarithms appearing in QCD calculations.

Throughout this writeup we will use the terms *jets and final state partons* synonymously. This is not really correct once we include jet algorithms and hadronization. On the other hand, in Sect. 3.1.2 we will see that the purpose of a jet algorithm is to take us from some kind of energy deposition in the calorimeter to the parton radiated in the hard process. The two should therefore be closely related.

2.3.1 Single Jet Radiation

Let us get back to the radiation of additional partons in the Drell–Yan process. We can start for example by computing the cross section for the partonic process $q\bar{q} \to Zg$. However, this partonic process involves renormalization of ultraviolet divergences as well as loop diagrams which we have to include before we can say anything reasonable, i.e. ultraviolet and infrared finite.

To make life easier and still learn about the structure of collinear infrared divergences we instead look at the crossed process $qg \to Zq$. It should behave similar to any other $(2 \to 2)$ jet radiation, except that it has a different incoming state than the leading-order Drell–Yan process and hence does not involve virtual corrections. This means we do not have to deal with ultraviolet divergences and renormalization, and can concentrate on parton or jet radiation from the initial state. Moreover, let us go back to Z production instead of a photon, to avoid confusion with massless particles which are not radiated jets.

The amplitude for this $(2 \to 2)$ process is—modulo charges and averaging factors, but including all Mandelstam variables

$$|\mathscr{M}|^2 \sim -\frac{t}{s} - \frac{s^2 - 2m_Z^2(s+t-m_Z^2)}{st}. \tag{2.80}$$

The Mandelstam variable t for one massless final state particle can be expressed as $t = -s(1-\tau)y$ in terms of the rescaled gluon-emission angle $y = (1-\cos\theta)/2$ and $\tau = m_Z^2/s$. Similarly, we obtain $u = -s(1-\tau)(1-y)$, so as a first check we can confirm that $t + u = -s(1-\tau) = -s + m_Z^2$. The collinear limit when the gluon is radiated in the beam direction is given by $y \to 0$, corresponding to negative $t \to 0$ with finite $u = -s + m_Z^2$. In this limit the matrix element can also be written as

$$|\mathscr{M}|^2 \sim \frac{s^2 - 2sm_Z^2 + 2m_Z^4}{s(s-m_Z^2)} \; \frac{1}{y} + \mathscr{O}(y). \tag{2.81}$$

This expression is divergent for collinear gluon radiation or splitting, i.e. for small angles y. We can translate this $1/y$ divergence for example into the transverse momentum of the gluon or Z

$$sp_T^2 = tu = s^2(1-\tau)^2\; y(1-y) = (s-m_Z^2)^2 y + \mathscr{O}(y^2) \tag{2.82}$$

In the collinear limit our matrix element squared in Eq. 2.81 becomes

$$|\mathscr{M}|^2 \sim \frac{s^2 - 2sm_Z^2 + 2m_Z^4}{s^2} \; \frac{(s-m_Z^2)}{p_T^2} + \mathscr{O}(p_T^0). \tag{2.83}$$

The matrix element for the tree-level process $qg \to Zq$ has a leading divergence proportional to $1/p_T^2$. To compute the total cross section for this process we need to integrate the matrix element over the entire two-particle phase space. Starting from

Eq. 2.41 and using the appropriate Jacobian this integration can be written in terms of the reduced angle y. Approximating the matrix element as C'/y or C/p_T^2, we then integrate

$$\int_{y^{\min}}^{y^{\max}} dy\, \frac{C'}{y} = \int_{p_T^{\min}}^{p_T^{\max}} dp_T^2\, \frac{C}{p_T^2} = 2\int_{p_T^{\min}}^{p_T^{\max}} dp_T\; p_T\; \frac{C}{p_T^2}$$
$$\simeq 2C \int_{p_T^{\min}}^{p_T^{\max}} dp_T \frac{1}{p_T} = 2C\, \log \frac{p_T^{\max}}{p_T^{\min}} \tag{2.84}$$

The form C/p_T^2 for the matrix element is of course only valid in the collinear limit; in the non-collinear phase space C is not a constant. However, Eq. 2.84 describes well the collinear divergence arising from quark radiation at the LHC.

Next, we follow the same strategy as for the ultraviolet divergence. First, we regularize the divergence for example using dimensional regularization. Then, we find a well-defined way to get rid of it. Dimensional regularization means writing the two-particle phase space in $n = 4 - 2\varepsilon$ dimensions. Just for reference, the complete formula in terms of the angular variable y reads

$$s\, \frac{d\sigma}{dy} = \frac{\pi (4\pi)^{-2+\varepsilon}}{\Gamma(1-\varepsilon)} \left(\frac{\mu_F^2}{m_Z^2}\right)^{\varepsilon} \frac{\tau^{\varepsilon}(1-\tau)^{1-2\varepsilon}}{y^{\varepsilon}(1-y)^{\varepsilon}} |\mathscr{M}|^2 \sim \left(\frac{\mu_F^2}{m_Z^2}\right)^{\varepsilon} \frac{|\mathscr{M}|^2}{y^{\varepsilon}(1-y)^{\varepsilon}}\,. \tag{2.85}$$

In the second step we only keep the factors we are interested in. The additional factor $1/y^{\varepsilon}$ regularizes the integral at $y \to 0$, as long as $\varepsilon < 0$ by slightly increasing the suppression of the integrand in the infrared regime. After integrating the leading collinear divergence $1/y^{1+\varepsilon}$ we are left with a pole $1/(-\varepsilon)$. This regularization procedure is symmetric in $y \leftrightarrow (1-y)$. What is important to notice is again the appearance of a scale $\mu_F^{2\varepsilon}$ with the n-dimensional integral. This scale arises from the infrared regularization of the phase space integral and is referred to as *factorization scale*. The actual removal of the infrared pole—corresponding to the renormalization in the ultraviolet case—is called *mass factorization* and works exactly the same way as renormalizing a parameter: in a well-defined scheme we simply subtract the pole from the fixed-order matrix element squared.

2.3.2 Parton Splitting

From the discussion of the process $qg \to Zq$ we can at least hope that after taking care of all other infrared and ultraviolet divergences the collinear structure of the process $q\bar{q} \to Zg$ will be similar. In this section we will show that we can indeed write all collinear divergences in a universal form, independent of the hard process which we choose as the Drell–Yan process. In the collinear limit, the radiation of additional partons or the splitting into additional partons will be described by universal *splitting functions*.

Infrared divergences occur for massless particles in the initial or final state, so we need to go through all ways incoming or outgoing gluons and quark can split into each other. The description of the factorized phase space, with which we will start, is common to all these different channels. The first and at the LHC most important case is the splitting of one gluon into two, shown in Fig. 2.1, where the two daughter gluons are close to mass shell while the mother has to have a finite positive invariant mass $p_a^2 \gg p_b^2, p_c^2$. We again assign the direction of the momenta as $p_a = -p_b - p_c$, which means we have to take care of minus signs in the particle energies. The kinematics of this approximately collinear process we can describe in terms of the energy fractions z and $1-z$ defined as

$$z = \frac{|E_b|}{|E_a|} = 1 - \frac{|E_c|}{|E_a|}, \tag{2.86}$$

which means for the four momentum of the splitting particle

$$\begin{aligned} p_a^2 &= 2(p_b p_c) = 2z(1-z)(1-\cos\theta)E_a^2 = z(1-z)E_a^2\theta^2 + \mathcal{O}(\theta^4) \\ \Leftrightarrow \quad \theta &\equiv \theta_b + \theta_c \simeq \frac{1}{|E_a|}\sqrt{\frac{p_a^2}{z(1-z)}}, \end{aligned} \tag{2.87}$$

in the collinear limit and in terms of the opening angle θ between $\vec{p}_b$ and $\vec{p}_c$. Because $p_a^2 > 0$ we call this final state splitting configuration *time-like branching*. For this configuration we can write down the so-called *Sudakov decomposition* of the four-momenta

$$-p_a = p_b + p_c = (-zp_a + \beta n + p_T) \; + \; (-(1-z)p_a - \beta n - p_T). \tag{2.88}$$

It defines an arbitrary unit four-vector n, a component orthogonal to the mother momentum and n, i.e. $p_a(p_a p_T) = 0 = (np_T)$, and a free factor β. This way, we can specify n such that it defines the direction of the $p_b - p_c$ decay plane. In this decomposition we can set only one invariant mass to zero, for example that of a radiated gluon $p_c^2 = 0$. The second final state will have a finite invariant mass $p_b^2 \neq 0$.

Relative to $\vec{p}_a$ we can split the opening angle θ for massless partons according to Fig. 2.1

$$\begin{aligned} & \theta = \theta_b + \theta_c \quad \text{and} \quad \frac{\theta_b}{\theta_c} = \frac{p_T}{|E_b|}\left(\frac{p_T}{|E_c|}\right)^{-1} = \frac{1-z}{z} \\ \Leftrightarrow \quad & \theta = \frac{\theta_b}{1-z} = \frac{\theta_c}{z} \end{aligned} \tag{2.89}$$

Using this specific phase space parameterization we can divide an $(n+1)$-particle process into an n-particle process and a *splitting process* of quarks and gluons. First, this requires us to split the $(n+1)$-particle phase space alone into an n-particle phase space and the collinear splitting. The general $(n+1)$-particle phase space separating off the n-particle contribution

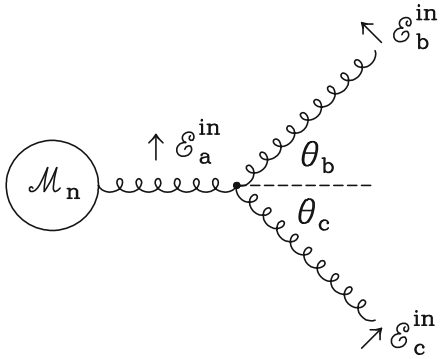

Fig. 2.1 Splitting of one gluon into two gluons. Figure from Ref. [1]

$$
\begin{aligned}
d\Phi_{n+1} &= \cdots \frac{d^3\vec{p}_b}{2(2\pi)^3|E_b|}\,\frac{d^3\vec{p}_c}{2(2\pi)^3|E_c|} \\
&= \cdots \frac{d^3\vec{p}_a}{2(2\pi)^3|E_a|}\,\frac{d^3\vec{p}_c}{2(2\pi)^3|E_c|}\frac{|E_a|}{|E_b|} \quad \text{at fixed} p_a \\
&= d\Phi_n\,\frac{dp_{c,3}dp_T\,p_T d\phi}{2(2\pi)^3|E_c|}\,\frac{1}{z} \\
&= d\Phi_n\,\frac{dp_{c,3}dp_T^2 d\phi}{4(2\pi)^3|E_c|}\,\frac{1}{z}
\end{aligned}
\tag{2.90}
$$

is best expressed in terms of the energy fraction z and the azimuthal angle ϕ.

In other words, separating the $(n+1)$-particle space into an n-particle phase space and a $(1 \to 2)$ splitting phase space is possible without any approximation, and all we have to take care of is the correct prefactors in the new parameterization. The third direction of p_c we can translate into z in a convenient reference frame for the momenta appearing in the Sudakov decomposition

$$
p_a = \begin{pmatrix} |E_a| \\ 0 \\ 0 \\ p_{a,3} \end{pmatrix} = |E_a| \begin{pmatrix} 1 \\ 0 \\ 0 \\ 1+\mathcal{O}(\theta) \end{pmatrix} \qquad n = \begin{pmatrix} 1 \\ 0 \\ 0 \\ -1 \end{pmatrix} \qquad p_T = \begin{pmatrix} 0 \\ p_{T,1} \\ p_{T,2} \\ 0 \end{pmatrix}. \tag{2.91}
$$

This choice has the special feature that $n^2 = 0$ which allows us to derive β from the momentum parameterization shown in Eq. 2.88 and the additional condition that $p_c^2 = 0$

$$
\begin{aligned}
p_c^2 &= (-(1-z)p_a - \beta n - p_T)^2 \\
&= (1-z)^2 p_a^2 + p_T^2 + 2\beta(1-z)(np_a) \\
&= (1-z)^2 p_a^2 + p_T^2 + 4\beta(1-z)|E_a|(1+\mathcal{O}(\theta)) \overset{!}{=} 0 \\
\Leftrightarrow \beta &\simeq -\frac{p_T^2 + (1-z)^2 p_a^2}{4(1-z)|E_a|}.
\end{aligned}
\tag{2.92}
$$

Starting from Eq. 2.88 for the z component of p_c, expressing p_a and p_T following Eq. 2.91 and inserting this value for β gives us

$$\begin{aligned}
\frac{dp_{c,3}}{dz} &= \frac{d}{dz}\left[-(1-z)|E_a|(1+\mathcal{O}(\theta))+\beta\right] \\
&= \frac{d}{dz}\left[-(1-z)|E_a|(1+\mathcal{O}(\theta)) - \frac{p_T^2+(1-z)^2p_a^2}{4(1-z)|E_a|}\right] \\
&= |E_a|(1+\mathcal{O}(\theta)) - \frac{p_T^2}{4(1-z)^2E_a} + \frac{p_a^2}{4|E_a|} \\
&= \frac{|E_c|}{1-z}(1+\mathcal{O}(\theta)) - \frac{\theta^2z^2E_c^2}{4(1-z)^2E_a} + \frac{z(1-z)E_a^2\theta^2+\mathcal{O}(\theta^4)}{4|E_a|} \\
&= \frac{|E_c|}{1-z} + \mathcal{O}(\theta) \quad \Leftrightarrow \quad \frac{dp_{c,3}}{|E_c|} \simeq \frac{dz}{1-z}.
\end{aligned} \tag{2.93}$$

In addition to substituting $dp_{c,3}$ by dz in Eq. 2.90 we also replace dp_T^2 with dp_a^2 according to

$$\frac{p_T^2}{p_a^2} = \frac{E_b^2\theta_b^2}{z(1-z)E_a^2\theta^2} = \frac{z^2(1-z)^2E_a^2\theta^2}{z(1-z)E_a^2\theta^2} = z(1-z). \tag{2.94}$$

This gives us the final result for the separated *collinear phase space*

$$\boxed{d\Phi_{n+1} = d\Phi_n \frac{dz dp_a^2 d\phi}{4(2\pi)^3} = d\Phi_n \frac{dz dp_a^2}{4(2\pi)^2}}, \tag{2.95}$$

where in the second step we assume a spherical symmetry.

Adding the transition matrix elements to this factorization of the phase space and ignoring the initial-state flux factor which is common to both processes we can now postulate a full factorization for one collinear emission and in the collinear approximation

$$\begin{aligned}
d\sigma_{n+1} &= \overline{|\mathcal{M}_{n+1}|^2}\, d\Phi_{n+1} \\
&= \overline{|\mathcal{M}_{n+1}|^2}\, d\Phi_n \frac{dp_a^2 dz}{4(2\pi)^2} \\
&= \frac{2g_s^2}{p_a^2}\,\hat{P}(z)\,\overline{|\mathcal{M}_n|^2}\, d\Phi_n \frac{dp_a^2 dz}{16\pi^2} \quad \text{assuming} \quad \boxed{\overline{|\mathcal{M}_{n+1}|^2} = \frac{2g_s^2}{p_a^2}\,\hat{P}(z)\,\overline{|\mathcal{M}_n|^2}}.
\end{aligned} \tag{2.96}$$

This last step is an assumption we will now proceed to show step by step by constructing the appropriate *splitting kernels* $\hat{P}(z)$ for all different quark and gluon configurations. If Eq. 2.96 holds true it means we can compute the $(n+1)$ particle

amplitude squared from the n-particle case convoluted with the appropriate splitting kernel. Using $d\sigma_n \sim \overline{|\mathscr{M}_n|^2}\, d\Phi_n$ and $g_s^2 = 4\pi\alpha_s$ we can write this relation in its most common form

$$\boxed{\sigma_{n+1} = \int \sigma_n \frac{dp_a^2}{p_a^2} dz \frac{\alpha_s}{2\pi} \hat{P}(z)}. \tag{2.97}$$

Reminding ourselves that relations of the kind $\overline{|\mathscr{M}_{n+1}|^2} = p\overline{|\mathscr{M}_n|^2}$ can typically be summed, for example for the case of successive soft photon radiation in QED, we see that Eq. 2.97 is not the final answer. It does not include the necessary phase space factor $1/n!$ from identical bosons in the final state which leads to the simple exponentiation.

As the first parton splitting in QCD we study a *gluon splitting into two gluons*, shown in Fig. 2.1. To compute its transition amplitude we parameterize all gluon momenta and polarizations. With respect to the scattering plane opened by $\vec{p}_b$ and $\vec{p}_c$ all three gluons have two transverse polarizations, one in the plane, $\varepsilon^{\parallel}$, and one perpendicular to it, $\varepsilon^{\perp}$. In the limit of small scattering angles, the three parallel as well as the three perpendicular polarization vectors are aligned. The perpendicular polarizations are also orthogonal to all three gluon momenta, while the polarizations in the plane are only proportional to their corresponding momenta, which altogether means for the three-vectors

$$\begin{aligned} (\varepsilon_i^{\parallel}\varepsilon_j^{\parallel}) &= -1 + \mathscr{O}(\theta) \qquad (\varepsilon_i^{\perp}\varepsilon_j^{\perp}) = -1 \quad (\varepsilon_i^{\perp}\varepsilon_j^{\parallel}) = \mathscr{O}(\theta) \\ (\varepsilon_i^{\perp} p_j) &= 0 \qquad\qquad (\varepsilon_j^{\parallel} p_j) = 0, \end{aligned} \tag{2.98}$$

with general $i \neq j$ and exactly one and zero for $i = j$. The finite combinations between polarization vectors and momenta which we need are, in terms of the three-dimensional opening angles $\angle(\vec{\varepsilon}, \vec{p})$

$$\begin{aligned} (\varepsilon_a^{\parallel} p_b) &= -E_b \cos\angle(\vec{\varepsilon}_a^{\parallel}, \vec{p}_b) = -E_b \cos\left(\frac{\pi}{2} - \theta_b\right) = +E_b \sin\theta_b \\ &\simeq +E_b\theta_b = z(1-z)E_a\theta \\ (\varepsilon_b^{\parallel} p_c) &= -E_c \cos\angle(\vec{\varepsilon}_b^{\parallel}, \vec{p}_c) = -E_c \cos\left(\frac{\pi}{2} + \theta\right) = -E_c \sin\theta \\ &\simeq -E_c\theta = -(1-z)E_a\theta \\ (\varepsilon_c^{\parallel} p_b) &= -E_b \cos\angle(\vec{\varepsilon}_c^{\parallel}, \vec{p}_b) = -E_b \cos\left(\frac{\pi}{2} - \theta\right) = +E_b \sin\theta \\ &\simeq +E_b\theta = zE_a\theta. \end{aligned} \tag{2.99}$$

Using these kinematic relations we can tackle the actual splitting amplitude. For three gluons the splitting amplitude will be proportional to the vertex, now switching back to the symmetric definition of all incoming momenta

$$
\begin{aligned}
V_{ggg} &= igf^{abc}\ \varepsilon_a^\alpha \varepsilon_b^\beta \varepsilon_c^\gamma [g_{\alpha\beta}(p_a - p_b)_\gamma \\
&\quad + g_{\beta\gamma}(p_b - p_c)_\alpha + g_{\gamma\alpha}(p_c - p_a)_\beta] \\
&= igf^{abc}\ \varepsilon_a^\alpha \varepsilon_b^\beta \varepsilon_c^\gamma [g_{\alpha\beta}(-p_c - 2p_b)_\gamma \\
&\quad + g_{\beta\gamma}(p_b - p_c)_\alpha + g_{\gamma\alpha}(2p_c + p_b)_\beta] && \text{with } p_a = -p_b - p_c \\
&= igf^{abc}\ [-2(\varepsilon_a\varepsilon_b)(\varepsilon_c p_b) + (\varepsilon_b\varepsilon_c)(\varepsilon_a p_b) \\
&\quad - (\varepsilon_b\varepsilon_c)(\varepsilon_a p_c) + 2(\varepsilon_c\varepsilon_a)(\varepsilon_b p_c)] && \text{with } (\varepsilon_j p_j) = 0 \\
&= -2igf^{abc}\,[(\varepsilon_a\varepsilon_b)(\varepsilon_c p_b) - (\varepsilon_b\varepsilon_c)(\varepsilon_a p_b) \\
&\quad - (\varepsilon_c\varepsilon_a)(\varepsilon_b p_c)] && \text{with } (\varepsilon_a p_c) = -(\varepsilon_a p_b) \\
&= -2igf^{abc}\ \Big[(\varepsilon_a\varepsilon_b)(\varepsilon_c^\parallel p_b) - (\varepsilon_b\varepsilon_c)(\varepsilon_a^\parallel p_b) \\
&\quad - (\varepsilon_c\varepsilon_a)(\varepsilon_b^\parallel p_c)\Big] && \text{with } (\varepsilon_i^\perp p_j) = 0.
\end{aligned}
\tag{2.100}
$$

Squaring the splitting matrix element to compute the $(n+1)$ and n particle matrix elements squared for the unpolarized case gives us

$$
\begin{aligned}
\overline{|\mathscr{M}_{n+1}|^2} &= \frac{1}{2}\left(\frac{1}{p_a^2}\right)^2 4g_s^2\ \frac{1}{N_c^2-1}\ \frac{1}{N_a}\left[\sum_{3\text{ terms}} \pm f^{abc}\ (\varepsilon\cdot\varepsilon)(\varepsilon\cdot p)\right]^2 \overline{|\mathscr{M}_n|^2} \\
&= \frac{2g_s^2}{p_a^2}\ \frac{f^{abc}f^{abc}}{N_c^2-1}\ \frac{1}{N_a}\left[\sum \frac{(\varepsilon\cdot\varepsilon)^2(\varepsilon\cdot p)^2}{p_a^2}\right] \overline{|\mathscr{M}_n|^2},
\end{aligned}
\tag{2.101}
$$

where the sum originally includes the three terms in the brackets of Eq. 2.100. Each term in this sum is symmetric in two indices but gets multiplied with the anti-symmetric color factor. The final result will only be finite if we square each term individually as a product of two symmetric and two anti-symmetric terms. In other words, the sum over the external gluons becomes an incoherent polarization sum.

Going through all possible combinations we know what can contribute inside the brackets of Eq. 2.100: $(\varepsilon_a^\parallel\varepsilon_b^\parallel)$ as well as $(\varepsilon_a^\perp\varepsilon_b^\perp)$ can be combined with $(\varepsilon_c^\parallel p_b)$; $(\varepsilon_b^\parallel\varepsilon_c^\parallel)$ or $(\varepsilon_b^\perp\varepsilon_c^\perp)$ with $(\varepsilon_a^\parallel p_b)$; and last but not least we can combine $(\varepsilon_a^\parallel\varepsilon_c^\parallel)$ and $(\varepsilon_a^\perp\varepsilon_c^\perp)$ with $(\varepsilon_b^\parallel p_c)$. These six combinations contribute to the splitting matrix element as

$\varepsilon_a\ \varepsilon_b\ \varepsilon_c$	$\pm(\varepsilon\cdot\varepsilon)(\varepsilon\cdot p)$	$\frac{(\varepsilon\cdot\varepsilon)^2(\varepsilon\cdot p)^2}{p_a^2}$
$\parallel\ \parallel\ \parallel$		
$\perp\ \perp\ \parallel$	$(-1)(-z)E_a\theta$	$\frac{z}{1-z}$
$\parallel\ \parallel\ \parallel$		
$\parallel\ \perp\ \perp$	$-(-1)(-z)(1-z)E_a\theta$	$z(1-z)$
$\parallel\ \parallel\ \parallel$		
$\perp\ \parallel\ \perp$	$-(-1)(1-z)E_a\theta$	$\frac{1-z}{z}$

These six cases correspond to four different polarizations of the three external gluons. For the coherent sum in Eq. 2.101 we find

$$\begin{aligned}
\overline{|\mathscr{M}_{n+1}|^2} &= \frac{2g_s^2}{p_a^2}\, N_c\, \frac{1}{N_a} \left[\sum \frac{(\varepsilon\cdot\varepsilon)^2(\varepsilon\cdot p)^2}{p_a^2}\right] \overline{|\mathscr{M}_n|^2} \qquad \text{with } f^{abc} f^{abd} = N_c \delta^{cd} \\
&= \frac{2g_s^2}{p_a^2}\, N_c \left[\frac{z}{1-z} + \frac{1-z}{z} + z(1-z)\right] \overline{|\mathscr{M}_n|^2} \qquad \text{with } N_a = 2 \\
&\equiv \frac{2g_s^2}{p_a^2}\, \hat{P}_{g\leftarrow g}(z)\, \overline{|\mathscr{M}_n|^2} \\
\Leftrightarrow \quad & \boxed{\hat{P}_{g\leftarrow g}(z) = C_A \left[\frac{z}{1-z} + \frac{1-z}{z} + z(1-z)\right]}, \qquad (2.102)
\end{aligned}$$

using $C_A = N_c$ and averaging over the color $(N_c^2 - 1)$ and polarization N_a of the mother particle a. The factor $1/2$ in the first line takes into account that for two final state gluons the $(n+1)$-particle phase space is only half its usual size. The form of the splitting kernel is symmetric when we exchange the two gluons z and $(1-z)$. It diverges if either of the gluons become soft. The notation $\hat{P}_{i\leftarrow j} \sim \hat{P}_{ij}$ is inspired by a matrix notation which we can use to multiply the splitting matrix from the right with the incoming parton vector to get the final parton vector. Following the logic described above, with this calculation we prove that the factorized form of the $(n+1)$-particle matrix element squared in Eq. 2.96 holds for gluons only.

The same kind of splitting kernel we can compute for a *gluon into two quarks* and a *quark into a quark and a gluon*

$$g(p_a) \to q(p_b) + \bar{q}(p_c) \qquad \text{and} \qquad q(p_a) \to q(p_b) + g(p_c). \qquad (2.103)$$

Both splittings include the quark–quark–gluon vertex, coupling the gluon current to the quark and antiquark spinors. The spinors of the massless quark $u(p_b)$ and the massless antiquark $v(p_c)$ we can write in terms of two-component spinors

$$\begin{aligned}
u(p) = \sqrt{E}\begin{pmatrix}\chi_\pm \\ \pm\chi_\pm\end{pmatrix} \quad \text{with} \quad \chi_+ &= \begin{pmatrix}1 \\ \theta/2\end{pmatrix} \qquad \text{(spin up)} \\
\chi_- &= \begin{pmatrix}-\theta/2 \\ 1\end{pmatrix} \qquad \text{(spin down).} \qquad (2.104)
\end{aligned}$$

For the massless antiquark we need to replace $\theta \to -\theta$ and take into account the different relative spin–momentum directions $(\sigma\,\hat{p})$, leading to the additional sign in the lower two spinor entries. The antiquark spinors then become

$$\begin{aligned}
v(p) = -i\sqrt{E}\begin{pmatrix}\mp\varepsilon\chi_\pm \\ \varepsilon\chi_\pm\end{pmatrix} \quad \text{with} \quad \chi_+ &= \begin{pmatrix}1 \\ -\theta/2\end{pmatrix} \quad \varepsilon\chi_+ = \begin{pmatrix}-\theta/2 \\ -1\end{pmatrix} \quad \text{(spin up)} \\
\chi_- &= \begin{pmatrix}\theta/2 \\ 1\end{pmatrix} \quad \varepsilon\chi_- = \begin{pmatrix}1 \\ -\theta/2\end{pmatrix} \quad \text{(spin down).} \qquad (2.105)
\end{aligned}$$

Our calculations we again limit to the leading terms in the small scattering angle θ. In addition to the fermion spinors, for the coupling to a gluonic current we need the *Dirac matrices* which we can conveniently express in terms of the Pauli matrices defined in Sect. 1.1.2

$$\gamma^0 = \begin{pmatrix} \mathbb{1} & 0 \\ 0 & -\mathbb{1} \end{pmatrix} \qquad \gamma^j = \begin{pmatrix} 0 & \sigma^j \\ -\sigma^j & 0 \end{pmatrix} \quad \Rightarrow \quad \gamma^0\gamma^0 = \mathbb{1} \qquad \gamma^0\gamma^j = \begin{pmatrix} 0 & \sigma^j \\ \sigma^j & 0 \end{pmatrix} \tag{2.106}$$

In the notation introduced in Eq. 2.102 we first compute the splitting kernel $\hat{P}_{q\leftarrow g}$, sandwiching the qqg vertex between an outgoing quark $\bar{u}_\pm(p_b)$ and an outgoing antiquark $v_\pm(p_a)$ for all possible spin combinations. We start with all four gluon polarizations, i.e. all four gamma matrices, between two spin-up quarks and their spinors written out in Eqs. 2.104 and 2.105

$$\begin{aligned}
\frac{\bar{u}_+(p_b)\gamma^0 v_-(p_c)}{-iE} &= \left(1, \frac{\theta_b}{2}, 1, \frac{\theta_b}{2}\right) \begin{pmatrix} 1 & & & \\ & 1 & & \\ & & 1 & \\ & & & 1 \end{pmatrix} \begin{pmatrix} 1 \\ -\theta_c/2 \\ 1 \\ -\theta_c/2 \end{pmatrix} \\
&= \left(1, \frac{\theta_b}{2}, 1, \frac{\theta_b}{2}\right) \begin{pmatrix} 1 \\ -\theta_c/2 \\ 1 \\ -\theta_c/2 \end{pmatrix} = 2 \\
\frac{\bar{u}_+(p_b)\gamma^1 v_-(p_c)}{-iE} &= \left(1, \frac{\theta_b}{2}, 1, \frac{\theta_b}{2}\right) \begin{pmatrix} & & & 1 \\ & & 1 & \\ & 1 & & \\ 1 & & & \end{pmatrix} \begin{pmatrix} 1 \\ -\theta_c/2 \\ 1 \\ -\theta_c/2 \end{pmatrix} \\
&= \left(1, \frac{\theta_b}{2}, 1, \frac{\theta_b}{2}\right) \begin{pmatrix} -\theta_c/2 \\ 1 \\ -\theta_c/2 \\ 1 \end{pmatrix} = \theta_b - \theta_c \\
\frac{\bar{u}_+(p_b)\gamma^2 v_-(p_c)}{-iE} &= \left(1, \frac{\theta_b}{2}, 1, \frac{\theta_b}{2}\right) \begin{pmatrix} & & & -i \\ & & i & \\ & -i & & \\ i & & & \end{pmatrix} \begin{pmatrix} 1 \\ -\theta_c/2 \\ 1 \\ -\theta_c/2 \end{pmatrix} \\
&= i\left(1, \frac{\theta_b}{2}, 1, \frac{\theta_b}{2}\right) \begin{pmatrix} \theta_c/2 \\ 1 \\ \theta_c/2 \\ 1 \end{pmatrix} = i(\theta_b + \theta_c) \\
\frac{\bar{u}_+(p_b)\gamma^3 v_-(p_c)}{-iE} &= \left(1, \frac{\theta_b}{2}, 1, \frac{\theta_b}{2}\right) \begin{pmatrix} & & 1 & \\ & & & -1 \\ 1 & & & \\ & -1 & & \end{pmatrix} \begin{pmatrix} 1 \\ -\theta_c/2 \\ 1 \\ -\theta_c/2 \end{pmatrix} \\
&= \left(1, \frac{\theta_b}{2}, 1, \frac{\theta_b}{2}\right) \begin{pmatrix} 1 \\ \theta_c/2 \\ 1 \\ \theta_c/2 \end{pmatrix} = 2,
\end{aligned} \tag{2.107}$$

Somewhat surprisingly the unphysical scalar and longitudinal gluon polarizations seem to contribute to this vertex. However, after adding the two unphysical degrees of freedom they cancel because of the form of our metric. For transverse gluons we can compute this vertex factor also for the other diagonal spin combination

$$\begin{aligned}
\frac{\bar{u}_-(p_b)\gamma^1 v_+(p_c)}{-iE} &= \left(-\frac{\theta_b}{2}, 1, \frac{\theta_b}{2}, -1\right)\begin{pmatrix} & & & 1\\ & & 1 & \\ & 1 & & \\ 1 & & & \end{pmatrix}\begin{pmatrix} \theta_c/2\\ 1\\ -\theta_c/2\\ -1\end{pmatrix}\\
&= \left(-\frac{\theta_b}{2}, 1, \frac{\theta_b}{2}, -1\right)\begin{pmatrix} -1\\ -\theta_c/2\\ 1\\ \theta_c/2\end{pmatrix} = \theta_b - \theta_c\\
\frac{\bar{u}_-(p_b)\gamma^2 v_+(p_c)}{-iE} &= \left(-\frac{\theta_b}{2}, 1, \frac{\theta_b}{2}, -1\right)\begin{pmatrix} & & & -i\\ & & i & \\ & -i & & \\ i & & & \end{pmatrix}\begin{pmatrix} \theta_c/2\\ 1\\ -\theta_c/2\\ -1\end{pmatrix}\\
&= i\left(-\frac{\theta_b}{2}, 1, \frac{\theta_b}{2}, -1\right)\begin{pmatrix} 1\\ -\theta_c/2\\ -1\\ \theta_c/2\end{pmatrix} = -i(\theta_b + \theta_c). \qquad (2.108)
\end{aligned}$$

Before collecting the prefactors for this gluon-quark splitting, we also need the same-spin case

$$\begin{aligned}
\frac{\bar{u}_+(p_b)\gamma^1 v_+(p_c)}{-iE} &= \left(1, \frac{\theta_b}{2}, 1, \frac{\theta_b}{2}\right)\begin{pmatrix} & & & 1\\ & & 1 & \\ & 1 & & \\ 1 & & & \end{pmatrix}\begin{pmatrix} \theta_c/2\\ 1\\ -\theta_c/2\\ -1\end{pmatrix}\\
&= \left(1, \frac{\theta_b}{2}, 1, \frac{\theta_b}{2}\right)\begin{pmatrix} -1\\ -\theta_c/2\\ 1\\ \theta_c/2\end{pmatrix} = 0\\
\frac{\bar{u}_+(p_b)\gamma^2 v_+(p_c)}{-iE} &= \left(1, \frac{\theta_b}{2}, 1, \frac{\theta_b}{2}\right)\begin{pmatrix} & & & -i\\ & & i & \\ & -i & & \\ i & & & \end{pmatrix}\begin{pmatrix} \theta_c/2\\ 1\\ -\theta_c/2\\ -1\end{pmatrix}\\
&= i\left(1, \frac{\theta_b}{2}, 1, \frac{\theta_b}{2}\right)\begin{pmatrix} 1\\ -\theta_c/2\\ -1\\ \theta_c/2\end{pmatrix} = 0, \qquad (2.109)
\end{aligned}$$

which vanishes. The gluon current can only couple to two fermions via a spin flip. For massless fermions this means that the gluon splitting into two quarks involves

two quark spin cases, each of them coupling to two transverse gluon polarizations. Keeping track of all the relevant factors our vertex function for the splitting $g \to q\bar{q}$ becomes for each of the two quark spins

$$\begin{aligned} V_{qqg} &= -ig_s T^a\, \bar{u}_\pm(p_b)\gamma_\mu \varepsilon_a^\mu v_\mp(p_c) \equiv -ig_s T^a\, \varepsilon_a^j\, F_\pm^{(j)} \\ \frac{|F_+^{(1)}|^2}{p_a^2} &= \frac{|F_-^{(1)}|^2}{p_a^2} = \frac{E_b E_c(\theta_b-\theta_c)^2}{p_a^2} = \frac{E_a^2 z(1-z)(1-z-z)^2\theta^2}{E_a^2 z(1-z)\theta^2} = (1-2z)^2 \\ \frac{|F_+^{(2)}|^2}{p_a^2} &= \frac{|F_-^{(2)}|^2}{p_a^2} = \frac{E_b E_c(\theta_b+\theta_c)^2}{p_a^2} = \frac{E_a^2 z(1-z)(1-z+z)^2\theta^2}{E_a^2 z(1-z)\theta^2} = 1, \end{aligned} \tag{2.110}$$

omitting irrelevant factors i and (-1) which will drop out once we compute the absolute value squared. In complete analogy to the gluon splitting case we can factorize the $(n+1)$-particle matrix element into

$$\begin{aligned} \overline{|\mathscr{M}_{n+1}|^2} &= \left(\frac{1}{p_a^2}\right)^2 g_s^2\, \frac{\mathrm{Tr} T^a T^a}{N_c^2-1}\, \frac{1}{N_a} \left[|F_+^{(1)}|^2 + |F_-^{(1)}|^2 + |F_+^{(2)}|^2 + |F_-^{(2)}|^2\right] \overline{|\mathscr{M}_n|^2} \\ &= \frac{g_s^2}{p_a^2}\, T_R \frac{N_c^2-1}{N_c^2-1} \left[(1-2z)^2+1\right] \overline{|\mathscr{M}_n|^2} \quad \text{with } \mathrm{Tr} T^a T^b = T_R \delta^{ab},\ N_a = 2 \\ &= \frac{2g_s^2}{p_a^2}\, T_R \left[z^2+(1-z)^2\right] \overline{|\mathscr{M}_n|^2} \\ &\equiv \frac{2g_s^2}{p_a^2} \hat{P}_{q\leftarrow g}(z) \overline{|\mathscr{M}_n|^2} \\ &\Leftrightarrow \quad \boxed{\hat{P}_{q\leftarrow g}(z) = T_R\left[z^2+(1-z)^2\right]}, \end{aligned} \tag{2.111}$$

with $T_R = 1/2$. In the first line we implicitly assume that the internal quark propagator can be written as something like $u\bar{u}/p_a^2$ and we only need to consider the denominator. This splitting kernel is again symmetric in z and $(1-z)$ because QCD does not distinguish between the outgoing quark and the outgoing antiquark.

The third splitting we compute is gluon radiation off a quark, i.e. $q(p_a) \to q(p_b) + g(p_c)$, sandwiching the qqg vertex between an outgoing quark $\bar{u}_\pm(p_b)$ and an incoming quark $u_\pm(p_a)$. From the splitting of a gluon into a quark-antiquark pair we already know that we can limit our analysis to the physical gluon polarizations and a spin flip in the quarks. Inserting the spinors from Eq. 2.104 and the two relevant gamma matrices gives us

$$\begin{aligned} \frac{\bar{u}_+(p_b)\gamma^1 u_+(p_a)}{E} &= \left(1, \frac{\theta_b^*}{2}, 1, \frac{\theta_b^*}{2}\right) \begin{pmatrix} & & & 1 \\ & & 1 & \\ & 1 & & \\ 1 & & & \end{pmatrix} \begin{pmatrix} 1 \\ \theta_a^*/2 \\ 1 \\ \theta_a^*/2 \end{pmatrix} \\ &= i \left(1, \frac{\theta_b^*}{2}, 1, \frac{\theta_b^*}{2}\right) \begin{pmatrix} \theta_a^*/2 \\ 1 \\ \theta_a^*/2 \\ 1 \end{pmatrix} = \theta_b^* + \theta_a^* \end{aligned}$$

$$\frac{\bar{u}_+(p_b)\gamma^2 u_+(p_a)}{E} = \left(1, \frac{\theta_b^*}{2}, 1, \frac{\theta_b^*}{2}\right) \begin{pmatrix} & & & -i \\ & & i & \\ & -i & & \\ i & & & \end{pmatrix} \begin{pmatrix} 1 \\ \theta_a^*/2 \\ 1 \\ \theta_a^*/2 \end{pmatrix}$$
$$= i \left(1, \frac{\theta_b^*}{2}, 1, \frac{\theta_b^*}{2}\right) \begin{pmatrix} -\theta_a^*/2 \\ 1 \\ -\theta_a^*/2 \\ 1 \end{pmatrix} = i(\theta_b^* - \theta_a^*), \qquad (2.112)$$

with the angles θ_b^* and θ_a^* relative to the final state gluon direction $\vec{p}_c$. Comparing to the situation shown in Fig. 2.1 for the angle relative to the scattered gluon we find $\theta_b^* = \theta$ while for the incoming quark $\theta_a^* = -\theta_c = -z\theta$. As expected, the spin-down case gives the same result, modulo a complex conjugation

$$\frac{\bar{u}_-(p_b)\gamma^1 u_-(p_a)}{E} = \left(-\frac{\theta_b^*}{2}, 1, \frac{\theta_b^*}{2}, -1\right) \begin{pmatrix} & & & 1 \\ & & 1 & \\ & 1 & & \\ 1 & & & \end{pmatrix} \begin{pmatrix} -\theta_a^*/2 \\ 1 \\ \theta_a^*/2 \\ -1 \end{pmatrix}$$
$$= \left(-\frac{\theta_b^*}{2}, 1, \frac{\theta_b^*}{2}, -1\right) \begin{pmatrix} -1 \\ \theta_a^*/2 \\ 1 \\ -\theta_a^*/2 \end{pmatrix} = \theta_a^* + \theta_b^*$$
$$\frac{\bar{u}_-(p_b)\gamma^2 u_-(p_a)}{E} = \left(-\frac{\theta_b^*}{2}, 1, \frac{\theta_b^*}{2}, -1\right) \begin{pmatrix} & & & -i \\ & & i & \\ & -i & & \\ i & & & \end{pmatrix} \begin{pmatrix} -\theta_a^*/2 \\ 1 \\ \theta_a^*/2 \\ -1 \end{pmatrix}$$
$$= i \left(-\frac{\theta_b^*}{2}, 1, \frac{\theta_b^*}{2}, -1\right) \begin{pmatrix} 1 \\ \theta_a^*/2 \\ -1 \\ -\theta_a^*/2 \end{pmatrix} = i(\theta_a^* - \theta_b^*). \qquad (2.113)$$

The vertex function for gluon radiation off a quark then becomes

$$V_{qqg} = -ig_s T^a \, \bar{u}_\pm(p_b)\gamma_\mu \varepsilon_a^\mu u_\pm(p_c) \equiv -ig_s T^a \, \varepsilon_a^j \, F_\pm^{(j)}$$
$$\frac{|F_+^{(1)}|^2}{p_a^2} = \frac{|F_-^{(1)}|^2}{p_a^2} = \frac{E_a E_b(\theta_a^* + \theta_b^*)^2}{p_a^2} = \frac{E_a^2 z(z-1)^2\theta^2}{E_a^2 z(1-z)\theta^2} = (1-z)$$
$$\frac{|F^{(2)}|_+^2}{p_a^2} = \frac{|F^{(2)}|_-^2}{p_a^2} = \frac{E_a E_b(\theta_b^* - \theta_a^*)^2}{p_a^2} = \frac{E_a^2 z(1+z)^2\theta^2}{E_a^2 z(1-z)\theta^2} = \frac{(1+z)^2}{1-z}, \qquad (2.114)$$

again dropping irrelevant prefactors. The factorized matrix element for this channel reads

$$
\begin{aligned}
\overline{|\mathcal{M}_{n+1}|^2} &= \left(\frac{1}{p_a^2}\right)^2 g_s^2 \, \frac{\mathrm{Tr} T^a T^a}{N_c} \, \frac{1}{N_a} \left[|F_+^{(1)}|^2 + |F_-^{(1)}|^2 + |F_+^{(2)}|^2 + |F_-^{(2)}|^2\right] \overline{|\mathcal{M}_n|^2} \\
&= \frac{g_s^2}{p_a^2} \, \frac{N_c^2 - 1}{2N_c} \, \frac{(1+z)^2 + (1-z)^2}{1-z} \, \overline{|\mathcal{M}_n|^2} \\
&= \frac{2g_s^2}{p_a^2} \, C_F \, \frac{1+z^2}{1-z} \, \overline{|\mathcal{M}_n|^2} \\
&\equiv \frac{2g_s^2}{p_a^2} \hat{P}_{q\leftarrow g}(z) \overline{|\mathcal{M}_n|^2} \\
&\Leftrightarrow \quad \boxed{\hat{P}_{q\leftarrow q}(z) = C_F \frac{1+z^2}{1-z}} \, .
\end{aligned}
\tag{2.115}
$$

The averaging factor $1/N_a = 2$ now is the number of quark spins in the intermediate state. Just switching $z \leftrightarrow (1-z)$ we can read off the kernel for a quark splitting written in terms of the final state gluon

$$
\boxed{\hat{P}_{g\leftarrow q}(z) = C_F \frac{1+(1-z)^2}{z}} \, . \tag{2.116}
$$

This result finalizes our calculation of *all QCD splitting kernels* $\hat{P}_{i\leftarrow j}(z)$ between quarks and gluons. As alluded to earlier, similar to ultraviolet divergences which get removed by counter terms these splitting kernels are universal, i.e. they do not depend on the hard n-particle matrix element which is part of the original $(n+1)$-particle process. The four results we show in Eqs. 2.102, 2.111, 2.115, and 2.116. This means that by construction of the kernels $\hat{P}$ we have shown that the collinear factorization Eq. 2.97 holds at this level in perturbation theory.

Before using this splitting property to describe QCD effects at the LHC we need to look at the splitting of partons in the initial state, meaning $|p_a^2|, p_c^2 \ll |p_b^2|$ where p_b is the momentum entering the hard interaction. The difference to the final state splitting is that now we can consider the split parton momentum $p_b = p_a - p_c$ as a t-channel diagram, so we already know $p_b^2 = t < 0$ from our usual Mandelstam variables argument. This *space-like splitting* version of Eq. 2.88 we can solve for p_b^2

$$
\begin{aligned}
t \equiv p_b^2 &= (-z p_a + \beta n + p_T)^2 \\
&= p_T^2 - 2z\beta(p_a n) && \text{with } p_a^2 = n^2 = (p_a p_T) = (n p_T) = 0 \\
&= p_T^2 + \frac{p_T^2 z}{1-z} && \text{using Eq. 2.92} \\
&= \frac{p_T^2}{1-z} = -\frac{p_{T,1}^2 + p_{T,2}^2}{1-z} < 0.
\end{aligned}
\tag{2.117}
$$

The calculation of the splitting kernels and matrix elements is the same as for the time-like case, with the one exception that for splitting in the initial state the flow

factor has to be evaluated at the reduced partonic energy $E_b = zE_a$ and that the energy fraction entering the parton density needs to be replaced by $x_b \to zx_b$. The factorized matrix element for initial state splitting then reads just like Eq. 2.97

$$\sigma_{n+1} = \int \sigma_n \frac{dt}{t} dz \frac{\alpha_s}{2\pi} \hat{P}(z). \tag{2.118}$$

How to use this property to make statements about the quark and gluon content in the proton will be the focus of the next section.

2.3.3 DGLAP Equation

What we now know about collinear parton splitting we can use to describe incoming partons. For example in $pp \to Z$ production incoming partons inside the protons transform into each other via collinear splitting until they enter the Z production process as quarks. Taking Eq. 2.118 seriously the parton density we insert into Eq. 2.28 then depends on two parameters, the final energy fraction and the virtuality $f(x_n, -t_n)$ where the second parameter t is new compared to the purely probabilistic picture in Eq. 2.28. It cannot be neglected unless we convince ourselves that it is unphysical. As we will see later it corresponds exactly to the artificial renormalization scale which appears when we re-sum the scaling logarithms which appear in counter terms.

More quantitatively, we start with a quark inside the proton with an energy fraction x_0, as it enters the hadronic phase space integral shown in Sect. 2.1.4. Since this quark is confined inside the proton it can only have small transverse momentum, which means its four-momentum squared t_0 is negative and its absolute value $|t_0|$ is small. The variable t we call *virtuality* because for the incoming partons which if on-shell have $p^2 = 0$ it gives the distance to the mass shell. Let us simplify our kinematic argument by assuming that there exists only one splitting, namely successive gluon radiation $q \to qg$ off an incoming quark, where the outgoing gluons are not relevant

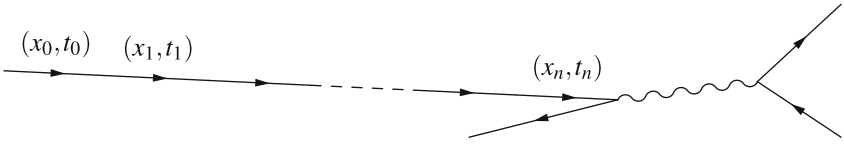

In that case each collinear gluon radiation will decrease the quark energy $x_{j+1} < x_j$ and through recoil increase its virtuality $|t_{j+1}| = -t_{j+1} > -t_j = |t_j|$.

From the last section we know what the successive splitting means in terms of splitting probabilities. We can describe how the parton density $f(x, -t)$ evolves in the $(x - t)$ plane as depicted in Fig. 2.2. The starting point (x_0, t_0) is at least probabilistically given by the energy and kind of the hadron, for example the proton.

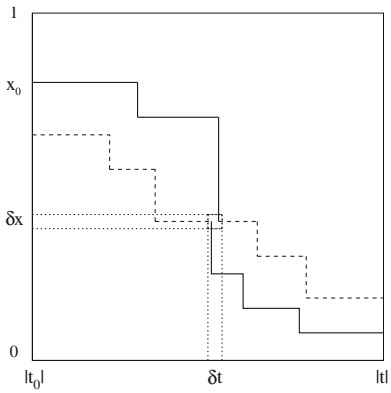

Fig. 2.2 Path of an incoming parton in the $(x - t)$ plane. Because we define t as a negative number its axis is labelled $|t|$

For a given small virtuality $|t_0|$ we start at some kind of fixed x_0 distribution. We then interpret each branching as a step strictly downward in $x_j \to x_{j+1}$ where the t value we assign to this step is the ever increasing virtuality $|t_{j+1}|$ after the branching. Each splitting means a synchronous shift in x and t, so the actual path in the $(x - t)$ plane really consists of discrete points. The probability of such a splitting to occur is given by $\hat{P}_{q \leftarrow q}(z) \equiv \hat{P}(z)$ as it appears in Eq. 2.118

$$\frac{\alpha_s}{2\pi}\, \hat{P}(z)\, \frac{dt}{t}\, dz. \tag{2.119}$$

In this picture we consider this probability a smooth function in t and z. At the end of the path we will probe this evolved parton density, where x_n and t_n enter the hard scattering process and its energy-momentum conservation.

When we convert a partonic into a hadronic cross section numerically we need to specify the probability of the parton density $f(x, -t)$ residing in an infinitesimal square $[x_j, x_j + \delta x]$ and, if this second parameter has anything to do with physics, $[|t_j|, |t_j| + \delta t]$. Using our (x, t) plane we compute the flow into this square and out of this square which together defines the net shift in f in the sense of a differential equation, similar to the derivation of Gauss' theorem for vector fields inside a surface

$$\delta f_{\text{in}} - \delta f_{\text{out}} = \delta f(x, -t). \tag{2.120}$$

The incoming and outgoing flow we compute from the history of the (x, t) evolution. At this stage our picture becomes a little subtle; the way we define the path between two splittings in Fig. 2.2 it can enter and leave the square either vertically or horizontally, but we have to decide which we choose. If we define a splitting as a vertical drop in x at the target value t_{j+1} an incoming path hitting the square at some value t can come from any x value above the square. Using this convention and

following the fat solid lines in Fig. 2.2 the vertical flow into (and out of) the square (x,t) square is proportional to δt

$$\begin{aligned}\delta f_{\rm in}(-t) &= \delta t \left(\frac{\alpha_s \hat{P}}{2\pi t}\otimes f\right)(x,-t) = \frac{\delta t}{t}\int_x^1 \frac{dz}{z}\,\frac{\alpha_s}{2\pi}\,\hat{P}(z) f\left(\frac{x}{z},-t\right)\\ &= \frac{\delta t}{t}\int_0^1 \frac{dz}{z}\,\frac{\alpha_s}{2\pi}\,\hat{P}(z) f\left(\frac{x}{z},-t\right) \quad \text{assuming } f(x',-t)=0 \text{ for } x'>1,\end{aligned} \tag{2.121}$$

where δt is the size of the interval covered by the virtuality value t. We use the definition of a *convolution*

$$\begin{aligned}(f\otimes g)(x) &= \int_0^1 dx_1 dx_2 f(x_1) g(x_2)\,\delta(x-x_1x_2)\\ &= \int_0^1 \frac{dx_1}{x_1} f(x_1) g\left(\frac{x}{x_1}\right) = \int_0^1 \frac{dx_2}{x_2} f\left(\frac{x}{x_2}\right) g(x_2).\end{aligned} \tag{2.122}$$

The outgoing flow we define in complete analogy, again leaving the infinitesimal square vertically. Following the fat solid line in Fig. 2.2 the outgoing flow is also proportional to δt

$$\delta f_{\rm out}(-t) = \delta t \int_0^1 dy \frac{\alpha_s \hat{P}(y)}{2\pi t}\, f(x,-t) = \frac{\delta t}{t} f(x,-t)\int_0^1 dy\,\frac{\alpha_s}{2\pi}\,\hat{P}(y). \tag{2.123}$$

The y integration, unlike the z integration for the incoming flow is not a convolution. This integration appears because we do not know the normalization of $\hat{P}(z)$ distribution which we interpret as a probability. The reason why it is not a convolution is that for the outgoing flow we know the starting condition and integrate over the final configurations; this aspect will become important later. Combining Eqs. 2.121 and 2.123 we can compute the change in the parton density of the quarks as

$$\begin{aligned}\delta f(x,-t) &= \frac{\delta t}{t}\left[\int_0^1 \frac{dz}{z}\,\frac{\alpha_s}{2\pi}\,\hat{P}(z)\, f\left(\frac{x}{z},-t\right) - \int_0^1 dy\,\frac{\alpha_s}{2\pi}\,\hat{P}(y)\, f(x,-t)\right]\\ &= \frac{\delta t}{t}\int_0^1 \frac{dz}{z}\,\frac{\alpha_s}{2\pi}\left[\hat{P}(z) - \delta(1-z)\int_0^1 dy\hat{P}(y)\right] f\left(\frac{x}{z},-t\right)\\ &\equiv \frac{\delta t}{t}\int_x^1 \frac{dz}{z}\,\frac{\alpha_s}{2\pi}\,\hat{P}(z)_+\, f\left(\frac{x}{z},-t\right)\\ \Leftrightarrow\quad \frac{\delta f(x,-t)}{\delta(-t)} &= \frac{1}{(-t)}\int_x^1 \frac{dz}{z}\,\frac{\alpha_s}{2\pi}\,\hat{P}(z)_+\, f\left(\frac{x}{z},-t\right),\end{aligned} \tag{2.124}$$

again assuming $f(x)=0$ for $x>1$, strictly speaking requiring α_s to only depend on t but not on z, and using the specifically defined *plus subtraction* scheme

$$\boxed{F(z)_+ \equiv F(z) - \delta(1-z)\int_0^1 dy\; F(y)}, \tag{2.125}$$

or equivalently

$$\int_0^1 dz\, \frac{f(z)}{(1-z)_+} = \int_0^1 dz\, \left(\frac{f(z)}{1-z} - \frac{f(1)}{1-z} \right). \tag{2.126}$$

For the second definition we choose $F(z) = 1/(1-z)$, multiply it with an arbitrary test function $f(z)$ and integrate over z. In contrast to the original z integral the plus-subtracted integral is by definition finite in the limit $z \to 1$ where some of the splitting kernels diverge. For example the quark splitting kernel including the plus prescription becomes of this form $C_F((1+z^2)/(1-z))_+$. At this stage the plus prescription is simply a convenient way of writing a complicated combination of splitting kernels, but we will see that it also has a physics meaning.

We can check that the plus prescription indeed acts as a regularization technique for the parton densities. Obviously, the integral over $f(z)/(1-z)$ is divergent at the boundary $z \to 1$, which we know we can cure using *dimensional regularization*. The special case $f(z) = 1$ illustrates how dimensional regularization of infrared divergences in the phase space integration Eq. 2.85 works

$$\int_0^1 dz\, \frac{1}{(1-z)^{1-\varepsilon}} = \int_0^1 dz\, \frac{1}{z^{1-\varepsilon}} = \frac{z^\varepsilon}{\varepsilon}\bigg|_0^1 = \frac{1}{\varepsilon} \quad \text{with } \varepsilon > 0, \tag{2.127}$$

for $4 + 2\varepsilon$ dimensions. This change in sign avoids the analytic continuation of the usual value $n = 4 - 2\varepsilon$ to $\varepsilon < 0$. The dimensionally regularized integral we can write as

$$\begin{aligned}
\int_0^1 dz\, \frac{f(z)}{(1-z)^{1-\varepsilon}} &= \int_0^1 dz\, \frac{f(z)-f(1)}{(1-z)^{1-\varepsilon}} + f(1) \int_0^1 dz\, \frac{1}{(1-z)^{1-\varepsilon}} \\
&= \int_0^1 dz\, \frac{f(z)-f(1)}{1-z}\,(1+\mathcal{O}(\varepsilon)) + \frac{f(1)}{\varepsilon} \\
&= \int_0^1 dz\, \frac{f(z)}{(1-z)_+}\,(1+\mathcal{O}(\varepsilon)) + \frac{f(1)}{\varepsilon} \quad \text{by definition} \\
\int_0^1 dz\, \frac{f(z)}{(1-z)^{1-\varepsilon}} - \frac{f(1)}{\varepsilon} &= \int_0^1 dz\, \frac{f(z)}{(1-z)_+}\,(1+\mathcal{O}(\varepsilon)).
\end{aligned} \tag{2.128}$$

The dimensionally regularized integral minus the pole, i.e. the finite part of the dimensionally regularized integral, is the same as the plus-subtracted integral modulo terms of the order ε. The third line in Eq. 2.128 shows that the difference between a dimensionally regularized splitting kernel and a plus-subtracted splitting kernel manifests itself as terms proportional to $\delta(1-z)$. Physically, they represent contributions to a soft-radiation phase space integral.

Before we move on introducing a gluon density we can slightly reformulate the splitting kernel $\hat{P}_{q\leftarrow q}$ in Eq. 2.115. If the plus prescription regularizes the pole at $z \to 1$, what happens when we include the numerator of the regularized function, e.g. the quark splitting kernel, as compared to leaving it out? The finite difference between these results is

$$\left(\frac{1+z^2}{1-z}\right)_+ - (1+z^2)\left(\frac{1}{1-z}\right)_+ = \frac{1+z^2}{1-z} - \delta(1-z)\int_0^1 dy\ \frac{1+y^2}{1-y} - \frac{1+z^2}{1-z} + \delta(1-z)\int_0^1 dy\ \frac{1+z^2}{1-y}$$
$$= -\delta(1-z)\int_0^1 dy\left(\frac{1+y^2}{1-y} - \frac{2}{1-y}\right)$$
$$= \delta(1-z)\int_0^1 dy\ \frac{y^2-1}{y-1}$$
$$= \delta(1-z)\int_0^1 dy\ (y+1) = \frac{3}{2}\delta(1-z). \tag{2.129}$$

We can therefore write the quark's splitting kernel in two equivalent ways

$$\boxed{P_{q\leftarrow q}(z) = C_F\left(\frac{1+z^2}{1-z}\right)_+ = C_F\left[\frac{1+z^2}{(1-z)_+} + \frac{3}{2}\delta(1-z)\right]}. \tag{2.130}$$

The infinitesimal version of Eq. 2.124 is the Dokshitzer–Gribov–Lipatov—Altarelli–Parisi or DGLAP *integro-differential equation* which describes the scale dependence of the quark parton density. As we already know quarks do not only appear in $q \to q$ splitting, but also in gluon splitting. Therefore, we generalize Eq. 2.124 to include the full set of QCD partons, i.e. quarks and gluons. This generalization involves a sum over all allowed splittings and the plus-subtracted splitting kernels. For the quark density on the left hand side it is

$$\boxed{\frac{df_q(x,-t)}{d\log(-t)} = -t\ \frac{df_q(x,-t)}{d(-t)} = \sum_{j=q,g}\int_x^1 \frac{dz}{z}\ \frac{\alpha_s}{2\pi}\ P_{q\leftarrow j}(z)\ f_j\left(\frac{x}{z},-t\right)}, \tag{2.131}$$

with $P_{q\leftarrow j}(z) \equiv \hat{P}_{q\leftarrow j}(z)_+$. Going back to Eq. 2.124 we add all relevant parton indices and splittings and arrive at

$$\delta f_q(x,-t) = \frac{\delta t}{t}\left[\int_0^1 \frac{dz}{z}\ \frac{\alpha_s}{2\pi}\hat{P}_{q\leftarrow q}(z)\ f_q\left(\frac{x}{z},-t\right) + \int_0^1 \frac{dz}{z}\ \frac{\alpha_s}{2\pi}\hat{P}_{q\leftarrow g}(z) f_g\left(\frac{x}{z},-t\right) - \int_0^1 dy\ \frac{\alpha_s}{2\pi}\ \hat{P}_{q\leftarrow q}(y)\ f_q(x,-t)\right]. \tag{2.132}$$

Of the three terms on the right-hand side the first and the third together define the plus-subtracted splitting kernel $P_{q\leftarrow q}(z)$, just following the argument above. The second term is a proper convolution and the only term proportional to the gluon parton density. Quarks can be produced in gluon splitting but cannot vanish into it. Therefore, we have to identify the second term with $P_{q\leftarrow g}$ in Eq. 2.131 without adding a plus-regulator

$$\boxed{P_{q\leftarrow g}(z) \equiv \hat{P}_{q\leftarrow g}(z) = T_R\left[z^2 + (1-z)^2\right]}. \tag{2.133}$$

In principle, the splitting kernel $\hat{P}_{g\leftarrow q}$ also generates a quark, in addition to the final state gluon. However, comparing this to the terms proportional to $\hat{P}_{q\leftarrow q}$ they both arise from the same splitting, namely a quark density leaving the infinitesimal square in the $(x-t)$ plane via the splitting $q \to qg$. Including the additional $\hat{P}_{g\leftarrow q}(y)$ would be double counting and should not appear, as the notation $g \leftarrow q$ already suggests.

The second QCD parton density we have to study is the gluon density. The incoming contribution to the infinitesimal square is given by the sum of four splitting scenarios each leading to a gluon with virtuality $-t_{j+1}$

$$\begin{aligned}
\delta f_{\text{in}}(-t) &= \frac{\delta t}{t}\int_0^1 \frac{dz}{z}\,\frac{\alpha_s}{2\pi}\left[\hat{P}_{g\leftarrow g}(z)\left(f_g\left(\frac{x}{z},-t\right) + f_g\left(\frac{x}{1-z},-t\right)\right)\right.\\
&\qquad\left. + \hat{P}_{g\leftarrow q}(z)\left(f_q\left(\frac{x}{z},-t\right) + f_{\bar{q}}\left(\frac{x}{z},-t\right)\right)\right]\\
&= \frac{\delta t}{t}\int_0^1 \frac{dz}{z}\,\frac{\alpha_s}{2\pi}\left[2\hat{P}_{g\leftarrow g}(z) f_g\left(\frac{x}{z},-t\right)\right.\\
&\qquad\left. + \hat{P}_{g\leftarrow q}(z)\left(f_q\left(\frac{x}{z},-t\right) + f_{\bar{q}}\left(\frac{x}{z},-t\right)\right)\right],
\end{aligned} \tag{2.134}$$

using $P_{g\leftarrow g}(1-z) = P_{g\leftarrow g}(z)$. To leave the volume element in the (x,t) space a gluon can either split into two gluons or radiate one of n_f light-quark flavors. Combining the incoming and outgoing flows we find

$$\begin{aligned}
\delta f_g(x,-t) =& \frac{\delta t}{t}\int_0^1 \frac{dz}{z}\,\frac{\alpha_s}{2\pi}\left[2\hat{P}_{g\leftarrow g}(z) f_g\left(\frac{x}{z},-t\right)\right.\\
&\qquad\left. + \hat{P}_{g\leftarrow q}(z)\left(f_q\left(\frac{x}{z},-t\right) + f_{\bar{q}}\left(\frac{x}{z},-t\right)\right)\right]\\
&- \frac{\delta t}{t}\int_0^1 dy\,\frac{\alpha_s}{2\pi}\left[\hat{P}_{g\leftarrow g}(y) + n_f\hat{P}_{q\leftarrow g}(y)\right] f_g(x,-t)
\end{aligned} \tag{2.135}$$

Again, for the gluon density there exists a contribution to δf_{in} proportional to f_q or $f_{\bar{q}}$ which is not matched by the outgoing flow. On the other hand, from the quark case we already know how to deal with it, namely by defining without a second plus subtraction

$$\boxed{P_{g\leftarrow q}(z) \equiv \hat{P}_{g\leftarrow q}(z) = C_F\,\frac{1+(1-z)^2}{z}}. \tag{2.136}$$

This ensures that the off-diagonal contribution to the gluon density is taken into account following Eq. 2.131.

Three regularized splitting kernels entering the DGLAP equation we give in Eqs. 2.130, 2.133 and 2.136. The generic structure of the DGLAP equation implies that the two off-diagonal splitting kernels do not include any plus prescription $\hat{P}_{i\leftarrow j} = P_{i\leftarrow j}$. We could have expected this because these off-diagonal kernels are finite in the soft limit $z \to 0, 1$. Applying a plus prescription would only have modified the splitting kernels at the isolated (zero-measure) point $y = 1$ which for a finite value of the integrand does not affect the integral on the right-hand side of the DGLAP equation.

The final splitting kernel $P_{g\leftarrow g}$ from the diagonal relation on the right-hand side of Eq. 2.135 requires some more work. The y integral not involving the gluon parton densities we can explicitly carry out for the gluon splitting into a quark pair

$$\begin{aligned} -\int_0^1 dy\ \frac{\alpha_s}{2\pi}\ n_f\ \hat{P}_{q\leftarrow g}(y) &= -\frac{\alpha_s}{2\pi}\ n_f\ T_R\ \int_0^1 dy\ \left[1-2y+2y^2\right] \\ &= -\frac{\alpha_s}{2\pi}\ n_f\ T_R\ \left[y-y^2+\frac{2y^3}{3}\right]_0^1 \\ &= -\frac{2}{3}\ \frac{\alpha_s}{2\pi}\ n_f\ T_R. \end{aligned} \tag{2.137}$$

The second y integral for gluon radiation has to consist of a finite term and a term we can use to define the plus prescription for $\hat{P}_{g\leftarrow g}$

$$\begin{aligned} \int_0^1 dy \frac{\alpha_s}{2\pi} \hat{P}_{g\leftarrow g}(y) =& \frac{\alpha_s}{2\pi} C_A\ \int_0^1 dy\ \left[\frac{y}{1-y}+\frac{1-y}{y}+y(1-y)\right] \\ =& \frac{\alpha_s}{2\pi}\ C_A\ \int_0^1 dy\ \left[\frac{2y}{1-y}+y(1-y)\right] \\ =& \frac{\alpha_s}{2\pi}\ C_A\ \int_0^1 dy\ \left[\frac{2(y-1)}{1-y}+y(1-y)\right] + \frac{\alpha_s}{2\pi}\ C_A\ \int_0^1 dy\ \frac{2}{1-y} \\ =& \frac{\alpha_s}{2\pi}\ C_A\ \int_0^1 dy\ \left[-2+y-y^2\right] + \delta(1-z)\ \frac{\alpha_s}{2\pi}\ 2C_A\ \int_0^1 dy\ \frac{z}{1-y} \\ =& \frac{\alpha_s}{2\pi}\ C_A\ \left[-2+\frac{1}{2}-\frac{1}{3}\right] + \delta(1-z)\ \frac{\alpha_s}{2\pi}\ 2C_A\ \int_0^1 dy\ \frac{z}{1-y} \\ =& -\frac{\alpha_s}{2\pi}\ \frac{11}{6}\ C_A\ + \delta(1-z)\ \frac{\alpha_s}{2\pi}\ 2C_A\ \int_0^1 dy\ \frac{z}{1-y}. \end{aligned} \tag{2.138}$$

The contribution proportional to $\delta(1-z)$ is necessary to give a finite result and is absorbed into the plus prescription of the convoluted $\hat{P}_{g\leftarrow g}(z)$, including the factor two in front. This defines the last remaining regularized splitting kernel

$$\boxed{P_{g\leftarrow g}(z) = 2C_A\left(\frac{z}{(1-z)_+}+\frac{1-z}{z}+z(1-z)\right)+\frac{11C_A}{6}\delta(1-z)+\frac{2n_f T_R}{3}\delta(1-z)} \tag{2.139}$$

and concludes our computation of all four regularized splitting functions which appear in the DGLAP equation Eq. 2.131.

Before discussing and solving the DGLAP equation, let us briefly recapitulate: for the full quark and gluon particle content of QCD we have derived the DGLAP equation which describes a (so-called factorization) scale dependence of the quark and gluon parton densities. The universality of the splitting kernels is obvious from the way we derive them—no information on the n-particle process ever enters the derivation.

The DGLAP equation is formulated in terms of four splitting kernels of gluons and quarks which are linked to the splitting probabilities, but which for the DGLAP equation have to be regularized. With the help of a plus-subtraction the kernels $P_{i\leftarrow j}(z)$ are all finite, including in the soft limit $z \to 1$. However, splitting kernels are only regularized when needed, so the finite off-diagonal quark-gluon and gluon-quark splittings are unchanged. This means the plus prescription really acts as an infrared renormalization, moving universal infrared divergences into the definition of the parton densities. The original collinear divergence has vanished as well.

The only approximation we make in the computation of the splitting kernels is that in the y integrals we implicitly assume that the running coupling α_s does not depend on the momentum fraction. In its standard form and in terms of the factorization scale $\mu_F^2 \equiv -t$ the *DGLAP equation* reads

$$\boxed{\frac{df_i(x,\mu_F)}{d\log\mu_F^2} = \sum_j \int_x^1 \frac{dz}{z}\,\frac{\alpha_s}{2\pi}\,P_{i\leftarrow j}(z)\,f_j\left(\frac{x}{z},\mu_F\right) = \frac{\alpha_s}{2\pi}\sum_j \left(P_{i\leftarrow j}\otimes f_j\right)(x,\mu_F)}\,. \tag{2.140}$$

2.3.4 Parton Densities

Solving the integro-differential DGLAP equation Eq. 2.140 for the parton densities is clearly beyond the scope of this writeup. Nevertheless, we will sketch how we would approach this. This will give us some information on the structure of its solutions which we need to understand the physics of the DGLAP equation.

One simplification we can make in this illustration is to postulate eigenvalues in parton space and solve the equation for them. This gets rid of the sum over partons on the right hand side. One such parton density is the *non-singlet parton density*, defined as the difference of two parton densities $f_q^{\text{NS}} = (f_u - f_{\bar{u}})$. Since gluons cannot distinguish between quarks and antiquarks, the gluon contribution to their evolution cancels, at least in the massless limit. This will be true at arbitrary loop order, since flavor $SU(3)$ commutes with the QCD gauge group. The corresponding DGLAP equation with leading order splitting kernels now reads

$$\frac{df_q^{\text{NS}}(x,\mu_F)}{d\log\mu_F^2} = \int_x^1 \frac{dz}{z}\,\frac{\alpha_s}{2\pi}\,P_{q\leftarrow q}(z)\,f_q^{\text{NS}}\left(\frac{x}{z},\mu_F\right) = \frac{\alpha_s}{2\pi}\,\left(P_{q\leftarrow q}\otimes f_q^{\text{NS}}\right)(x,\mu_F). \tag{2.141}$$

To solve it we need some kind of transformation which disentangles the convolution, namely a *Mellin transform*. Starting from a function $f(x)$ of a real variable x we define the Mellin transform into moment space m

$$\boxed{\mathscr{M}[f](m) \equiv \int_0^1 dx x^{m-1} f(x)} \qquad f(x) = \frac{1}{2\pi i} \int_{c-i\infty}^{c-i\infty} dn \, \frac{\mathscr{M}[f](m)}{x^n}. \tag{2.142}$$

The integration contour for the inverse transformation lies to the right of all singularities of the analytic continuation of $\mathscr{M}[f](m)$, which fixes the offset c. The Mellin transform of a convolution is the product of the two Mellin transforms, which gives us the transformed DGLAP equation

$$\begin{aligned} \mathscr{M}[P_{q\leftarrow q} \otimes f_q^{\mathrm{NS}}](m) &= \mathscr{M}\left[\int_0^1 \frac{dz}{z} P_{q\leftarrow q}\left(\frac{x}{z}\right) f_q^{\mathrm{NS}}(z)\right](m) \\ &= \mathscr{M}[P_{q\leftarrow q}](m)\, \mathscr{M}[f_q^{\mathrm{NS}}](m,\mu_F) \\ \frac{d\mathscr{M}[f_q^{\mathrm{NS}}](m,\mu_F)}{d\log\mu_F^2} &= \frac{\alpha_s}{2\pi}\, \mathscr{M}[P_{q\leftarrow q}](m)\, \mathscr{M}[f_q^{\mathrm{NS}}](m,\mu_F) \end{aligned} \tag{2.143}$$

and its solution

$$\begin{aligned} \mathscr{M}[f_q^{\mathrm{NS}}](m,\mu_F) &= \mathscr{M}[f_q^{\mathrm{NS}}](m,\mu_{F,0})\, \exp\left(\frac{\alpha_s}{2\pi}\, \mathscr{M}[P_{q\leftarrow q}](m) \log\frac{\mu_F^2}{\mu_{F,0}^2}\right) \\ &= \mathscr{M}[f_q^{\mathrm{NS}}](m,\mu_{F,0}) \left(\frac{\mu_F^2}{\mu_{F,0}^2}\right)^{\frac{\alpha_s}{2\pi}\mathscr{M}[P_{q\leftarrow q}](m)} \\ &\equiv \mathscr{M}[f_q^{\mathrm{NS}}](m,\mu_{F,0}) \left(\frac{\mu_F^2}{\mu_{F,0}^2}\right)^{\frac{\alpha_s}{2\pi}\gamma(m)}, \end{aligned} \tag{2.144}$$

defining $\gamma(m) = \mathscr{M}[P](m)$. Instead of assuming a fixed α_s in the transformed DGLAP equation Eq. 2.143 we can include $\alpha_s(\mu_R^2)$ in the running of the DGLAP equation, identifying the renormalization scale μ_R of the strong coupling with the factorization scale $\mu_F = \mu_R \equiv \mu$. This allows us to replace $\log\mu^2$ in the DGLAP equation by α_s, including the leading order Jacobian

$$\frac{d}{d\log\mu^2} = \frac{d\log\alpha_s}{d\log\mu^2}\, \frac{d}{d\log\alpha_s} = \frac{1}{\alpha_s}\, \frac{d\alpha_s}{d\log\mu^2}\, \frac{d}{d\log\alpha_s} = -\alpha_s b_0\, \frac{d}{d\log\alpha_s}. \tag{2.145}$$

This additional factor of α_s on the left-hand side will cancel the factor α_s on the right hand side of the DGLAP equation Eq. 2.143

$$\frac{d\mathcal{M}[f_q^{\rm NS}](m,\mu)}{d\log\alpha_s} = -\frac{1}{2\pi b_0}\gamma(m)\ \mathcal{M}[f_q^{\rm NS}](m,\mu)$$

$$\begin{aligned}\mathcal{M}[f_q^{\rm NS}](m,\mu) &= \mathcal{M}[f_q^{\rm NS}](m,\mu_0)\ \exp\left(-\frac{1}{2\pi b_0}\ \gamma(m)\log\frac{\alpha_s(\mu^2)}{\alpha_s(\mu_0^2)}\right)\\ &= \mathcal{M}[f_q^{\rm NS}](m,\mu_{F,0})\ \left(\frac{\alpha_s(\mu_0^2)}{\alpha_s(\mu^2)}\right)^{\frac{\gamma(m)}{2\pi b_0}}. \end{aligned} \tag{2.146}$$

Among other things in this derivation we neglect that some splitting functions have singularities and therefore the Mellin transform is not obviously well-defined. Our convolution is not really a convolution either, because we cut it off at Q_0^2, etc.; but the final structure in Eq. 2.146 really holds.

Because we will need it in the next section we emphasize that the same kind of solution appears in pure Yang–Mills theory, i.e. in QCD without quarks. Looking at the different color factors in QCD this limit can also be derived as the leading terms in N_c. In that case there exists also only one splitting kernel defining an anomalous dimension γ, and we find in complete analogy to Eq. 2.146

$$\boxed{\mathcal{M}[f_g](m,\mu) = \mathcal{M}[f_g](m,\mu_0)\ \left(\frac{\alpha_s(\mu_0^2)}{\alpha_s(\mu^2)}\right)^{\frac{\gamma(m)}{2\pi b_0}}}. \tag{2.147}$$

To remind ourselves that in this derivation we unify the renormalization and factorization scales we denote them just as μ. This solution to the DGLAP equation is not completely determined: as a solution to a differential equation it also includes an integration constant which we express in terms of μ_0. The DGLAP equation therefore does not determine parton densities, it only describes their evolution from one scale μ_F to another, just like a renormalization group equation in the ultraviolet.

The structure of Eq. 2.147 already shows something we will in more detail discuss in the following Sect. 2.3.5: the splitting probability we find in the exponent. To make sense of such a structure we remind ourselves that such ratios of α_s values to some power can appear as a result of a re-summed series. Such a series would need to include powers of $(\mathcal{M}[\hat{P}])^n$ summed over n which corresponds to a sum over splittings with a varying number of partons in the final state. Parton densities cannot be formulated in terms of a fixed final state because they include effects from any number of collinearly radiated partons summed over the number of such partons. For the processes we can evaluate using parton densities fulfilling the DGLAP equation this means that they always have the form

$$\boxed{pp \to \mu^+\mu^- + X} \qquad \text{where } X \text{ includes any number of collinear jets} \tag{2.148}$$

Why is γ is referred to as the *anomalous dimension* of the parton density? This is best illustrated using a running coupling with a finite mass dimension, like the gravitational coupling $G_{\rm Planck} \sim 1/M^2_{\rm Planck}$. When we attach a renormalization constant

Z to this coupling we first define a dimensionless running bare coupling g. In n dimensions this gives us

$$g^{\text{bare}} = M^{n-2}\, G_{\text{Planck}} \quad g^{\text{bare}} = M^{n-2}\, G_{\text{Planck}} \to Z g(M^2). \tag{2.149}$$

For the dimensionless gravitational coupling we can compute the running

$$\begin{aligned}\frac{dg(M^2)}{d\log M} &= \frac{d}{d\log M}\left(\frac{1}{Z} M^{n-2}\, G_{\text{Planck}}\right) \\ &= G_{\text{Planck}}\left(\frac{1}{Z} M \frac{dM^{n-2}}{dM} - \frac{1}{Z^2}\frac{dZ}{d\log M} M^{n-2}\right) \\ &= g(M)\,(n-2+\eta) \quad \text{with} \quad \eta = -\frac{1}{Z}\frac{dZ}{d\log M}\end{aligned} \tag{2.150}$$

Hence, there are two sources of running for the renormalized coupling $g(M^2)$: first, there is the mass dimension of the bare coupling $n-2$, and secondly there is η, a quantum effect from the coupling renormalization. For obvious reasons we call η the anomalous dimension of G_{Planck}.

This is similar to the running of the parton densities in Mellin space, as shown in Eq. 2.143 with $\gamma(m)$ defined in Eq. 2.144, so we refer to γ as an anomalous dimension as well. The entire running of the transformed parton density arises from collinear splitting, parameterized by a finite γ. There is only a slight stumbling step in this analogy: usually, an anomalous dimension arises through renormalization involving a ultraviolet divergence and the renormalization scale. In our case we are discussing an infrared divergence and the factorization scale dependence.

2.3.5 Re-Summing Collinear Logarithms

Remembering how we arrive at the DGLAP equation we notice an analogy to the case of ultraviolet divergences and the running coupling. We start from universal infrared divergences. Those we describe in terms of splitting functions which we regularize using the plus prescription. The DGLAP equation plays the role of a renormalization group equation for example for the running coupling. It links parton densities evaluated at different scales μ_F.

In analogy to the scaling logarithms considered in Sect. 2.2.3 we now test if we can point to a *type of logarithm* the DGLAP equation re-sums by reorganizing our perturbative series of parton splitting. To identify these re-summed logarithms we build a physical model based on collinear splitting but without using the DGLAP equation. We then solve it to see the resulting structure of the solutions and compare it to the structure of the DGLAP solutions in Eq. 2.147.

We start from the basic equation defining the physical picture of parton splitting in Eq. 2.97. Only taking into account gluons in pure Yang–Mills theory it precisely

corresponds to the starting point of our discussion leading to the DGLAP equation, schematically written as

$$\sigma_{n+1} = \int \sigma_n \, \frac{dt}{t} dz \, \frac{\alpha_s}{2\pi} \, \hat{P}_{g\leftarrow g}(z). \tag{2.151}$$

What we now need is an exact physical definition of the virtuality variable t describing initial-state splitting. If we remember that $t = p_b^2 < 0$ we can follow Eq. 2.117 and introduce a positive transverse momentum variable $\vec{p}_T^{\,2}$ such that

$$-t = -\frac{p_T^2}{1-z} = \frac{\vec{p}_T^{\,2}}{1-z} > 0 \quad \Rightarrow \quad \frac{dt}{t} = \frac{dp_T^2}{p_T^2} = \frac{d\vec{p}_T^{\,2}}{\vec{p}_T^{\,2}}. \tag{2.152}$$

From the definition of p_T in the Sudakov decomposition Eq. 2.88 we see that $\vec{p}_T^{\,2}$ is really the transverse three-momentum of the parton pair after splitting.

If beyond the single parton radiation discussed in Sect. 2.3.1 we consider a ladder of successive splittings of one gluon into two and we for a moment forget about the actual parton densities we can write the hadronic cross section in the collinear limit including the appropriate convolution as

$$\begin{aligned}\sigma_{n+1}(x,\mu_F) &= \int_{\mu_0^2}^{\mu_F^2} \frac{d\vec{p}_{T,n}^{\,2}}{\vec{p}_{T,n}^{\,2}} \frac{\alpha_s(\mu_R^2)}{2\pi} \int_{x_0}^1 \frac{dx_n}{x_n} \, \hat{P}_{g\leftarrow g}\left(\frac{x}{x_n}\right) \sigma_n(x_n,\mu_0) \\ &= \int_{x_0}^1 \frac{dx_n}{x_n} \, \hat{P}_{g\leftarrow g}\left(\frac{x}{x_n}\right) \sigma_n(x_n,\mu_0) \int_{\mu_0^2}^{\mu_F^2} \frac{d\vec{p}_{T,n}^{\,2}}{\vec{p}_{T,n}^{\,2}} \frac{\alpha_s(\mu_R^2)}{2\pi}. \end{aligned} \tag{2.153}$$

The dz in Eq. 2.151 we replace by the proper convolution $\hat{P} \otimes \sigma_n$, evaluated at the momentum fraction x. Because the splitting kernel is infrared divergent we cut off the convolution integral at x_0. Similarly, the transverse momentum integral is bounded by an infrared cutoff μ_0 and the physical external scale μ_F. For the split of the two integrals in Eq. 2.153 it is crucial that μ_0 is the only scale the final matrix element σ_1 depends on.

Identifying μ_F with the upper boundary of the transverse momentum integration for collinear splitting is the first assumption we make for our model. The recursion in Eq. 2.153 we can then apply iteratively

$$\begin{aligned}\sigma_{n+1}(x,\mu_F) \sim &\int_{x_0}^1 \frac{dx_n}{x_n} \, \hat{P}_{g\leftarrow g}\left(\frac{x}{x_n}\right) \cdots \int_{x_0}^1 \frac{dx_1}{x_1} \, \hat{P}_{g\leftarrow g}\left(\frac{x_2}{x_1}\right) \sigma_1(x_1,\mu_0) \\ &\times \int_{\mu_0}^{\mu_F} \frac{d\vec{p}_{T,n}^{\,2}}{\vec{p}_{T,n}^{\,2}} \frac{\alpha_s(\mu_R^2)}{2\pi} \cdots \int_{\mu_0}^{\mu_F} \frac{d\vec{p}_{T,1}^{\,2}}{\vec{p}_{T,1}^{\,2}} \frac{\alpha_s(\mu_R^2)}{2\pi}. \end{aligned} \tag{2.154}$$

The two sets of integrals in this equation we will solve one by one, starting with the $\vec{p}_T$ integrals.

The crucial physics assumption in our multiple-splitting model concerns the integration boundaries, in addition to the global upper limit μ_F: as the second assumption the transverse momenta of the splittings should be *strongly ordered*; the first splitting

integrated over $\vec{p}_{T,1}^{\,2}$ is bounded from above by the next external scale $\vec{p}_{T,2}^{\,2}$, which is then bounded by $\vec{p}_{T,3}^{\,2}$, etc. For the n-fold $\vec{p}_T^{\,2}$ integration this means

$$\mu_0^2 < \vec{p}_{T,1}^{\,2} < \vec{p}_{T,2}^{\,2} < \cdots < \mu_F^2 \tag{2.155}$$

The transverse momentum integrals in Eq. 2.154 then become

$$\begin{aligned}
&\int_{\mu_0}^{\mu_F} \frac{d\vec{p}_{T,n}^{\,2}}{\vec{p}_{T,n}^{\,2}} \frac{\alpha_s(\vec{p}_{T,n}^{\,2})}{2\pi} \cdots \int_{\mu_0}^{p_{T,3}} \frac{d\vec{p}_{T,2}^{\,2}}{\vec{p}_{T,2}^{\,2}} \frac{\alpha_s(\vec{p}_{T,2}^{\,2})}{2\pi} \int_{\mu_0}^{p_{T,2}} \frac{d\vec{p}_{T,1}^{\,2}}{\vec{p}_{T,1}^{\,2}} \frac{\alpha_s(\vec{p}_{T,1}^{\,2})}{2\pi} \cdots \\
&= \int_{\mu_0}^{\mu_F} \frac{d\vec{p}_{T,n}^{\,2}}{\vec{p}_{T,n}^{\,2}} \frac{1}{2\pi b_0 \log \frac{\vec{p}_{T,n}^{\,2}}{\Lambda_{\text{QCD}}^2}} \cdots \int_{\mu_0}^{p_{T,3}} \frac{d\vec{p}_{T,2}^{\,2}}{\vec{p}_{T,2}^{\,2}} \frac{1}{2\pi b_0 \log \frac{\vec{p}_{T,2}^{\,2}}{\Lambda_{\text{QCD}}^2}} \\
&\quad \times \int_{\mu_0}^{p_{T,2}} \frac{d\vec{p}_{T,1}^{\,2}}{\vec{p}_{T,1}^{\,2}} \frac{1}{2\pi b_0 \log \frac{\vec{p}_{T,1}^{\,2}}{\Lambda_{\text{QCD}}^2}} \cdots \\
&= \frac{1}{(2\pi b_0)^n} \int_{\mu_0}^{\mu_F} \frac{d\vec{p}_{T,n}^{\,2}}{\vec{p}_{T,n}^{\,2}} \frac{1}{\log \frac{\vec{p}_{T,n}^{\,2}}{\Lambda_{\text{QCD}}^2}} \cdots \int_{\mu_0}^{p_{T,3}} \frac{d\vec{p}_{T,2}^{\,2}}{\vec{p}_{T,2}^{\,2}} \frac{1}{\log \frac{\vec{p}_{T,2}^{\,2}}{\Lambda_{\text{QCD}}^2}} \\
&\quad \times \int_{\mu_0}^{p_{T,2}} \frac{d\vec{p}_{T,1}^{\,2}}{\vec{p}_{T,1}^{\,2}} \frac{1}{\log \frac{\vec{p}_{T,1}^{\,2}}{\Lambda_{\text{QCD}}^2}} \cdots .
\end{aligned} \tag{2.156}$$

Note that just as in Eq. 2.146 as our third assumption we identify the scale of the strong coupling α_s with the transverse momentum scale of the splitting $\mu_R^2 = \vec{p}_T^{\,2}$. These integrals we can solve by switching variables, for example in the last integral

$$\begin{aligned}
\int_{\mu_0}^{p_{T,2}} \frac{d\vec{p}_{T,1}^{\,2}}{\vec{p}_{T,1}^{\,2}} \frac{1}{\log \frac{\vec{p}_{T,1}^{\,2}}{\Lambda_{\text{QCD}}^2}} &= \int_{\mu_0}^{p_{T,2}} d \log\log \frac{\vec{p}_{T,1}^{\,2}}{\Lambda_{\text{QCD}}^2} \quad \text{with} \quad \frac{d(ax)}{(ax)\log x} = d\log\log x \\
&= \int_{\mu_0}^{p_{T,2}} d\left(\log\log \frac{\vec{p}_{T,1}^{\,2}}{\Lambda_{\text{QCD}}^2} - \log\log \frac{\mu_0^2}{\Lambda_{\text{QCD}}^2} \right) \\
&= \left[\log\log \frac{\vec{p}_{T,1}^{\,2}}{\Lambda_{\text{QCD}}^2} - \log\log \frac{\mu_0^2}{\Lambda_{\text{QCD}}^2} \right]_{\vec{p}_{T,1}^{\,2}=\mu_0^2}^{\vec{p}_{T,1}^{\,2}=\vec{p}_{T,2}^{\,2}} \\
&= \log \frac{\log \vec{p}_{T,2}^{\,2}/\Lambda_{\text{QCD}}^2}{\log \mu_0^2/\Lambda_{\text{QCD}}^2}.
\end{aligned} \tag{2.157}$$

In the second line we shift the integration variable by a constant. To simplify the notation we throughout keep the integration boundaries in terms of $|\vec{p}_{T,j}|$. The chain of

integrals over $\vec{p}^{\,2}_{T,j}$ we can solve, provided the integrand does not have any additional $\vec{p}^{\,2}_{T,j}$ dependence. This gives us

$$\begin{aligned}
&\int_{\mu_0}^{\mu_F} d\log\frac{\log\vec{p}^{\,2}_{T,n}/\Lambda^2_{\rm QCD}}{\log\mu_0^2/\Lambda^2_{\rm QCD}}\int_{\mu_0}^{p_{T,n}} d\log\frac{\log\vec{p}^{\,2}_{T,n-1}/\Lambda^2_{\rm QCD}}{\log\mu_0^2/\Lambda^2_{\rm QCD}}\cdots\\
&\quad\times\int_{\mu_0}^{p_{T,3}} d\log\frac{\log\vec{p}^{\,2}_{T,2}/\Lambda^2_{\rm QCD}}{\log\mu_0^2/\Lambda^2_{\rm QCD}}\int_{\mu_0}^{p_{T,2}} d\log\frac{\log\vec{p}^{\,2}_{T,1}/\Lambda^2_{\rm QCD}}{\log\mu_0^2/\Lambda^2_{\rm QCD}}\\
=&\int_{\mu_0}^{\mu_F} d\log\frac{\log\vec{p}^{\,2}_{T,n}/\Lambda^2_{\rm QCD}}{\log\mu_0^2/\Lambda^2_{\rm QCD}}\int_{\mu_0}^{p_{T,n}} d\log\frac{\log\vec{p}^{\,2}_{T,n-1}/\Lambda^2_{\rm QCD}}{\log\mu_0^2/\Lambda^2_{\rm QCD}}\cdots\\
&\quad\times\int_{\mu_0}^{p_{T,3}} d\log\frac{\log\vec{p}^{\,2}_{T,2}/\Lambda^2_{\rm QCD}}{\log\mu_0^2/\Lambda^2_{\rm QCD}}\left(\log\frac{\log\vec{p}^{\,2}_{T,2}/\Lambda^2_{\rm QCD}}{\log\mu_0^2/\Lambda^2_{\rm QCD}}\right)\\
=&\int_{\mu_0}^{\mu_F} d\log\frac{\log\vec{p}^{\,2}_{T,n}/\Lambda^2_{\rm QCD}}{\log\mu_0^2/\Lambda^2_{\rm QCD}}\int_{\mu_0}^{p_{T,n}} d\log\frac{\log\vec{p}^{\,2}_{T,n-1}/\Lambda^2_{\rm QCD}}{\log\mu_0^2/\Lambda^2_{\rm QCD}}\cdots\\
&\quad\times\frac{1}{2}\left(\log\frac{\log\vec{p}^{\,2}_{T,3}/\Lambda^2_{\rm QCD}}{\log\mu_0^2/\Lambda^2_{\rm QCD}}\right)^2\\
=&\int_{\mu_0}^{\mu_F} d\log\frac{\log\vec{p}^{\,2}_{T,n}/\Lambda^2_{\rm QCD}}{\log\mu_0^2/\Lambda^2_{\rm QCD}}\left(\frac{1}{2}\cdots\frac{1}{n-1}\right)\left(\log\frac{\log\vec{p}^{\,2}_{T,n}/\Lambda^2_{\rm QCD}}{\log\mu_0^2/\Lambda^2_{\rm QCD}}\right)^{n-1}\\
=&\frac{1}{n!}\left(\log\frac{\log\mu_F^2/\Lambda^2_{\rm QCD}}{\log\mu_0^2/\Lambda^2_{\rm QCD}}\right)^n=\frac{1}{n!}\left(\log\frac{\alpha_s(\mu_0^2)}{\alpha_s(\mu_F^2)}\right)^n.
\end{aligned}\tag{2.158}$$

This is the final result for the chain of transverse momentum integrals in Eq. 2.154. Again, we see that the strong coupling is evaluated at the factorization scale μ_F, which means we identify $\mu_R \equiv \mu_F$ following our third assumption.

To compute the convolution integrals over the momentum fractions in the same equation

$$\begin{aligned}
\sigma_{n+1}(x,\mu)\sim&\frac{1}{n!}\left(\frac{1}{2\pi b_0}\log\frac{\alpha_s(\mu_0^2)}{\alpha_s(\mu^2)}\right)^n\\
&\times\int_{x_0}^1\frac{dx_n}{x_n}\,\hat{P}_{g\leftarrow g}\left(\frac{x}{x_n}\right)\cdots\int_{x_0}^1\frac{dx_1}{x_1}\,\hat{P}_{g\leftarrow g}\left(\frac{x_2}{x_1}\right)\,\sigma_1(x_1,\mu_0),
\end{aligned}\tag{2.159}$$

we again Mellin transform the equation into moment space

$$\begin{aligned}\mathcal{M}[\sigma_{n+1}](m,\mu) \sim & \frac{1}{n!}\left(\frac{1}{2\pi b_0}\log\frac{\alpha_s(\mu_0^2)}{\alpha_s(\mu^2)}\right)^n \\ & \times \mathcal{M}\left[\int_{x_0}^1 \frac{dx_n}{x_n}\hat{P}_{g\leftarrow g}\left(\frac{x}{x_n}\right)\cdots\int_{x_0}^1\frac{dx_1}{x_1}\hat{P}_{g\leftarrow g}\left(\frac{x_2}{x_1}\right)\sigma_1(x_1,\mu_0)\right](m) \\ = & \frac{1}{n!}\left(\frac{1}{2\pi b_0}\log\frac{\alpha_s(\mu_0^2)}{\alpha_s(\mu^2)}\right)^n \gamma(m)^n \mathcal{M}[\sigma_1](m,\mu_0) \\ = & \frac{1}{n!}\left(\frac{1}{2\pi b_0}\log\frac{\alpha_s(\mu_0^2)}{\alpha_s(\mu^2)}\gamma(m)\right)^n \mathcal{M}[\sigma_1](m,\mu_0), \end{aligned} \tag{2.160}$$

where we define $\gamma(m) \equiv \mathcal{M}[P](m)$. We can now sum the production cross sections for n collinear jets and obtain

$$\begin{aligned}\sum_{n=0}^{\infty}\mathcal{M}[\sigma_{n+1}](m,\mu) = & \mathcal{M}[\sigma_1](m,\mu_0)\ \sum_n \frac{1}{n!}\left(\frac{1}{2\pi b_0}\log\frac{\alpha_s(\mu_0^2)}{\alpha_s(\mu^2)}\ \gamma(m)\right)^n \\ = & \mathcal{M}[\sigma_1](m,\mu_0)\ \exp\left(\frac{\gamma(m)}{2\pi b_0}\ \log\frac{\alpha_s(\mu_0^2)}{\alpha_s(\mu^2)}\right). \end{aligned} \tag{2.161}$$

This way we can write the Mellin transform of the $(n+1)$ particle production rate as the product of the n-particle rate times a ratio of the strong coupling at two scales

$$\boxed{\sum_{n=0}^{\infty}\mathcal{M}[\sigma_{n+1}](m,\mu) = \mathcal{M}[\sigma_1](m,\mu_0)\left(\frac{\alpha_s(\mu_0^2)}{\alpha_s(\mu^2)}\right)^{\frac{\gamma(m)}{2\pi b_0}}}. \tag{2.162}$$

This is the same structure as the DGLAP equation's solution in Eq. 2.147. It means that we should be able to understand the physics of the DGLAP equation using our model calculation of a gluon ladder emission, including the generically variable number of collinear jets in the form of $pp \to \mu^+\mu^- + X$, as shown in Eq. 2.148.

We should remind ourselves of the three assumptions we need to make to arrive at this form. There are two assumptions which concern the transverse momenta of the successive radiation: first, the global upper limit on all transverse momenta should be the factorization scale μ_F, with a strong ordering in the transverse momenta. This gives us a physical picture of the successive splittings as well as a physical interpretation of the factorization scale. Second, the strong coupling should be evaluated at the transverse momentum or factorization scale, so all scales are unified, in accordance with the derivation of the DGLAP equation.

Bending the rules of pure Yang–Mills QCD we can come back to the hard process σ_1 as the Drell–Yan process $q\bar{q} \to Z$. Each step in n means an additional parton in the final state, so σ_{n+1} is Z production with n collinear partons On the left hand side of Eq. 2.162 we have the sum over any number of additional collinear partons;

on the right-hand side we see fixed order Drell–Yan production without any additional partons, but with an exponentiated correction factor. Comparing this to the running parton densities we can draw the analogy that any process computed with a scale dependent parton density where the scale dependence is governed by the DGLAP equation includes *any number* of collinear partons.

The logarithms which are re-summed by scale dependent parton densities we can also identify. Going back to Eq. 2.84 reminds us that we start from the divergent collinear logarithms $\log p_T^{\max}/p_T^{\min}$ arising from the collinear phase space integration. In our model for successive splitting we replace the upper boundary by μ_F. The collinear logarithm of successive initial state parton splitting diverges for $\mu_0 \to 0$, but it gets absorbed into the parton densities and determines the structure of the DGLAP equation and its solutions. The upper boundary μ_F tells us to what extent we assume incoming quarks and gluons to be a coupled system of splitting partons and what the maximum momentum scale of these splittings is. Transverse momenta $p_T > \mu_F$ generated by hard parton splitting are not covered by the DGLAP equation and hence not a feature of the incoming partons anymore. They belong to the hard process and have to be consistently simulated, as we will see in Sects. 2.5.3 and 2.6. While this scale can be chosen freely we have to make sure that it does not become too large, because at some point the *collinear approximation* $C \simeq$ constant in Eq. 2.84 ceases to hold and with it our entire argument. Only if we do everything correctly, the DGLAP equation re-sums logarithms of the maximal *transverse momentum size* of the incoming gluon. They are universal and arise from simple kinematics.

The ordering of the splittings we have to assume is not relevant unless we simulate this splitting, as we will see in the next section. For the details of this we have to remember that our argument follows from the leading collinear approximation introduced in Sect. 2.3.1. Therefore, the strong p_T ordering can in practice mean angular ordering or rapidity ordering as well, just applying a linear transformation.

2.4 Scales in LHC Processes

Looking back at Sects. 2.2 and 2.3 we introduced the factorization and renormalization scales step by step completely in parallel: first, computing perturbative higher order contributions to scattering amplitudes we encounter ultraviolet and infrared divergences. Both of them we regularize using dimensional regularization with $n = 4 - 2\varepsilon < 4$ for ultraviolet and $n > 4$ for infrared divergences, linked by analytic continuation. For both kinds of divergences we notice that they are universal, i.e. not process or observable dependent. This allows us to absorb ultraviolet and infrared divergences into a re-definition of the strong coupling and the parton density. This nominally infinite shift of parameters we refer to as renormalization for example of the strong coupling or as mass factorization absorbing infrared divergences into the parton distributions.

After renormalization as well as after mass factorization we are left with a *scale artifact*. Scales arise as part of a the pole subtraction: together with the pole $1/\varepsilon$ we

have a choice of finite contributions which we subtract with this pole. Logarithms of the renormalization and factorization scales will always be part of these finite terms. Moreover, in both cases the re-definition of parameters is not based on fixed order perturbation theory. Instead, it involves summing logarithms which otherwise can become large and spoil the convergence of our perturbative series in α_s. The only special feature of infrared divergences as compared to ultraviolet divergences is that to identify the resummed logarithms we have to unify both scales to one.

The hadronic production cross section for the Drell–Yan process or other LHC production channels, now including both scales, reads

$$\sigma_{\text{tot}}(\mu_F, \mu_R) = \int_0^1 dx_1 \int_0^1 dx_2 \sum_{ij} f_i(x_1, \mu_F) f_j(x_2, \mu_F) \hat{\sigma}_{ij}(x_1 x_2 S, \alpha_s(\mu_R^2), \mu_F, \mu_R). \tag{2.163}$$

The Drell–Yan process has the particular feature that at leading order $\hat{\sigma}_{q\bar{q}}$ only involves weak couplings, it does not include α_s with its implicit renormalization scale dependence at leading order. Strictly speaking, in Eq. 2.163 the parton densities also depend on the renormalization scale because in their extraction we identify both scales. Carefully following their extraction we can separate the two scales if we need to. Lepton pair production and Higgs production in weak boson fusion are the two prominent electroweak production processes at the LHC.

The evolution of all running parameters from one renormalization/factorization scale to another is described either by renormalization group equation in terms of a beta function in the case of renormalization and by the DGLAP equation in the case of mass factorization. Our renormalization group equation for α_s is a single equation, but in general they are sets of coupled differential equations for all relevant parameters, which again makes them more similar to the DGLAP equation.

There is one formal difference between these two otherwise very similar approaches. The fact that we can absorb ultraviolet divergences into process-independent, i.e. universal counter terms is called renormalizability and has been proven to all orders for the kind of gauge theories we are dealing with. The universality of infrared splitting kernels has not (yet) in general been proven, but on the other hand we have never seen an example where is fails for sufficiently inclusive observables like production rates. For a while we thought there might be a problem with factorization in supersymmetric theories using the $\overline{\text{MS}}$ scheme, but this issue has been resolved. A summary of the properties of the two relevant scales for LHC physics we show in Table 2.2.

The way we introduce factorization and renormalization scales clearly labels them as an artifact of perturbation theories with divergences. What actually happens if we include *all orders* in perturbation theory? For example, the re-summation of the self energy bubbles simply deals with one class of diagrams which have to be included, either order-by-order or rearranged into a re-summation. Once we include all orders in perturbation theory it does not matter according to which combination of couplings and logarithms we order it. An LHC production rate will then not depend on arbitrarily chosen renormalization or factorization scales μ.

Table 2.2 Comparison of renormalization and factorization scales appearing in LHC cross sections

	Renormalization scale μ_R	Factorization scale μ_F
Source	Ultraviolet divergence	Collinear (infrared) divergence
Poles cancelled	Counter terms (renormalization)	Parton densities (mass factorization)
Summation	Re-sum self energy bubbles	Re-sum parton splittings
Parameter	Running coupling $\alpha_s(\mu_R^2)$	Running parton density $f_j(x, \mu_F)$
Evolution	RGE for α_s	DGLAP equation
Large scales	Decrease of σ_{tot}	Increase of σ_{tot} for gluons/sea quarks
Theory background	Renormalizability Proven for gauge theories	Factorization Proven all orders for DIS Proven order-by-order DY...

Practically, in Eq. 2.163 we evaluate the renormalized parameters and the parton densities at some scale. This scale dependence will only cancel once we include all implicit and explicit appearances of the scales at all orders. Whatever scale we choose for the strong coupling or parton densities will eventually be compensated by explicit scale logarithms. In the ideal case, these logarithms are small and do not spoil perturbation theory. In a process with one distinct external scale, like the Z mass, we know that all scale logarithms should have the form $\log(\mu/m_Z)$. This logarithm vanishes if we evaluate everything at the 'correct' external energy scale, namely m_Z. In that sense we can think of the running coupling as a proper *running observable* which depends on the external energy of the process. This dependence on the external energy is not a perturbative artifact, because a cross section even to all orders does depend on the energy. The problem in particular for LHC analyses is that after analysis cuts every process will have more than one external energy scale.

We can turn around the argument of vanishing scale dependence to all orders in perturbation theory. This gives us an estimate of the minimum *theoretical error* on a rate prediction set by the scale dependence. The appropriate interval of what we consider reasonable scale choices depends on the process and the taste of the people doing this analysis. This error estimate is not at all conservative; for example the renormalization scale dependence of the Drell–Yan production rate or Higgs production in weak boson fusion is zero because α_s only enters are next-to-leading order. At the same time we know that the next-to-leading order correction to the Drell–Yan cross section is of the order of 30%, which far exceeds the factorization scale dependence. Moreover, the different scaling behavior of a hadronic cross section shown in Table 2.2 implies that for example gluon-induced processes at typical x values around 10^{-2} show a cancellation of the factorization and renormalization scale variation. Estimating theoretical uncertainties from scale dependence therefore requires a good understanding of the individual process and the way it is affected by the two scales.

Guessing the right scale choice for a process is hard, often impossible. For example in Drell–Yan production at leading-order there exists only one scale, m_Z. If we set $\mu = m_Z$ all scale logarithms vanish. In reality, LHC observables include several different scales. Some of them appear in the hard process, for example in the production of two or three particles with different masses. Others enter through the QCD environment where at the LHC we only consider final state jets above a certain minimal transverse momentum. Even others appear though background rejection cuts in a specific analysis, for example when we only consider the Drell–Yan background for $m_{\mu\mu} > 1$ TeV to Kaluza–Klein graviton production. Using likelihood methods does not improve the situation because the phase space regions dominated by the signal will introduce specific energy scales which affect the perturbative prediction of the backgrounds. This is one of the reasons why an automatic comparison of LHC events with signal or background predictions is bound to fail once it requires an estimate of the theoretical uncertainty on the background simulation.

All that means that in practice there is no way to define a 'correct' scale. On the other hand, there are definitely *poor scale choices*. For example, using $1,000 \times m_Z$ as a typical scale in the Drell–Yan process will if nothing else lead to logarithms of the size $\log 1,000$ whenever a scale logarithm appears. These logarithms eventually have to be cancelled to all orders in perturbation theory, inducing unreasonably large higher order corrections.

When describing jet radiation, we usually introduce a phase-space dependent renormalization scale, evaluating the strong coupling at the transverse momentum of the radiated jet $\alpha_s(\vec{p}_{T,j}^{\,2})$. This choice gives the best kinematic distributions for the additional partons because in Sect. 2.3.5 we have shown that it re-sums large collinear logarithms.

The transverse momentum of a final state particle is one of scale choices allowed by factorization; in addition to poor scale choices there also exist *wrong scale choices*, i.e. scale choices violating physical properties we need. Factorization or the Kinoshita–Lee–Nauenberg theorem which ensures that soft divergences cancel between real and virtual emission diagrams are such properties we should not violate—in QED the same property is called the Bloch–Nordsieck cancellation. Imagine picking a factorization scale defined by the partonic initial state, for example the partonic center-of-mass energy $s = x_1 x_2 S$. We know that this definition is not unique: for any final state it corresponds to the well defined sum of all momenta squared. However, virtual and real gluon emission generate different multiplicities in the final state, which means that the two sources of soft divergences only cancel until we multiply each of them with numerically different parton densities. Only scales which are uniquely defined in the final state can serve as factorization scales. For the Drell–Yan process such a scale could be m_Z, or the mass of heavy new-physics states in their production process. So while there is no such thing as a correct scale choice, there are more or less smart choices, and there are definitely very poor choices, which usually lead to an unstable perturbative behavior.

2.5 Parton Shower

In LHC phenomenology we are usually less interested in fixed-order perturbation theory than in logarithmically enhanced QCD effects. Therefore, we will not deepen our discussion of hadronic rates as shown in Eq. 2.163 based on fixed-order partonic cross sections convoluted with parton densities obeying the DGLAP equation. In Sect. 2.3.5 we have already seen that there exist more functions with the same structure as solutions to the DGLAP equation. In this section we will look for other structures which obey the DGLAP equation, leading us to Sudakov form factors and the parton shower. In Sect. 2.5.2 we will discuss some of the physical properties of the parton shower. Per se it is not clear how jet radiation described by the parton shower and jet radiation described by fixed-order QCD processes are linked. In Sect. 2.5.3 we will discuss ways to combine the two approaches in realistic LHC simulations, bringing us very close to contemporary research topics.

2.5.1 Sudakov Form Factor

The splitting kernels $\hat{P}_{i\leftarrow j}(z)$ we introduce as something like splitting probabilities, but we never apply a probabilistic approach to parton splitting. The basis of such an interpretation are *Sudakov form factors* describing the splitting of a parton i into any of the partons j based on the factorized form Eq. 2.97

$$\boxed{\Delta_i(t) \equiv \Delta_i(t,t_0) = \exp\left(-\sum_j \int_{t_0}^{t} \frac{dt'}{t'} \int_0^1 dy \frac{\alpha_s}{2\pi} \hat{P}_{j\leftarrow i}(y)\right)}. \tag{2.164}$$

Before we check that such a function can obey the DGLAP equation we confirm that such exponentials appear in probabilistic arguments, similar to our discussion of the central jet veto in Sect. 1.5.2. Using Poisson statistics for something expected to occur p times, the probability of observing it n times is given by

$$\mathcal{P}(n;\, p) = \frac{p^n e^{-p}}{n!} \qquad \mathcal{P}(0;\, p) = e^{-p}. \tag{2.165}$$

If the exponent in the Sudakov form factor in Eq. 2.164 describes the integrated splitting probability of a parton i this means that the Sudakov itself describes a *non-splitting probability* of the parton i into any final state j.

Based on such probabilistic Sudakov factors we can use a Monte Carlo (i.e. a *Markov process* without a memory of individual past steps) to compute a chain of parton splittings as depicted in Fig. 2.2. This will describe a quark or a gluon propagating forward in time. Starting from a point (x_1, t_1) in momentum-virtuality space we step by step move to the next splitting point (x_j, t_j). Following the original discussion t_2 is the target virtuality at x_2, and for time-like final state branching the

virtuality is positive $t_j > 0$ in all points j. The Sudakov factor is a function of t, so it gives us the probability of not seeing any branching between t_1 and t_2 as $\Delta(t_1)/\Delta(t_2) < 1$. The appropriate cutoff scale t_0 drops out of this ratio. Using a flat random number r_t the t_2 distribution is implicitly given by the solution to

$$\frac{\Delta(t_1)}{\Delta(t_2)} = r_t \in [0,1] \qquad \text{with} \quad t_1 > t_2 > t_0 > 0. \tag{2.166}$$

Beyond the absolute cutoff scale t_0 we assume that no resolvable branching occurs.

In a second step we need to compute the matching energy fraction x_2 or the ratio x_2/x_1 describing the momentum fraction which is kept in the splitting at x_2. The y integral in the Sudakov factor in Eq. 2.164 gives us this probability distribution which we can again implicitly solve for x_2 using a flat random number r_x

$$\frac{\int_0^{x_2/x_1} dy \frac{\alpha_s}{2\pi} \hat{P}(y)}{\int_0^1 dy \frac{\alpha_s}{2\pi} \hat{P}(y)} = r_x \in [0,1] \qquad \text{with } x_1 > x_2 > 0. \tag{2.167}$$

For splitting kernels with soft divergences at $y = 0$ or $y = 1$ we should include a numerical cutoff in the integration because the probabilistic Sudakov factor and the parton shower do not involve the regularized splitting kernels.

Of the four momentum entries of the radiated parton the two equations Eqs. 2.166 and 2.167 give us two. The on-shell mass constraint fixes a third, so all we are left is the azimuthal angle distribution. We know from symmetry arguments that QCD splitting is insensitive to this angle, so we can generate it randomly between zero and 2π. For final state radiation this describes probabilistic branching in a *Monte Carlo program*, just based on Sudakov form factors.

The same statement for initial state radiation including parton densities we will put on a more solid or mathematical footing. The derivative of the Sudakov form factor Eq. 2.164

$$\frac{1}{\Delta_i(t)} \frac{d\Delta_i(t)}{dt} = -\sum_j \frac{1}{t} \int_0^1 dy \frac{\alpha_s}{2\pi} \hat{P}_{j \leftarrow i}(y) \tag{2.168}$$

is precisely the second term in $df(x,t)/dt$ for diagonal splitting, as shown in Eq. 2.124

$$\begin{aligned} \frac{df_i(x,t)}{dt} &= \frac{1}{t} \sum_j \left[\int_0^1 \frac{dz}{z} \frac{\alpha_s}{2\pi} \hat{P}_{i \leftarrow j}(z) \, f_j\left(\frac{x}{z}, t\right) - \int_0^1 dy \, \frac{\alpha_s}{2\pi} \hat{P}_{j \leftarrow i}(y) \, f_i(x,t) \right] \\ &= \frac{1}{t} \sum_j \int_0^1 \frac{dz}{z} \frac{\alpha_s}{2\pi} \hat{P}_{i \leftarrow j}(z) \, f_j\left(\frac{x}{z}, t\right) + \frac{f_i(x,t)}{\Delta_i(t)} \frac{d\Delta_i(t)}{dt}. \end{aligned} \tag{2.169}$$

This relation suggests to consider the derivative of the f_i/Δ_i instead of the Sudakov factor alone to obtain something like the DGLAP equation

$$\begin{aligned}
\frac{d}{dt}\frac{f_i(x,t)}{\Delta_i(t)} &= \frac{1}{\Delta_i(t)}\frac{df_i(x,t)}{dt} - \frac{f_i(x,t)}{\Delta_i(t)^2}\frac{d\Delta_i(t)}{dt} \\
&= \frac{1}{\Delta_i(t)}\left(\frac{1}{t}\sum_j \int_0^1 \frac{dz}{z}\,\frac{\alpha_s}{2\pi}\,\hat{P}_{i\leftarrow j}(z)\,f_j\left(\frac{x}{z},t\right) + \frac{f_i(x,t)}{\Delta_i(t)}\frac{d\Delta_i(t)}{dt}\right) \\
&\quad - \frac{f_i(x,t)}{\Delta_i(t)^2}\frac{d\Delta_i(t)}{dt} \\
&= \frac{1}{\Delta_i(t)}\,\frac{1}{t}\sum_j \int_0^{1-\varepsilon} \frac{dz}{z}\,\frac{\alpha_s}{2\pi}\,\hat{P}_{i\leftarrow j}(z)\,f_j\left(\frac{x}{z},t\right).
\end{aligned} \tag{2.170}$$

In the last step we cancel what corresponds to the plus prescription for diagonal splitting, i.e. we remove the regularization of the splitting kernel at $z \to 1$. Therefore, we need to modify the upper integration boundary by a small parameter ε which can in principle depend on t. The resulting equation is the diagonal DGLAP equation with unsubtracted splitting kernels, solved by the ratio of parton densities and Sudakov factors

$$\boxed{t\frac{d}{dt}\frac{f_i(x,t)}{\Delta_i(t)} = \frac{d}{d\log t}\frac{f_i(x,t)}{\Delta_i(t)} = \sum_j \int_0^{1-\varepsilon} \frac{dz}{z}\,\frac{\alpha_s}{2\pi}\,\hat{P}_{i\leftarrow j}(z)\,\frac{f_j\left(\frac{x}{z},t\right)}{\Delta_i(t)}}\,. \tag{2.171}$$

We can study the structure of these solutions of the unsubtracted DGLAP equation by integrating f/Δ between appropriate points in t

$$\begin{aligned}
\frac{f_i(x,t)}{\Delta_i(t)} - \frac{f_i(x,t_0)}{\Delta_i(t_0)} &= \int_{t_0}^t \frac{dt'}{t'}\sum_j \int_0^{1-\varepsilon} \frac{dz}{z}\,\frac{\alpha_s}{2\pi}\,\hat{P}_{i\leftarrow j}(z)\,\frac{f_j\left(\frac{x}{z},t'\right)}{\Delta_i(t')} \\
f_i(x,t) &= \frac{\Delta_i(t)}{\Delta_i(t_0)}f_i(x,t_0) + \int_{t_0}^t \frac{dt'}{t'}\,\frac{\Delta_i(t)}{\Delta_i(t')}\sum_j \int_0^{1-\varepsilon} \frac{dz}{z}\,\frac{\alpha_s}{2\pi}\,\hat{P}_{i\leftarrow j}(z)\,f_j\left(\frac{x}{z},t'\right) \\
&= \Delta_i(t)\,f_i(x,t_0) + \int_{t_0}^t \frac{dt'}{t'}\,\frac{\Delta_i(t)}{\Delta_i(t')}\sum_j \int_0^{1-\varepsilon} \frac{dz}{z}\,\frac{\alpha_s}{2\pi}\,\hat{P}_{i\leftarrow j}(z)\,f_j\left(\frac{x}{z},t'\right) \\
&\equiv \Delta_i(t,t_0)\,f_i(x,t_0) + \int_{t_0}^t \frac{dt'}{t'}\,\Delta_i(t,t')\sum_j \int_0^{1-\varepsilon} \frac{dz}{z}\,\frac{\alpha_s}{2\pi}\,\hat{P}_{i\leftarrow j}(z)\,f_j\left(\frac{x}{z},t'\right),
\end{aligned} \tag{2.172}$$

where we choose t_0 such that $\Delta(t_0) = 1$ and introduce the notation $\Delta(t_1,t_2) = \Delta(t_1,t_0)/\Delta(t_2,t_0)$ for the ratio of two Sudakov factors in the last line. This formula for the dependence of the parton density $f_i(x,t)$ on x and t has a suggestive interpretation: corresponding to Eq. 2.165 the first term can be interpreted as 'nothing happening to f between t_0 and t' because it is weighted by the Sudakov no-branching probability Δ_i. The second term includes the ratio of Sudakov factors which just like in Eq. 2.166 means no branching between t' and t. Integrating this factor times the splitting probability over $t' \in [t_0,t]$ implies at least one branching between t_0 and t.

The issue of this interpretation of the Sudakov form factor in conjunction with the parton densities is its numerical usability in a probabilistic approach: starting from a parton density somewhere in $(x - t)$ space we need to evolve it to a fixed point (x_n, t_n) given by the hard subprocess, e.g. $q\bar{q} \to Z$ with m_Z giving the scale and energy fraction of the two quarks. Numerically it would be much easier to simulate *backwards evolution* where we start from the known kinematics of the hard process and the corresponding point in the $(x - t)$ plane and evolve towards the partons in the proton, ideally to a point where the probabilistic picture of collinear, stable, non-radiating quarks and gluons in the proton holds. This means we need to define a probability that a parton evolved backwards from a space-like $t_2 < 0$ to $t_1 < 0$ with $|t_2| > |t_1|$ does not radiate or split.

For this final step we define a probability measure for the backwards evolution of partons $\Pi(t_1, t_2; x)$. Just like the two terms in Eq. 2.172 it links the splitting probability to a probability of an undisturbed evolution. For example, we can write the probability that a parton is generated by a splitting in the interval $[t, t + \delta t]$, evaluated at (t_2, x), as $dF(t; t_2)$. The measure corresponding to a Sudakov survival probability is then

$$\Pi(t_1, t_2; x) = 1 - \int_{t_1}^{t_2} dF(t; t_2). \tag{2.173}$$

Comparing the definition of dF to the relevant terms in Eq. 2.172 and replacing $t \to t_2$ and $t' \to t$ we know what happens for the combination

$$\begin{aligned} f_i(x, t_2) dF(t; t_2) &= \frac{dt}{t} \frac{\Delta_i(t_2)}{\Delta_i(t)} \sum_j \int_0^{1-\varepsilon} \frac{dz}{z} \frac{\alpha_s}{2\pi} \hat{P}_{i \leftarrow j}(z) f_j\left(\frac{x}{z}, t\right) \\ &= dt \; \Delta_i(t_2) \frac{1}{t} \sum_j \int_0^{1-\varepsilon} \frac{dz}{z} \frac{\alpha_s}{2\pi} \hat{P}_{i \leftarrow j}(z) \frac{f_j\left(\frac{x}{z}, t\right)}{\Delta_i(t)} \\ &= dt \; \Delta_i(t_2) \frac{d}{dt} \frac{f_i(x, t)}{\Delta_i(t)} \qquad \text{using Eq. 2.171.} \end{aligned} \tag{2.174}$$

This means

$$\Pi(t_1, t_2; x) = 1 - \frac{f_i(x, t) \Delta_i(t_2)}{f_i(x, t_2) \Delta_i(t)} \Bigg|_{t_1}^{t_2} = \frac{f_i(x, t_1) \Delta_i(t_2)}{f_i(x, t_2) \Delta_i(t_1)}, \tag{2.175}$$

and gives us a probability measure for backwards evolution: the probability of evolving back from t_2 to t_1 is described by a Markov process with a flat random number as

$$\frac{f_i(x, t_1) \Delta_i(t_2)}{f_i(x, t_2) \Delta_i(t_1)} = r \in [0, 1] \qquad \text{with } |t_2| > |t_1|. \tag{2.176}$$

While we cannot write down this procedure in a closed form, it shows how we can algorithmically generate initial state as well as final state parton radiation patterns based on the unregularized DGLAP equation and the Sudakov factors solving this

equation. One remaining issue is that in our derivation of the collinear re-summation interpretation of the parton shower we assume some a strong ordering of the radiated partons which we will discuss in the next section.

2.5.2 Soft Gluon Emission

To this point we have built our parton shower on collinear parton splitting or radiation and its universal properties indicated by Eq. 2.97. Deriving the diagonal splitting kernels in Eqs. 2.102 and 2.115 we encounter an additional source of infrared divergences, namely *soft gluon emission* corresponding to energy fractions $z \to 0, 1$. Its radiation pattern is also universal, just like the collinear case. One way to study this soft divergence without an overlapping collinear pole is gluon radiation off a massive quark with momentum $q + k$ and mass m, which could be attached to some hard process as a splitting final state. The initial quark momentum $q + k$ splits into a hard quark q and a soft gluon k with $k^2 \ll q^2 = m^2$

$$
\begin{aligned}
\mathscr{M}_{n+1} &= g_s T^a \, \varepsilon_\mu^*(k) \, \bar{u}(q) \gamma^\mu \frac{\not{q} + \not{k} + m}{(q+k)^2 - m^2} \, \mathscr{M}_n \\
&= g_s T^a \, \varepsilon_\mu^*(k) \, \bar{u}(q) \left[-\not{q} \gamma^\mu + 2q^\mu + m\gamma^\mu - \gamma^\mu \not{k} \right] \frac{1}{2(qk) + \mathscr{O}(k^2)} \, \mathscr{M}_n \\
&= g_s T^a \, \varepsilon_\mu^*(k) \, \bar{u}(q) \frac{q^\mu + \mathscr{O}(k)}{(qk) + \mathscr{O}(k^2)} \, \mathscr{M}_n \quad \text{Dirac equation} \quad \bar{u}(q)(\not{q} - m) = 0 \\
&\sim g_s T^a \, \varepsilon_\mu^*(k) \, \frac{q^\mu}{(qk)} \, \bar{u}(q) \, \mathscr{M}_n \\
&\to g_s \, \varepsilon_\mu^*(k) \left(\sum_j \hat{T}_j^a \frac{q_j^\mu}{(q_j k)} \right) \bar{u}(q) \, \mathscr{M}_n
\end{aligned}
\tag{2.177}
$$

The conventions are similar to Eq. 2.102, $\mathscr{M}_n$ includes all additional terms except for the spinor of the outgoing quark with momentum $q + k$. Neglecting the gluon momentum altogether defines the leading term of the *eikonal approximation*.

In the last step we simply add all possible sources j of gluon radiation. This defines a color operator which we insert into the matrix element and which assumes values of $+T_{ij}^a$ for radiation off a quark, $-T_{ji}^a$ for radiation off an antiquark and $-if_{abc}$ for radiation off a gluon. For a color neutral process like our favorite Drell–Yan process adding an additional soft gluon $q\bar{q} \to Zg$ it returns $\sum_j \hat{T}_j = 0$.

The matrix element in Eq. 2.177 we need to square. It includes a polarization sum and will therefore depend on the gauge. We choose the general *axial gauge* for massless gauge bosons

$$
\sum_{\text{pol}} \varepsilon_\mu^*(k) \varepsilon_\nu(k) = -g_{\mu\nu} + \frac{k_\mu n_\nu + n_\mu k_\nu}{(nk)} - n^2 \frac{k_\mu k_\nu}{(nk)^2} = -g_{\mu\nu} + \frac{k_\mu n_\nu + n_\mu k_\nu}{(nk)},
\tag{2.178}
$$

with a light-like reference vector n obeying $n^2 = 0$. The matrix element squared then reads

$$\begin{aligned}
\overline{|\mathscr{M}_{n+1}|^2} &= g_s^2 \left(-g_{\mu\nu} + \frac{k_\mu n_\nu + n_\mu k_\nu}{(nk)}\right) \left(\sum_j \hat{T}_j^a \frac{q_j^\mu}{(q_j k)}\right)^\dagger \left(\sum_j \hat{T}_j^a \frac{q_j^\nu}{(q_j k)}\right) \overline{|\mathscr{M}_n|^2} \\
&= g_s^2 \left(- \left(\sum_j \hat{T}_j^a \frac{q_j^\mu}{(q_j k)}\right)^\dagger \left(\sum_j \hat{T}_j^a \frac{q_{j\mu}}{(q_j k)}\right) \right. \\
&\qquad \left. + \frac{2}{(nk)} \left(\sum_j \hat{T}_j^a\right)^\dagger \left(\sum_j \hat{T}_j^a \frac{(q_j n)}{(q_j k)}\right) \right) \overline{|\mathscr{M}_n|^2} \\
&= -g_s^2 \left(\sum_j \hat{T}_j^a \frac{q_j^\mu}{(q_j k)}\right)^\dagger \left(\sum_j \hat{T}_j^a \frac{q_{j\mu}}{(q_j k)}\right) \overline{|\mathscr{M}_n|^2}.
\end{aligned} \tag{2.179}$$

The insertion operator in the matrix element has the form of an insertion current multiplied by its hermitian conjugate. This current describes the universal form of soft gluon radiation off an n-particle process

$$\boxed{\overline{|\mathscr{M}_{n+1}|^2} \equiv -g_s^2 \, (J^\dagger \cdot J) \, \overline{|\mathscr{M}_n|^2}} \quad \text{with} \quad J^{a\mu}(k, \{q_j\}) = \sum_j \hat{T}_j^a \, \frac{q_j}{(q_j k)}. \tag{2.180}$$

The squared current appearing in the matrix element squared, Eq. 2.179, we can further simplify to

$$\begin{aligned}
(J^\dagger \cdot J) &= \sum_j \hat{T}_j^a \hat{T}_j^a \, \frac{q_j^2}{(q_j k)^2} + 2 \sum_{i<j} \hat{T}_i^a \hat{T}_j^a \, \frac{(q_i q_j)}{(q_i k)(q_j k)} \\
&= \sum_j \hat{T}_j^a \left(-\sum_{i \neq j} \hat{T}_i^a\right) \frac{q_j^2}{(q_j k)^2} + 2 \sum_{i<j} \hat{T}_i^a \hat{T}_j^a \, \frac{(q_i q_j)}{(q_i k)(q_j k)} \\
&= -\left(\sum_{i<j} + \sum_{i>j}\right) \hat{T}_i^a \hat{T}_j^a \frac{q_j^2}{(q_j k)^2} + 2 \sum_{i<j} \hat{T}_i^a \hat{T}_j^a \, \frac{(q_i q_j)}{(q_i k)(q_j k)} \\
&= 2 \sum_{i<j} \hat{T}_i^a \hat{T}_j^a \left(\frac{(q_i q_j)}{(q_i k)(q_j k)} - \frac{q_i^2}{2(q_i k)^2} - \frac{q_j^2}{2(q_j k)^2}\right) \quad \text{massive case} \\
&= 2 \sum_{i<j} \hat{T}_i^a \hat{T}_j^a \, \frac{(q_i q_j)}{(q_i k)(q_j k)} \qquad \text{massless partons} \\
&= 2 \sum_{i<j} \hat{T}_i^a \hat{T}_j^a \, \frac{(q_i q_j)}{(q_i k) + (q_j k)} \left(\frac{1}{(q_i k)} + \frac{1}{(q_j k)}\right).
\end{aligned} \tag{2.181}$$

In the last step we only bring the eikonal factor into a different form which sometimes comes in handy because it separates the two divergences associated with q_i and with q_j.

At this point we return to massless QCD partons, keeping in mind that the ansatz Eq. 2.177 ensures that the insertion currents only model soft, not collinear radiation. Just as a side remark at this stage—our definition of the insertion current $J^{a\mu}$ in Eq. 2.180 we can generalize to colored processes, where the current becomes dependent on the gauge vector n to cancel the n dependence of the polarization sum

$$J^{a\mu}(k, \{p_j\}) = \sum_j \hat{T}_j^a \left(\frac{p_j}{(p_j k)} - \frac{n}{(nk)} \right) \tag{2.182}$$

This *dipole radiation term* in Eqs. 2.180 and 2.182 we can study to see how successive soft gluon radiation will be organized for example in terms of emission angles. Given that in the interpretation of the DGLAP equation and its solutions the ordering of the collinear emissions plays a crucial role this is an important question. As it will turn out, the soft emission case will help us understand this feature.

At this stage, calling the terms in Eq. 2.182 a dipole is a little bit of a stretch if we compare it to a multi-pole series. To see the actual dipole structure we would need to look at the color structure. We start by symmetrizing the soft radiation dipole with respect to the two hard momenta in a particular way

$$\begin{aligned}
(J^\dagger \cdot J)_{ij} \sim W_{ij} &= \frac{(q_i q_j)}{(q_i k)(q_j k)} \\
&= \frac{1 - \cos\theta_{ij}}{(1 - \cos\theta_{ig})(1 - \cos\theta_{jg})} \qquad \text{in terms of opening angles } \theta \\
&= \frac{1}{2} \left(\frac{1 - \cos\theta_{ij}}{(1 - \cos\theta_{ig})(1 - \cos\theta_{jg})} + \frac{1}{1 - \cos\theta_{ig}} - \frac{1}{1 - \cos\theta_{jg}} \right) + (i \leftrightarrow j) \\
&\equiv W_{ij}^{[i]} + W_{ij}^{[j]}.
\end{aligned} \tag{2.183}$$

Each of the two terms we need to integrate over the gluon's phase space, including the azimuthal angle integration

$$\begin{aligned}
\int_0^{2\pi} d\phi_{ig} W_{ij}^{[i]} &= \frac{1}{2} \int_0^{2\pi} d\phi_{ig} \left(\frac{1 - \cos\theta_{ij}}{(1 - \cos\theta_{ig})(1 - \cos\theta_{jg})} + \frac{1}{1 - \cos\theta_{ig}} - \frac{1}{1 - \cos\theta_{jg}} \right) \\
&= \frac{1}{2} \int_0^{2\pi} d\phi_{ig} \left[\frac{1}{1 - \cos\theta_{ig}} + \frac{1}{1 - \cos\theta_{jg}} \left(\frac{1 - \cos\theta_{ij}}{1 - \cos\theta_{ig}} - 1 \right) \right].
\end{aligned} \tag{2.184}$$

To disentangle the different angular integrations we express the three parton vectors in polar coordinates where the initial parton i propagates into the x direction, the interference partner j in the $(x - y)$ plane, and the soft gluon in the full three-dimensional space

$$\begin{aligned}
\vec{n}_i &= (1,0,0) && \text{hard parton} \\
\vec{n}_j &= (\cos\theta_{ij}, \sin\theta_{ij}, 0) && \text{interference partner} \\
\vec{n}_g &= (\cos\theta_{ig}, \sin\theta_{ig}\cos\phi_{ig}, \sin\theta_{ig}\sin\phi_{ig}) && \text{soft gluon} \\
1-\cos\theta_{jg} \equiv (\vec{n}_j\vec{n}_g) &= 1-\cos\theta_{ij}\cos\theta_{ig} + \sin\theta_{ij}\sin\theta_{ig}\cos\phi_{ig}, && (2.185)
\end{aligned}$$

From the scalar product between these four-vectors we see that of the terms appearing in Eq. 2.184 only the opening angle θ_{jg} is related to ϕ_{ig}, which for the azimuthal angle integration means

$$\begin{aligned}
\int_0^{2\pi} d\phi_{ig}\; W_{ij}^{[i]} &= \frac{\pi}{1-\cos\theta_{ig}} + \frac{1}{2}\left(\frac{1-\cos\theta_{ij}}{1-\cos\theta_{ig}} - 1\right)\int_0^{2\pi} d\phi_{ig}\;\frac{1}{1-\cos\theta_{jg}} \\
&= \frac{1}{1-\cos\theta_{ig}}\left[\pi + \frac{\cos\theta_{ig}-\cos\theta_{ij}}{2}\int_0^{2\pi} d\phi_{ig}\;\frac{1}{1-\cos\theta_{jg}}\right]. \qquad (2.186)
\end{aligned}$$

The azimuthal angle integral in this expression for $W_{ij}^{[i]}$ we can solve

$$\begin{aligned}
\int_0^{2\pi} d\phi_{ig}\frac{1}{1-\cos\theta_{jg}} &= \int_0^{2\pi} d\phi_{ig}\frac{1}{1-\cos\theta_{ij}\cos\theta_{ig}+\sin\theta_{ij}\sin\theta_{ig}\cos\phi_{ig}} \\
&= \int_0^{2\pi} d\phi_{ig}\frac{1}{a-b\cos\phi_{ig}} \\
&= \oint_{\text{unit circle}} dz\;\frac{1}{iz}\frac{1}{a-b\frac{z+1/z}{2}} \\
&= \frac{2}{i}\oint dz\;\frac{1}{2az-b-bz^2} \\
&= \frac{2i}{b}\oint \frac{dz}{(z-z_-)(z-z_+)} \qquad \text{with } z_\pm = \frac{a}{b} \pm \sqrt{\frac{a^2}{b^2}-1} \\
&= \frac{2i}{b}\,2\pi i\,\frac{1}{z_- - z_+} \qquad z_- \text{ inside contour} \\
&= \frac{2\pi}{\sqrt{a^2-b^2}} \\
&= \frac{2\pi}{\sqrt{(\cos\theta_{ig}-\cos\theta_{ij})^2}} = \frac{2\pi}{|\cos\theta_{ig}-\cos\theta_{ij}|}. \qquad (2.187)
\end{aligned}$$

The crucial coordinate transformation is $z = \exp(i\phi_{ig})$ and $\cos\phi_{ig} = (z+1/z)/2$ in the third line. For the entire integral in Eq. 2.184 this gives us

$$\int_0^{2\pi} d\phi_{ig}\; W_{ij}^{[i]} = \frac{1}{1-\cos\theta_{ig}} \left[\pi + \frac{\cos\theta_{ig}-\cos\theta_{ij}}{2} \frac{2\pi}{|\cos\theta_{ig}-\cos\theta_{ij}|}\right]$$
$$= \frac{\pi}{1-\cos\theta_{ig}} \left[1+\text{sign}(\cos\theta_{ig}-\cos\theta_{ij})\right]$$
$$= \begin{cases} \dfrac{\pi}{1-\cos\theta_{ig}} & \text{if} \quad \theta_{ig} < \theta_{ij} \\ 0 & \text{else.} \end{cases} \tag{2.188}$$

The soft gluon is only radiated at angles between zero and the opening angle of the initial parton i and its hard interference partner or spectator j. The same integral over $W_{ij}^{[j]}$ gives the same result, with switched roles of i and j. After combining the two permutations the probability of radiating a soft gluon at an angle larger than the earlier branching is zero; successive emission of soft gluons obeys an *angular ordering*.

Going back to collinear radiation, we know from Eqs. 2.83 and 2.152 that the different variables describing parton splitting, namely the angle θ, the transverse momentum p_T, or the virtuality $\sqrt{t}$, are equivalent as long as we are only interested in the leading logarithm arising from the collinear phase space integration. They can be transformed into each other by a simple linear transformation.

Different implementations of the parton shower order their jet radiation by different variables: historically, of the two most widely used event generators PYTHIA uses the virtuality or the transverse momentum while HERWIG uses the angle. Once we re-sum the collinear logarithms the finite shifts which appear in the transformation between the ordering parameters are also re-summed, so the underlying variable in the parton shower does matter in the comparison to data. This is even more true for the matching of the parton shower and the matrix element which we will discuss in the next section.

In this section we have learned an argument for using the angle to order parton radiation: soft radiation is ordered in the angle θ, and a parton shower would be well advised to match this behavior. On the other hand, in Sect. 2.3.5 we have learned that the physical interpretation of the collinear logarithms re-summed by the parton shower is based on a transverse momentum ordering. If theory does not define the golden way to order parton radiation we will have to rely on Tevatron or LHC measurements to tell us which implementation works best. This includes the new SHERPA parton shower which is not based on the collinear splitting kernels but on the soft-collinear QCD dipoles introduced in this section.

2.5.3 CKKW and MLM Schemes

The main problem with QCD at the LHC is the range of energy scales of the jets we encounter. *Collinear jets* with their small transverse momenta are well described by a parton shower. From Sect. 2.3.5 we know that strictly speaking the parton shower only

fills the phase space region up to a maximum transverse momentum $p_T < \mu_F$. In contrast, *hard jets* with large transverse momentum are described by matrix elements which we compute using the QCD Feynman rules. They fill the non-collinear part of phase space which is not covered by the parton shower. Because of the collinear logarithmic enhancement we discussed in Sect. 2.3.5 we expect many more collinear and soft jets than hard jets at the LHC.

The natural question then becomes: what is the range of 'soft' or 'collinear' and what is 'hard'? Applying a consistency condition we can define collinear jet radiation by the validity of the collinear approximation in Eq. 2.84. The maximum p_T of a collinear jet is the upper end of the region for which the jet radiation cross section behaves like $1/p_T$ or the point where the distribution $p_T d\sigma/dp_T$ leaves its plateau. For harder and harder jets we will at some point become limited by the partonic energy available at the LHC, which means the p_T distribution of additional jets will start dropping faster than $1/p_T$. Collinear logarithms will become numerically irrelevant and jets will be described by the regular matrix element squared without any re-summation.

Quarks and gluons produced in association with gauge bosons at the Tevatron behave like collinear jets for $p_T \lesssim 20\,\text{GeV}$, because quarks at the Tevatron are limited in energy. At the LHC, jets produced in association with tops behave like collinear jets to $p_T \sim 150\,\text{GeV}$, jets produced with 500 GeV gluinos behave like collinear jets to p_T scales larger than 300 GeV. This is not good news, because collinear jets means many jets, and many jets produce *combinatorial backgrounds* and ruin the missing momentum resolution of the detector: if we are looking for example for two jets to reconstruct an invariant mass you can simply plot all events as a function of this invariant mass and remove the backgrounds by requiring all event to sit around a peak in m_{jj}. If we have for example three jets in the event we have to decide which of the three jet-jet combinations should go into this distribution. If this is not possible we have to consider two of the three combinations as uncorrelated 'background' events. In other words, we make three histogram entries out of each signal or background event and consider all three background events plus two of the three signal combinations as background. This way the signal-to-background ratio decreases from N_S/N_B to $N_S/(3N_B+2N_S)$. A famous victim of such combinatorics was for a long time the Higgs discovery channel $pp \to t\bar{t}H$ with $H \to b\bar{b}$.

For theorists this means that at the LHC we have to reliably model collinear and hard jets. For simplicity, in this section we will first limit our discussion to final state radiation, for example off the R-ratio process $e^+e^- \to q\bar{q}$ from Sect. 2.1.1. Combining collinear and hard jets in the final state has to proceed in two steps. The first of them has nothing to do with the parton shower: the problem we need to solve is that the parton shower by construction generates a definitive number of jets. We can categorize the generated events by counting the number of jets in the final state, i.e. the parton shower events are jet-exclusive. On the other hand, the total rate for the hard process we compute as $e^+e^- \to q\bar{q} + X$, with any number of collinear jets in the final state denoted by X. Predictions involving parton densities and the DGLAP equation are jet-inclusive. Any scheme combining the parton shower and hard matrix elements has to follow the path

1. Define jet-exclusive events from the hard matrix elements and the parton shower
2. Combine final states with *different numbers of final state particles*
3. Reproduce matrix element results in high-p_T and well separated phase space region
4. Reproduce parton shower results for collinear and soft radiation
5. Interpolate smoothly and avoid double counting of events.

For specific processes at the Tevatron the third and fourth point on this list have actually been tackled by so-called matrix element corrections in the parton shower Monte Carlos PYTHIA and HERWIG.

For example the final state of the process $e^+e^- \to q\bar{q}+X$ often involves more than two jets due to final state splitting. Even for the first step of defining jet-exclusive predictions from the matrix element we have to briefly consider the geometry of different jets. To separate jet-inclusive event samples into jet-exclusive event samples we have to define some kind of jet separation parameter. As a start, we radiate a gluon off one of the quark legs, which gives us a $q\bar{q}g$ final state. This additional gluon can either be collinear with and hence geometrically close to one of the quarks or not. Jet algorithms which decide if we count such a splitting as one or two jets we describe in detail in Sect. 3.1.1. They are based on a choice of collinearity measure y_{ij} which we can for example construct as a function of the distance in R space, introduced in Eq. 2.35, and the transverse momenta. We define two jets as collinear and hence as one jet if $y_{ij} < y_{\text{resol}}$ where y_{resol} we give to the algorithm. As a result, the number of jets in an event will of course depend on this resolution parameter y_{resol}.

For the second step of combining hard and collinear jet simulation the same resolution parameter appears in a form where it becomes a collinear vs hard matching parameter y_{match}, i.e. it allows us to clearly assign each hadron collider event a number of collinear jets and a number of hard jets. Such an event with its given number of more or less hard jets we can then describe either using matrix elements or using a parton shower, where 'describe' means computing the relative probability of different phase space configurations. The parton shower will do well for jets with $y_{ij} < y_{\text{match}}$. In contrast, if for our closest jets we find $y_{ij} > y_{\text{match}}$, we know that collinear logarithms did not play a major role, so we should use the hard matrix element. If we assign the hard process a typical energy or virtuality scale t_{hard} we can translate the matching parameter y_{match} into a virtuality scale $t_{\text{match}} = y^2_{\text{match}} t_{\text{hard}}$, below which we do not trust the hard matrix element. For example for the Drell–Yan process the hard scale would be something like the Z mass.

The CKKW jet combination scheme first tackles the problem of defining jet-exclusive final states. While an *exclusive rate* requires a process to have exactly a given number of jets, an *inclusive rate* is defined as the number of events in which we for example identify n jets and ignore everything else appearing in the event. For example, additional collinear jets which we usually denote as '$+X$' will be included.

The main ingredient to translating one into the other are non-splitting probabilities, i.e. Sudakov factors. They can transform inclusive n-particle rates into exact n-particle rates, with no additional final state jet outside a given resolution scale. Analytically we can compute integrated splitting probabilities $\Gamma_j(t_{\text{hard}}, t)$ which for quarks and

gluons are implicitly defined through the Sudakov factors which we introduce in Eq. 2.164

$$\begin{aligned}\Delta_q(t_{\text{hard}}, t_{\text{match}}) &= \exp\left(-\int_{t_{\text{match}}}^{t_{\text{hard}}} \frac{dt}{t} \int_0^1 dy \frac{\alpha_s}{2\pi} \hat{P}_{q\leftarrow q}(y)\right) \\ &\equiv \exp\left(-\int_{t_{\text{match}}}^{t_{\text{hard}}} dt\ \Gamma_q(t_{\text{hard}}, t)\right) \\ \Delta_g(t_{\text{hard}}, t_{\text{match}}) &\equiv \exp\left(-\int_{t_{\text{match}}}^{t_{\text{hard}}} dt\ \left[\Gamma_g(t_{\text{hard}}, t) + \Gamma_f(t)\right]\right). \end{aligned} \tag{2.189}$$

For final state radiation t corresponds to the original $\sqrt{p_a^2}$ and, moving forward in time, is ordered according to $t_{\text{hard}} > t > t_{\text{match}}$. The resolution of individual jets we identify with the matrix element-shower matching scale t_{match}. The y integration in the original definition we can carry out in the leading logarithm approximation, giving us

$$\begin{aligned}\Gamma_q(t_{\text{hard}}, t) \equiv \Gamma_{q\leftarrow q}(t_{\text{hard}}, t) &= \frac{C_F}{\pi} \frac{\alpha_s(t)}{t} \left(\frac{1}{2} \log \frac{t_{\text{hard}}}{t} - \frac{3}{4}\right) \\ \Gamma_g(t_{\text{hard}}, t) \equiv \Gamma_{g\leftarrow g}(t_{\text{hard}}, t) &= \frac{C_A}{\pi} \frac{\alpha_s(t)}{t} \left(\frac{1}{2} \log \frac{t_{\text{hard}}}{t} - \frac{11}{12}\right) \\ \Gamma_f(t) \equiv \Gamma_{q\leftarrow g}(t) &= \frac{n_f}{6\pi} \frac{\alpha_s(t)}{t}. \end{aligned} \tag{2.190}$$

The virtualities $t_{\text{hard}} > t$ correspond to the incoming (mother) and outgoing (daughter) parton. Unfortunately, this formula is somewhat understandable from a probabilistic picture of parton splitting, but not quite. Terms arising from next-to-leading logarithms spoil the limit $t_{\text{match}} \to t_{\text{hard}}$, where the probability of no splitting should approach unity. Technically, we can deal with the finite terms in the Sudakov factors by requiring them to be positive semi-definite, i.e. by replacing $\Gamma(t_{\text{hard}}, t_{\text{match}}) < 0$ by zero. For the general argument this problem with the analytic expressions for the splitting functions is irrelevant; to avoid unnecessary approximations in the y integration more recent CKKW implementations integrate the splitting kernels numerically.

To get a first idea how to transform inclusive into exact n-jet rates we compute the probability to see exactly *two jets* in the process $e^+e^- \to q\bar{q}$. Looking at Fig. 2.3 this means that none of the two quarks in the final state radiate a resolved gluon between the virtualities t_{hard} (given by the qqZ vertex) and $t_{\text{match}} < t_{\text{hard}}$. As will become important later we specify that this no-radiation statement assumes a jet resolution as given by end point of the external quark and gluon legs. The probability we have to multiply the inclusive two-jet rate with is then $\left[\Delta_q(t_{\text{hard}}, t_{\text{match}})\right]^2$, once for each quark. Whatever happens at virtualities below t_{match} will be governed by the parton shower and does not matter anymore. Technically, this requires us to define a vetoed parton shower which we will describe in Sect. 2.6.3.

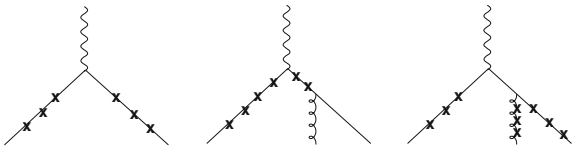

Fig. 2.3 Vetoed showers on two-jet and three-jet contributions. The scale at the gauge boson vertex is t_{hard}. The two-jet (three-jet) diagram implies exactly two (three) jets at the resolution scale t_{match}, below which we rely on the parton shower. Figure from Ref. [2]

Next, what is the probability that the initially two-jet final state evolves exactly into *three jets*, again following Fig. 2.3? We know that it contains a factor $\Delta_q(t_{\text{hard}}, t_{\text{match}})$ for one untouched quark.

After splitting at t_q with the probability $\Gamma_q(t_q, t_{\text{hard}})$ the second quark survives to t_{match}, giving us a factor $\Delta_q(t_q, t_{\text{match}})$. If we assign the virtuality t_g to the radiated gluon at the splitting point we find the gluon's survival probability $\Delta_g(t_g, t_{\text{match}})$. So together we find

$$\Delta_q(t_{\text{hard}}, t_{\text{match}})\ \Gamma_q(t_{\text{hard}}, t_q)\ \Delta_q(t_q, t_{\text{match}})\ \Delta_g(t_g, t_{\text{match}}) \cdots \tag{2.191}$$

That is all there is, with the exception of the intermediate quark. If we label the quark virtuality at which the second quark radiates a gluon by t_q there has to appear another factor describing that the quark, starting from t_{hard}, gets to t_q untouched. Naively we would guess that this probability is given by $\Delta_q(t_{\text{hard}}, t_q)$. However, this implies no splittings resolved at the fixed lower scale t_q, but what we really mean is no splitting between t_{hard} and t_q resolved at a third scale $t_{\text{match}} < t_q$ given by the quark leg hitting the parton shower regime. We therefore better compute the probability of no splitting between t_{hard} and t_q, namely $\Delta_q(t_{\text{hard}}, t_{\text{match}})$, but under the condition that splittings from t_q down to t_{match} are explicitly allowed.

If zero splittings gives us a probability factor $\Delta_q(t_{\text{hard}}, t_{\text{match}})$, to describe exactly one splitting from t_q on we add a factor $\Gamma(t_q, t)$ with an unknown splitting point t. This point t we integrate over between the resolution point t_{match} and the original splitting point t_q. This is the same argument as in our physical interpretation of the Sudakov factors solving the DGLAP equation Eq. 2.172. For an arbitrary number of possible splittings between t_q and t_{match} we find the sum

$$\begin{aligned}\Delta_q(t_{\text{hard}}, t_{\text{match}}) &\left[1 + \int_{t_{\text{match}}}^{t_q} dt\ \Gamma_q(t_q, t) + \text{more splittings}\right] \\ &= \Delta_q(t_{\text{hard}}, t_{\text{match}})\ \exp\left[\int_{t_{\text{match}}}^{t_q} dt\ \Gamma_q(t_q, t)\right] = \frac{\Delta_q(t_{\text{hard}}, t_{\text{match}})}{\Delta_q(t_q, t_{\text{match}})}.\end{aligned} \tag{2.192}$$

The factors $1/n!$ in the Taylor series appear because for example radiating two jets in the same t interval can proceed ordered in two ways, both of which lead to the same final state. Once again: the probability of nothing happening between t_{hard} and

t_q we compute from the probability of nothing happening between t_{hard} and t_{match} times any number of possible splittings between t_q and t_{match}.

Collecting all factors from Eqs. 2.191 and 2.192 gives us the probability to find exactly three partons resolved at t_{match} as part of the inclusive sample

$$\begin{aligned}\Delta_q(t_{\text{hard}}, t_{\text{match}})\ \Gamma_q(t_{\text{hard}}, t_q)\ \Delta_q(t_q, t_{\text{match}})\ \Delta_g(t_g, t_{\text{match}})\ \frac{\Delta_q(t_{\text{hard}}, t_{\text{match}})}{\Delta_q(t_q, t_{\text{match}})} \\ = \Gamma_q(t_{\text{hard}}, t_q)\ [\Delta_q(t_{\text{hard}}, t_{\text{match}})]^2\ \Delta_g(t_g, t_{\text{match}}).\end{aligned} \tag{2.193}$$

This result is what we expect: both quarks go through untouched, just like in the two-parton case. In addition, we need exactly one splitting producing a gluon, and this gluon cannot split further. This example illustrates how we can compute these probabilities using Sudakov factors: adding a gluon corresponds to adding a splitting probability times the survival probability for this gluon, everything else magically drops out. At the end, we only integrate over the splitting point t_q.

This discussion allows us to write down the first step of the *CKKW algorithm*, combining different hard n-jet channels into one consistent set of events. One by one we turn inclusive n-jet events into exact n-jet events. We can write down the slightly simplified algorithm for final state radiation. As a starting point, we compute all leading-order cross sections for n-jet production with a lower jet radiation cutoff at t_{match}. This cutoff ensures that all jets are hard and that all corresponding cross sections $\sigma_{n,i}$ are finite. The second index i describes different non-interfering parton configurations for a given number of final state jets, like $q\bar{q}gg$ and $q\bar{q}q\bar{q}$ for $n = 4$. The purpose of the algorithm is to assign a weight (probability, matrix element squared,...) to a given phase space point, statistically picking the correct process and combining them properly. It proceeds event by event:

1. For each jet final state (n, i) compute the relative probability $P_{n,i} = \sigma_{n,i} / \sum_{k,j} \sigma_{k,j}$
2. Select a final state (n, i) with its probability $P_{n,i}$
3. Assign the momenta from the phase space generator to, assumed, hard external particles
4. Compute the transition matrix element $|\mathcal{M}|^2$ including parton shower below t_{match}
5. Use a jet algorithm to compute the shower history, i.e. all splitting virtualities t_j in each event
6. Check that this history corresponds to possible Feynman diagrams and does not violate any symmetries
7. For each internal and external line compute the Sudakov non-splitting probability down to t_{match}
8. Re-weight the α_s values of each splitting using the k_T scale from the shower history
9. Combine matrix element, Sudakovs, and α_s into a final weight

This final event weight we can use to compute distributions from weighted events or to decide if to keep or discard an event when producing unweighted events. The construction ensures that the relative weight of the different n-jet rates is identical to the probabilities we initially computed. In step 4 the CKKW event generation first chooses the appropriate hard scale in the event; in step 5 we compute the individual starting scale for the parton shower applied to each of the legs. Following our example, this might be t_{hard} for partons leaving the hard process itself or t_g for a parton appearing via later splitting.

In a second step of the CKKW scheme we match this combined hard matrix element with the parton shower, given the matching point t_{match}. From the final experimental resolution scale t_{resol} up to a matching scale t_{match} we rely on the parton shower to describe jet radiation while above the matching scale jet radiation is explicitly forbidden by the Sudakov non-splitting probabilities. Individually, both regimes consistently combine different n-jet processes. All we need to make sure is that there is no double counting.

From the discussion of Eq. 2.192 we know that Sudakovs describing the evolution between two scales and using a third scale as the resolution are going to be the problem. Carefully distinguishing the scale of the actual splitting from the scale of jet resolution is the key. The CKKW scheme starts each parton shower at the point where the parton first appears, and it turns out that we can use this argument to keep the resolution regimes $y > y_{\text{match}}$ and $y < y_{\text{match}}$ separate. There is a simple way to check this, namely if the y_{match} *dependence* drops out of the final combined probabilities. The answer for final state radiation is yes, as proven in the original paper, including a hypothetical next-to-leading logarithm parton shower. The CKKW scheme is implemented in the publicly available SHERPA and MadEvent event generators.

An alternative to the CKKW scheme which has been developed independently but incorporates essentially the same physics is the *MLM scheme*, for example implemented in ALPGEN or MadEvent. Its main difference to the CKKW scheme is that it avoids computing the survival properties using Sudakov form factors. Instead, it vetos those events which CKKW removes by applying the Sudakov non-splitting probabilities. This way MLM avoids problems with splitting probabilities beyond the leading logarithms, for example the finite terms appearing in Eq. 2.190, which can otherwise lead to a mismatch between the actual shower evolution and the analytic expressions of the Sudakov factors. In addition, the veto approach allows the MLM scheme to combine a set of independently generated n-parton events, which can be convenient.

In the MLM scheme we veto events which are simulated the wrong way after the hard matrix element and the parton shower have defined a set of complete events. This avoids double counting of events which on the one hand are generated with n hard jets from the matrix element and on the other hand appear for example as $(n-1)$ hard jets with an additional jet from the parton shower. After applying a jet algorithm (which in the case of ALPGEN is a cone algorithm and in case of MadEvent is a k_T algorithm) we compare the showered event with the un-showered hard event by identifying each reconstructed showered jet with the partons we started from. If all

jet–parton combinations match and there exist no additional resolved jets we know that the showering has not altered the hard structure of the event. This corresponds to adding the Sudakov non-splitting probabilities in the CKKW scheme. If there is a significant change between the original hard parton event and the showered event this event has to go. The only exception to this rule is the set of events with the highest jet multiplicity for which additional jets can only come from the parton shower. After defining the proper exclusive n-jet event sets we can again use the parton shower to describe more collinear jet radiation between t_{match} and t_{resol}.

After combining the samples we still need a backwards evolution of a generated event to know the virtuality scales which fix $\alpha_s(Q^2)$. As a side effect, if we also know the Feynman diagrams describing an event we can check that a certain splitting with its color structure is actually possible. For the parton shower or splitting simulation we need to know the interval of virtualities over which for example the additional gluon in the previous two-jet example can split. The lower end of this interval is universally given by t_{match}, but the upper end we cannot extract from the record event by event. Therefore, to compute the α_s values at each splitting point we start the parton shower at an universal hard scale, chosen as the hard(est) scale of the process.

Aside from such technical details all merging schemes are conceptually similar enough that we should expect them to reproduce each others' results, and they largely do. But the devil is in the details, so experiment will tell which scheme as part of which event generator produces the most usable results to understand LHC data.

To summarize, we can use the CKKW and MLM schemes to first combine n-jet events with variable n and then consistently add the parton shower. In other words, we can for example simulate $Z+n$ jets production at the LHC to arbitrarily large numbers of jets, limited only by computational resources and the physical argument that at some point any additional jet radiation will be described by the parton shower. This combination will describe all jets correctly over the entire collinear and hard phase space. In Fig. 2.4 we show the number of jets expected to be produced in association with a pair of top quarks and a pair of heavy new states at the LHC. The details of these heavy scalar gluons are secondary for the basic features of these distributions, the only parameter which matters is their mass, i.e. the hard scale of the process which sets the factorization scale and defines the upper limit of collinearly enhanced initial-state radiation. We see that heavy states come with many jets radiated at $p_T \lesssim 30\,\text{GeV}$, where most of these jets vanish once we require transverse momenta of at least 100 GeV. This figure tells us that an analysis which asks for a reconstruction of two W-decay jets may well be swamped by combinatorics.

Looking at the individual columns in Fig. 2.4 there is one thing we have to keep in mind: each of the merged matrix elements combined into this sample is computed at leading order. The emission of real particles is included, virtual corrections are not. In other words, the CKKW and MLM schemes give us all *jet distributions*, but only to leading order in the strong coupling. When we combine the different jet multiplicities to evaluate total rates, jet merging improves the rate prediction because it includes contributions from all orders in α_s, provided they come with a potentially large logarithm from jet emission. From all we know, these leading logarithms dominate

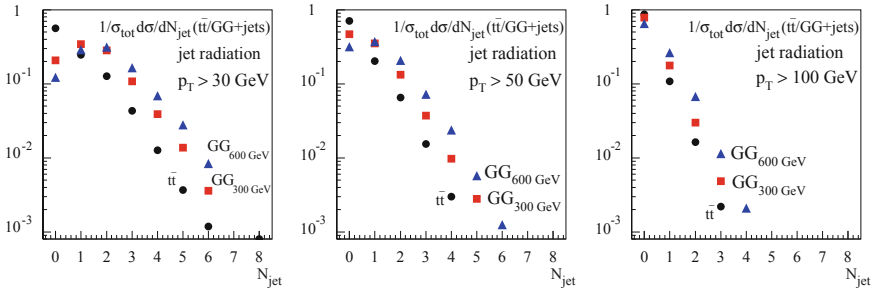

Fig. 2.4 Number of additional jets with a transverse momentum of at least 30, 50 or 100 GeV radiated off top pair production and the production of heavy states at the LHC. An example for such heavy states are scalar gluons with a mass of 300 or 600 GeV, pair-produced in gluon fusion. Figures from Ref. [3]

the higher order QCD corrections for most LHC processes, but it is not obvious how general this feature is and how we can quantify it. This is certainly true for all cases where higher order effects appear unexpectedly large and can be traced back to new partonic processes or phase space configurations opening up at higher jet multiplicities. Systematically curing some of this shortcoming (but at a prize) will be the topic of the next section.

Before moving on to an alternative scheme we will illustrate why Higgs or exotics searches at the LHC really care about progress in QCD simulations: one way to look for heavy particles decaying into jets, leptons and missing energy is the variable

$$\begin{aligned} m_{\text{eff}} &= \not{E}_T + \sum_j E_{T,j} + \sum_\ell E_{T,\ell} \\ &= \not{p}_T + \sum_j p_{T,j} + \sum_\ell p_{T,\ell} \qquad \text{(for massless quarks, leptons)} \end{aligned} \tag{2.194}$$

This variable and its relatives we will discuss in detail in Sect. 3.3.2. For gluon-induced QCD processes the effective mass should be small while the new physics signal's effective mass scale will be determined by the heavy masses.

For QCD jets as well as for W and Z plus jets backgrounds we can study the production of many jets using the CKKW scheme. Figure 2.5 shows the two critical distributions. First, in the number of hard jets we see the so-called staircase scaling behavior, namely constant ratios of exclusive $(n+1)$-jet and n-jet rates σ_{n+1}/σ_n. Such a scaling is closely related to the pattern we discuss in Eq. 2.133, in the context of the central jet veto of Sect. 1.5.2. The particularly interesting aspect of staircase scaling is that the constant ratio is the same for jet-inclusive and jet-exclusive cross sections $P_{\text{incl}} = P_{\text{excl}}$, as shown in Eq. 2.134.

The consistent variation of α_s gives a small parametric uncertainty on these rates. A common scaling factor μ/μ_0 for all factorization, renormalization and shower scales in the process following our argument of Sect. 2.4 is strictly speaking not

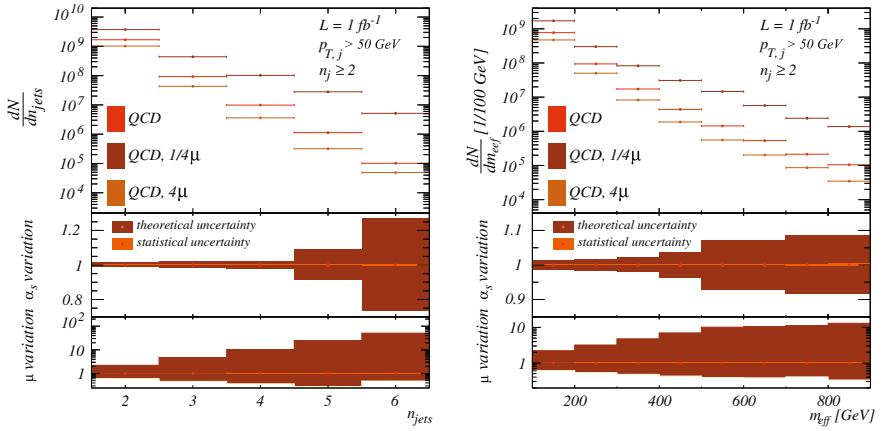

Fig. 2.5 Exclusive number of jets and effective mass distributions for pure QCD jet events at the LHC with a center-of-mass energy of 7 TeV and $p_{T,j} > 50$ GeV. The curves including the α_s uncertainty and a scale variation (tuning parameter) are computed with SHERPA and a fully merged sample including up to six hard jets. These distributions describe typical backgrounds for searches for jets plus missing energy with fake missing energy, which could originate from supersymmetric squark and gluino production. Figures from Ref. [4]

fixed by our physical interpretation in terms of resummation; such a factor as part of the leading logarithm can be factored out as a subleading finite term, so it should really be considered a tuning parameters for each simulation tool. Using the same simulation we also show the effective mass and observe a drop towards large values of m_{eff}. However, this drop is nowhere as pronounced as in parton shower predictions. This analysis shows that the naive parton shower is not a good description of QCD background processes to the production of heavy particles. Using a very pragmatic approach and tune the parton shower to correctly describe LHC data even in this parameter region will most likely violate basic concepts like factorization, so we would be well advised to use merging schemes like CKKW or MLM for such predictions.

2.6 Next-to-Leading Orders and Parton Shower

As we know for example for the R ratio from Sect. 2.1.1 the precision of a leading order QCD calculation in terms of the strong coupling constant α_s is not always sufficient to match the experimental accuracy. In such a case we need to compute observables to higher order in QCD. On the other hand, in Sect. 2.3.5 we have seen that the parton shower does not respect a fixed order perturbation theory. With its collinear logarithm it sums particular terms to all orders in α_s. So how can we on the one hand compute higher order corrections to for example the Drell–Yan cross

section and distributions and in addition consistently combine them with the parton shower?

Such a combination would remove one of the historic shortcomings of parton shower Monte Carlos. Apart from the collinear approximation for jet radiation they were always limited by the fact that in the words of one of the authors they 'only do shapes'. In other words, the normalization of the simulated event sample will always be leading order in perturbative QCD and hence subject to large theoretical uncertainties. The reason for this shortcoming is that collinear jet radiation relies on a hard process and the corresponding production cross section and works with splitting probabilities, but never touches the total cross section it started from.

As a solution we compute higher order cross sections to normalize the total cross section entering the respective Monte Carlo simulation. This is what we call a *K factor*: $K = \sigma^{\text{improved}}/\sigma^{\text{MC}} = \sigma^{\text{improved}}/\sigma^{\text{LO}}$. It is crucial to remember that higher order cross sections integrate over unobserved additional jets in the final state. So when we normalize the Monte Carlo we assume that we can first integrate over additional jets and obtain σ^{improved} and then just normalize the Monte Carlo which puts back these jets in the collinear approximation. Obviously, we should try to do better than that, and there are two ways to improve this traditional Monte Carlo approach, the MC@NLO scheme and the POWHEG scheme.

2.6.1 Next-to-Leading Order in QCD

When we compute the next-to-leading order correction to a cross section, for example to Drell–Yan production, we consider all contributions of the order $G_F\alpha_s$. There are three obvious sets of Feynman diagrams we have to square and multiply, namely the Born contribution $q\bar{q} \to Z$, the virtual gluon exchange for example between the incoming quarks, and the real gluon emission $q\bar{q} \to Zg$. An additional set of diagrams we should not forget are the crossed channels $qg \to Zq$ and $\bar{q}g \to Z\bar{q}$. Only amplitudes with the same external particles can be squared, so we find the matrix-element-squared contributions

$$\begin{aligned} |\mathcal{M}_B|^2 &\propto G_F \\ 2\text{Re}\,\mathcal{M}_V^*\mathcal{M}_B \propto G_F\alpha_s \quad |\mathcal{M}_{Zg}|^2 &\propto G_F\alpha_s \quad |\mathcal{M}_{Zq}|^2, |\mathcal{M}_{Z\bar{q}}|^2 \propto G_F\alpha_s. \end{aligned} \tag{2.195}$$

Strictly speaking, we have to include counter terms, which following Eq. 2.54 are a modification of $|\mathcal{M}_{\hat{\mathcal{B}}}|^{\in}$. These counter terms we add to the interference of Born and virtual gluon diagrams to remove the ultraviolet divergences. However, this is not the issue we want to discuss.

Infrared poles arise from two sources, soft and collinear divergences. To avoid the complication of overlapping collinear and soft divergences we will follow a toy model by Bryan Webber. It describes simplified particle radiation off a hard process: the energy of the system before radiation is x_s and the energy of the outgoing particle (call it photon or gluon) is x, so $x < x_s < 1$. When we compute *next-to-leading*

order corrections to a hard process, the different contributions, neglecting crossed channels, are

$$\left.\frac{d\sigma}{dx}\right|_B = B\delta(x) \qquad \left.\frac{d\sigma}{dx}\right|_V = \alpha_s\left(-\frac{B}{2\varepsilon}+V\right)\delta(x) \qquad \left.\frac{d\sigma}{dx}\right|_R = \alpha_s\frac{R(x)}{x}. \tag{2.196}$$

The constant B describes the Born process and the factorizing poles in the virtual contribution. The coupling constant α_s ignores factors 2 and π or color factors. We immediately see that the integral over x in the real emission rate is logarithmically divergent in the soft limit, similar to the collinear divergences we know. From factorization which we have illustrated based on the universality of the leading splitting kernels we know that in the collinear and soft limits the real emission has to follow the Born matrix element

$$\boxed{\lim_{x\to 0} R(x) = B}. \tag{2.197}$$

An *observable* computed beyond leading order includes contributions from real gluon emission and virtual gluon exchange. If the observable is infrared safe it will have a smooth limit towards vanishing gluon energy $O(x) \to O(0)$. The virtual corrections alone diverge, but the expectation value including virtual and real gluon contributions after dimensional regularization is finite. Because we are interested in infrared divergences we choose $n = 4 + 2\varepsilon$ dimensions with $\varepsilon > 0$, just like in Sect. 2.3.3, and schematically obtain the two divergent contributions

$$\langle O\rangle \sim \int_0^1 dx\, \frac{O(x)}{x^{1-2\varepsilon}} - \frac{O(0)}{2\varepsilon}. \tag{2.198}$$

This kind of combination has a finite limit for $\varepsilon \to 0$. However, for numerical applications and event simulation we need to implement this cancellation differently.

The expectation value of any *infrared safe observable* over the entire phase space, including Born terms, virtual corrections and real emission, is given by

$$\langle O\rangle \equiv \langle O\rangle_B + \langle O\rangle_V + \langle O\rangle_R = \mu_F^{-2\varepsilon}\int_0^1 dx\, \frac{O(x)}{x^{-2\varepsilon}}\left[\left.\frac{d\sigma}{dx}\right|_B + \left.\frac{d\sigma}{dx}\right|_V + \left.\frac{d\sigma}{dx}\right|_R\right]. \tag{2.199}$$

The same way the renormalization and factorization scales appear, dimensional regularization now yields an additional factor $1/x^{-2\varepsilon}$. Because we know its structure, we will omit this factorization scale factor in the following.

When we compute for example a distribution of the energy of one of the heavy particles in the process, we can extract a histogram from of the integral for $\langle O\rangle$ in Eq. 2.199 and obtain a normalized distribution. The problem is that we have to numerically integrate over x, and the individual parts of the integrand in Eq. 2.199 are not integrable.

There exist two methods to combine the virtual and real contributions to an observable and produce a finite physics result. The first way historically introduced by the

Dutch loop school for example to compute QCD corrections to top pair production is the numerically highly efficient *phase space slicing*: we divide the divergent phase space integral into a finite part and a pole, by introducing a small parameter Δ, which acts like

$$\begin{aligned}
\langle O\rangle_R + \langle O\rangle_V &= \int_0^1 dx\ \frac{O(x)}{x^{-2\varepsilon}}\ \frac{d\sigma}{dx}\Big|_R + \langle O\rangle_V \\
&= \left(\int_0^\Delta + \int_\Delta^1\right) dx\ \alpha_s \frac{R(x)O(x)}{x^{1-2\varepsilon}} + \langle O\rangle_V \\
&= \alpha_s R(0)\ O(0) \int_0^\Delta dx\ \frac{1}{x^{1-2\varepsilon}} + \alpha_s \int_\Delta^1 dx\ \frac{R(x)O(x)}{x} + \langle O\rangle_V \\
&= \alpha_s B\ O(0)\ \frac{\Delta^{2\varepsilon}}{2\varepsilon} + \alpha_s \int_\Delta^1 dx\ \frac{R(x)O(x)}{x} + \langle O\rangle_V \\
&= \alpha_s \frac{B\ O(0)}{2}\ \frac{2\varepsilon \log\Delta + \mathcal{O}(\varepsilon^2)}{\varepsilon} + \alpha_s \int_\Delta^1 dx\ \frac{R(x)O(x)}{x} + \alpha_s V O(0) \\
&= \alpha_s B O(0)\ \log\Delta + \alpha_s \int_\Delta^1 dx\ \frac{R(x)O(x)}{x} + \alpha_s V O(0) + \mathcal{O}(\varepsilon).
\end{aligned} \tag{2.200}$$

The two sources of $\log\Delta$ dependence have to cancel in the final expression, so we can evaluate the integral at finite but small values of Δ. An amusing numerical trick is to re-write the explicit $\log\Delta$ contribution into a NLO-type phase space integral. If the eikonal approximation is given in terms of a Mandelstam variable $\delta(s_4)$ and the cut-off has mass dimension two we can write

$$\log\frac{\Delta}{\mu^2} = \int_0^{s_4^{\max}} ds_4\ \log\frac{\Delta}{\mu^2}\ \delta(s_4) = \int_0^{s_4^{\max}} ds_4 \left[\frac{\log\frac{s_4^{\max}}{\mu^2}}{s_4^{\max}-\Delta} - \frac{1}{s_4}\right] \tag{2.201}$$

and similarly for $\log^2\Delta$. This representation we can integrate along with the real emission phase space. The result will be a finite value for the next-to-leading order rate in the limit $\Delta \to 0$ and exactly $\varepsilon = 0$.

The fundamental shortcoming of phase space slicing is that it requires an analytical integration to produce sensible observable distributions. To avoid cancellations between integrals and replace them by cancellations among integrands we use a *subtraction method* to define integrable functions under the x integral in Eq. 2.199. While our toy model appears more similar to the Frixione–Kunszt–Signer subtraction scheme than to the *Catani–Seymour* scheme, both of them really are equivalent at the level of the soft-collinear toy model. Starting from the individually divergent virtual and real contributions we first subtract and then add again a smartly chosen term, in this toy model identical to a plus-subtraction following Eq. 2.125

$$\begin{aligned}
\langle O\rangle_R + \langle O\rangle_V &= \int_0^1 dx\ \alpha_s \frac{R(x)O(x)}{x^{1-2\varepsilon}} + \langle O\rangle_V \\
&= \int_0^1 dx \left(\frac{\alpha_s R(x)O(x)}{x^{1-2\varepsilon}} - \frac{\alpha_s R(0)O(0)}{x^{1-2\varepsilon}}\right) + \int_0^1 dx \frac{\alpha_s B O(0)}{x^{1-2\varepsilon}} + \langle O\rangle_V \\
&= \alpha_s \int_0^1 dx\ \frac{R(x)O(x) - BO(0)}{x} + \alpha_s \frac{B\ O(0)}{2\varepsilon} + \langle O\rangle_V \\
&= \alpha_s \int_0^1 dx\ \frac{R(x)O(x) - BO(0)}{x} + \alpha_s V O(0) \quad \text{using Eq. 2.196.}
\end{aligned} \tag{2.202}$$

In the subtracted real emission integral we take the limit $\varepsilon \to 0$ because the asymptotic behavior of $R(x \to 0)$ regularizes this integral without any dimensional regularization required. The first integral precisely cancels the divergence from the virtual correction. We end up with a perfectly finite x integral for the sum of all three contributions, even in the limit $\varepsilon = 0$, i.e. there is no numerically small parameter in the expression

$$\begin{aligned}
\langle O\rangle = \langle O\rangle_B + \langle O\rangle_V + \langle O\rangle_R &= B\ O(0) + \alpha_s V\ O(0) + \alpha_s \int_0^1 dx\ \frac{R(x)\ O(x) - B\ O(0)}{x} \\
&= \int_0^1 dx\ \left[O(0)\ \left(B + \alpha_s V - \alpha_s \frac{B}{x}\right) + O(x)\ \alpha_s\ \frac{R(x)}{x}\right].
\end{aligned} \tag{2.203}$$

This subtraction procedure is a standard method to compute next-to-leading order corrections involving one-loop virtual contributions and the emission of one additional parton.

As a side remark, we can numerically improve this expression using a distribution relation

$$\begin{aligned}
\int_0^1 dx\ \frac{f(x)}{x^{1-2\varepsilon}} &= \int_0^1 dx\ \frac{f(x) - \theta(x_c - x) f(0)}{x^{1-2\varepsilon}} + f(0) \int_0^{x_c} dx\ x^{-1+2\varepsilon} \\
&= \int_0^1 dx\ \frac{f(x) - \theta(x_c - x) f(0)}{x} \left(1 + 2\varepsilon \log x + \mathcal{O}(\varepsilon^2)\right) + f(0)\ \frac{x_c^{2\varepsilon}}{2\varepsilon} \\
&= \int_0^1 dx \left(\frac{f(x) - \theta(x_c - x) f(0)}{x}\right. \\
&\qquad \left. + 2\varepsilon\ \frac{f(x) - \theta(x_c - x) f(0)}{x} \log x + \frac{x_c^{2\varepsilon}}{2\varepsilon}\ f(x)\delta(x)\right).
\end{aligned} \tag{2.204}$$

In terms of appropriately defined distributions we can write this relation as

$$\frac{1}{x^{1-2\varepsilon}} = \frac{x_c^{2\varepsilon}}{2\varepsilon}\ \delta(x) + \left(\frac{1}{x}\right)_c + 2\varepsilon \left(\frac{\log x}{x}\right)_c. \tag{2.205}$$

This c-subtraction first introduced as part of the Frixione–Kunszt–Signer subtraction scheme is defined as

$$\int_0^1 dx\ f(x)\ g(x)_c = \int_0^1 dx\ \left(f(x)g(x) - f(0)g(x)\theta(x_c - x)\right), \tag{2.206}$$

and is a generalization of the plus subtraction defined in Eq. 2.125 which we reproduce choosing $x_c = 1$. Linking the delta distribution to the divergent integral over $1/x$ it is also reminiscent of the principal value integration, but for an endpoint singularity and a dimensionally regularized phase space. Effectively combining phase space subtraction Eq. 2.202 and phase space slicing Eq. 2.200, we include a cutoff in the integrals holding the subtraction terms

$$\begin{aligned}\langle O\rangle_R &= \alpha_s \int_0^1 dx\ \frac{R(x)O(x)}{x^{1-2\varepsilon}} \\ &= \alpha_s \int_0^1 dx\ \frac{R(x)O(x) - \theta(x_c - x)BO(0)}{x}\,(1 + 2\varepsilon \log x) \\ &\quad + \alpha_s BO(0)\ \frac{x_c^{2\varepsilon}}{2\varepsilon} + \mathcal{O}(\varepsilon^2).\end{aligned} \tag{2.207}$$

The dependence on the finite cutoff parameter x_c drops out of the final result. The numerical behavior, however, should be improved if we subtract the infrared divergence only close to the actual pole where following Eq. 2.197 we understand the behavior of the real emission amplitude.

The formula Eq. 2.203 is, in fact, a little tricky: usually, the Born-type kinematics would come with an explicit factor $\delta(x)$, which in this special case we can omit because of the integration boundaries. We can re-write the same formula in a more appropriate way to compute distributions, possibly including experimental cuts

$$\boxed{\frac{d\sigma}{dO} = \int_0^1 dx\ \left[I(O)_{\text{LO}}\ \left(B + \alpha_s V - \alpha_s \frac{B}{x}\right) + I(O)_{\text{NLO}}\ \alpha_s\ \frac{R(x)}{x}\right]}. \tag{2.208}$$

The *transfer function* $I(O)$ is defined in a way that formally does precisely what we require: at leading order we evaluate $I(O)$ using the Born kinematics $x = 0$ while for the real emission kinematics it allows for general $x = 0 \ldots 1$.

2.6.2 MC@NLO Method

For example in Eq. 2.199 we integrate over the entire phase space of the additional parton. For a hard additional parton or jet the cross section looks well defined and finite, provided we fully combine real and virtual corrections. An infrared divergence appears after integrating over small but finite $x \to 0$ from real emission, and we cancel it with an infrared divergence in the virtual corrections proportional to a Born-type momentum configuration $\delta(x)$. In terms of a histogram in x we encounter the real emission divergence at small x, and this divergence is cancelled by a negative

delta distribution at $x = 0$. Obviously, this will only give a well behaved distribution after integrating over at least a range of x values just above zero.

This soft and collinear subtraction scheme for next-to-leading order calculations leads us to the first method of combining or matching next-to-leading order calculations with a parton shower. Instead of the contribution from the virtual corrections contributing at $\delta(x)$ what we would rather want is a smeared virtual corrections pole which coincides with the justified collinear approximation and cancels the real emission over the entire low-x range. This contribution we can view as events with a negative weight, i.e. counter-events. Negative events negative reactions with experimentalists, because they cause problems in a chain of probabilistic statements like a detector simulation. Fundamentally, there is really no problem with them as long as any physical prediction we make after adding all leading order and next-to-leading order contributions gives a positive cross section.

Because we know they describe collinear jet radiation correctly such a modification will make use of Sudakov factors. We can write them as a function of the energy fraction z and find $d\mathscr{P} = \alpha_s P(z)/z dz$. Note that we avoid the complicated proper two-dimensional description of Eq. 2.164 in favor of the simpler picture just in terms of particle energy fractions as introduced in the last section.

Once we integrate over the entire phase space this modified subtraction scheme has to give the same result as the *next-to-leading order rate*. Smearing the integrated soft-collinear subtraction term using the splitting probabilities entering the parton shower means that the MC@NLO subtraction scheme has to be adjusted to the parton shower we use.

Let us consider the perturbatively critical but otherwise perfectly fine observable, the radiated *photon spectrum* as a function of the (external) energy scale z. We know what this spectrum looks like for the collinear and hard kinematic configurations

$$\left.\frac{d\sigma}{dz}\right|_{\text{LO}} = \alpha_s \frac{B P(z)}{z} \qquad \left.\frac{d\sigma}{dz}\right|_{\text{NLO}} = \alpha_s \frac{R(z)}{z}. \tag{2.209}$$

The first term describes parton shower radiation from the Born diagram at order α_s, while the second term is the hard real emission defined in Eq. 2.196. The transfer functions we would have to include in the general form of Eq. 2.208 to arrive at this equation are

$$\begin{aligned} I(z,1)\Big|_{\text{LO}} &= \alpha_s \frac{P(z)}{z} \\ I(z,x_M)\Big|_{\text{NLO}} &= \delta(z-x) + \alpha_s \frac{P(z)}{z}\,\theta(x_M(x)-z). \end{aligned} \tag{2.210}$$

The second term in the real radiation transfer function arises because at the next order in perturbation theory the parton shower also acts on the real emission process. It requires that enough energy to radiate a photon with an energy z be available, where x_M is the energy available at the respective stage of showering, i.e. $z < x_M$.

These transfer functions we can include in Eq. 2.208

$$\begin{aligned}\frac{d\sigma}{dz} &= \int_0^1 dx \left[I(z,1) \left(B + \alpha_s V - \alpha_s \frac{B}{x} \right) + I(z, x_M)\, \alpha_s \frac{R(x)}{x} \right] \\ &= \int_0^1 dx \left[\alpha_s \frac{P(z)}{z} \left(B + \alpha_s V - \alpha_s \frac{B}{x} \right) + (\delta(x-z) + \mathcal{O}(\alpha_s))\, \alpha_s \frac{R(x)}{x} \right] \\ &= \int_0^1 dx \left[\alpha_s \frac{BP(z)}{z} + \alpha_s \frac{R(z)}{z} \right] + \mathcal{O}(\alpha_s^2) \\ &= \alpha_s \frac{BP(z) + R(z)}{z} + \mathcal{O}(\alpha_s^2). \end{aligned} \tag{2.211}$$

All Born terms proportional to $\delta(z)$ vanish because their contributions would be unphysical. This already fulfills the first requirement for our scheme, without having done anything except for including a transfer function. Now, we can integrate over z and calculate the total cross section σ_{tot} with a cutoff $z_{\min}$ for consistency. However, Eq. 2.211 includes an additional term which spoils the result: the same kind of jet radiation is included twice, once through the matrix element and once through the shower. This is precisely the double counting which we avoid in the CKKW scheme. So we are still missing something.

We also knew we would fall short, because our strategy includes a smeared virtual subtraction term which for finite x should cancel the real emission. This subtraction is not yet included. Factorization tells us how to write such a subtraction term using the splitting function P as defined in Eq. 2.209 to turn the real emission term into a finite contribution

$$\frac{R(x)}{x} \quad \longrightarrow \quad \frac{R(x) - BP(x)}{x}. \tag{2.212}$$

Because this is an ad hoc subtraction term we also have to add it to the Born-type contribution. This leads us to a modified version of Eq. 2.208, now written for general observables

$$\boxed{\frac{d\sigma}{dO} = \int_0^1 dx \left[I(O,1) \left(B + \alpha_s V - \frac{\alpha_s B}{x} + \frac{\alpha_s BP(x)}{x} \right) + I(O, x_M) \alpha_s \frac{R(x) - BP(x)}{x} \right]}. \tag{2.213}$$

Looking back at different methods of removing ultraviolet divergences this modification from the minimal soft and collinear subtraction in Eq. 2.208 to a physical subtraction term corresponding to the known radiation pattern reminds us of different renormalization schemes. The minimal $\overline{\text{MS}}$ scheme will always guarantee finite results, but for example the on-shell scheme with its additional finite terms has at least to a certain degree beneficial properties when it comes to understanding its physical meaning. This is the same for the MC@NLO method: we replace the minimal subtraction terms by physically motivated non-minimal subtraction terms such that the radiation pattern of the additional parton is described correctly.

So when we use this form to compute the z spectrum to order α_s it will in addition to Eq. 2.211 include an integrated subtraction term contributing to the Born-type kinematics

$$\begin{aligned}\frac{d\sigma}{dz} &\longrightarrow \int_0^1 dx \left[\alpha_s \frac{BP(z)}{z} + \alpha_s\, \delta(x-z) \left(\frac{R(x)}{x} - \frac{BP(x)}{x}\right)\right] + \mathcal{O}(\alpha_s^2) \\ &= \int_0^1 dx\, \alpha_s \frac{BP(z) + R(z) - BP(z)}{z} + \mathcal{O}(\alpha_s^2) \\ &= \alpha_s \frac{R(z)}{z} + \mathcal{O}(\alpha_s^2).\end{aligned} \tag{2.214}$$

This is exactly the distribution we expect.

Following the above argument the subtraction scheme implemented in the Monte Carlo generator MC@NLO describes hard emission just like a next-to-leading order calculation. This includes the next-to-leading order normalization of the rate as well as the *next-to-leading order distributions* for those particles produced in the original hard process. For example for W+jets production such corrections to the W and leading jet distributions matter, while for the production of heavy new particles their distributions hardly change at next-to-leading order. The distribution of the first radiated parton is included at leading order, as we see in Eq. 2.214. Finally, additional collinear particle emissions is simulated using Sudakov factors, precisely like a parton shower.

Most importantly, it avoids double counting between the first hard emission and the collinear jets, which means it describes the entire p_T range of jet emission for the *first and hardest* radiated jet consistently. Those additional jets, which do not feature in the next-to-leading order calculation, are added through the parton shower, i.e. in the collinear approximation. As usually, what looked fairly easy in our toy example is much harder in QCD reality, but the setup is the same.

2.6.3 POWHEG Method

As described in Sect. 2.6.2 the MC@NLO matching scheme for a next-to-leading order correction and the parton shower is based on an extended subtraction scheme. It starts from a given parton shower and avoids double counting by modifying the next-to-leading corrections. An interesting question is: can we also combine a next-to-leading order calculation by keeping the next-to-leading order structure and apply a modified parton shower? The main ingredient to this structure are Sudakov factors introduced in Sect. 2.5.1 and used for the CKKW merging scheme in Sect. 2.5.3.

In contrast to the MC@NLO scheme the POWHEG (Positive Weight Hardest Emission Generator) scheme does not introduce counter events or subtraction terms. It considers the next-to-leading order calculation of a cross section a combination of an m-particle and an $(m+1)$-particle process and attempts to adjust the parton shower attached to each of these two contributions such that there is no double counting.

Our starting point is the next-to-leading order computation of a cross section following Eq. 2.196. We can combine it with appropriate soft and collinear subtraction terms C in the factorized $(m+1)$-particle phase space where for simplicity we assume that the integrated subtraction terms exactly cancel the divergences from the virtual corrections:

$$\begin{aligned} d\sigma &= B\, d\phi_m + \alpha_s \left(-\frac{B}{2\varepsilon} + V\right) d\phi_m + \alpha_s R\, dz\, dt' d\phi_m \\ &= B\, d\phi_m + \alpha_s V\, d\phi_m + \alpha_s\, (R - C\mathbb{P})\; d\phi_m dz dt' \quad \text{soft-collinearly subtracted} \\ &= [\alpha_s V + \alpha_s (R - C)\mathbb{P}\, dz\, dt]\; d\phi_m + B\, d\phi_m \left[1 + \frac{\alpha_s R}{B}\,(1 - \mathbb{P})\, dz\, dt'\right]. \end{aligned} \tag{2.215}$$

The $(m+1)$-particle phase we factorize into the m-particle phase space and the azimuthally symmetric remainder $dz\, dt'$, as suggested by Eq. 2.97. With these two proper integration variables we cannot assume a toy form R/x for the real emission, so we denote the real emission as R alone. The projector $\mathbb{P}$ maps the nominal $(m+1)$-particle phase space of the real emission onto the m-particle phase space of the leading order process.

The first term in Eq. 2.215 is suppressed by one power of α_s, so we can add a parton shower to it without any worry. The second term consists of the Born contribution and the hard emission of one parton, so we have to avoid double counting when defining the appropriate Sudakov factors. Moreover, a serious problem appears in Eq. 2.215 when we interpret it probabilistically: nothing forces the combination of virtual and subtracted real emission in the first brackets to be positive. To cure this shortcoming we can instead combine all m-particle contributions into one term

$$\begin{aligned} d\sigma &= \left[B + \alpha_s V + \alpha_s (R - C)\mathbb{P}\, dz\; dt'\right]\; d\phi_m \left[1 + \frac{\alpha_s R}{B}\,(1 - \mathbb{P})\, dz\, dt'\right] + \mathcal{O}(\alpha_s^2) \\ &\equiv \overline{B}\; d\phi_m \left[1 + \frac{\alpha_s R}{B}\,(1 - \mathbb{P})\, dz\; dt'\right] + \mathcal{O}(\alpha_s^2) \\ &= \overline{B}\; d\phi_m \left[1 + \frac{\alpha_s R}{B}\theta\left(p_T(t', z) - p_T^{\min}\right) dz\; dt'\right] + \mathcal{O}(\alpha_s^2), \end{aligned} \tag{2.216}$$

where the combination $\overline{B}$ can only become negative if the regularized next-to-leading contribution over-compensates the Born term which would indicate a breakdown of perturbation theory. The second term in the brackets needs to project the real emission onto the hard $(m+1)$-particle phase space. If we replace the symbolic projection $(1-\mathbb{P})$ by a step function in terms of the transverse momentum of the radiated parton $p_T(t', z)$ we can ensure that it really only appears for hard radiation above $p_T^{\min}$ and at the same time keep the integral over the radiation phase space finite.

From CKKW jet merging we know what we have to do to combine an m-particle process with an $(m+1)$-particle process, even in the presence of the parton shower: the m-particle process has to be exclusive, which means we need to attach a Sudakov factor Δ to veto additional jet radiation to the first term in the brackets of Eq. 2.216.

In the CKKW scheme the factor in the front of the brackets would be B and not $\overline{B}$. The introduction of $\overline{B}$ is nothing but a re-weighting factor for the events contributing to the m-particle configuration which we need to maintain the next-to-leading order normalization of the combined m-particle and $(m+1)$-particle rates. The second factor $\alpha_s R/B$ is essentially the multiplicative PYTHIA or HERWIG matrix element correction used for an improved simulation for example of $W+$jet events.

The appropriate Sudakov factor for the real emission has to veto only hard jet radiation from an additional parton shower. This way we ensure that for the $(m+1)$-particle contribution the hardest jet radiation is given by the matrix element R, i.e. no splitting occurs in the hard regime $p_T > p_T^{\min}$. Such a *vetoed shower* we can define in analogy to the (diagonal) Sudakov survival probability Eq. 2.164 by adding a step function which limits the unwanted splittings to $p_T > p_T^{\min}$

$$\Delta(t, p_T^{\min}) = \exp\left(-\int_{t_0}^{t} \frac{dt'}{t'} \int_0^1 dz\, \frac{\alpha_s}{2\pi} \hat{P}(z)\, \theta\left(p_T(t', z) - p_T^{\min}\right)\right), \tag{2.217}$$

omitting the resolution t_0 in the argument. This modified Sudakov factor indicates that in contrast to the MC@NLO method we now modify the structure of the parton shower which we combine with the higher order matrix elements.

For the vetoed Sudakov factors to make sense we need to show that they obey a DGLAP equation like Eq. 2.172, including the veto condition in the splitting kernel

$$\begin{aligned} f(x,t) &= \Delta(t, p_T^{\min})\, f(x, t_0) \\ &\quad + \int_{t_0}^{t} \frac{dt'}{t'}\, \Delta(t, t', p_T^{\min}) \int_0^1 \frac{dz}{z}\, \frac{\alpha_s}{2\pi}\, \hat{P}(z)\, \theta\left(p_T(t', z) - p_T^{\min}\right) f\left(\frac{x}{z}, t'\right), \end{aligned} \tag{2.218}$$

where we again show the diagonal case to simplify the notation. The proof of this formula starts from Eq. 2.172 with the modification of an explicit veto. Using $1 = \theta(g) + (1 - \theta(g))$ we find Eq. 2.218 more or less straight away. The bottom line is that we can consistently write down vetoed Sudakov probabilities and build a parton shower out of them.

Inserting both Sudakov factors into Eq. 2.216 gives us for the combined next-to-leading order exclusive contributions

$$\boxed{d\sigma = \overline{B}\, d\phi_m \left[\Delta(t, 0) + \Delta(t', p_T^{\min}) \frac{\alpha_s R}{B} \theta\left(p_T(t', z) - p_T^{\min}\right) dt' dz\right] + \mathcal{O}(\alpha_s^2)}\,. \tag{2.219}$$

The first Sudakov factor is not vetoed which means it is evaluated at $p_T^{\min} = 0$.

Based on the next-to-leading order normalization of the integrated form of Eq. 2.219 we can determine the form of the splitting probability entering the Sudakov factor from the perturbative series: the term in brackets integrated over the entire phase space has to give unity. Starting from Eq. 2.218 we first compute the derivative of the Sudakov factor with respect to one of its integration boundaries, just like in Eq. 2.168

$$\begin{aligned}\frac{d\Delta(t,p_T^{\min})}{dt} &= \frac{d}{dt}\exp\left(-\int_{t_0}^{t}\frac{dt'}{t'}\int_0^1 dz\frac{\alpha_s}{2\pi}\hat{P}(z)\,\theta\left(p_T(t',z)-p_T^{\min}\right)\right)\\ &= \Delta(t,p_T^{\min})\,\frac{(-1)}{t}\int_0^1 dz\frac{\alpha_s}{2\pi}\hat{P}(z)\,\theta\left(p_T(t,z)-p_T^{\min}\right).\end{aligned} \tag{2.220}$$

Using this relation we indeed find for the integral over the second term in the brackets of Eq. 2.219

$$\begin{aligned}&\int_{t_0}^{t} dt'dz\Delta(t',p_T^{\min})\frac{\alpha_s R}{B}\theta\left(p_T(t',z)-p_T^{\min}\right)\\ &= -\int_{t_0}^{t} dt'\,\frac{d\Delta(t',p_T^{\min})}{dt'}\,\frac{\int dz\frac{\alpha_s R}{B}\theta\left(p_T(t',z)-p_T^{\min}\right)}{\int dz\frac{\alpha_s}{2\pi t'}\hat{P}(z)\,\theta\left(p_T(t',z)-p_T^{\min}\right)}\\ &= -\int_{t_0}^{t} dt'\,\frac{d\Delta(t',p_T^{\min})}{dt'}\\ &= -\Delta(t,p_T^{\min}) \qquad \Leftrightarrow \qquad \boxed{\frac{\alpha_s R}{B}=\frac{\alpha_s}{2\pi t'}\hat{P}(z)}\,.\end{aligned} \tag{2.221}$$

Looking back at Eq. 2.97 this corresponds to identifying $B=\sigma_n$ and $\alpha_s R=\sigma_{n+1}$. In the POWHEG scheme the Sudakov factors are based on the simulated splitting probability $\alpha_s R/B$ instead of the splitting kernels. This replacement is nothing new, though. We can already read it off Eq. 2.97.

A technical detail which we have not mentioned yet is that the POWHEG scheme assumes that our Sudakov factors can be ordered in such a way that the hardest emission always occurs first. Following the discussion in Sect. 2.5.2 we expect any collinear transverse momentum ordering to be disrupted by soft radiation, ordered by the angle. The first emission of the parton shower might well appear at large angles but with small energy, which means it will not be particularly hard.

For the POWHEG shower this soft radiation has to be removed or moved to a lower place in the ordering of the splittings. The condition to treat soft emission separately we know from CKKW merging, namely Eq. 2.192: the scale at which we resolve a parton splitting does not have to identical with the lower boundary of simulated splittings. We can construct a parton shower taking into account such splitting kernels, defining a *truncated shower*. This modified shower is the big difference between the MC@NLO scheme and the POWHEG scheme in combining next-to-leading order corrections with a parton shower. In the MC@NLO scheme we modify the next-to-leading order correction for a given shower, but the shower stays the same. In the POWHEG scheme the events get re-weighted according to standard building blocks of a next-to-leading order calculation, but the shower has to be adapted.

In Sects. 2.5.3, 2.6.2 and 2.6.3 we have introduced different ways to simulate jet radiation at the LHC. The main features and shortcomings of the matching and merging approaches we summarize in Table 2.3.

At this stage it is up to the competent user to pick the scheme which describes their analysis best. First of all, if there is a well defined and sufficiently hard scale in the

Table 2.3 Comparison of the MC@NLO and CKKW schemes combining collinear and hard jets

	MC@NLO/POWHEG matching	CKKW/MLM merging
Hard jets	First jet correct	All jets correct
Collinear jets	All jets correct, tuned	All jets correct, tuned
Normalization	Correct to NLO	Correct to LO plus real emission
Implementations	MC@NLO, POWHEG, SHERPA, HERWIG	SHERPA, Alpgen, MadEvent,...

process, the old-fashioned Monte Carlo with a tuned parton shower will be fine, and it is by far the fastest method. When for some reason we are mainly interested in one hard jet we can use MC@NLO or POWHEG and benefit from the next-to-leading order normalization. This is the case for example when a gluon splits into two bottoms in the initial state and we are interested in the radiated bottom jet and its kinematics. In cases where we really need a large number of jets correctly described we will end up with CKKW or MLM simulations. However, just like the old-fashioned parton shower Monte Carlo we need to include the normalization of the rate by hand. Or we are lucky and combined versions of CKKW and POWHEG, as currently developed by both groups, will be available.

I am not getting tired of emphasizing that the conceptual progress in QCD describing jet radiation for all transverse momenta is absolutely crucial for LHC analyses. If I were a string theorist I would definitely call this achievement a revolution or even two, like 1917 but with the trombones and cannons of Tchaikovsky's 1812. In contrast to a lot of other progress in theoretical physics jet merging solves a problem which would otherwise have limited our ability to understand LHC data, no matter what kind of Higgs or new physics we are looking for.

2.7 Further Reading

Just like the Higgs part the QCD part of these lecture notes is something in between a text book chapter and a review of QCD and mostly focused on LHC searches. Some corners I cut, in particular when calculations do not affect the main topic, namely the resummation of logarithms in QCD and the physical meaning of these logarithms. There is no point in giving a list of original references, but I will list a few books and review articles which should come in handy if you would like to know more:

- I started learning high energy theory including QCD from Otto Nachtmann's book. I still use his appendices for Feynman rules because I have not seen another book with as few (if not zero) typos [5].
- Similar, but maybe a little more modern is the Standard Model primer by Cliff Burgess and Guy Moore [6]. At the end of it you will find more literature.

- The best source to learn QCD at colliders is the pink book by Keith Ellis, James Stirling, and Bryan Webber. It includes everything you ever wanted to know about QCD [1] and more. This QCD section essentially follows its Chap. 5.
- A little more phenomenology you can find in Günther Dissertori, Ian Knowles and Michael Schmelling's book [7]. Again, I borrowed some of the discussions in the QCD section from there.
- If you would like to learn how to for example compute higher order cross sections to Drell–Yan production, Rick Field works it all out [8].
- For those of you who are now hooked on QCD and jet physics at hadron colliders there are two comprehensive reviews by Steve Ellis [9] and by Gavin Salam [10].
- Aimed more at perturbative QCD at the LHC is the QCD primer by John Campbell, Joey Huston, and James Stirling [11].
- Coming to the usual brilliant TASI lectures, there are Dave Soper's [12] and George Sterman's [13] notes. Both of them do not exactly use my kind of notations and are comparably formal, but they are a great read if you know something about QCD already. More on the phenomenological side there are Mike Seymour's lecture notes [14].
- The only review on leading order jet merging is by Michelangelo Mangano and Tim Stelzer [15]. The original CKKW paper beautifully explains the general idea for final state radiation, and I follow their analysis [2]. For other approaches there is a very concise discussion included with the comparison of the different models [16].
- To understand MC@NLO there is nothing like the original papers by Bryan Webber and Stefano Frixione [17].
- The POWHEG method is really nicely described in the original paper by Paolo Nason [18]. Different processes you can find discussed in detail in a later paper by Stefano Frixione, Paolo Nason, and Carlo Oleari [19].
- Even though they are just hand written and do not include a lot of text it might be useful to have a look at Michael Spira's QCD lecture notes [20] to view some of the topics from a different angle.

References

1. Ellis, R.K., Stirling, W.J., Webber, B.R.: QCD and collider physics camb. Monogr. Part. Phys. Nucl. Phys. Cosmol **8**, 1 (1996)
2. Catani, S., Krauss, F., Kuhn, R., Webber, B.R.: QCD matrix elements + parton showers. JHEP **0111**, 063 (2001)
3. Plehn, T., Tait, T.M.P.: Seeking Sgluons. J. Phys. G **36**, 075001 (2009)
4. Englert, C., Plehn, T., Schichtel P., Schumann, S.: Jets plus missing energy with an autofocus. Phys. Rev. D **83**, 095009 (2011)
5. Nachtmann, O.: Elementary particle physics: concepts and phenomena, pp. 559. Springer, Berlin (1990)
6. Burgess, C.P., Moore, G.D.: The standard model: a primer cambridge, pp. 542. Cambridge University Press, Cambridge

7. Dissertori, G., Knowles, I.G., Schmelling, M.: QCD—high energy experiments and theory oxford, pp. 538. Clarendon, UK (2003)
8. Field R.D.: Applications of perturbative QCD Redwood City. Addison-Wesley, USA, p. 366 (Frontiers in Physics, 77) (1989)
9. Ellis, S.D., Huston, J., Hatakeyama, K., Loch, P., Tonnesmann, M.: Jets in hadron–hadron collisions. Prog. Part. Nucl. Phys. **60**, 484 (2008)
10. Salam G.P.: Towards jetography, arXiv:0906.1833 [hep-ph]
11. Campbell, J.M., Huston, J.W., Stirling, W.J.: Hard interactions of quarks and gluons: a primer for LHC physics. Rept. Prog. Phys. **70**, 89 (2007)
12. Soper D.E.: Basics of QCD perturbation theory, arXiv:hep-ph/0011256
13. Sterman G.: QCD and jets arXiv:hep-ph/0412013
14. Seymour M.H.: Quantum chromodynamics, arXiv:hep-ph/0505192
15. Mangano M.L., Stelzer T.J.: Tools for the simulation of hard hadronic collisions. Ann. Rev. Nucl. Part. Sci. **55**, 555 CERN-PH-TH-2005-074 (2005)
16. Alwall, J. et al.: Study of various algorithms for the merging of parton showers and matrix elements in hadronic collisions. Eur. Phys. J. C **53**, 473 (2008)
17. Frixione, S., Webber, B.R.: Matching NLO QCD computations and parton shower simulations. JHEP **0206**, 029 (2002)
18. Nason, P.: A new method for combining NLO QCD with shower monte carlo algorithms. JHEP **0411**, 040 (2004)
19. Frixione, S., Nason, P., Oleari, C.: Matching NLO QCD computations with Parton Shower simulations: the POWHEG method. JHEP **0711**, 070 (2007)
20. Spira M.: QCD, people.web.psi.ch/spira/vorlesung/qcd

Chapter 3
LHC Phenomenology

While the first two parts of these lecture notes focus on Higgs physics and on QCD, biased towards aspects relevant to the LHC, they do not yet justify the title of the lecture notes. In addition, both introductions really are theoretical physics. The third section will reflect what many theorists working on LHC topics need to know. It goes beyond what you find in theoretical physics text books and is usually referred to as 'phenomenology'.[1]

This terms indicate that these topics are not really theoretical physics in the sense that they rely on for example field theory. They are not experimental physics either, because they go beyond understanding the direct results of the LHC detectors. Instead, they lie in between the two fields and need to be well understood to allow theorists and experimentalists to interact with each other.

Sometimes, phenomenology has the reputation of not being proper theoretical physics. From these lecture notes it is clear that LHC physics is field theory, either electroweak symmetry breaking, QCD, or—not covered in these notes—physics models describing extensions of our Standard Model at the TeV scale. This chapter supplements the pure theory aspects and links them to experimental issues of the ATLAS and CMS experiments. In Sect. 3.1 we start by filling in some blanks from Sects. 1.4.3, 1.6 and 2.5.3. We first discuss jets and how to link the asymptotic final states of QCD amplitudes, partons, to experimentally observed QCD objects, jets. Then, we turn to a current field of research, so-called fat jets. In Sect. 3.2 we introduce a particularly efficient way of computing transition amplitudes from Feynman rules, the helicity method. Most professional tools for the computation of LHC cross sections or for simulating LHC events use this method instead of squaring amplitudes analytically. Section 3.3 discusses how to reconstruct particles which interact too weakly to be observed in LHC detectors. In the Standard Model those would

[1] The term 'phenomenology' is borrowed from philosophy where it means exactly the opposite from what it means in physics. Originally, phenomenology is a school based on Edmund Husserl. Unlike other fields of philosophy their main interest are not observations but the actual nature of things. Doing exactly the opposite, physicist phenomenologists are theorists who really care about measurements.

T. Plehn, *Lectures on LHC Physics*, Lecture Notes in Physics 844,
DOI: 10.1007/978-3-642-24040-9_3, © Springer-Verlag Berlin Heidelberg 2012

be neutrinos, but as part of the LHC program we hope to find dark matter candidates that way. Finally, in Sect. 3.4 we very briefly discuss LHC uncertainties from a theory point of view. In the public arXiv version more sections will follow, hopefully triggered by LHC measurements challenging theorists and their simulations.

3.1 Jets and Fat Jets

Throughout Chap. 2 we pretend that quarks and gluons produced at the LHC are actually what we observe in the LHC detectors. In perturbative QCD those particles are the final states, even though they cannot exist individually because QCD is asymptotically free. For example, in Eq. 2.63 we apply wave function renormalization factors to them. On the other hand, in Sect. 2.2.2 we see that the strong coupling explodes at low energy scales around Λ_{QCD} which means that something has to happen with quarks and gluons on their way through the detectors. Indeed, the gluon and all quarks except for the top quark *hadronize* before they decay and form bunches of baryons and mesons which in turn decay in many stages. These particles carry a lot of energy, around the typical energy scales $\mathcal{O}(m_H)$ we are interested in at the LHC. Relativistic kinematics then tells us that these baryons and mesons are strongly boosted together to form *jets*. Those jets we measure at hadron colliders and link to the partons produced in the hard interaction.

Consequently, in Chap. 2 we use the terms parton and jet synonymously, essentially assuming that each parton at the LHC turns into a jet and that the measured jet four-momentum can be linked to the parton four-momentum. The way we usually define jets are so-called recombination algorithms including for example the Cambridge–Aachen or (anti-) k_T algorithms. Imagine we observe a large number of energy depositions in the ATLAS or CMS calorimeter which we would like to combine into jets. We know that they come from a small number of partons which originate in the hard QCD process and which since have undergone a sizeable number of splittings, hadronized and decayed to stable particles. Can we try to reconstruct the original partons?

The answer is yes, in the sense that we can combine a large number of proto-jets into smaller numbers, where unfortunately nothing tells us what the final number of jets should be. We know from Chap. 2 that in QCD we can produce an arbitrary number of hard jets in a hard matrix element and another arbitrary number via soft or collinear radiation. Therefore, we need to tell the jet algorithm either how many jets it should arrive at or what should be the resolution of the smallest proto-jets we consider partons, whatever the measure for this resolution might be. In the coming section we will therefore discuss what criteria exist for a proto-jet recombination to correspond to an assumed physical jet.

3.1.1 Jet Algorithms

The basic idea of recombination algorithms is to ask if a given proto-jet has a soft or collinear partner. This follows from the physics arguments in Chap. 2 from which we

know that partons produced in a hard process preferably turn into collinear pairs of partons as approximately described by the parton shower. To decide if two proto-jets have arisen from one parton leaving the hard process we have to define a collinearity measure. This measure will on the one hand include the distance in R space as introduced in Eq. 2.35 and on the other hand the transverse momentum of one proto-jet with respect to another or to the beam axis. Explicit measures are, weighted by the relative power of the two ingredients

$$\begin{aligned} k_T \qquad & y_{ij} = \frac{\Delta R_{ij}}{D} \min\left(p_{T,i}, p_{T,j}\right) && y_{iB} = p_{T,i} \\ \text{C/A} \qquad & y_{ij} = \frac{\Delta R_{ij}}{D} && y_{iB} = 1 \\ \text{anti-}k_T \qquad & y_{ij} = \frac{\Delta R_{ij}}{D} \min\left(p_{T,i}^{-1}, p_{T,j}^{-1}\right) && y_{iB} = p_{T,i}^{-1}. \end{aligned} \tag{3.1}$$

The parameter D is a measure of the angular size of the jet and can range anywhere between 0.4 and 1.5. It balances the jet–jet and jet-beam criteria; small values of D increase y_{ij}, so $y_{ij} > y_{iB}$ becomes more likely. Because of the power dependence on the transverse momenta the three algorithms start with soft constituents (k_T), purely geometric (*Cambridge–Aachen C/A*) or hard constituents (anti-k_T) to form a jet. All of them have in common that they link physical objects, namely calorimeter towers, to other more or less physical objects, namely partons from the hard process. As we can see from the different choices in Eq. 3.1 we have all the freedom in the world to weight the angular and transverse momentum distances relative to each other. While for the k_T and the *C/A* algorithms it is fairly clear that the intermediate steps have a physical interpretation, this is not clear at all for the anti-k_T algorithm.

We define two proto-jets as coming from one jet if $y_{ij} < y_{\text{cut}}$, where y_{cut} is the scale we give to the algorithm. The jet algorithm proceeds as

(1) for all combinations of two proto-jets in the event find the minimum $y^{\min} = \min_{ij}(y_{ij}, y_{iB})$
(2a) if $y^{\min} = y_{ij} < y_{\text{cut}}$ merge proto-jets i and j and their momenta, go back to (1)
(2b) if $y^{\min} = y_{iB} < y_{\text{cut}}$ remove proto-jet i, call it beam radiation, go back to (1)
(2c) if $y^{\min} > y_{\text{cut}}$ keep all proto-jets, done

The result of the algorithm will of course depend on the resolution y_{cut}. Alternatively, we can give the algorithm the minimum number of physical jets and stop there. The technical question is what 'combine jets' means in terms of the four-momentum of the new jet. The three-momentum vectors we simply add $\vec{k}_i + \vec{k}_j \to \vec{k}_i$. For the zero component we can assume that the new physical jet have zero invariant mass, which is inspired by the massless parton we are usually looking for. If instead we add the four-momenta we can compute the invariant mass of the jet constituents, the *jet mass*. As we will see in the next section this allows us to extend the concept of jet algorithms to massive particles like a W or Z boson, the Higgs boson, or the top quark.

From Chap. 2 and the derivation of the collinear splitting kernels it is obvious why theorists working on perturbative QCD often prefer the k_T algorithm: we know

that the showering probability or the collinear splitting probability is best described in terms of virtuality or transverse momentum. A transverse momentum distance between jets is therefore best suited to combine the correct proto-jets into the original parton from the hard interaction, following a series of actual physical intermediate splittings. Moreover, this transverse momentum measure is intrinsically infrared safe, which means the radiation of an additional soft parton cannot affect the global structure of the reconstructed jets. For other algorithms we have to ensure this property explicitly, and you can find examples in QCD lectures by Mike Seymour.

The problem of the k_T algorithm arises with pile-up or underlying event, i.e. very soft QCD activity entering the detectors undirectionally. Such noise is easiest understood geometrically in a probabilistic picture. Basically, the low-energy jet activity is constant all over the detector, so we *subtract it from each event*. How much energy deposit we have to subtract from a reconstructed jet depends on the area the jet covers in the detector. Therefore, it is a major step that even for the k_T algorithm we can compute an IR-safe geometric jet size. The C/A and anti-k_T algorithms are more compact and easier to interpret experimentally.

3.1.2 Fat Jets

Starting from the way the experiments at the Tevatron and the LHC search for bottom jets, including several detailed requirements on the content of such jets, the question arises if we can look for other *heavy objects* inside a jet. Such jets involving heavy particles and (usually) a large geometrical size are referred to as fat jets. Three main motivations lead us into the direction of fat jets: first, dependent on our physics model heavy objects like W bosons or top quarks might be boosted enough to fit into a regular jet of angular size $R \lesssim 0.7$. Secondly, a jet algorithm might include hadronic decay products which we would not trust to include in a regular mass reconstruction based on reconstructed detector objects. And finally, even if only a fraction of the heavy particles we are searching for are sufficiently boosted such an algorithm automatically resolves signal combinatorics known to limit LHC analyses.

At the LHC, we are guaranteed to encounter the experimental situation $p_T/m \gtrsim 1$ for electroweak gauge bosons, Higgs bosons, and top quarks. The more extreme case of $p_T \gg m$, for example searching for top quarks with a transverse momentum in excess of 1 TeV is unlikely to appear in the Standard Model and will only become interesting if we encounter very heavy resonances decaying to a pair of top quarks. This is why we focus on the moderate scenario.

Historically, fat jet searches were first designed to look for strongly interacting W bosons. Based on the k_T algorithm they look for structures in the chain of y values introduced in Eq. 3.1, which define the kinematics of each jet. For such an analysis of y values it is helpful but not crucial that the intermediate steps of the jet algorithm have a physics interpretation. More recent fat jet algorithms looking for not too highly boosted heavy particles are based on the C/A algorithm which appears to be best suited to extract massive splittings inside the jet clustering history. A comparison

of different jet algorithms can be found in the original paper on associated Higgs and gauge boson production. Using a C/A algorithm we can search for hadronically decaying boosted W and Z bosons. The problem is that for those we only have one hard criterion based on which we can reject QCD backgrounds: the mass of the W/Z resonance. Adding a second W/Z boson and possibly the mass of a resonance decaying to these two, like a heavy Higgs boson, adds to the necessary QCD rejection. For Higgs and top decays the situation is significantly more promising.

Starting with the *Higgs tagger* we search for jets which include two bottom quarks coming from a massive Higgs boson with $m_H \gtrsim 120\,\text{GeV}$. First, we run the C/A algorithm over the event, choosing a large geometric size $R = 1.2$ estimated to cover

$$R_{b\bar{b}} \sim \frac{1}{\sqrt{z(1-z)}} \frac{m_H}{p_{T,H}} > \frac{2m_H}{p_{T,H}}, \tag{3.2}$$

in terms of the transverse momentum of the boosted Higgs and the momentum fractions z and $1-z$ of the two bottom jets.

We then uncluster again this *fat jet*, searching for a drop in jet mass indicating the decay of the massive Higgs to two essentially massless quarks. The iterative unclustering we start by undoing the last clustering of the jet j, giving two subjets j_1, j_2 ordered such that $m_{j_1} > m_{j_2}$. If the mass drop between the original jet and its more massive splitting product is small, i.e. $m_{j_1} > 0.8\, m_j$, we conclude that j_2 is soft enough to come from the underlying event or soft-collinear QCD emission and discard j_2 while keeping j_1; otherwise we keep both j_1 and j_2; each surviving subjet j_i we further decompose recursively until it reaches some minimum value, e.g. $m_{j_i} < 30\,\text{GeV}$ ensuring it does not involve heavy states. This way we obtain a splitting pattern which should only include massive splittings and which for the Higgs jet uniquely identifies the $H \to b\bar{b}$ decay. Making use of the scalar nature of the Higgs boson we can add an additional requirement on the balance based on $\min(p_{Tj_1}^2, p_{Tj_2}^2)\Delta R_{j_1 j_2}^2$. Of course, all actual numbers in this selection are subject to experimental scrutiny and can only be determined after testing the algorithm on LHC data.

Experimentally, the goal of such a Higgs search is a distribution of the invariant mass of the bottom quarks which gives us a signal peak and side bins to estimate the background. However, applying jet algorithms with very large R size makes us increasingly vulnerable to underlying event, pile-up, or even regular initial state radiation as described in Sect. 2.3.2. Therefore, we cannot simply use the mass of a set of constituents of the fat jet. Instead, we apply a filtering procedure looking at the same constituent with a higher resolution which can for example be $R_{\text{filt}} = \min(0.3, R_{b\bar{b}}/2)$. This filtering significantly reduces the $y - \phi$ surface area of the relevant constituents and thereby the destructive power of the underlying event and pile-up. The invariant mass we include in the histogram is the mass of the three hardest constituents, the two bottom quarks and possibly a radiated gluon.

In a *busy QCD environment* another problem arises: errand jets from initial state radiation or other particles in the final state enter the fat jet algorithm and give

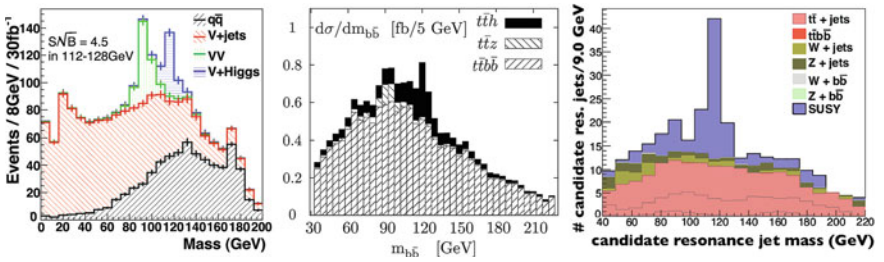

Fig. 3.1 Invariant mass distributions for Higgs searches using fat jets from $H \to b\bar{b}$ decays. For a Standard Model Higgs boson the production mechanisms are $pp \to WH/ZH$ (*left*) and $pp \to t\bar{t}H$ (*center*). In cascade decays of supersymmetric squarks and gluinos we can apply the same search for the light Higgs boson (*right*). Figures from Refs. [1–3] (*left* to *right*)

us several mass drops in the fat jet history. To avoid shaping the background side bins we can include several (filtered) subjet combinations, ordered in the modified Jade distance $p_{T,1}\,p_{T,2}(\Delta R_{12})^4$—the original Jade distance includes is given by $p_{T,1}\,p_{T,2}(\Delta R_{12})^2$. Examples for the invariant mass distributions for different Higgs search channels we show in Fig. 3.1. They include Standard Model Higgs searches in *WH/ZH* production, in $t\bar{t}H$ production, and light supersymmetric Higgs searches in the decays of squarks and gluinos.

From the above discussion we see that Higgs taggers rely only on *one kinematic criterion* the mass of the $b\bar{b}$ pair. In terms of background rejection this is not much, so we usually add two bottom tags on the constituents which according to detector simulations can be very efficient. The two combined add to a QCD rejection of at least 10^{-4}, which might even allows us to run a Higgs tagger over any kind of event sample and see if we find any Higgs bosons for example in new physics decays.

While fat jet Higgs searches are targeted mostly at the Standard Model, looking for other boosted heavy particles is usually motivated by new physics scenarios. Looking for massive particles decaying to heavy quarks *top taggers* should be the next step. Starting from a C/A jet of size up to $R = 1.5$ we again search for mass drops, this time corresponding to the top and W masses. After appropriate filtering we apply these two mass windows conditions; the entire fat jet has to reproduce the top mass. Next, we require a mass drop corresponding to the W decay and effectively constrain a second combination of two decay jets evaluating the helicity angle of the left handed W decay. Instead of these two distinct steps we can also apply a two-dimensional condition on the kinematics of the three top decay products which avoids assigning the two W decay jets in cases where two combinations of decay jets give similar invariant masses. On the simulation level both methods give equivalent results.

Applying these three kinematic conditions for example in the HEPTopTagger implementation gives a QCD rejection of a few per-cent. If this should not be sufficient for a given analysis we can increase the rejection rate by requiring a bottom tag which as a bonus also tells us which of the three top decay jets should reconstruct the

W mass. When we use top taggers to look for new particles decaying to top quarks we are not only interested in finding boosted top quarks, but we would like to know their invariant mass. This means we would like to reconstruct their direction and their energy. Such a reconstruction is possible in a reasonably clean sample without too many QCD jets, i.e. provided the top quarks have large enough energy to boost all three decay jets into a small enough cone.

While it seems like the C/A jet algorithm with its purely geometric selection has the best potential to search for massive particles in its jet history there exists a multitude of algorithms searching for boosted top quarks. Once the top quarks have very large transverse momenta the two-step mass drop criterion becomes less critical because the three decay jets are too close to be cleanly resolved. In this situation analyses based on the k_T or anti-k_T algorithms can be very promising, as could be event shapes which do not involve any jet algorithm.

3.2 Helicity Amplitudes

When we simulate LHC events we do not actually rely on the approach usually described in text books. This is most obvious when it comes to the computation of a transition matrix elements in modern LHC Monte Carlo tools, which you will not even recognize when looking at the codes. In Sect. 2.1 we compute the cross section for Z production by writing down all external spinors, external polarization vectors, interaction vertices and propagators and squaring the amplitude analytically. The amplitude itself inherits external indices for example from the polarization vectors, while $|\mathscr{M}|^2$ is a real positive number with a fixed mass dimension depending on the number of external particles.

For the LHC nobody calculates gamma matrix traces by hand anymore. Instead, we use powerful tools like Form to compute traces of Dirac matrices in the calculation of $|\mathscr{M}|^2$. Nevertheless, a major problem with squaring Feynman diagrams and computing polarization sums and gamma matrix traces is that once we include more than three particles in the final state, the number of terms appearing in $|\mathscr{M}|^2$ soon becomes very large. Moreover, this approach requires symbolic computer manipulation instead of pure numerics. In this section we illustrate how we can transform the computation of $|\mathscr{M}|^2$ at the tree level into a purely numerical problem.

As an example, we consider our usual toy process

$$u\bar{u} \to \gamma^* \to \mu^+\mu^-. \tag{3.3}$$

The structure of the amplitude $\mathscr{M}$ with two internal Dirac indices μ and ν involves one vector current on each side $(\bar{u}_f \gamma_\mu u_f)$ where $f = u, \mu$ are massless fermions, so we do not have to be careful with the different spinors u and v. The entries in the external spinors are given by the spin of the massless fermions obeying the Dirac equation. For each value of $\mu = 0 \cdots 3$ each current is a complex number, computed from the four component of each spinor and the respective 4×4 gamma matrix γ^μ

shown in Eq. 2.106. The intermediate photon propagator has the form $g_{\mu\nu}/s$, which is a real number for each value of $\mu = \nu$. Summing over μ and ν in both currents forms the matrix element. To square this matrix element we need to sum $\mathscr{M}^* \times \mathscr{M}$ over all possible spin directions of the external fermions.

Instead of squaring this amplitude symbolically we can follow exactly the steps described above and compute an array of numbers for different spin and helicity combinations numerically. Summing over the internal Dirac indices we compute the matrix element; however, to compute the matrix element squared we need to sum over external fermion spin directions or gauge boson polarizations. The helicity basis we have to specify externally. This is why this method is called helicity amplitude approach. To explain the way this method works, we illustrate it for muon pair production based on the implementation in the *MadGraph/Helas* package.

MadGraph as part of the event generator MadEvent is a tool to compute matrix elements this way. Other event generators have corresponding codes serving the same purposes. In our case, MadGraph automatically produces a Fortran routine which then calls functions to compute spinors, polarization vectors, currents of all kinds, etc. These functions are available as the so-called Helas library. For our toy process Eq. 3.3 the MadGraph output reads

```
      REAL*8 FUNCTION UUB_MUPMUM(P,NHEL)
C
C FUNCTION GENERATED BY MADGRAPH
C RETURNS AMPLITUDE SQUARED SUMMED/AVG OVER COLORS
C FOR PROCESS : u u~ -> mu+ mu-
C
      INTEGER    NGRAPHS,    NEIGEN,    NEXTERNAL
      PARAMETER (NGRAPHS=   1,NEIGEN=  1,NEXTERNAL=4)
      INTEGER    NWAVEFUNCS     , NCOLOR
      PARAMETER (NWAVEFUNCS=   5, NCOLOR=   1)

      REAL*8 P(0:3,NEXTERNAL)
      INTEGER NHEL(NEXTERNAL)

      INCLUDE 'coupl.inc'

      DATA Denom(1  )/            1/
      DATA (CF(i,1  ),i=1  ,1  ) /     3/

      CALL IXXXXX(P(0,1   ),ZERO ,NHEL(1   ),+1,W(1,1   ))
      CALL OXXXXX(P(0,2   ),ZERO ,NHEL(2   ),-1,W(1,2   ))
      CALL IXXXXX(P(0,3   ),ZERO ,NHEL(3   ),-1,W(1,3   ))
      CALL OXXXXX(P(0,4   ),ZERO ,NHEL(4   ),+1,W(1,4   ))
      CALL JIOXXX(W(1,1   ),W(1,2   ),GAU ,ZERO    ,ZERO    ,W(1,5   ))
      CALL IOVXXX(W(1,3   ),W(1,4   ),W(1,5   ),GAL ,AMP(1   ))
      JAMP(   1) = +AMP(   1)

      DO I = 1, NCOLOR
          DO J = 1, NCOLOR
              ZTEMP = ZTEMP + CF(J,I)*JAMP(J)
          ENDDO
          UUB_MUPMUM =UUB_MUPMUM+ZTEMP*DCONJG(JAMP(I))/DENOM(I)
      ENDDO
      END
```

The input to this function are the external four-momenta $p(0:3, 1:4)$ and the helicities of all fermions $n_{\text{hel}}(1:4)$ in the process. Remember that helicity and chirality are identical only for massless fermions because chirality is defined as the

eigenvalue of the projectors $(\mathbb{1} \pm \gamma_5)/2$, while helicity is defined as the projection of the spin onto the momentum direction, i.e. as the left or right handedness. The entries of n_{hel} will be either $+1$ or -1. For each point in phase space and each helicity combination the MadGraph subroutine `SUUB_MUPMUM` computes the matrix element using standard *Helas routines*.

- `IXXXXX`$(p, m, n_{\text{hel}}, n_{\text{sf}}, F)$ computes the wave function of a fermion with incoming fermion number, so either an incoming fermion or an outgoing anti-fermion. As input it requires the four-momentum, the mass and the helicity of this fermion. Moreover, $n_{\text{sf}} = +1$ marks the incoming fermion u and $n_{\text{sf}} = -1$ the outgoing anti-fermion μ^+, because by convention MadGraph defines its particles as u and μ^-.

  The fermion wave function output is a complex array $F(1:6)$. Its first two entries are the left-chiral part of the fermionic spinor, i.e. $F(1:2) = (\mathbb{1} - \gamma_5)/2\, u$ or $F(1:2) = (\mathbb{1} - \gamma_5)/2\, v$ for $n_{\text{sf}} = \pm 1$. The entries $F(3:4)$ are the right-chiral spinor. These four numbers can directly be computed from the four-momentum if we know the helicity. The four entries correspond to the size of one γ matrix, so we can compute the trace of the chain of gamma matrices. Because for massless particles helicity and chirality are identical our quarks and leptons will only have finite entries $F(1:2)$ for $n_{\text{hel}} = -1$ and $F(3:4)$ for $n_{\text{hel}} = +1$.

  The last two entries of F contain the four-momentum in the direction of the fermion flow, namely $F(5) = n_{\text{sf}}(p(0) + ip(3))$ and $F(6) = n_{\text{sf}}(p(1) + ip(2))$.
- `OXXXXX`$(p, m, n_{\text{hel}}, n_{\text{sf}}, F)$ does the same for a fermion with outgoing fermion flow, i.e. our incoming $\bar{u}$ and our outgoing μ^-. The left-chiral and right-chiral components now read $F(1:2) = \bar{u}(\mathbb{1} - \gamma_5)/2$ and $F(3:4) = \bar{u}(\mathbb{1} + \gamma_5)/2$, and similarly for the spinor $\bar{v}$. The last two entries are $F(5) = n_{\text{sf}}(p(0) + ip(3))$ and $F(6) = n_{\text{sf}}(p(1) + ip(2))$.
- `JIOXXX`$(F_i, F_o, g, m, \Gamma, J_{io})$ computes the (off-shell) current for the vector boson attached to the two external fermions F_i and F_o. The coupling $g(1:2)$ is a complex array with the interaction of the left-chiral and right-chiral fermion in the upper and lower index. For a general Breit–Wigner propagator we need to know the mass m and the width Γ of the intermediate vector boson. The output array J_{io} again has six components which for the photon with momentum q are

$$\begin{aligned} J_{io}(\mu+1) &= -\frac{i}{q^2}\, F_o^T\, \gamma^\mu \left(g(1)\, \frac{\mathbb{1} - \gamma_5}{2} + g(2)\, \frac{\mathbb{1} + \gamma_5}{2} \right) F_i \\ J_{io}(5) &= -F_i(5) + F_o(5) \sim -p_i(0) + p_o(0) + i\,(-p_i(3) - p_o(3)) \\ J_{io}(6) &= -F_i(6) + F_o(6) \sim -p_i(1) + p_o(1) + i\,(-p_i(2) + p_o(2)). \end{aligned} \tag{3.4}$$

  The first four entries in J_{io} correspond to the index μ or the dimensionality of the Dirac matrices in this vector current. The spinor index is contracted between F_o^T and F_i.

  As two more arguments J_{io} includes the four-momentum flowing through the gauge boson propagator. They allow us to reconstruct q^μ from the last two entries

$$q^\mu = (\mathrm{Re}J_{io}(5), \mathrm{Re}J_{io}(6), \mathrm{Im}J_{io}(6), \mathrm{Im}J_{io}(5)). \tag{3.5}$$

- `IOVXXX`(F_i, F_o, J, g, V) computes the amplitude of a fermion–fermion–vector coupling using the two external fermionic spinors F_i and F_o and an incoming vector current J which in our case comes from `JIOXXX`. Again, the coupling $g(1:2)$ is a complex array, so we numerically compute

$$F_o^T \boldsymbol{J} \left(g(1) \frac{\mathbb{1} - \gamma_5}{2} + g(2) \frac{\mathbb{1} + \gamma_5}{2} \right) F_i. \tag{3.6}$$

  All spinor and Dirac indices of the three input arguments are contracted in the final result. Momentum conservation is not enforced by `IOVXXX`, so we have to take care of it by hand.

Given the list above it is easy to follow how MadGraph computes the amplitude for $u\bar{u} \to \gamma^* \to \mu^+\mu^-$. First, it calls wave functions for all external particles and puts them into the array $W(1:6, 1:4)$. The vectors $W(*, 1)$ and $W(*, 3)$ correspond to $F_i(u)$ and $F_i(\mu^+)$, while $W(*, 2)$ and $W(*, 4)$ mean $F_o(\bar{u})$ and $F_o(\mu^-)$.

The first vertex we evaluate is the incoming quark-photon vertex. Given the wave functions $F_i = W(*, 1)$ and $F_o = W(*, 2)$ `JIOXXX` computes the vector current for the massless photon in the s channel. Not much changes if we instead choose a massive Z boson, except for the arguments m and Γ in the `JIOXXX` call. Its output is the photon current $J_{io} \equiv W(*, 5)$.

The last step combines this current with the two outgoing muons coupling to the photon. Since this number gives the final amplitude, it should return a complex number, not an array. MadGraph calls `IOVXXX` with $F_i = W(*, 3)$ and $F_o = W(*, 4)$, combined with the photon current $J = W(*, 5)$. The result `AMP` is copied into `JAMP` without an additional sign which could have come from the relative ordering of external fermions in different Feynman diagrams contributing to the same process.

The only remaining sum left to compute before we square `JAMP` is the color structure, which in our simple case means one color structure with a color factor $N_c = 3$.

As an added bonus MadGraph produces a file with all Feynman diagrams in which the numbering of the external particles corresponds to the second argument of W and the numbering of the Feynman diagrams corresponds to the argument of `AMP`. This helps us identify intermediate results W, each of which is only computed once, even if is appears several times in the different Feynman diagrams.

As mentioned above, to calculate the transition amplitude MadGraph requires all masses and couplings. They are transferred through common blocks in the file coupl.inc and computed elsewhere. In general, MadGraph uses unitary gauge for all vector bosons, because in the helicity amplitude approach it is easy to accommodate complicated tensors, in exchange for a large number of Feynman diagrams.

The function `UUB_MUPMUM` described above is not yet the full story. When we square $\mathscr{M}$ symbolically we need to sum over the spins of the outgoing states to transform a spinor product of the kind $u\bar{u}$ into the residue or numerator of a fermion

propagator. To obtain the full transition amplitude numerically we correspondingly sum over all *helicity combinations* of the external fermions, in our case $2^4 = 16$ combinations.

```
      SUBROUTINE SUUB_MUPMUM(P1,ANS)
C
C FUNCTION GENERATED BY MADGRAPH
C RETURNS AMPLITUDE SQUARED SUMMED/AVG OVER COLORS
C AND HELICITIES FOR THE POINT IN PHASE SPACE P(0:3,NEXTERNAL)
C
C FOR PROCESS : u u~ -> mu+ mu-
C
      INTEGER    NEXTERNAL,   NCOMB,
      PARAMETER (NEXTERNAL=4, NCOMB= 16)
      INTEGER    THEL
      PARAMETER (THEL=NCOMB*1)

      REAL*8 P1(0:3,NEXTERNAL),ANS

      INTEGER NHEL(NEXTERNAL,NCOMB),NTRY
      REAL*8 T, UUB_MUPMUM
      INTEGER IHEL,IDEN,IC(NEXTERNAL)
      INTEGER IPROC,JC(NEXTERNAL)
      LOGICAL GOODHEL(NCOMB)

      DATA GOODHEL/THEL*.FALSE./
      DATA NTRY/0/

      DATA (NHEL(IHEL,  1),IHEL=1,4) / -1, -1, -1, -1/
      DATA (NHEL(IHEL,  2),IHEL=1,4) / -1, -1, -1,  1/
      DATA (NHEL(IHEL,  3),IHEL=1,4) / -1, -1,  1, -1/
      DATA (NHEL(IHEL,  4),IHEL=1,4) / -1, -1,  1,  1/
      DATA (NHEL(IHEL,  5),IHEL=1,4) / -1,  1, -1, -1/
      DATA (NHEL(IHEL,  6),IHEL=1,4) / -1,  1, -1,  1/
      DATA (NHEL(IHEL,  7),IHEL=1,4) / -1,  1,  1, -1/
      DATA (NHEL(IHEL,  8),IHEL=1,4) / -1,  1,  1,  1/
      DATA (NHEL(IHEL,  9),IHEL=1,4) /  1, -1, -1, -1/
      DATA (NHEL(IHEL, 10),IHEL=1,4) /  1, -1, -1,  1/
      DATA (NHEL(IHEL, 11),IHEL=1,4) /  1, -1,  1, -1/
      DATA (NHEL(IHEL, 12),IHEL=1,4) /  1, -1,  1,  1/
      DATA (NHEL(IHEL, 13),IHEL=1,4) /  1,  1, -1, -1/
      DATA (NHEL(IHEL, 14),IHEL=1,4) /  1,  1, -1,  1/
      DATA (NHEL(IHEL, 15),IHEL=1,4) /  1,  1,  1, -1/
      DATA (NHEL(IHEL, 16),IHEL=1,4) /  1,  1,  1,  1/
      DATA (  IC(IHEL,  1),IHEL=1,4) /  1,  2,  3,  4/
      DATA (IDEN(IHEL),IHEL=  1,  1) /  36/

      NTRY=NTRY+1
      DO IHEL=1,NEXTERNAL
         JC(IHEL) = +1
      ENDDO

      DO IHEL=1,NCOMB
         IF (GOODHEL(IHEL,IPROC) .OR. NTRY .LT. 2) THEN
            T = UUB_MUPMUM(P1,NHEL(1,IHEL),JC(1))
            ANS = ANS + T
            IF (T .GT. 0D0 .AND. .NOT. GOODHEL(IHEL,IPROC)) THEN
               GOODHEL(IHEL,IPROC)=.TRUE.
            ENDIF
         ENDIF
      ENDDO
      ANS = ANS/DBLE(IDEN)

      END
```

The important part of this subroutine is the list of possible helicity combinations stored in the array $n_{\text{hel}}(1:4, 1:16)$. Adding all different helicity combinations means a loop over the second argument and a call of `UUB_MUPMUM` with the respective helicity combination. Because of the naive helicity combinations many are not allowed the array `GOODHEL` keeps track of valid combinations. After an initialization to all 'false' this array is only switched to 'true' if `UUB_MUPMUM` returns a finite value, otherwise MadGraph does not waste time to compute the matrix element. At the very end, a complete spin-color averaging factor is included as `IDEN` and in our case given by $2 \times 2 \times N_c^2 = 36$.

Altogether, MadGraph provides us with the subroutine `SUUB_MUPMUM` and the function `UUB_MUPMUM` which together compute $\overline{|\mathscr{M}|^2}$ for each phase space point, i.e. for each external momentum configuration. This helicity method might not seem particularly appealing for a simple $(2 \to 2)$ process, but it makes it possible to compute processes with four and more particles in the final state and typically up to 10,000 Feynman diagrams which we could never square symbolically, no matter how many graduate students' live times we throw in.

3.3 Missing Transverse Energy

Some of the most interesting signatures at the LHC involve dark matter particles. From cosmological constraints we know that dark matter definitely interacts gravitationally and that it cannot carry electromagnetic or color charges. Weak interactions are allowed because of their limited reach. It turns out that a weakly interacting particle with a mass around the electroweak scale typically gives the observed relic density in the universe. This is called the *WIMP miracle*. It is the reason why in modern TeV-scale model building every model (and its dog) predict a stable WIMP. From supersymmetry we know that this is not hard to achieve: all we need is a $\mathbb{Z}_2$ symmetry, i.e. a *multiplicative quantum number* for (a sector of) newly introduced particles. In supersymmetry this is called R parity, in Little–Higgs models T parity, and in extra dimensional models Kaluza–Klein parity.

At the LHC we typically produce strongly interacting new particles, provided they exist. If a conserved dark matter quantum number exists we will always produce them in pairs. Each of them decays to the weakly interacting sector which includes a stable dark matter agent. On the way, the originally produced particles have to radiate quarks or gluons to get shed their color charge. If in some kind of cascade decays they also radiate leptons or photons those can be very useful to trigger on and to reduce QCD backgrounds, but this depends on the details of the weakly interacting new physics sector. The decay steps ideally are two body decays from on-shell particle to on-shell particle, but they do not have to be. What we therefore look for is jets in association with pairs of only weakly interacting, hence invisible particles in the ATLAS and CMS detectors.

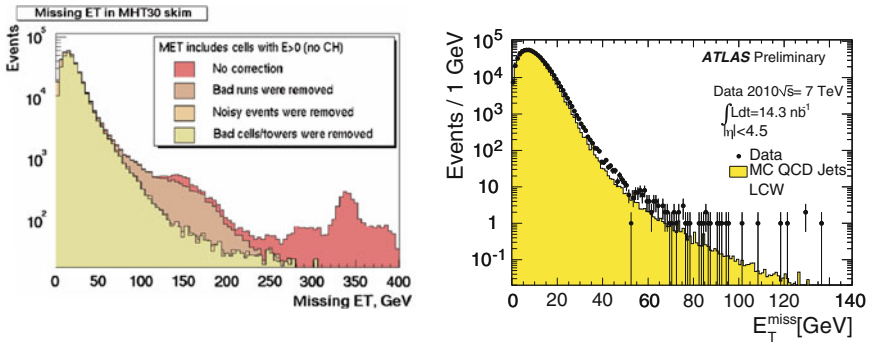

Fig. 3.2 *Left* Missing energy distribution from the early running phase of the DZero experiment at the Tevatron. Figure from Beate Heinemann. *Right* Corrected missing energy distribution in QCD events at ATLAS using only data from April/May 2010 at 7 TeV collider energy. Figure from Ref. [4]

From Eq. 2.28 and the discussion of parton densities we remember that at hadron colliders we do not know the kinematics of the initial state. In beam direction we only know its boost statistically, whereas in the transverse plane by definition the incoming partons have zero momentum. The way to look for invisible particles therefore is a mis-balance of three-momentum in the transverse plane. The actual observable is the *missing transverse momentum* i.e. the vector sum of the transverse momenta of all invisible particles. We can convert it into a missing transverse energy which in the absence of any information on particle masses is defined as the absolute value of the two-dimensional missing momentum vector. LHC events including dark matter are characterized by a high jet multiplicity and large missing transverse energy.

At the end of Sect. 2.5.3 we focus on the proper simulation of W+jets and Z+jets samples, which are the Standard Model backgrounds to such signals. It will turn out that jet merging is needed to reliably predict the missing transverse momentum distributions in Standard Model processes. After all our studies in Chap. 2 we are at least theoretically on safe ground. However, this is not the whole story of missing transverse momentum.

3.3.1 Measuring Missing Energy

The left panel of Fig. 3.2 is a historic missing transverse energy distribution from DZero. It nicely illustrates that by just measuring missing transverse energy, Tevatron would have discovered supersymmetry based on two beautiful peaks around 150 GeV and around 350 GeV. However, this preliminary experimental result has nothing to do with physics, it is purely a detector effect.

The problem of missing energy we can illustrate using a simple number: to identify and measure a lepton we need around 500 out of 200,000 calorimeter cells in an

experiment like ATLAS, while for missing transverse energy we need all of them. To cut on a variable like missing transverse momentum we need to understand our detectors really well, and for this level of understanding we need time.

There are several sources of missing energy which we have to understand before we get to search for new physics:

- First, we have to subtract bad runs. They happen if for a few hours parts of the detector does not work properly. We can identify them by looking at the detector response and its correlation. One example is a so-called ring of fire where we see coherent effects in detector modules of circular shape around the beam axis.
- Next, there will be coherent noise in the calorimeter. With 200,000 cells we know that some of them will individually fail or produce noise. Some sources of noise, like leaking voltage or other electronic noise can be correlated geometrically and lead to beautiful missing momentum signals. The way to get rid of such noise event by event is to again look for usual detector response. Combined with bad runs such events can constitute $\mathcal{O}(0.1\%)$ of all events and get removed from the data sample.
- In addition, there might be particles crossing our detector, but not coming from the interaction point. They can be cosmic rays and lead to unbalanced energy deposition as well. Such events will have reconstructed particle tracks which are not compabible with the measured primary vertex.
- Another source of fake missing energy is failing calorimeter cells, like continuously hot cells or dead cells. ATLAS for example has developed such a hole by 2010. Events where missing energy points into such a region can often be removed once we understand the detector.
- While not really a detector fake the main source of missing energy at hadron colliders are mis-measured QCD jets. If parts of jets point into regions with poor calorimetry, like support structures, the jet energy will be wrongly measured, and the corresponding QCD event will show missing transverse energy. One way to tackle this problem is to require a geometric separation of the missing momentum vector and hard jets in the event. ATLAS detector studies indicate that up to $\mathcal{O}(0.1-1\%)$ of all hard QCD events at the LHC lead to more than 100 GeV of well separated fake missing transverse energy. Figure 1.5 in Sect. 1.4.3 shows that this is not at all a negligible number of events.

Once we understand all sources of fake missing momentum we can focus on real missing momentum. This missing transverse momentum we compute from the momenta of all tracks seen in the detector. This means that any uncertainty on these measurements, like the jet or lepton energy scale will smear the missing momentum. Moreover, we know that there is for example dead matter in the detector, so we have to compensate for this. This compensation is a global correction to individual events, which means it will generally smear the missing energy distribution. The right panel of Fig. 3.2 shows a very early missing transverse energy distribution of ATLAS after some of the corrections described above.

To simulate a realistic missing transverse momentum distribution at the LHC we have to smear all jet and lepton momenta, and in addition apply a Gaussian *smearing*

of the order

$$\frac{\Delta \not{E}_T}{\text{GeV}} \sim \frac{1}{2}\sqrt{\frac{\sum E_T}{\text{GeV}}} \gtrsim 20. \tag{3.7}$$

While this sounds like a trivial piece of information I cannot count the number of papers where people forget this smearing and discover great channels to look for Higgs bosons or new physics. They fall apart when experimentalists take a careful look. The simple rule is: phenomenological studies are right or wrong based on if they can be reproduced by real experimentalists and real detectors or not.

3.3.2 Missing Energy in the Standard Model

In the Standard Model there exists a particle which only interacts weakly: the neutrino. At colliders we produce them in reasonably large numbers in W decays. This means that in W+ jets production we can learn how to reconstruct the mass of a leptonically decaying W, i.e. one observed and one missing particle. We construct a *transverse mass* in analogy to an invariant mass, but neglecting the longitudinal momenta of the decay products

$$\begin{aligned} m_T^2 &= \left(E_{T,\text{miss}} + E_{T,\ell}\right)^2 - \left(\vec{p}_{T,\text{miss}} + \vec{p}_{T,\ell}\right)^2 \\ &= m_\ell^2 + m_{\text{miss}}^2 + 2\left(E_{T,\ell} E_{T,\text{miss}} - \vec{p}_{T,\ell} \cdot \vec{p}_{T,\text{miss}}\right), \end{aligned} \tag{3.8}$$

in terms of a transverse energy $E_T^2 = \vec{p}_T^{\,2} + m^2$. Since the transverse mass is always smaller than the actual W mass and reaches this limit for realistic phase space regions we can extract m_W from the upper edge in the $m_{T,W}$ distribution. Obviously, we can define the transverse mass in many different reference frames. However, its value is invariant under—or better independent of—longitudinal boosts. Moreover, given that we construct it as the transverse projection of an invariant mass it is also invariant under transverse boosts. By construction we cannot analyze the transverse mass event by event, so this W mass measurement only uses the fraction of events which populate the upper end of the transverse mass distribution.

Alternatively, from single top production and the production of mixed leptonically and hadronically decaying top pairs we know another method to conditionally reconstruct masses and momenta involving one invisible particle: from a leptonically decaying top quark we only miss the longitudinal momentum of the neutrino. On the other hand, we know at least for the signal events that the neutrino and the lepton come from an on-shell W boson, so we can use this *on-shell condition* to reconstruct the longitudinal neutrino momentum under the assumption that the neutrino have zero mass. Recently, we have seen that sufficiently boosted top quarks with leptonic decays can be fully reconstructed even without using the measured missing energy vector. Instead, we rely on the W and t on-shell conditions and on an assumption about the neutrino momentum in relation to the bottom-lepton decay plane.

From Higgs searches we know how to extend the transverse mass to two leptonic W decays, i.e. two neutrinos in the final state. The definition of this transverse mass

$$\begin{aligned} m_{T,WW}^2 &= \left(E_{T,\text{miss}} + E_{T,\ell\ell}\right)^2 - \left(\vec{p}_{T,\text{miss}} + \vec{p}_{T,\ell\ell}\right)^2 \\ &= m_{\ell\ell}^2 + m_{\text{miss}}^2 + 2\left(E_{T,\ell\ell}E_{T,\text{miss}} - \vec{p}_{T,\ell\ell}\cdot\vec{p}_{T,\text{miss}}\right) \end{aligned} \tag{3.9}$$

is not unique because it is not clear how to define m_{miss}, which also enters the definition of $E_{T,\text{miss}}$. From Monte Carlo studies it seems that identifying $m_{\text{miss}} \equiv m_{\ell\ell}$, which is correct at threshold, is most strongly peaked. On the other hand, setting $m_{\text{miss}} = 0$ to define a proper bounded-from-above transverse mass variable seems to improve the Higgs mass extraction.

For an unspecified number of visible and invisible particles in the final state there also exist global observables we can rely on. The *visible mass* is based on the assumption that we are looking for the decay of two heavy new states where the parton densities will ensure that these two particles are non-relativistic. We can then approximate the partonic energy $\sqrt{\hat{s}} \sim m_1 + m_2$ by some kind of visible energy. If the heavy states are produced with little energy, boost invariance is not required for this construction. Without taking into account missing energy and adding leptons ℓ and jets j the visible mass looks like

$$m_{\text{visible}}^2 = \left[\sum_{\ell,j} E\right]^2 - \left[\sum_{\ell,j} \vec{p}\right]^2 . \tag{3.10}$$

Similarly, the Tevatron experiments have for a long time used an effective transverse mass scale which is usually evaluated for jets only, but can trivially be extended to leptons:

$$H_T = \sum_{\ell,j} E_T = \sum_{\ell,j} p_T , \tag{3.11}$$

where the last step assumes that all final state particles are massless. In an alternative definition of H_T we sum over a number of jets plus the missing energy and skip the hardest jet in this sum.

When combining such a measure with missing transverse momentum the question arises: Do we want to pair up the missing transverse momentum with the visible transverse momenta or with the complete visible momenta? For example, we can use the scalar sum of all transverse momenta in the event, now including the missing transverse momentum

$$m_{\text{eff}} = \sum_{\ell,j,\text{miss}} E_T = \sum_{\ell,j,\text{miss}} p_T . \tag{3.12}$$

This effective mass is known to trace the mass of the heavy new particles decaying for example to jets and missing energy. This interpretation relies on the non-relativistic nature of the production process and our confidence that all jets included are really decay jets.

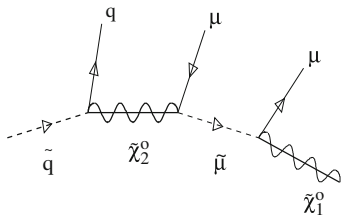

Fig. 3.3 Feynman diagram for the long decay chain shown in Eq. 3.13

3.3.3 Missing Energy and New Physics

The methods described in the last section are well studied for different Standard Model processes and can be applied in new physics searches for various lengths of decay chains. However, there is need for one significant modification, namely to account for a finite *unknown mass* of the carrier of the missing energy. This is a problem of relativistic kinematics and at leading order does not require any knowledge of QCD or new physics models.

The chain of three successive three-body decays shown in Fig. 3.3 is the typical left handed *squark cascade decay* in supersymmetry. The same topology we can interpret in extra-dimensional models (universal extra dimensions or UED) as the decay of a Kaluza–Klein quark excitation

$$\tilde{q}_L \to \tilde{\chi}_2^0 q \to \tilde{\ell}^{\pm}\ell^{\mp} q \to \tilde{\chi}_1^0 \ell^+\ell^- q \qquad Q_L^{(1)} \to Z^{(1)} q \to \ell^{(1)^{\pm}}\ell^{\mp} q \to \gamma^{(1)}\ell^+\ell^- q. \tag{3.13}$$

In both cases the last particle in the chain, the lightest neutralino or the Kaluza–Klein photon excitation pass the detectors unobserved. The branching ratio for such decays might not be particularly large; for example in the supersymmetric parameter point SPS1a with a mass spectrum we will discuss later in Fig. 3.7 the long squark decay ranges around 4%. On the other hand, strongly interacting new particles should be generously produced at the LHC, so we usually assume that there will be enough events to study. The question is how we can then extract the four masses of the new particles appearing in this decay from the three observed external momenta.

The proposals to solve this problem can be broadly classified into four classes. While all of them should in principle work and would then differ mostly by statistics, only for the first strategy we know how QCD and detector smearing affect them.

1. *Endpoint methods* extract masses from lower (threshold) and upper (edge) kinematic endpoints of invariant mass distributions of visible decay products. This method is best suited for long decay chains, where the number of independent endpoint measurements in one leg at least matches the number of unknown masses in the cascade. An implicit assumption of these endpoint techniques is that the form of the matrix element populates the phase space close to the endpoint well. Otherwise, the endpoint will be soft and difficult to identify on top of the continuum background.

The squark decay Eq. 3.13 has a particular kinematic feature: the invariant mass distributions of the two leptons $m_{\ell\ell}$. Looked at from the rest frame of the intermediate slepton it is a current–current interaction, similar to the Drell–Yan process computed in Eq. 2.11. Because in the s channel there now appears a scalar particle there cannot be any angular correlations between the two currents, which means the $m_{\ell\ell}$ distribution will have a triangular shape. Its upper limit, called the *dilepton edge*, we can compute: in the rest frame of the scalar lepton the three-momenta of the incoming and outgoing pair of particles have the absolute values $|\vec{p}| = |m^2_{\tilde{\chi}^0_{1,2}} - m^2_{\tilde{\ell}}|/(2m_{\tilde{\ell}})$. The lepton mass we set to zero. The invariant mass of the two lepton reaches its maximum if the two leptons are back-to-back, i.e. the scattering angle is $\cos\theta = -1$

$$\begin{aligned} m^2_{\ell\ell} &= (p_{\ell^+} + p_{\ell^-})^2 \\ &= 2\,(E_{\ell^+}E_{\ell^-} - |\vec{p}_{\ell^+}||\vec{p}_{\ell^-}|\cos\theta) \\ &< 2\,(E_{\ell^+}E_{\ell^-} + |\vec{p}_{\ell^+}||\vec{p}_{\ell^-}|) \\ &= 4\frac{m^2_{\tilde{\chi}^0_2} - m^2_{\tilde{\ell}}}{2m_{\tilde{\ell}}}\,\frac{m^2_{\tilde{\ell}} - m^2_{\tilde{\chi}^0_1}}{2m_{\tilde{\ell}}} \qquad \text{using} \quad E^2_{\ell^\pm} = \vec{p}^{\,2}_{\ell^\pm}. \end{aligned} \tag{3.14}$$

This kinematic statement is independent of the shape of the $m_{\ell\ell}$ distribution. For the particle assignments shown in Eq. 3.13 the kinematic endpoint are given by

$$0 < m^2_{\ell\ell} < \frac{(m^2_{\tilde{\chi}^0_2} - m^2_{\tilde{\ell}})(m^2_{\tilde{\ell}} - m^2_{\tilde{\chi}^0_1})}{m^2_{\tilde{\ell}}} \qquad 0 < m^2_{\ell\ell} < \frac{(m^2_{Z^{(1)}} - m^2_{\ell^{(1)}})(m^2_{\ell^{(1)}} - m^2_{\gamma^{(1)}})}{m^2_{\ell^{(1)}}}. \tag{3.15}$$

A problem in realistic applications of endpoint methods is combinatorics. We need to either clearly separate the decays of two heavy new states, or we need to combine a short decay chain on one side with a long chain on the other side. In supersymmetry this is naturally the case for associated squark and gluino production. A right handed squark often decays directly to the lightest neutralino which is the dark matter candidate in the model. The gluino has to radiate two quark jets to reach the weakly interacting sector of the model and can then further decay in many different ways. In other models this feature is less generic. The impressive potential of endpoint methods in the case of supersymmetry we will illustrate later in this section.

When looking at long cascade decays for example with two leptons we usually cannot tell which of the two leptons is radiated first. Therefore, endpoint techniques will always be plagued with *combinatorial background* from the mapping of the particle momenta on the decay topology. The same applies to QCD jet radiation vs decay jets. In this situation it is useful to consider the correlation of different invariant masses and their endpoints. The endpoint method can be extended to use invariant mass distributions from both sides of the event (hidden threshold techniques), and correlations between the distributions from each leg (wedgebox techniques).

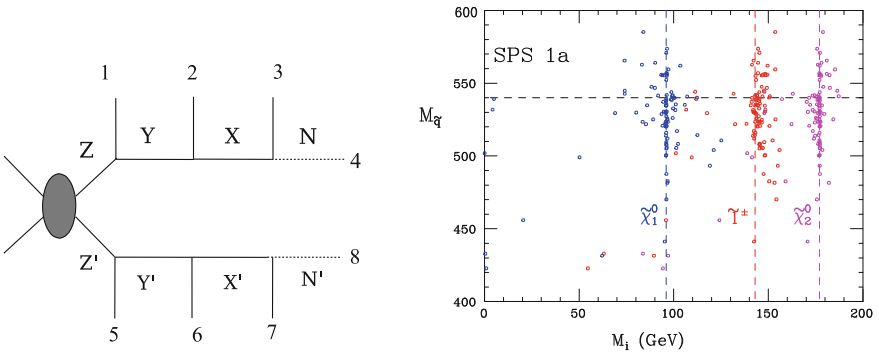

Fig. 3.4 Example for the mass relation method using three successive two-body decays on both sides of the events (*left*). After detector smearing we can reconstruct the masses for the supersymmetric parameter point SPS1a with the squark decay chain shown in Eq. 3.13 (*right*). Figure from Ref. [5]

2. *Mass relation methods* generalize the single-top example in Sect. 3.3.2 and completely reconstruct the kinematics event by event. For each event this construction provides a set of kinematic constraints. While for one event the number of parameters can be larger than the number of measurements, adding signal events increases the number of measurements while keeping the number of unknowns constant. Eventually, the system of equations will solve, provided all events are really signal events. Implicitly, we always assume that all decaying particles are on-shell, but we do not expect off-shell effects to have a huge effect on the results at the LHC.
   In Fig. 3.4 we show the general topology of a three-step cascade decay on each side of the event, like we expect it for a pair of left handed squarks following Eq. 3.13. To extract the masses of the new particles we need to solve the system of equations

$$\begin{aligned} (p_1 + p_2 + p_3 + p_4)^2 &= m_Z^2 \\ (p_2 + p_3 + p_4)^2 &= m_Y^2 \\ (p_3 + p_4)^2 &= m_X^2 \\ p_4^2 &= m_N^2 \end{aligned} \tag{3.16}$$

   for each side of the event. For each event there are eight unknown masses and six unknown missing momentum components of which we measure two combinations as the missing transverse momentum. All of these 12 unknowns we can determine if we add a sufficiently large number of events.
   One way to solve this starts with eight test masses $m = (m_Z^2, m_Y^2, m_X^2, m_N^2, \ldots)$, uses the three first equations in Eq. 3.16 for each event plus the two missing transverse momentum components to determine both missing four-momenta, and tests the consistency of this solution using the last line of Eq. 3.16 for each of the two legs. In this consistency test we combine the information from several events.

The first three lines in Eq. 3.16 we can conveniently solve for the missing momentum

$$\begin{aligned} -2(p_1 p_4) \equiv s_1 &= m_Y^2 - m_Z^2 + 2(p_1 p_2) + 2(p_1 p_3) \\ -2(p_2 p_4) \equiv s_2 &= m_X^2 - m_Y^2 + 2(p_2 p_3) \\ -2(p_3 p_4) \equiv s_3 &= m_N^2 - m_X^2, \end{aligned} \tag{3.17}$$

for simplicity assuming massless Standard Model decay products. Similarly, we define the measured combinations $s_{5,6,7}$ from the opposite chain. In addition, we measure the two-dimensional missing transverse momentum, so we can collect the two missing four-momenta into $p_{\text{miss}} = (\vec{p}_4, E_4, \vec{p}_8, E_8)$ and define two additional e ntries of the vector s in terms of measured quantities and masses like

$$\begin{aligned} (\hat{x}\, p_4) + (\hat{x}\, p_8) &= s_4 \\ (\hat{y}\, p_4) + (\hat{y}\, p_8) &= s_8. \end{aligned} \tag{3.18}$$

Combining the first equal signs of Eqs. 3.17 and 3.18 for both halves of the events reads $A \cdot p_{\text{miss}} = s$, where the matrix A includes only components of measured momenta and is almost block diagonal, so it can be inverted. Following the second equal sign in Eq. 3.17 we can then write $s = B \cdot m + c$, where the matrix B only contains non-zero entries ± 1 and the vector c consists of measured quantities. Together, this gives us

$$p_{\text{miss}} = A^{-1} s = A^{-1} B m + A^{-1} c. \tag{3.19}$$

The result for all masses in the decay chain using 25 events per set and including all combinatorics we show in Fig. 3.4. The mass relation method has also been successfully applied to single legs as well as in combination with kinematic endpoints.

3. *MT2 methods* are based on a global variable m_{T2}. It generalizes the transverse mass known from W decays to the case of two massive invisible particles, one from each leg of the event. The observed missing energy in the event we can divide into two scalar fractions $p_{T,\text{miss}} = q_1 + q_2$. Given the two fractions q_j we can construct a transverse mass for each side of the event, assuming we know the invisible particle's mass $m_{T,j}(q_j; \hat{m}_{\text{miss}})$; the second argument is an external assumption, i.e. $\hat{m}_{\text{miss}}$ is an assumed value for m_{miss}.
Inspired by the usual transverse mass we are interested in a mass variable with a well-defined upper edge, so we need to construct some kind of minimum of $m_{T,j}$ as a function of the splitting of $p_{T,\text{miss}}$. Naively, this minimum will simply be the zero transverse momentum limit of m_T on one leg, which is not very interesting. On the other hand, in this case the transverse mass from the other leg reaches a maximum, so we can instead define

$$m_{T2}(\hat{m}_{\text{miss}}) = \min_{p_{T,\text{miss}} = q_1 + q_2} \left[\max_j \; m_{T,j}(q_j; \hat{m}_{\text{miss}}) \right] \tag{3.20}$$

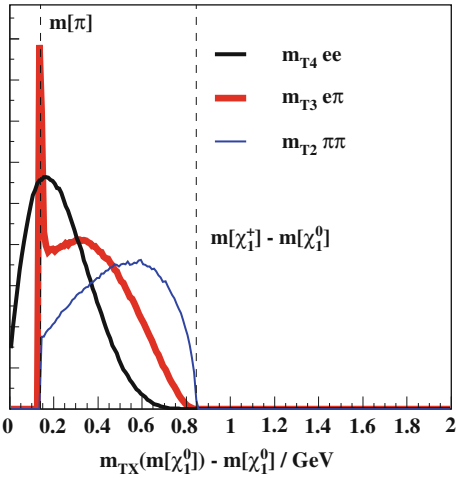

Fig. 3.5 Simulations for different m_{TX}, for the decay $\tilde{\chi}_1^+ \to \tilde{\chi}_1^0 \pi$ or $\tilde{\chi}_1^+ \to \tilde{\chi}_1^0 e^+ \nu$. The *blue* m_{T2} line applies to the two-body decay. Figure from Ref. [6]

as a function of the unknown missing particle mass. There are a two properties we know by construction

$$\begin{aligned} m_{\text{light}} + \hat{m}_{\text{miss}} &< m_{T2}(\hat{m}_{\text{miss}}) \\ m_{\text{light}} + m_{\text{miss}} &< m_{T2}(m_{\text{miss}}) < m_{\text{heavy}}. \end{aligned} \tag{3.21}$$

The first line means that each of the $m_{T,j}$ lie between the sum of the two decay products' masses and the mass of the decaying particle, so for massless Standard Model decay products there will be a global m_{T2} threshold at the missing particle's mass.

Moreover, for the correct value of m_{miss} the m_{T2} distribution has a sharp edge at the mass of the parent particle. In favorable cases m_{T2} may allow the measurement of both the parent particle and the LSP based on a single-step decay chain. These two aspects for the correct value $\hat{m}_{\text{miss}} = m_{\text{miss}}$ we can see in Fig. 3.5: the lower threshold is indeed given by $m_{T2} - m_{\tilde{\chi}_1^0} = m_\pi$, while the upper edge of $m_{T2} - m_{\tilde{\chi}_1^0}$ coincides with the dashed line for $m_{\tilde{\chi}_1^+} - m_{\tilde{\chi}_1^0}$.

An interesting aspect of m_{T2} is that it is boost invariant if and only if $\hat{m}_{\text{miss}} = m_{\text{miss}}$. For a wrong assignment of m_{miss} it has nothing to do with the actual kinematics and hence with any kind of invariant, and house numbers are not boost invariant. This aspect we can exploit by scanning over m_{miss} and looking for so-called kinks, i.e. points where different events kinematics all return the same value for m_{T2}.

Similar to the more global m_{eff} variable we can generalize m_{T2} to the case where we do not have a clear assignment of the two decay chains involved. This modification $M_{T\text{Gen}}$ again has an upper edge, which unfortunately is not as sharp as the one in m_{T2}. Similarly, the procedure can be generalized to any one-step decay, for example a three-body decay with either one or two missing particles on each

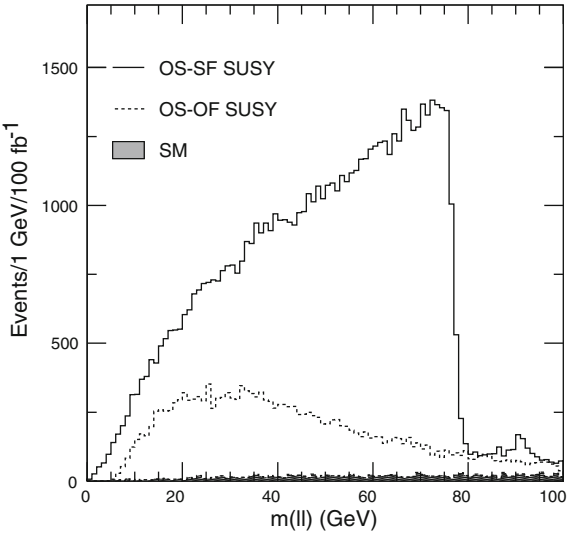

Fig. 3.6 Invariant mass of two leptons after selection cuts for the SPS1a parameter point: SUSY signal Opposite Sign Same Flavor (OS-SF): *full line*; SUSY signal Opposite Sign Opposite Flavor (OS-OF): *dotted line*; Standard Model background: *grey*. Figure from Giacomo Polesello (ATLAS)

side of the event. Such $M_{T\,X}$ distributions are useful as long as they have a sharp enough edge, as illustrated in Fig. 3.5.

4. *Extreme kinematics* can also give us a handle on mass reconstruction from an incomplete set of observables. One such phase space region are points close kinematic endpoints where particles are produced at rest. Other examples are the approximate collinear Higgs mass reconstruction in a decay to boosted tau pairs described in Sect. 1.5.3 or the boosted leptonic top decays mentioned before.

The way mass measurements can lead to proper *model reconstruction* we sketch for one scenario. The classic example for the endpoint method is the long supersymmetric left handed squark decay chain shown in Eq. 3.13 and in Fig. 3.3. When we use such kinematic endpoints or other methods to extract mass parameters it is crucial to start from a signal-rich sample to avoid combinatorics and washed out endpoints vanishing in a fluctuating or even sculptured background. For jets, leptons and missing energy a major background will be top pairs. The key observation is that in long cascade decays the leptons are flavor-locked, which means the combination $e^+e^- + \mu^+\mu^- - e^-\mu^+ - e^+\mu^-$ becomes roughly twice $\mu^+\mu^-$ for the signal, while it cancels for top pairs. Using such a combination for the endpoint analysis means the top background is subtracted purely from data, as illustrated in Fig. 3.6.

The long squark decay in SPS1a-like parameter points with squark masses in the 500 to 600 GeV range has an important advantage: for a large *mass hierarchy* we should be able to isolate the one decay jet just based on its energy. In complete analogy to the dilepton edge shown in Eq. 3.15, but with somewhat reduced elegance we can measure the threshold and edge of the $\ell^+\ell^- q$ distribution and the edges of the two $\ell^\pm q$ combinations. Then, we solve the system for the intermediate masses without any model assumption, which allows us to even measure the dark matter

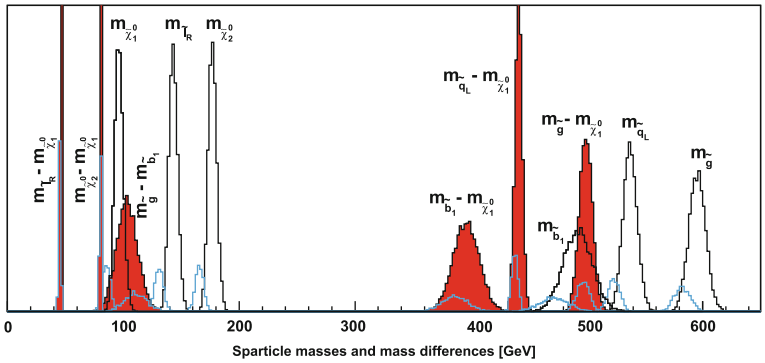

Fig. 3.7 Masses extracted from the gluino-sbottom decay chain, including estimated errors. The faint *blue lines* indicate wrong solutions when inverting the endpoint-mass relations. The supersymmetric mass spectrum is given by the SPS1a parameter point. Figure from Ref. [7]

mass to $\mathcal{O}(10\%)$. The limiting factors will likely be our chances to observe enough endpoints in addition to $m_{\ell\ell}^{\max}$ and the jet energy scale uncertainty. An interesting question is how well we will do with tau leptons, where the edge is softened by neutrinos from tau decays.

Provided the gluino or heavy gluon is heavier than the squarks or heavy quarks we can measure its mass by extending the squark chain by one step: $\tilde{g} \to q\tilde{q}$. This measurement is hard if one of the two jets from the gluino decay is not very hard, because its information will be buried by the combinatorial error due to QCD jet radiation. The way around is to ask for two bottom jets from the strongly interacting decay: $\tilde{g} \to b\tilde{b}^*$ or $G^{(1)} \to b\bar{B}^{(1)}$. The summary of all measurements in Fig. 3.7 shows that for example the gluino mass we can extract at the per-cent level, a point at which we might have to start thinking about off-shell propagators and at some point even define what exactly we mean by 'masses as appearing in cascade decays'.

A generic feature or all methods relying on decay kinematics is that it is easier to constrain the differences of squared masses than the absolute mass scale. This is also visible in Fig. 3.7. It is due to the form of the endpoint formulas which involve the difference of mass squares $m_1^2 - m_2^2 = (m_1 + m_2)(m_1 - m_2)$. This combination is much more sensitive to $(m_1 - m_2)$ than it is to $(m_1 + m_2)$. Experimentally, correlated jet and lepton energy scale uncertainties do not make life easier either. Nevertheless, the common lore that kinematics only constrain mass differences is obviously not true for two body decays.

Alternatively, we can use the same gluino decay to first reconstruct the intermediate neutralino or Kaluza–Klein Z momentum for lepton pairs residing near the $m_{\ell\ell}$ edge. In that case the invisible heavy state is produced approximately at rest, and the momenta are correlated as

$$\vec{p}_{\tilde{\chi}_2^0} = \left(1 - \frac{m_{\tilde{\chi}_1^0}}{m_{\ell\ell}}\right) \vec{p}_{\ell\ell} \qquad \vec{p}_{Z^{(1)}} = \left(1 - \frac{m_{\gamma^{(1)}}}{m_{\ell\ell}}\right) \vec{p}_{\ell\ell} \tag{3.22}$$

If both neutralino masses (or the Kaluza–Klein photon and Z masses) are known we can extract the sbottom (Kaluza–Klein bottom) and gluino (Kaluza–Klein gluon) masses by adding the measured bottom momenta to this neutralino (Kaluza–Klein photon) momentum. Again, for the mass spectrum shown in Fig. 3.7 we can measure the gluino mass to few per-cent, depending on the systematic errors.

For a complete analysis, kinematic endpoints can be supplemented by any other method to measure new physics masses. For short decay chains m_{T2} is best suited to measure the masses of particles decaying directly to the dark matter agent. In supersymmetry, this happens for right handed sleptons or right-handed squarks. The issue with short decay chains is that they often require on some kind of jet veto, which following Sects. 2.5.3 and 1.5.2 is problematic for low-p_T jets.

Keeping in mind that endpoint analyses only use a small fraction of the events, namely those with extreme kinematics, an obvious way to improve their precision is to include the complete shape of the invariant mass distributions. However, this strategy bears a serious danger. Invariant masses are just an invariant way of writing angular correlations between outgoing particles. Those depend on the *spin and quantum numbers* of all particles involved. For example, in the case of the $m_{\ell\ell}$ endpoint the triangular shape implies the absence of angular correlations, because the intermediate particle is a scalar. This means that we should be careful when extracting information for example from kinematic endpoints we do not observe. Depending on the quantum numbers and mixing angles in the new physics scenario, kinematic endpoints can for example be softened, so they vanish in the background noise.

This argument we can turn around. Measuring discrete quantum numbers, like the spin of new particles, is hard in the absence of fully reconstructed events. The usual threshold behavior is not observable at hadron colliders, in particular when the final state includes missing transverse energy. Instead, we rely on angular correlation in decays. For the squark decay chain given in Eq. 3.13 there exists a promising method to simultaneously determine the spin of all new particles in the chain:

1. Instead of trying to measure spins in a general parameterization we start from the observation that cascade decays radiate particles with known spins. This is most obvious for long gluino decays where we know that the radiated bottom quarks as well as muons are fermions. The spins inside the decay chain can only alternate between fermions and bosons. Supersymmetry switches this fermion/boson nature compared to the corresponding Standard Model particle, so we can contrast it with another hypothesis where the spins in the decay chain follow the Standard Model assignments. Such a model are Universal Extra Dimensions, where each Standard Model particle acquires a Kaluza–Klein partner from the propagation in the bulk of the additional dimensions.
2. Thresholds and edges of all invariant masses of the radiated fermions are completely determined by the masses inside the decays chain. Kinematic endpoints cannot distinguish between supersymmetry and universal extra dimensions. In contrast, the shape of the distribution between the endpoints is nothing but an angular correlation in some reference frame. For example, the $m_{j\ell}$ distribution in principle allows us to analyze spin correlations in squark decays in a Lorentz

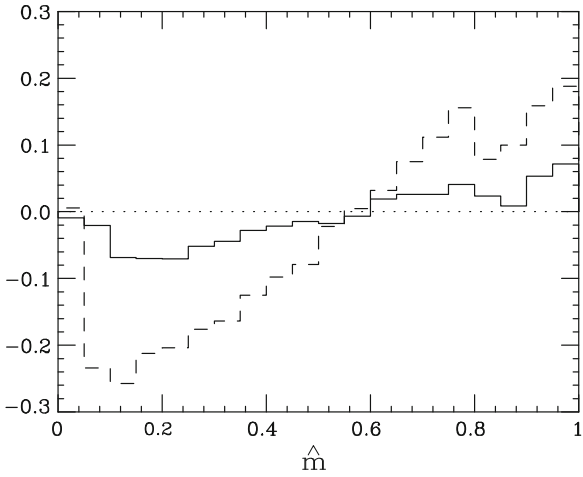

Fig. 3.8 Asymmetry in $m_{j\ell}/m_{j\ell}^{\max}$ for supersymmetry (*dashed*) and universal extra dimensions (*solid*). The spectrum is assumed to be hierarchical, typical for supersymmetric theories. Figure taken from Ref. [8]

invariant manner. The only problem is the link between $\ell^{\pm}$ and their ordering in decay chain.

3. A proton–proton collider like the LHC produces considerably more squarks than antisquarks in the squark-gluino associated channel. For the SPS1a spectrum at 14 TeV collider energy their ratio ranges around 2:1. A decaying squark radiates a quark while an antisquark radiates an antiquark, which means that we can define a non-zero production-side asymmetry between $m_{j\ell^+}$ and $m_{j\ell^-}$. Such an asymmetry we show in Fig. 3.8, for the SUSY and for the UED hypotheses. Provided the masses in the decay chain are not too degenerate we can indeed distinguish the two hypotheses.

This basic idea has since been applied to many similar situations, like decays including gauge bosons, three-body decays, gluino decays with decay-side asymmetries, cascades including charginos, weak-boson-fusion signatures, etc. They show that the LHC can do much more than just discover some kind of particle beyond the Standard Model. It actually allows us to study underlying models and symmetries.

3.4 Uncertainties

As we argue in the very beginning of the lecture, LHC physics always means extracting signals from often large backgrounds. This means, a correct error estimate is crucial. For LHC calculations we are usually confronted with three types of errors.

The first and easiest one are the *statistical errors*. For small numbers of events these experimental errors are described by Poisson statistics, and for large numbers

they converge to the Gaussian limit. In that limit the number of standard deviations in terms of the number of signal and background events is $n_\sigma = N_{\text{sig}}/\sqrt{N_{\text{back}}}$. The two event numbers are proportional to the integrated luminosity $\mathscr{L}$ which means that the statistical significance in the Gaussian limit increases with $\sqrt{\mathscr{L}}$. In high energy physics five standard deviations above a known background we call a discovery, three sigma is often referred to as an evidence. The Poisson region is the only complication we encounter for statistical errors. It means that for small number of signal and background events we need more luminosity than the Gaussian limit suggests.

The second set of errors are *systematic errors*, like the calibration of the jet and lepton energy scales, the measurements of the luminosity, or the efficiencies to for instance identify a muon as a muon. Some readers might remember a bunch of theorists mistaking a forward pion for an electron—that happened right around my TASI in 1997 and people not only discovered supersymmetry but also identified its breaking mechanism. Of course, our experimentalist CDF lecturer told us that the whole thing was a problem of identifying a particle in the detector with an efficiency which does not have to be zero or one.

Naively, we would not assume that systematic errors follow a Gaussian distribution, but experimentally we determine efficiencies and scaling factors largely from well understood background processes. Such counting experiments in background channels like $Z \to$ leptons and their extracted parameters also follow a Gaussian distribution. The only caveat is the shape of far-away tails, which often turn out to be higher than the exponentially suppressed Gaussian tails.

Systematic errors which do not follow a Gaussian distribution we quantify in terms of $n_\sigma = N_{\text{sig}}/N_{\text{back}}$ which means they do not improve with increasing luminosity. Again, five standard deviations are required to claim a discovery, and once we are systematics dominated waiting for more data does not help.

The third source of errors are *theoretical errors*. They are hardest to model because they are often dominated by higher-order QCD effects in fixed order perturbation theory. From Chap. 2 we know that higher order corrections for example to LHC production rates do not follow a naive power counting in α_s but are enhanced by large logarithms. If we can compute or reliably estimate some higher order terms in the perturbative QCD series we call this a prediction. In other words, once we consider a statement about perturbative QCD a statement about its uncertainty we are probably only giving a wild guess.

To model theoretical uncertainties it is crucial to realize that higher order effects are not any more likely to give a K factor of 1.0 than 0.9 or 1.1. In other words, likelihood distributions accounting for theoretical errors do not have a peak and are definitely not Gaussian. There is a good reason to choose the Gaussian short cut, which is that folding three Gaussian shapes for statistical, systematic and theoretical errors gives us a Gaussian distribution altogether, which makes things numerically much easier. But this approach assumes that we know much more about QCD than we actually do which means it is not conservative at all.

On the other hand, we also know that theoretical errors cannot be arbitrarily large. Unless there is a very good reason, a K factor for a total LHC cross section should

not be larger than something like two or three. If that happens we need to conclude that perturbative QCD breaks down, and the proper description of error bars is our smallest problem. In other words, the centrally flat theory probability distribution for an LHC observable has to go to zero for very large deviations from the currently best value.

In the Bayesian picture we define individual *likelihood distributions* for the different errors and integrate over the corresponding uncertainties. This is where the convolution of several Gaussians comes from. The same thing we can do for a Gaussian experimental error and a flat theory errors. The integral returns a two-sided error distribution which still has a peak.

An intuitively better solution which gives a centrally flat likelihood distributions for the combined errors is the *Rfit scheme*, used for example by CKMfitter or SFitter. It is a frequentist of *profile likelihood* construction marginalizing the unknown errors. Such a marginalization of an unwanted direction in the parameter space of our likelihood is a mathematical problem: to keep the mathematical properties of a likelihood as a probability measure we prefer to integrate over unwanted directions. This is what the Bayesian pictures does. The downside is that any integration needs a measure, and a measure in model space or error space is not defined by physics. We therefore assume such a prior and have to test our final result by varying this prior in what we consider a reasonable range.

A profile likelihood instead projects the best fitting point of the unwanted direction onto the new parameter space; for each binned parameter point in the $(n-1)$-dimensional space we explore the nth direction which is to be removed $\mathscr{L}(x_{1,\ldots,n-1}, x_n)$. Along this direction we pick the best value and it with the lower-dimensional parameter point $\mathscr{L}(x_{1,\ldots,n-1}) \equiv \mathscr{L}^{\max(n)}(x_{1,\ldots,n-1}, x_n)$. Such a projection avoids defining a measure but it does not maintain for example the normalization of the likelihood distribution.

The Rfit scheme projects away a flat theory error as well as a Gaussian experimental error. For the center of the distribution this means we need to cut open the experimental Gaussian distribution and insert a flat theory piece. For the log-likelihood $\chi^2 = -2 \log \mathscr{L}$ given a set of measurements $\vec{d}$ and in the presence of a general correlation matrix C this gives us

$$\begin{aligned} \chi^2 &= \vec{\chi}_d^{\,T}\, C^{-1}\, \vec{\chi}_d \\ \chi_{d,i} &= \begin{cases} 0 & |d_i - \bar{d}_i| < \sigma_i^{(\text{theo})} \\ \frac{d_i - \bar{d}_i + \sigma_i^{(\text{theo})}}{\sigma_i^{(\text{exp})}} & d_i - \bar{d}_i < -\sigma_i^{(\text{theo})} \\ \frac{d_i - \bar{d}_i - \sigma_i^{(\text{theo})}}{\sigma_i^{(\text{exp})}} & d_i - \bar{d}_i > \sigma_i^{(\text{theo})}. \end{cases} \end{aligned} \tag{3.23}$$

This distribution implies that for very large deviations there will always be tails from the experimental errors, so we can neglect the impact of the theoretical errors on this range. In the center the distribution is flat, reflecting our ignorance of the theory prediction. The impact of the size of the flat box we need to test.

3.5 Further Reading

Again, there exist several good review articles with more in-depth discussions of different aspects touched in this section:

- As mentioned in Chap. 2 two very useful reviews of jet physics are available by Steve Ellis and collaborators [9] and by Gavin Salam [10].
- For the general phenomenology of the heaviest Standard Model particles, the top quark, have a look at Sally Dawson's TASI lectures [11].
- If you use MadGraph/HELAS to compute helicity amplitudes there is the original documentation which describes every routine [12].
- A lot of experimental knowledge on new physics searches well described and theoretically sound you can find in the CMS technical design report. Some key analyses are described in detail while most of the documentation focuses on the physics expectations [13].
- More on the magical variable m_{T2} you can find in an article by Alan Barr, Chris Lester and Phil Stephens [6]. Chris Lester's thesis [14] is a good point to start with. Recently, Alan Barr and Chris Lester published a broad review on techniques to measure masses in models with dark matter particles [15].
- As mentioned in the introduction, there is our more advanced review on new physics at the LHC which includes an extensive chapter on LHC signatures [16].
- A lot of insight into new physics searches at the LHC and at a linear collider you can find in a huge review article collected by Georg Weiglein [17].
- The pivotal work on determining spins in cascade decays is Jennifer Smillie's Ph.D. thesis [8]. On the same topic there exists a nicely written review by Liantao Wang and Itay Yavin [18].
- Many useful pieces of information on mass extraction, errors, and the statistical treatment of new-physics parameter spaces you can find in the big SFitter publication [19]. The SFitter analysis of the Higgs sector [20] is very similar in structure, but different in the physics application.

References

1. Butterworth, J.M., Davison, A.R., Rubin, M., Salam, G.P.: Jet substructure as a new Higgs search channel at the LHC. Phys. Rev. Lett. **100**, 242001 (2008)
2. Plehn, T., Salam, G.P., Spannowsky, M.: Fat jets for a light higgs. Phys. Rev. Lett. **104**, 111801 (2010)
3. Kribs, G.D., Martin, A., Roy, T.S., Spannowsky, M.: Discovering the Higgs boson in new physics events using jet substructure. Phys. Rev. D **81**, 111501 (2010)
4. ATLAS Collaboration, Performance of the missing transverse energy reconstruction and calibration in proton–proton collisions at a center-of-mass energy of $\sqrt{s} = 7$ TeV with the ATLAS Detector ATLAS-CONF-2010-057
5. Webber, B.: Mass determination in sequential particle decay chains. JHEP **0909**, 124 (2009)
6. Barr, A., Lester, C., Stephens, P.: m(T2): The truth behind the glamour. J. Phys. G **29**, 2343 (2003)

7. Gjelsten, B.K., Miller, D.J., Osland, P.: Measurement of the gluino mass via cascade decays for SPS 1a. JHEP **0506**, 015 (2005)
8. Smillie, J.M., Webber, B.R.: Distinguishing spins in supersymmetric and universal extra dimension models at the large hadron collider. JHEP **0510**, 069 (2005)
9. Ellis, S.D., Huston, J., Hatakeyama, K., Loch, P., Tonnesmann, M.: Jets in hadron–hadron collisions. Prog. Part. Nucl. Phys. **60**, 484 (2008)
10. Salam, G.P.: Towards jetography. arXiv:0906.1833 [hep-ph]
11. Dawson, S.: The top quark, QCD, and new physics. arXiv:hep-ph/0303191
12. Murayama, H., Watanabe, I.., Hagiwara, K.: HELAS: HELicity amplitude subroutines for Feynman diagram evaluations KEK-91-11
13. Bayatian, G.L., et al.: CMS collaboration, CMS technical design report, vol. II, Physics performance. J. Phys. G **34**, 995, (2007)
14. Lester, C.: Model independent sparticle mass measurement at ATLAS. CERN-THESIS-2004-003, http://www.hep.phy.cam.ac.uk/lester/thesis/index.html
15. Barr, A.J., Lester, C.G.: A review of the mass measurement techniques proposed for the large hadron collider. J. Phys. G **37**, 123001 (2010)
16. Morrissey, D.E., Plehn, T., Tait, T.M.P.: New physics at the LHC. arXiv:0912.3259 [hep-ph]
17. Weiglein, G. et al.: LHC/LC study group physics interplay of the LHC and the ILC. Phys. Rept. **426**, 47 (2006)
18. Wang, L.T., Yavin, I.: A review of spin determination at the LHC. Int. J. Mod. Phys. A **23**, 4647 (2008)
19. Lafaye, R., Plehn, T., Rauch, M., Zerwas, D.: Measuring supersymmetry. Eur. Phys. J. C **54**, 617 (2008)
20. Lafaye, R., Plehn, T., Rauch, M., Zerwas, D., Dührssen, M.: Measuring the Higgs sector. JHEP **0908**, 009 (2009)

Index

T. Plehn, *Lectures on LHC Physics*, Lecture Notes in Physics 844,
DOI: 10.1007/978-3-642-24040-9, © Springer-Verlag Berlin Heidelberg 2012